Technical Report

TR-10-06

# Landscape dose conversion factors used in the safety assessment SR-Site

Rodolfo Avila, Per-Anders Ekström, Per-Gustav Åstrand
Facilia AB

December 2010

**Svensk Kärnbränslehantering AB**
Swedish Nuclear Fuel
and Waste Management Co

Box 250, SE-101 24 Stockholm
Phone +46 8 459 84 00

ISSN 1404-0344
SKB TR-10-06
ID 1272381
Updated 2013-08

# Landscape dose conversion factors used in the safety assessment SR-Site

Rodolfo Avila, Per-Anders Ekström, Per-Gustav Åstrand
Facilia AB

December 2010

**Updated 2013-08**

The original report, dated December 2010, was found to contain factual errors which have been corrected in this updated version. The corrected factual errors are presented below.

**Updated 2013-08**

| Location | Original text | Corrected text |
|---|---|---|
| Page 159, Appendix B, last line, column 1 | Aqu_z_regoMid_pg | Aqu_z_rego_pg |
| Page 159, Appendix B, last line, column 2 | Depth of postglacial clay in aquatic middle regolith layer… | Depth of aquatic postglacial sediments… |

# Summary

In this report two types of Dose Convesion Factors have been derived: i) a Landscape Dose Conversion Factor (*LDF*) that is applicable to continuous long-term releases to the biosphere at a constant rate, and ii) a Landscape Dose Conversion Factor for pulse releases (*LDF pulse*) that is applicable to a radionuclide release that reaches the biosphere in a pulse within years to hundreds of years. In SR-Site these Dose Factors are multiplied with modelled release rates or pulse releases from the geosphere to obtain dose estimates used in assessment of compliance with the regulatory risk criterion. The *LDFs* were calculated for three different periods of the reference glacial cycle; a period of submerged conditions following the deglaciation, the temperate period, and a prolonged period of periglacial conditions. Additionally, *LDFs* were calculated for the global warming climate case. The *LDF pulse* was calculated only for temperate climate conditions. The *LDF* and *LDF pulse* can be considered as Best Estimate values, which can be used in calculations of Best Estimate values of doses to a representative individual of the most exposed group from potential releases from a future repository. A systematic analysis of the effects of system, model and parameter uncertainties on the *LDFs* has been carried out. This analysis has shown that the use of the derived *LDF* would lead to cautious or realistic dose estimates. The models and methods that were used for derivation of the *LDFs* and *LDF pulse* are also described in this report.

# Contents

# 1 Introduction

Radioactive waste and spent nuclear fuel from Swedish nuclear power plants are managed by the Swedish Nuclear Fuel and Waste Management Co, SKB. Both waste and spent fuel are planned to be placed in a geological repository. According to KBS-3, copper canisters with a cast iron insert containing spent fuel are to be enclosed by bentonite clay and deposited at approximately 500 m depth in granitic bedrock. Approximately 12,000 tonnes of spent nuclear fuel is forecasted to arise from the Swedish nuclear power programme, corresponding to roughly 6,000 canisters in a KBS-3 repository.

Between 2002 and 2008, SKB performed site investigations with the intention on finding a suitable location for a repository. Investigations were focused on two different sites along the eastern coast of southern Sweden; Forsmark in the municipality of Östhammar and Laxemar-Simpevarp in the municipality of Oskarshamn. Data from the site investigations have been used to produce comprehensive, multi-disciplinary site descriptions for each of the sites. The resulting site descriptions were reported in /SKB 2008/ (Forsmark) and /SKB 2009/ (Laxemar-Simpevarp). Based on available knowledge from the site descriptions and from preliminary safety assessments of the planned repository, SKB decided in June 2009 to put forward Forsmark as suggested site for the repository. The location of Forsmark is shown in Figure 1-1. An application for the construction of a geological repository for spent nuclear fuel at Forsmark is planned to be filed in 2011.

According to the regulations from the Swedish Radiation Safety Authority, SSM, a safety assessment of the planned repository, evaluating features, events and processes that potentially may lead to the release of radionuclides, has to be performed before the construction of the repository is started (SSMFS 2008:21 /SSM 2008a/). The evaluation of the long-term safety of the repository is reported in the /SKB 2011/ (SR-Site is the project of which the report is a product) and, accordingly, it is an important supporting document to the application.


***Figure 1-1.*** *Location of the Forsmark and Laxemar-Simpevarp.*

The safety assessment SR-Site, which is described in the /SKB 2011/, is focused on three major fields of investigation: the performance of the repository, the geosphere and the biosphere. The biosphere part of SR-Site, SR-Site Biosphere, provides estimates for human exposure given a unit release rate or a unit pulse release (*Landscape Dose Conversion Factors, LDFs*). These *LDFs* are multiplied with modelled release rates or pulse releases from the geosphere to obtain estimates of the annual doses to a representative individual of the most exposed group. Dose estimates for different release scenarios are used to assess compliance with the regulatory risk criterion. The present report is dedicated to the derivation of *LDFs* used in assessments of doses to humans. The effects on the environment of a potential release from the repository are also assessed in the biosphere component of SR-Site, but are addressed in a separate report.

The main document for the biosphere analysis within the SR-Site Safety assessment is the Biosphere synthesis report /SKB 2010a/. However, a number of background reports are produced where all details and data that are necessary for a detailed review and for a reproduction of the work done can be found. Figure 1-2 shows information flow between the reports and how the reports are linked together. The present report (marked red in red Figure 1-2) provides a definition of the *LDFs* and approaches for their derivation (Chapter 2), describes the Radionuclide Model for the biosphere and the model simulations for derivation of *LDFs* (Chapter 3), presents the *LDFs* for different climatic conditions and release types (Chapter 4). The report concludes with an analysis of uncertainties associated with the derived *LDFs* (Chapter 5). The equations and parameters used in the Radionuclide Model for the biosphere are presented in Appendices A and B, respectively. Appendix C presents sensitivity analysis results for a selection of radionuclides.

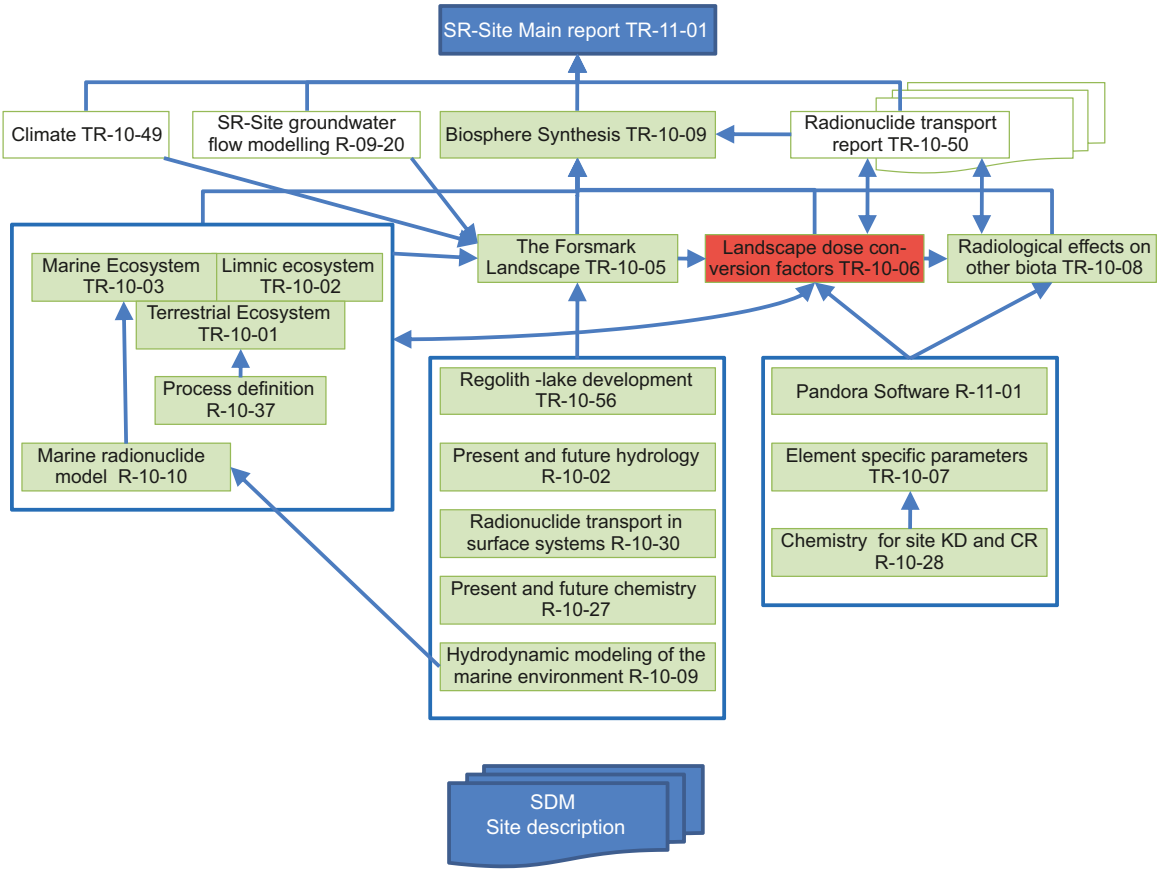


***Figure 1-2.*** *The hierarchy of reports produced in the SR-Site Biosphere project. This report (market red).*

# 2 Dose assessments using Landscape Dose Factors

In the corrosion and the shear load scenarios /SKB 2011/, radionuclides from the repository are unlikely to reach the biosphere within the first 100,000 years. However, after this period contaminated groundwater from the repository may reach the biosphere resulting in a continuous release of radionuclides during more than 1,000,000 years. When a release from the repository reaches the biosphere 100,000 years after closure, the peak release rates for most dose dominating nuclides will remain on a near-constant level for periods of 10,000 years or more /SKB 2011/**.** Under such release conditions it is appropriate to calculate doses to future inhabitants of potentially affected areas in the biosphere by multiplying the release rates to the biosphere by a constant Dose Conversion Factor, that relates annual doses to the release rate of each radionuclide. In SR-Site, this radionuclide-specific Dose Conversion Factor is called the Landscape Dose Conversion Factor (*LDF*). *LDF* for different climatic conditions have been derived from simulations with constant unit release rates during the whole time period when different climatic conditions prevail.

As mentioned above, under both the corrosion and the shear load scenarios, release from the fuel matrix and corroded metals will result in a continuous release of radionuclides during very long time spans (> million years). However, for some radionuclides the instantaneously accessible fraction from fuel dissolution may reach the biosphere in a pulse within years or tens of years after failure. Using the above *LDFs* for calculating doses from such pulse releases would result in large overestimation of the doses. To address such situation, a second type of Dose Conversion Factor has been derived, which relates annual doses to a unit pulse release. In SR-Site, this Dose Conversion Factor is called the Landscape Dose Factor for pulse releases (*LDF pulse*) and in some cases has also been called the "*modified LDF for pulse release*". The values of *LDF pulse* have been derived from simulations with a unit release of short duration occurring at different times during an interglacial period.

A more exact definition of the *LDF* and *LDF pulse* is given in Section 2.3. The general approach for their derivation is presented in Section 2.4. The models applied and the simulations made are described in Chapter 3. The *LDF*s have been derived for all radionuclides presented in Section 2.2.2, whereas *LDF pulse* have been derived only for radionuclides (see Table 2-1) that can be present in the instantaneously accessible fraction from fuel dissolution, at the start of the release in the corrosion and the shear load scenarios /SKB 2011/.

## 2.1 Assessment endpoints

The *LDF* and *LDF pulse* derived in this report are used in SR-Site for calculation of doses to a representative individual in the group that is exposed to the greatest risk. These doses are then multiplied by a factor of 7.3% per Sievert, which is the factor recommended in ICRP Publication 60 /ICRP 1991/ and the Swedish regulation /SSM 2008a/ for conversion of effective dose to risk. In this way, an estimate of the annual risk of harmful effects is obtained which can be compared with the risk criterion of $10^{-6}$ per year, established in the Swedish Regulation /SSM 2008a/.

As recognized in the Swedish regulations, the most exposed group to the releases from a repository cannot be described in an unequivocal, unique way. SSMFS 2008:37 /SSM 2008b/ states that "One way of defining the most exposed group is to include the individuals that receive a risk in the interval from the highest risk down to a tenth of this risk. If a larger number of individuals can be considered to be included in such a group, the arithmetic average of individual risks in the group can be used for demonstrating compliance with the criterion for individual risk in the regulations. One example of such an exposure situation is a release of radioactive substances into a large lake that can be used as a source of drinking water and for fishing".

SSMFS 2008:37 also states that "If the exposed group only consists of a few individuals, the criterion of the regulations for individual risk can be considered as being complied with if the highest calculated individual risk does not exceed $10^{-5}$ per year. An example of a situation of this

kind might be if consumption of drinking water from a drilled well is the dominant exposure path. In such a calculation example, the choice of individuals with the highest risk load should be justified by information about the spread in calculated individual risks with respect to assumed living habits and places of stay".

In SR-Site, the most exposed group is defined as the group of individuals exposed to the biosphere object (Section 2.4) with the potentially highest contamination, considering a glacial cycle from a submerged landscape to fully terrestrial conditions. A representative individual from the most exposed group is assumed to spend all time in this object, and get his/her entire supply of food and water from the object. The procedures applied for calculation of dose to a representative individual from this group (Section 3.2), also allow estimating the size of the group, i.e. the number of individuals in the group.

The Swedish regulations /SSM 2008a, b/ require that annual dose averaged over the lifetime of the individuals are calculated for comparison with the risk criteria, which means that it is not necessary to calculate doses to different age groups, as this average can be adequately represented by the annual dose to an adult /ICRP 1998/. Hence, in the derivation of *LDF* and *LDF pulse* values, doses to adults have been calculated. The term dose is taken to mean "effective dose", including, as appropriate, the committed dose from intakes of radionuclides and the contribution from external irradiation. This is the appropriate dose type that should be calculated for comparison with the Swedish regulatory criteria /SSM 2008a/. For calculation of effective doses to adults parameters that describe human demands for survival, (i.e. annual food and water consumption rates, and inhalation rates), and dose coefficients for internal and external irradiation on the individuals were taken from the literature (see Section 3.3). In line with international recommendations /ICRP 2006/ fixed, slightly conservative values were chosen for these parameters.

## 2.2 Scope of the assessments

The *LDF* and *LDF pulse* derived in this report are considered representative for the conditions at the Forsmark site, which are briefly described in Section 2.2.1. It is assumed that the landscape development at Forsmark during repeated glacial cycles will follow a path similar to the present glacial cycle. Thus, discharge areas will go through a similar succession from being part of the open sea, over a sea bay phase, to a lake, which eventually will transform into a wetland also after future deglaciations (see Section 3.1.1). Future sea and lake ecosystems are assumed to have similar characteristics as the current aquatic ecosystems in Forsmark. The wetlands that will develop from future lakes are assumed to be similar to the rich fens that presently are found in the area. If drained, these wetlands will provide an organic soil rich in nutrients that will be suitable for cultivation for a limited period of time.

### 2.2.1 The biosphere at Forsmark

This section provides a brief description of the present-day conditions at Forsmark, based on available knowledge from the site investigations. More detailed descriptions of the site can be found in the Site description Forsmark report /SKB 2008/ and in the report describing the surface systems at Forsmark /Lindborg 2008/. The section starts with a presentation of the abiotic characteristics of the Forsmark area, which describes the physical and chemical context of the ecosystems and continues with an overview of the present-day ecosystems of the site and the utilisation of the landscape by humans.

#### *Abiotic characteristics*

The topography of the Forsmark area is characterised by a low relief (Figure 2-1). In terrestrial areas, elevation differences are usually less than 20 metres. SKB has developed a digital elevation model (DEM) to describe the topography of the area. The DEM serves as input to other models for projection of both past and future conditions. Detailed descriptions of the DEM are provided in /Brydsten and Strömgren 2004/ and /Strömgren and Brydsten 2008/.

***Figure 2-1.*** *The Forsmark area seen from south-east, with the only larger arable land area, Storskäret, in the foreground.*

The regolith, which includes all unconsolidated material overlying the bedrock, consists to a large degree of glacial deposits, reworked during multiple glaciations and relocated by subsequent glacial and post-glacial processes. The distribution of regolith follows the general pattern for areas in Sweden below the highest postglacial coast-line. Elevated parts of the terrain are dominated by till or exposed bedrock and valleys have a higher percentage of clay and postglacial deposited fine-grained material. The upper part of the regolith is affected by deposition and decomposition of organic material. This leads to formation of soils in terrestrial areas and of organic matter rich sediments in aquatic areas. Terrestrial areas are also affected by weathering of the original material. A high content of calcium carbonate ($CaCO_3$) is recorded in a majority of the glacial deposits /Hedenström and Sohlenius 2008/. The carbonates originate from Palaeozoic limestone on the bottom of the Bothnian Sea, brought to Forsmark by glacial transport. A regolith depth model (RDM model) was created by /Hedenström et al. 2008/ where the regolith is subdivided into seven layers and three generalised lake sediment lenses. The total regolith depth in the model varies between 0.1 and 42 m.

The mean annual temperature at Forsmark is approximately +7°C. The dominating wind direction in the area is from the south-west. The annual corrected precipitation in the Forsmark area during the studied period was 546 mm/y /Johansson 2008/. On average, snow covers the ground for 105 and 80 days/season on forest land and open land, respectively. The period of snow cover is typically from the end of November until the beginning of April /Löfgren 2010/.

The small-scale topography of the area gives rise to many small catchments with local, shallow groundwater flow systems in the regolith. In combination with the decreasing hydraulic conductivity with regolith depth, this causes that a dominant part of the near-surface groundwater will move along shallow flow paths. Shallow groundwater flow paths imply strong interactions among evapotranspiration, soil moisture content, groundwater levels and flow. In Forsmark, the groundwater table in the regolith is very shallow; in general the depth to the groundwater table is less than a metre. Thus, the groundwater level in the regolith is highly correlated with the topography of the ground surface. This local flow system in the regolith overlies a larger-scale flow system in the bedrock.

In total, 25 lake-centred catchment areas, ranging in size from 0.03 to 8.67 km$^2$, have been delineated and described within the Forsmark area /Brunberg et al. 2004, Andersson 2010/. The 25 lakes are all small and shallow with mean and maximum depths ranging from approximately 0.1 to 1 m and 0.4 to 2 m, respectively. Wetlands are frequent and cover 25 to 35% of some of the catchments /Johansson 2008/. No major watercourses flow through the central part of the site investigation area, and most streams in the area dry out during parts of the year.

The marine part of the Forsmark area is located in Öregrundsgrepen, a funnel-shaped bay of the Bothnian Sea which is a part of the Baltic Sea with its wide end to the north and the narrow end southwards. The studied area was divided into 28 sub-basins, based on today's bathymetry and the projected pattern of future drainage areas arising in consequence of isostatic rebound /Brydsten 2006/. The sub-basins are presented in Figure 2-2, together with the DEM for the marine area at Forsmark. The major part of the area is shallow and most sub-basins show a mean depth shallower than 10 m. The water retention time in the 28 sub-basins varies between 13 and 34 days (22 on average) /Karlsson et al. 2010/.

The present chemical characteristics at Forsmark are a consequence of the past landscape development, together with the abiotic and biotic factors acting today. Fresh surface waters and shallow groundwaters in the Forsmark area are generally characterised by high contents of marine ions, high pH and high alkalinity, as well as very high concentrations of calcium compared with the general conditions in Sweden. These site-specific characteristics can be explained by marine remnants left by a regressing Baltic Sea, together with glacial remnants in the form of the calcite-rich till layer deposited during the Weichselian glaciation /Sonesten 2005, Tröjbom and Söderbäck 2006, Tröjbom et al. 2007/.

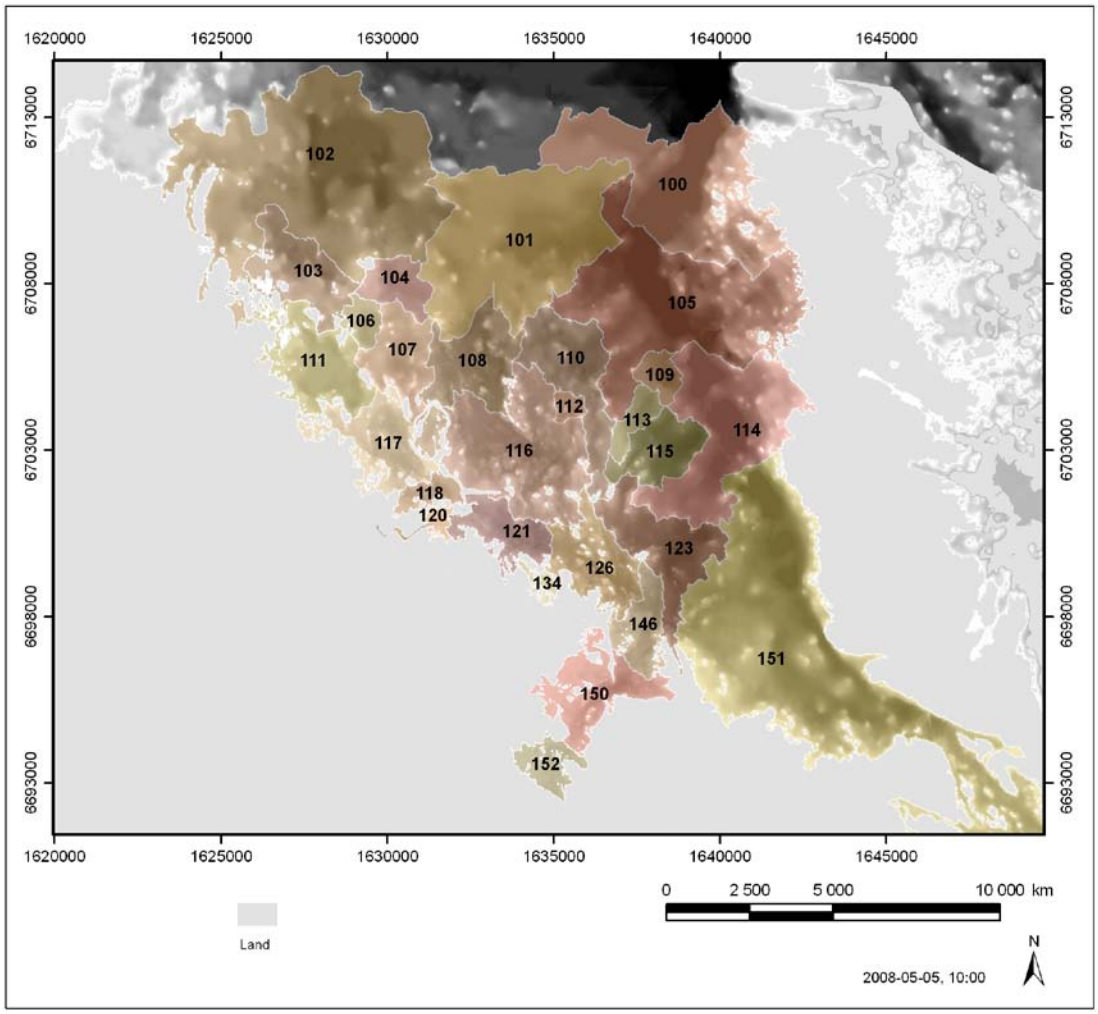


***Figure 2-2.*** *Marine sub-basins used in the SR-Site assessment, projected on the bathymetric map of Forsmark. Numbers are identification numbers of the sub-basins.*

The influence from calcite has had a strong effect on the development of the terrestrial and limnic ecosystems in the Forsmark area. Secondary precipitation of calcite, with co-precipitation of dissolved phosphorus, mediates the development of the nutrient-poor oligotrophic hardwater lakes that are typical of this region. The rich supply of calcium also influences soil formation and the development and structure of the terrestrial ecosystems /Löfgren 2010/.

### *Biotic characteristics*

This section presents a general description of the ecosystems in the Forsmark area. Detailed information on biomass, production, chemical composition, turnover of tissues and carbon content used in the ecosystem models can be found in the ecosystem reports; terrestrial ecosystems /Löfgren 2010/, limnic ecosystems /Andersson 2010/ and marine ecosystems /Aquilonius 2010/.

In Forsmark, 73% of the terrestrial area is covered by forests, dominated by Scots pine (*Pinus sylvestris*) and Norway spruce (*Picea abies*), which are the dominating tree species in the boreal forests of Scandinavia. The relatively large portion of deciduous trees is both a consequence of previous or present human land use and of the location by the coast. The field layer is characterised by herbs and broad-leaved grasses, along with a number of orchid species, favoured by the calcareous soils. The area has a long history of forestry, in recent times generally managed by clear-cutting.

A major part of the wetlands in the Forsmark area consist of coniferous forest swamps and open mires. The less mature wetlands consist of moderately to extremely rich fens /Jonsell and Jonsell 1995/, which is a consequence of the high calcareous content of the local regolith. Arable land and pastures are found close to settlements, including settlements now abandoned. The most common larger mammal species in the Forsmark area are roe deer and moose.

All present-day lakes in the Forsmark area are small and shallow, and are characterised as oligotrophic hardwater lakes /Andersson 2010/. The shallow depths and relatively clear water of the lakes permit photosynthesis in the entire benthic habitat of the lakes, and the bottoms are covered by dense stands of the macroalgae *Chara* sp. Moreover, many of the lakes also have a thick (>10 cm) microbial mat, consisting of cyanobacteria and diatoms, in the benthic habitat. The large amounts of macroalgae and microphytobenthos give rise to high primary production in the benthic habitat, whereas primary production in the water column is modest. The fish community in the lakes is dominated by species resistant to low oxygen concentrations, mainly due to poor oxygen conditions during the winter.

Shallow waters, a subdued bathymetry and restricted light penetration characterise the marine ecosystems in Forsmark. Together, these factors result in high primary production in the near-shore zone, were the highest biomasses and primary production are found. In deeper areas, where primary production is restricted to the pelagic zone, the production is lower. The marine system of the Forsmark area is a relatively productive coastal zone in a region of otherwise fairly low primary production. This is due to upwelling along the coast /Eriksson et al. 1977/. As in the rest of the Bothnian Sea, the fauna consists of mixed freshwater and saltwater species. The benthic fauna occurs in the highest densities in association with vegetation. In offshore areas, herring and sprat are the dominating fish species, whereas perch and pike are the most common species in the inner bays /Aquilonius 2010/.

### *Human utilization of natural resources*

Today, the Forsmark area has no permanent residents, but there are five holiday houses and three farms situated within the area /Miliander et al. 2004/. The only agricultural enterprise operating today is situated at Storskäret. It is focused on meat production and the cattle graze outdoors during the period of vegetation growth. The area used for agricultural purposes (pastures, meadows and fields) comprises 4% of the total area. The land use is dominated by forestry, and wood extraction is the only significant outflow of biomass from the area. The dominant leisure activity is hunting. Besides this, the area is only occasionally used for leisure as a result of the small local population, the relative inaccessibility of the locality and the distance from major urban areas. The area contains one large industrial plant, the Forsmark nuclear power plant, with more than 700 employees. Besides these, there are only a few work places within the area /Miliander et al. 2004/.

### 2.2.2 Radionuclides considered

For all radionuclides presented in Table 2-1 *LDFs* have been derived for all considered climatic conditions (see Section 2.3). Where appropriate the long-lived progeny has been taken into account in the *LDFs*. This means that doses obtained from multiplying the release rate of a radionuclide by the corresponding *LD*F include the contribution of longer-lived progeny that in-grow in the environment from decay of the parent radionuclides. The *LDF pulse* values were derived only for those radionuclides (marked in bold in Table 2-1) that can be present in the instantaneously accessible fraction from fuel dissolution at the start of the releases in the corrosion and the shear load scenarios /SKB 2011/.

**Table 2-1. Radionuclides for which *LDF* and *LDF pulse* (marked in bold) were derived.**

| Radionuclide | Decay half life (years) | Longer-lived progeny | | | | | | |
|---|---|---|---|---|---|---|---|---|
| Ac-227 | 2,280E+01 | | | | | | | |
| **Ag-108m** | 4,180E+02 | | | | | | | |
| Am-241 | 4,322E+02 | Np-237 | U-233 | Th-229 | | | | |
| Am-243 | 7,370E+03 | Pu-239 | U-235 | Pa-231 | | | | |
| C-14 | 5,730E+03 | | | | | | | |
| Ca-41 | 1,030E+05 | | | | | | | |
| Cd-113m | 1,410E+01 | | | | | | | |
| **Cl-36** | 3,010E+05 | | | | | | | |
| Cm-244 | 1,810E+01 | Pu-240 | U-236 | Th-232 | | | | |
| Cm-245 | 8,500E+03 | Am-241 | Np-237 | U-233 | Th-229 | | | |
| Cm-246 | 4,730E+03 | Pu-242 | U-238 | U-234 | Th-230 | Ra-226 | Pb-210 | Po-210 |
| **Cs-135** | 2,300E+06 | | | | | | | |
| Cs-137 | 3,010E+01 | | | | | | | |
| Ho-166m | 1,200E+03 | | | | | | | |
| **I-129** | 1,570E+07 | | | | | | | |
| Mo-93 | 3,999E+03 | | | | | | | |
| **Nb-94** | 2,030E+04 | | | | | | | |
| **Ni-59** | 7,600E+04 | | | | | | | |
| Ni-63 | 1,001E+02 | | | | | | | |
| Np-237 | 2,140E+06 | U-233 | Th-229 | | | | | |
| Pa-231 | 3,276E+04 | | | | | | | |
| Pb-210 | 2,230E+01 | Po-210 | | | | | | |
| Pd-107 | 6,500E+06 | | | | | | | |
| Po-210 | 4,000E–01 | | | | | | | |
| Pu-239 | 2,411E+04 | U-235 | Pa-231 | | | | | |
| Pu-240 | 6,563E+03 | U-236 | Th-232 | | | | | |
| Pu-242 | 3,730E+05 | U-238 | U-234 | Th-230 | Ra-226 | Pb-210 | Po-210 | |
| Ra-226 | 1,600E+03 | Pb-210 | Po-210 | | | | | |
| **Se-79** | 1,130E+06 | | | | | | | |
| Sm-151 | 9,000E+01 | | | | | | | |
| **Sn-126** | 1,000E+05 | | | | | | | |
| Sr-90 | 2,880E+01 | | | | | | | |
| **Tc-99** | 2,110E+05 | | | | | | | |
| Th-229 | 7,340E+03 | | | | | | | |
| Th-230 | 7,538E+04 | Ra-226 | Pb-210 | Po-210 | | | | |
| Th-232 | 1,410E+10 | | | | | | | |
| U-233 | 1,590E+05 | Th-229 | | | | | | |
| U-234 | 2,460E+05 | Th-230 | Ra-226 | Pb-210 | Po-210 | | | |
| U-235 | 7,040E+08 | Pa-231 | | | | | | |
| U-236 | 2,340E+07 | Th-232 | | | | | | |
| U-238 | 4,470E+09 | U-234 | Th-230 | Ra-226 | Pb-210 | Po-210 | | |
| Zr-93 | 1,530E+06 | | | | | | | |

## 2.3 Definition of Landscape Dose Conversion Factors

Two dose conversion factors were derived in SR-Site: i) the Landscape Dose Conversion Factor (*LDF*) that is applicable to continuous long-term releases at a constant rate, and ii) the Landscape Dose Conversion Factor for pulse releases (*LDF pulse*) that is applicable to a radionuclide release that reaches the biosphere in a pulse within years to hundreds of years. The definition of these Dose Conversion Factors is provided below.

The Landscape Dose Conversion Factor (*LDF*) of a radionuclide is defined as the annual effective dose to a representative individual from the most exposed group resulting from a constant unit release rate of this radionuclide to the biosphere. The annual effective dose comprises the sum of the annual effective dose from external exposure and the committed effective dose from internal exposure due to intakes. The exposure is averaged over the lifetime of an individual, and the units of the *LDFs* are Sv/y per Bq/y. *LDFs* were calculated for three different periods of the reference glacial cycle: the period of submerged conditions following the deglaciation, the interglacial period, and a prolonged period of periglacial conditions. Additionally, *LDFs* were calculated for the global warming climate case.

The modified Landscape Dose Conversion Factor for pulse releases (*LDF pulse*) of a radionuclide is defined as the annual effective dose to a representative individual from the most exposed group, resulting from a unit pulse release of this radionuclide to the biosphere. The exposure is averaged over the lifetime of an individual, and the unit of the *LDF pulse* is Sv/y per Bq. The *LDF pulse* has only been derived for temperate climate conditions.

#### *Reference glacial cycle*

The first part of the reference glacial cycle is represented by *temperate conditions*, i.e. climate conditions similar to those of today. For the derivation of *LDFs,* this interglacial period is assumed to exist for 18,400 years (i.e. at their first occurrence from –9000 to 9400 AD, but then recurring in each glacial-interglacial cycle). When the period starts, the landscape is covered by the sea (submerged conditions). As land emerges sufficiently out of the sea, wetlands are first created and then converted to arable land. In the derivation of *LDFs* it is assumed that drinking water for humans and livestock is supplied in equal parts from surface water and from a contaminated well drilled deep in the rock during this period.

The interglacial period with temperate conditions is followed by periods with *periglacial conditions*, representing a colder climate than today with deep permafrost. For the derivation of *LDFs* for permafrost, these conditions are assumed to prevail for 50,200 years (i.e. from 9400 to 59,600 AD at their first occurrence). In the derivation of *LDFs* it is assumed that during this period, agricultural practice is not possible and drinking water from a contaminated deep drilled well is not accessible.

Releases under *glacial conditions*, when the repository is covered by an inland ice, are unlikely. Nevertheless, if they occur then humans can only be exposed to radionuclides through ingestion of sea food, which can be contaminated from releases to the sea when the ice margin is situated above or close to the repository. The resulting doses in this case are expected to be lower than in temperate conditions, due to a larger dilution of radionuclides released to the sea. As a cautious estimate of annual exposures from releases during *glacial conditions*, the *LDFs* from the open-sea stage (submerged period) obtained for temperate conditions are used in the assessments.

#### *Global warming climate case*

In this climate case, it is assumed that global warming will extend the period of *temperate conditions*, which will prevail during the whole interglacial period (i.e. from –9000 to 59,600 AD). *LDFs* for the global warming climate case represent the maximum during this period. It is assumed that wetlands are converted to arable land when possible, and drinking water for humans and livestock is supplied by equal parts from surface water and water from a contaminated well drilled in the rock.

## 2.4 Approach for derivation of Landscape Dose Conversion Factors

In both of the main release scenarios in SR-Site /SKB 2011/, radionuclides that reach the biosphere are most likely originating from one single canister. In the corrosion scenario, the failing canister has been deposited in a position with a high groundwater flow rate, which is associated with low geosphere transport resistance. In the shear load scenario, the shearing fracture is assumed to be among the largest in the rock fracture network, and therefore radionuclide retention in the geosphere is pessimistically disregarded in the safety assessment, see further the SR-Site Main report /SKB 2011/. For releases which are associated with low or negligible geosphere transport retention, the shoreline position is expected to have limited effect on the geographical location of the discharge area, and discharge of contaminated groundwater may thus be restricted to one discharge area /Lindborg 2010/.

For the calculation of *LDFs*, it has been assumed that the release to the biosphere from the fuel matrix and corroded metals will be approximately constant on the time scale of the biosphere assessment (~20,000 years). It is cautiously assumed that the whole release of radionuclides will reach the discharge area where it will cause maximum exposure, i.e. the release will not be subdivided over several biosphere objects. For the calculations of the *LDF pulse*, it is assumed that the total instantaneously accessible fraction of radionuclides from fuel dissolution will reach the same discharge area that gives the maximum *LDF*.

The biosphere at Forsmark is represented by a set of interconnected biosphere objects. A biosphere object is defined as an area of the landscape that can receive radionuclides released, either through discharge of deep groundwater or in contaminated surface water, at any time during a glacial cycle. The identification of biosphere objects in the Forsmark area is based on the modelling of flow paths from the repository to the ground surface /Joyce et al. 2010/. Deep groundwater from the repository is primarily attracted to low points in the landscape, e.g. shallow parts of the sea, along the shoreline, and in lakes, streams and wetlands. The outer boundary of each biosphere object was determined from the hypsography of the sea basin during the submerged phase, whereas the shoreline of the lake at time of isolation from the sea delineates the biosphere object during the lake and terrestrial phases /Lindborg 2010/.

As the releases from the repository may be restricted to single biosphere objects (see above), it is considered appropriate to base the derivation of the *LDF* and *LDF pulse* on simulations for each biosphere object separately. The effect of releases to a biosphere object from an indirect release originating from a contaminated object located upstream has not been considered in simulations for calculation of *LDFs*. This simplification is appropriate for derivation of *LDF* values that represent the maximum doses across all biosphere objects in the Forsmark area during the whole simulation period (Chapter 5). Further, it has been assumed that in addition to reaching biosphere objects, the released radionuclides will also reach a well drilled in the bedrock (see Section 3.1.1) and contributions to the doses from ingestion of well water are also considered in the *LDF* and *LDF pulse*.

The same models and parameter values were used for deriving *LDFs* for the two climate cases. Although many features of the biosphere may be affected by the climate, it was assumed that quantitative changes in these biosphere features will be within the range of natural variation and the measurement uncertainties associated with the parameter values for present-day temperate conditions /Andersson 2010, Aquilonius 2010, Löfgren 2010/. Thus, the major difference in the calculations for the two climate cases is that global warming is expected to extend the period of temperate conditions within an interglacial, resulting in longer time of accumulation for released radionuclides.

The assessment philosophy in SR-Site has been to make as realistic as possible estimations of the radiological risks from potential releases from a future repository. The derivation of *LDFs* has been based on scenarios of the biosphere development, the climate evolution and the use of natural resources by humans, which are based on the knowledge of present-day conditions at Forsmark, and of the past and expected future development of the site. However, it is difficult to determine the level of realism in assumptions related to future development of the biosphere and human habits. In these cases, the uncertainties are large and therefore it is inevitable that some cautious assumptions have had to be introduced in the assessments.

There are also conceptual uncertainties associated with the Radionuclide model for the biosphere used for derivation of *LDFs*, and uncertainties associated with the values assigned to the model parameters. The effect of conceptual uncertainties in the model has been explored by deriving *LDFs* using alternative assumptions and models and comparing these with the *LDFs* used in the SR-Site dose assessments. The selection of Best Estimate (BE) values for model parameters has been based, as far as possible, on data obtained from the site investigation programs and knowledge of the site properties. The *LDFs* have been derived from deterministic simulations with the model using these BE values. In addition, probabilistic simulations have been used to quantify the impact of parameter uncertainties on the *LDFs*. A comprehensive analysis of uncertainties associated with the derived *LDFs* and of the approaches adopted for treatment of the uncertainties has been carried out and is presented in Chapter 5.

# 3 Methods for derivation of LDF values

This chapter describes the methods applied for derivation of the *LDF* and *LDF pulse* (see definitions in Section 2.3). The values of these Dose Conversion Factors have been derived from deterministic simulations with the Radionuclide Model for the biosphere for different climatic conditions. The section starts with a description of the conceptual and mathematical models used to simulate transport and accumulation of radionuclides in the biosphere, and the methods used to calculate the activity concentrations in the environment. This description is supported by a presentation of model equations in Appendix A and a description of the software implementation of the model in Section 3.4. A description of the methods used to calculate exposures of a representative individual of the most exposed group to potential releases from the repository is presented in Section 3.2. An overview of the input parameters used in model simulations is presented in Section 3.3 and a complete list of model parameters is given in Appendix B. The last section in the chapter describes the simulations made for derivation of values of *LDF* and *LDF pulse*.

## 3.1 The Radionuclide Model for the biosphere

The Radionuclide Model for the biosphere addresses the radionuclide transport and accumulation in biosphere objects that may potentially be affected by radionuclide releases from a future repository. A biosphere object is defined as an area of the landscape that can receive radionuclide releases; either through discharge of deep groundwater or in contaminated surface water, at any time during a glacial cycle (see Section 2.4). The identification of biosphere objects in the Forsmark area is based on the modeling of flow paths from the repository to the ground surface /Joyce et al. 2010/. The delineation of biosphere objects, and prediction of their development in time is described in detail in Chapter 6 in /Lindborg 2010/.

### 3.1.1 The conceptual model

The radionuclide model for the biosphere is a classical compartment model, where system components are considered internally homogeneous and are represented by distinct compartments. A graphical representation of the conceptual model is shown in Figure 3-1, where each box corresponds to a model compartment. Definitions of individual compartments are presented in Table 3-1. A basic assumption implicit in the model is that radionuclides that enter a compartment get homogeneously mixed in the compartment, within the relevant time scale of the model. When defining the compartments and their size, it was presumed that the model will be applied for simulations of the long-term transport and accumulation of radionuclides in the biosphere.

The arrows in Figure 3-1 represent radionuclide fluxes between compartments and fluxes in and out of a typical biosphere object with a central depression (in this case a lake). Radionuclide fluxes are linked to the main fluxes of matter in the biosphere, i.e. water fluxes (2 in Figure 3-1), gas fluxes (3) and particle fluxes (4). Radionuclide transfers mediated by biota (6), like uptake by primary producers, have also been considered. The arrow (1) reaching the lower regolith compartment represents radionuclide releases from the geosphere into the biosphere object. These releases are directed to the deeper parts of the regolith, which at the site normally consists of glacial till directly overlying bedrock.

Radionuclides released to the lower regolith compartment are distributed to the upper layers of the ecosystems by advection and diffusion. The representation of the waterborne transport of radionuclides between compartments is based on detailed hydrological modelling with MIKE-SHE /Bosson et al. 2010/. These studies have shown that the vertical hydrological fluxes in the deep regolith layer of sea basins and bays are small. Discharge areas above sea level may, on the other hand, have substantial vertical fluxes with preferential flow paths through areas of higher permeability within a biosphere object, as in wetlands surrounding lakes and streams.

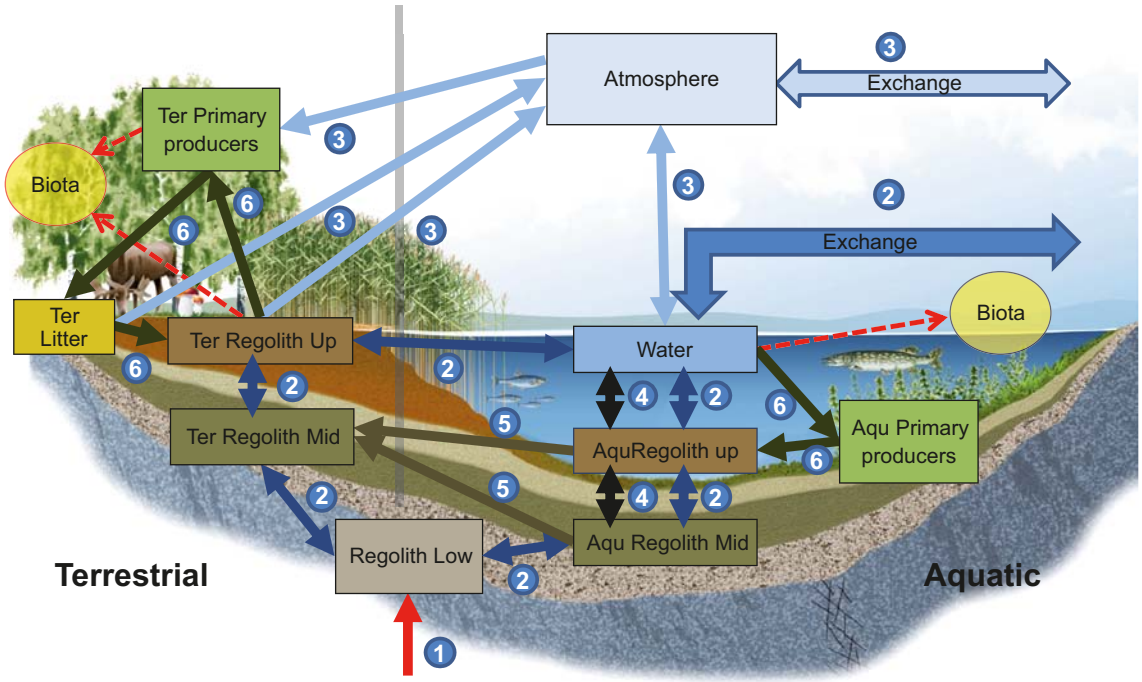


***Figure 3-1.*** *Conceptual illustration of the Radionuclide Model for the biosphere. Boxes represent compartments, thick arrows fluxes, and dotted arrows concentration computations for biota (these are not included in the mass balance calculations). The model represents one biosphere object which contains an aquatic (right) and a terrestrial part (left) with a common lower regolith and atmosphere. The release from the geosphere is represented by a red arrow (1). The radionuclide transport is mediated by different major transport processes, indicated with dark blue arrows for water fluxes (2), light blue for gas fluxes (3), black for sedimentation/resuspension fluxes (4), dark brown for the wetland growth (5), and green for biological uptake/decomposition (6). Import from and export to surrounding objects in the landscape is represented by arrows marked "exchange". Descriptions of the compartments are given in Table 3-1.*

**Table 3-1. Compartments included in the Radionuclide Model for the biosphere.**

| Model name | Description |
|---|---|
| Regolith Low | The lower part of the regolith overlying the bedrock, primarily composed of glacial till. |
| Aqu Regolith Mid | The middle part of the regolith in the aquatic part of biosphere objects, usually consisting of glacial and postglacial clay and gyttja. |
| Aqu Regolith Up | The part of the aquatic regolith with highest biological activity, comprising ca 5–10 cm of the upper aquatic sediments where resuspension and bioturbation can maintain an oxidizing environment. |
| Ter Regolith Mid | The middle part of the terrestrial regolith, containing glacial and postglacial fine material, i.e. sediments formed in a former seabed / lake bottom environment. |
| Ter Regolith Up | The upper part of the terrestrial regolith which has the highest biological activity, primarily composed of wetland peat. |
| Litter | Dead plant material overlying the regolith. |
| Water | The surface water (stream, lake, or sea water). |
| Aqu Primary Producers | The biotic community in aquatic habitats, comprising both primary producers and consumers. |
| Ter Primary Producers | Terrestrial primary producers. |
| Atmosphere | The lower part of the atmosphere (the troposphere) where released radionuclides are fully mixed. |

The effect of radionuclide sorption on the advective and diffusive transport of radionuclides is taken into account by assuming equilibrium between the pore water and the solid phase of the compartments. The model also considers the transport of radionuclides absorbed to suspended particles driven by surface water fluxes, sedimentation and resuspension processes.

The radionuclide transport mediated by biota is described in the model through fluxes driven by net primary production, in both terrestrial and aquatic ecosystems. It is assumed that equilibrium is established between the concentration of radionuclides in the newly produced biomass and the corresponding environmental media (regolith for terrestrial primary producers and water for aquatic primary producers). This is an improvement over traditional plant uptake models as plant uptake is a made a function of growth, while at the same time mass balances are maintained /Avila 2006, Andersson 2010/.

#### *Representation of the successional development of a biosphere object*

Simultaneous simulation of both aquatic and terrestrial ecosystems in the Radionuclide Model for the biosphere, has allowed representing the continuous development in time of biosphere objects and the landscape. When applied to each biosphere object the radionuclide model has two parts, one aquatic (right side in Figure 3-1) and one terrestrial (left side in Figure 3-1). The temporal development of an object is handled by varying the sizes and properties of these two parts in accordance with the simulated development of the specific biosphere object, resulting from natural processes such as shoreline displacement, sedimentation, and lake infilling (see Chapter 3 and 8 in /Andersson 2010/ and /Lindborg 2010/ for details on site development and biosphere objects).

Throughout the succession from open sea to a wetland, the model representation of a biosphere object changes as follows. During the sea stage, there are no terrestrial compartments, and all fluxes from the lower regolith are directed to aquatic sediments. During a transitional stage (~500 years), the sea bay is isolated and transforms into a lake, and a wetland starts to develop. Denomination of the compartments and processes will change as a consequence of a changing environment. For example the flux of radionuclides from the deep regolith will gradually shift from aquatic sediments to sediments under the wetland. During this phase, saltwater intrusions will still occur, although at reducing frequency, and consequently the values of the aquatic model parameters are varied continuously from sea to lake values. After isolation is completed, the surrounding wetland will continue to expand into the lake. Thus, during the lake stage, aquatic sediments are gradually covered by a layer of peat. In the model this process is represented by a flux of radionuclides from the aquatic sediments to the terrestrial regolith (arrows 5 in Figure 3-1). The natural end state of the biosphere objects is a wetland, usually drained by a small stream. At different points in time this wetland might or might not be converted into an agricultural land by future humans (see below).

#### Aquatic environment

When a marine basin is isolated from the sea and the surface water becomes fresh, by definition a lake is formed. During the sea stage there are no terrestrial compartments. The formation of wetland (further discussed in Chapter 8 in /Andersson 2010/) starts immediately upon lake isolation and thus terrestrial compartments are present throughout the lake stage. For the majority of biosphere objects, the end stage is a wetland that is drained by a small stream. The same fluxes are assumed to occur in the stream stage as in the lake stage, although the magnitude of some of the fluxes, like sedimentation fluxes, will change (see Chapter 6 and 11 in /Andersson 2010/).

Radionuclides released to the lower regolith compartment are distributed to the upper layers of the ecosystem by advection and diffusion. A flux of radionuclides enters the ecosystem going from the bedrock into the till (Regolith Low) and further through the sediments (Regolith_Mid) to the upper oxidizing sediment layer (Aqu_regoUp). Radionuclides are further transported to the surface water system. Representation of the waterborne transport of radionuclides between compartments is based on detailed hydrological modelling with MIKE-SHE /Bosson et al. 2010/. These studies have shown that the vertical hydrological fluxes in the deep regolith layer of sea basins and bays are small. Sorption of radionuclides will affect the advection and diffusion, i.e. affecting the transport to the water above the regolith.

Radionuclides may also be attached to particles in the water. Radionuclides dissolved in water or attached to particles in the water may be exported from the biosphere objects by water fluxes. This is considered for all stages of the aquatic objects. Sea objects interact with the entire Öregrundsgrepen via water exchange in both directions. Radionuclides from Öregrundsgrepen are then discharged to the rest of the Baltic Sea, which is treated as a sink in the model. Water fluxes from lakes are modelled as an addition to the next downstream object.

During spring, water from lakes and streams are sometimes transported to the surrounding wetland by flooding (further discussed in Chapter 3 in /Andersson 2010/). Radionuclides may, therefore, in addition to downstream export, be transported from the lake and stream object to the surrounding wetland. Fluxes of radionuclides from the mire to the lake by surface runoff will also occur.

Aquatic primary producers may incorporate radionuclides during primary production and this is a possible sink for radionuclides. It is assumed that equilibrium is established between the concentration of radionuclides in the newly produced biomass and water. However, most aquatic primary producers in Forsmark have a short life cycle compared with terrestrial producers (e.g. trees). Phytoplankton and microphytobenthos have life cycles of days to weeks and most macroalgae have a life cycle of less than a year, although there are a few perennial species (primary producers are further described in Chapter 3 in /Andersson 2010/). Therefore, a large fraction of radionuclides incorporated during primary production would be released back to the water compartment upon degradation and mineralisation of the organic matter driven by respiration. Only a small fraction of the primarily incorporated radionuclides is assumed to be retained in organic matter. Therefore, the flux of radionuclides into aquatic primary producers in the model is estimated as net primary production (i.e. primary production minus respiration). Concentrations in water are also used to calculate concentrations in other biota (e.g. fish and crayfish) utilised by humans (biota utilised by humans are further discussed in Chapters 3, 4, and 11 in /Andersson 2010/).

The model assumes that there is a flux of carbon dioxide across the air-water interface of lakes (further discussed in Chapter 5). The equilibrium of $CO_2$ between water and air is influenced by primary production (taking up $CO_2$) and respiration (releasing $CO_2$) in the aquatic objects. Carbon-14 is assumed to be exported from the lake via this gas flux, whereas the flux for other radionuclides is assumed to be insignificant.

Aquatic sediments (Aqu_Regolith_Up and Aqu_Regolith_Mid) are gradually covered by a layer of organic material, i.e. peat, during the process of growth of the wetland. This process is represented in the model by a flux of radionuclides from the aquatic sediments to the terrestrial regolith (arrows 5 in Figure 3-1). The duration of the transformation of the lake into wetland is dependent upon the lake depth and is driven by the accumulation of peat. This accumulation is based on the observed extension of vegetation in 25 lakes in the Forsmark area /Brydsten and Strömgren 2010/.

**Terrestrial environment**

The terrestrial part of the radionuclide model represents a forested wetland. A flux of radionuclides, driven by advective and diffusive transport, enters the ecosystem from bedrock into the glacial till (Regolith Low) and further through the sediments (glacial and post glacial clay) deposited during the aquatic stages. Plant uptake of radionuclides is driven by net primary production and the subsequent litter production continuously transports radionuclides from the peat and water into plants and back to the peat via a litter compartment. The major part of the litter will decompose, and thereby release radionuclides into the peat compartment (Ter Regolith Up) of the wetland for further uptake by plants or transport to the lake. Radionuclides are discriminated during decomposition, although to different degrees. The remaining non-decomposed material is regarded as recalcitrant material accumulated in the litter compartment and is not available for further transport /Löfgren 2010/. The wetland starts to develop from the lake margins and expands into the lake. Transport of radionuclides from the wetland to the lake occurs through runoff, whereas transport from the lake to the wetland occurs during flooding events (see above).

The natural end state of the biosphere objects is a fen, even though the fen would be replaced by a bog under the conditions prevailing in the Forsmark region. However, the raised bog is of less interest in the context of the safety assessment, taking into account that the radionuclides enter the ecosystem from below. The primary production in the bog is sustained by meteoric water and the

bog plane where the production occurs has restricted or non-existent connection to the groundwater table.

Carbon-14 is the only radionuclide that is assumed to be found in gas form in sufficient amounts in the terrestrial environment to be a potential risk to humans. C-14 may degas from the wetland and be incorporated into primary producers during photosynthesis. Once incorporated into biota, it is further cycled via the litter compartment and heterotrophic respiration to the atmosphere or by water fluxes to the lake environment.

**Transformation of wetlands into agricultural lands**

When the wetland has risen to a sufficiently high elevation to avoid periodic seawater intrusions, it is of potential use for agricultural purposes and can be drained. It has been assumed that human inhabitants will drain and subsequently use wetlands for production of crops and livestock fodder /Lindborg 2010, Löfgren 2010/. This is done for each simulation time point, starting from the moment when the use of the wetland for agricultural purposes is possible. The organic layers (peat and gyttja) on drained and cultivated wetlands will rapidly become oxidized and compacted, resulting in an agricultural soil /Lindborg 2010/, which in the model, is a mixture of contaminated organic matter and deeper mineral layers (postglacial and glacial deposits), where radionuclides may have accumulated since the early sea stage.

Once the wetlands have been drained, further contamination through groundwater is assumed to be of no quantitative importance. Instead, radionuclides can enter the agricultural land via irrigation with surface water and are leached from the soil through runoff. Accordingly, the highest concentrations of radionuclides in agricultural soil are expected in the period directly after drainage, and thus the 50 years immediately following drainage is used to assess the average exposure during a human life time from the use of contaminated agricultural soil.

### *Releases to drilled wells*

In addition to the radionuclides released into deeper parts of the regolith of a biosphere object, a unit release rate was also applied to a hypothetical well drilled through bedrock. The activity concentration in well water (Bq/m$^3$) has been calculated by dividing the release rate (Bq/y) by the well capacity (m$^3$/y). The value of the well capacity was taken from statistics of the capacity of wells existing in the area near the proposed repository location at Forsmark, where a drilled well that might receive 100% of the releases would be located. Drilled wells located farther away from the repository may have lower well capacity, but because of increased distance, they will also have a lower probability of receiving 100% of the releases. When a biosphere object has risen above the sea, these activity concentrations, together with the concentrations in surface water, have been used to estimate doses from drinking water by humans and for calculation of radionuclide concentration in meat and milk from cattle consuming this water. Sustainable irrigation of agricultural lands from a drilled well is considered unlikely at the site /Löfgren 2010/ and therefore it was not considered in the derivation of *LDFs*. The possible effect on the *LDFs* of irrigation with well water was studied as part of the uncertainty analyses presented in Chapter 5.

### *Spatial distribution of radionuclides in the landscape*

Deep groundwater from the repository is primarily attracted to low points in the landscape, e.g. shallow parts of the sea, along the shoreline, and in lakes, streams and wetlands. The outer boundary of each biosphere object was determined from the hypsography of the sea basin during the submerged phase, whereas the shoreline of the lake at time of isolation from the sea delineates the biosphere object during the lake and terrestrial phases. Key geometrical characteristics of the objects have been determined from the local (i.e. sea or lake basin) topography, whereas the regional geometry defined landscape characteristics, like hydrological links between biosphere objects and sizes of catchment areas. In total ten biosphere objects have been identified, containing a discharge area during any period of the present interglacial. Five additional biosphere objects located downstream of the discharge areas have also been identified. Finally, to represent discharge directly into a stream or a wetland without an initial lake stage, the basin of one of the original biosphere objects has been partitioned into three separate biosphere objects (objects 121-01, 121-02 and 121-03 in Figure 3-2).

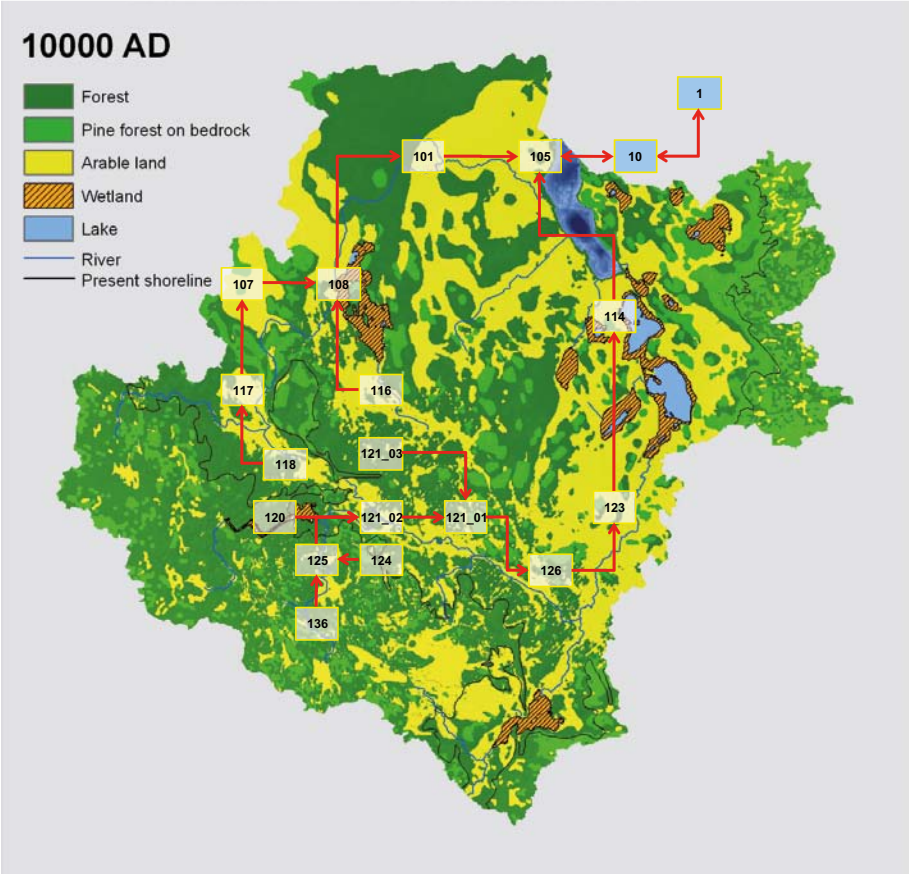


***Figure 3-2.*** *Illustration of the landscape model at 10,000 AD. The boxes shows biosphere objects (with id numbers) at their approximate locations in the landscape and red arrows indicate the surface water flow paths connecting the objects. The blue boxes represent the combined objects of Öregrundsgrepen (object 10) and the model area outlet, the Baltic Sea (object 1). Figure taken from /Lindborg 2010/.*

The Radionuclide Model for the biosphere is implemented for each biosphere object included in the landscape model. These models are then connected with each other to account for radionuclide fluxes between biosphere objects, driven by fluxes of surface waters and suspended particles. In the transitional, lake and terrestrial stages, the radionuclide fluxes from a biosphere object are directed to the connected downstream objects. Hence, all downstream objects will receive inputs from one or several upstream objects. In the Sea Stage, all objects interact only with the outer coastal area (Öregrundsgrepen) via water exchange in both directions. From Öregrundsgrepen, radionuclides are finally discharged to the Baltic Sea), which is treated as a sink in the model.

The simulations for derivation of *LDFs* (see Section 3.5) were carried out for each separate biosphere object and the maximum *LDF*, across all biosphere objects, was selected for use in the SR-Site assessments. The landscape model (Figure 3-2) was used in supporting simulations, reported in Chapter 5, to show that derivation of *LDFs* from simulations of separate biosphere objects does not lead to their underestimations.

### 3.1.2 The mathematical model

The mathematical model for each biosphere object consists of a System of Ordinary Differential Equations (ODEs). Each of the ODEs represents the rate of change of the radionuclide inventory (Bq) in a model compartment, as a function of the radionuclide fluxes (Bq/y) from and to the compartment, and of the radioactive decay and in-growth of progeny.

The model assumes that the radionuclide fluxes are proportional to the radionuclide inventory in the compartment, multiplied by a transfer rate coefficient (1/y). Radionuclide-specific behaviour is taken into account by using element-specific values for some of the model parameters, that describe retention (distribution coefficients or $K_d$ values) and biological uptake (concentration ratios or CR).

The radionuclide fluxes have been modelled in the same way for all radionuclides, except for C-14. In the case of C-14 the uptake by biota is modelled using a specific activity approach /Avila and Pröhl 2008/. Gas exchange between the peat and surface water on the one hand and the atmosphere on the other hand has been considered only for C-14. The effect on the *LDFs* of neglecting these processes for other radionuclides is discussed in Chapter 5.

The Radionuclide Model has the same mathematical formulation for all biosphere objects. The differences between biosphere objects have been captured by using object-specific values for parameters describing the geometry of the biosphere objects, the depths of regolith layers, and the rate and timing of transitions between sea, lake and terrestrial stages (see Section 3.3).

The ordinary differential equation for each model compartment (*k*) may includes inflows from outside the system, outflows from the system and transfer of radionuclides from and to other connected compartments (*i*), decay and in-growth of the radionuclide. The ODE of a compartment (*k*) has the following general form:

$$\frac{dA^j_k}{dt} = F^j_{out\ to\ k} - F^j_{k\ to\ out} + \sum_i F^j_{i\ to\ k} - \sum_i F^j_{k\ to\ i} - \lambda^j \cdot A^j_k + ingowth^j$$

$$F^j_{k\ to\ out} = TC^j_{k\ to\ out} \cdot A^j_k$$

$$F^j_{i\ to\ k} = TC^j_{i\ to\ k} \cdot A^j_i$$

$$F^j_{k\ to\ i} = TC^j_{k\ to\ i} \cdot A^j_k$$

where:

$A^j_k$ is in inventory of the *j-th* radionuclide in compartment k (Bq).

$\lambda^j$ is the decay constant for the *j-th* radionuclide (year$^{-1}$).

Ingrowth $^j$ is the in-growth of the *j-th* radionuclide from decay of the parents (Bq·year$^{-1}$).

$F^j_{out\ to\ k}$ is the inflow of the *j-th* radionuclide from outside the system to *k-th* compartment (Bq·year$^{-1}$).

$F_{k\ to\ out}$ is the outflow of the *j-th* radionuclide from *k-th* compartment out from the system (Bq·year$^{-1}$).

$F^j_{i\ to\ k}$ is the flux of the *j-th* radionuclide from *i-th* to *k-th* compartment (Bq·year$^{-1}$).

$F^j_{k\ to\ i}$ is the flux of the *j-th* radionuclide from *k-th* to *i-th* compartment (Bq·year$^{-1}$).

$TC^j_{k\ to\ out}$ is the transfer rate coefficient of the *j-th* radionuclide from *k-th* compartment out from the system (year$^{-1}$).

$TC^j_{k\ to\ i}$ is the transfer rate coefficient of the *j-th* radionuclide from *k-th* to *i-th* compartment compartment (year$^{-1}$).

$TC^j_{i\ to\ k}$ is the transfer rate coefficient rate of the *j-th* radionuclide from *i-th* to *k-th* compartment (year$^{-1}$).

The transfer rate coefficients, TC, represent the fraction of the inventory in one compartment that is transferred either to other compartments or out from the biosphere object. In the model they can be either constant or vary in time, depending on which process they described and which parameters are used in their mathematical formulation. The mathematical equations used for the different transfer rate coefficients are presented in Appendix A.

### 3.1.3 Calculation of activity concentrations in the environment

The Radionuclide Model dynamically models the radionuclide inventory in 10 compartments of the biosphere object. From these inventories, the activity concentrations in peat, agricultural soil, atmosphere, surface water, aquatic sediments and primary producers are calculated. The calculated environmental concentrations are used in assessments of doses to non-human biota /Torudd 2010/ and in calculations of doses to humans (see Section 3.2). The different concentrations are calculated as follows:

- Activity concentrations in *peat* (Bq/kg dw) are calculated by dividing the radionuclide inventory (Bq) in the upper terrestrial regolith compartment by the mass of this compartment (product of the peat density and volume).
- The activity concentrations in *aquatic sediments* (Bq/kg dw) are calculated by dividing the combined radionuclide inventories (Bq) in the upper and the middle aquatic regolith compartments by the summed mass of these compartments (where each mass is the product of the sediment density, the area and the depth).
- The activity concentrations in *surface waters* (Bq/$m^3$) are calculated by dividing the inventory in the water compartment (Bq) by its volume ($m^3$).
- The activity concentrations in *atmospheric air* (Bq/$m^3$) of all radionuclides, except for C-14, are calculated by multiplying the activity concentrations in peat and soil (Bq/kg dw) by the dust concentrations (kg dw/$m^3$) in air. For C-14 these concentrations are calculated by dividing the inventory (Bq) in the atmospheric air compartment by the volume ($m^3$) of this compartment.
- The activity concentration (Bq/kg dw) in soil is obtained by dividing the average radionuclide inventory (Bq) by the soil mass (kg dw), which is the product of agricultural soil density (kg dw/$m^3$), the area ($m^2$) and ploughing depth (m). The initial inventory in *agricultural soil* (Bq) is calculated by summing the radionuclide inventories in the upper terrestrial regolith compartment and in the top 25 cm (the ploughing depth) of the middle terrestrial compartment, assuming a uniform distribution through the depth of this compartment. The average inventory in the agricultural soil during a period of 50 years is then calculated assuming leaching due to runoff and, for vegetables, additional input via irrigation of vegetables with contaminated surface water.
- The activity concentrations in *terrestrial primary producers* (Bq/kg C) are calculated by dividing the inventory (Bq) of the compartment Ter_Primary Producers by the total biomass (kgC).

#### *Concentrations in food*

Biological uptake in organisms that are consumed by humans is not modelled dynamically (with exception of the concentration in terrestrial primary producers). Instead the activity concentrations in human food (Bq/kg C) are calculated from concentrations in environmental media (peat or soil and surface water), assuming an equilibrium between the concentrations in food and in the corresponding environmental media.

For aquatic foods (fish and crayfish), the activity concentrations are calculated by multiplying the activity concentration in water by a specific Concentration Ratio (Bq/kg C per Bq/$m^3$) for each food type. The concentrations in fish and crayfish are calculated for both freshwater and marine ecosystems, whereas the concentrations in mussels are only calculated for marine ecosystems.

For terrestrial food types, activity concentrations are calculated by multiplying the activity concentration in peat (for berries and mushrooms) and agricultural soil (for cereals, vegetables and root crops ) by the corresponding Concentration Ratio (Bq/kg C per Bq/kg dw) /Nordén et al. 2010/. In absence of CRs for calculation of concentrations in edible berries, these were set to be the same as the concentrations in terrestrial primary producers.

The activity concentrations in herbivores are calculated by assuming equilibrium between food consumed by the herbivore and the tissues of the herbivore. Since the herbivore diet consists of both green plants and mushrooms, the activity concentration in herbivore diet is calculated by summing the contributions from both sources and then dividing by the total mass consumed. The fractions of the diet taken to be green parts and mushrooms were estimated from statistics for similar sites /Nordén et al. 2010/.

To determine the activity concentration in meat from game or cattle and in dairy products, the concentrations in the animal diet (wetland vegetation or green fodder) are first calculated by multiplying activity concentrations in peat or soil by the corresponding Concentration Ratios (Bq/kg C per Bq/kg dw). Activity concentrations in meat and milk are then calculated from the concentrations in animal diet and animal consumption rates, using simple equilibrium models /Nordén et al. 2010/. Radionuclide intakes from contaminated water and ingestion of soil are also included in these calculations.

## 3.2 Exposure assessment

The activity concentrations in different environmental media are used to calculate doses to humans. For these calculations, it is assumed that the representative individual of the most exposed group spends all time in the contaminated biosphere object, and gets his/her full supply of food and water from this biosphere object.

The dose assessments performed in SR-Site are estimates of potential exposures, averaged over the lifetime, of individuals that may make use of the Forsmark area in the far future. Humans can be exposed both externally and internally to radionuclides in the environment. Based on earlier assessments, e.g. /Bergström et al. 1999, Avila and Bergström 2006/, it is concluded that the major long-term risk for human exposure to radionuclides from a repository is from internal exposure. The internal exposure is always preceded by incorporation of radionuclides into the human body. This can occur mainly by ingestion of contaminated water and food or inhalation of contaminated air. For most radionuclides the intake is dominated by food ingestion and/or water ingestion.

The internal exposure will, among other things, depend on the fraction of contaminated food and water consumed and the activity concentrations in the food and water. In this assessment, it is assumed that the annual demand of water and food is contaminated, but other situations can easily be addressed by introducing corrections to account for the fraction of consumed water and food that is not contaminated. The dietary composition can also have an impact on internal exposure, as different foods can have different contamination levels. However, for long-term assessments it is difficult to postulate a particular dietary composition, as human habits and choices may change.

Exposure via inhalation of contaminated air can occur both outdoors and indoors. However, usually exposure indoors will be lower than outdoors due to the filtering effects of buildings (see Chapter 5). In SR-Site, only outdoor exposure was considered, which gives a conservative estimate. Other pathways for radionuclide penetration into the human body, for example through the skin, are irrelevant in the context of this safety assessment.

The external exposure comes from radiation emitted by the radionuclides in surrounding environmental media; air, water and soils. Previous safety assessments of planned geologic repositories in Sweden and Finland /Bergström et al. 1999, Karlsson and Bergström 2000/ have shown that for dose-contributing radionuclides external exposure gives only a minor contribution to the total dose.

### 3.2.1 Exposure from external irradiation and inhalation

Dose rates via inhalation (Sv/y) are calculated by multiplying the activity concentration in air (Bq/m$^3$) by the inhalation rate (m$^3$/h), the exposure time (h/y) and the Dose Coefficient for inhalation (Sv/Bq). Dose rates from external irradiation (Sv/y) are calculated by multiplying volumetric concentrations in peat and agricultural soil (Bq/m$^3$) by the exposure time (h/y) and the Dose Coefficient for external exposure (Sv/h per Bq/m$^3$).

In the calculation of exposure via inhalation and external irradiation it has been assumed that the human inhabitants are exposed outdoors 24 hours per day.

### 3.2.2 Exposure from water consumption

Dose rates due to water consumption (Sv/y) are calculated by multiplying the activity concentration in drinking water (Bq/m$^3$) by the water ingestion rate (m$^3$/y) and the Dose Coefficient for ingestion (Sv/Bq).

The need of drinking water of future human inhabitants living in a biosphere object is assumed to be satisfied by equal contributions from a well drilled into the rock and from the surface water in the lake or stream passing through the object. This also covers the case of drinking water from a shallow well dug into the till, since lake and stream water is likely to intrude into a well that is in contact with contaminated sediments beneath the wetland.

Exposure from contaminated drinking water is considered from the point in time when a biosphere object has emerged from the sea. Livestock are assumed to consume water from the same sources as human inhabitants, i.e. equal water contributions from surface water and a drilled well.

### 3.2.3 Exposure from food consumption

Doses due to food ingestion (Sv/y) are calculated for each food type by multiplying the activity concentration in food (Bq/kg C) with the food ingestion rate (kg C/y), and the Dose Coefficient for ingestion (Sv/Bq). No assumptions have been made regarding food preferences of future individuals. Instead, in the calculation of food ingestion doses it is assumed that the human diet reflects the production capacity of different foods in the biosphere objects.

Further, it is assumed that future human inhabitants will be self-sustaining and will utilize all available food sources in proportion to their production. The production capacity of human food in a biosphere object is directly determined by the size of the contaminated object, (i.e. the size of the sea basin or the size of the wetland and the surface water), and the sustainable yield of natural food stuffs and agricultural products, which in turn may vary with climatic conditions. Assuming that food production is the limiting factor for humans living in the biosphere object, the number of individuals that can be sustained in a biosphere object is thus proportional to the area of the object. However, the size of the population that can be sustained also depends on land use, since the productivity per unit area of crop is two to three orders of magnitude larger than the productivity of natural food stuffs in a wetland.

All types of food sources from both aquatic and terrestrial parts of a biosphere object are considered in the dose calculations. It is assumed that wetlands will at least partly be converted to agricultural land when this is possible. Thus, when the object is submerged the human diet consists of sea food. When the object has been isolated from the sea, the diet consists of natural food stuffs from the lake/stream and from the wetland. When agriculture is possible, the diet will be a combination of natural food stuffs and agricultural produce. The contribution of each food type to the human diet is assumed to be proportional to the production of that food type in the object. When agriculture is possible, it is deemed equally likely that the wetland is used for production of natural food stuffs, cereals, root crops, vegetables or fodder for beef and dairy production.

The result is that biosphere objects with a large area that can be drained and cultivated can typically feed a population in the range of 170–1,300 persons (first and third quartiles, respectively). In contrast, biosphere objects that cannot be cultivated can only support a limited number of individuals, i.e. approximately 10 individuals during submerged or coastal conditions and typically one or a few individuals when inhabitants are limited to forage the lake and wetlands for natural food stuffs. It is important to note that the assumption of self-sustained future inhabitants of the area does not imply that this is a “stone-age”-like culture. It only sets the constraint that the population is obtaining all its food locally from available resources.

## 3.3 Input parameters

The Radionuclide Model for the biosphere uses approximately 140 input parameters, of which one third represent radionuclide- or element-specific properties. Parameters describe the development of the individual biosphere objects, characteristics of the ecosystems where radionuclides are likely to accumulate, and flows within and between biosphere objects. There are also parameters describing the exposed individuals and dose coefficients for external exposure, inhalation, and ingestion of food and drinking water.

For each parameter, a Best Estimate was derived from site and/or literature data, and the uncertainty of parameter values was described by a probability density function (PDF) (see Section 3.4.2 below).

The Best Estimates were used in the deterministic simulations for derivation of *LDFs* and *LDF pulse* (see Section 3.5). The PDFs were used to assess the impact of parameter uncertainty on *LDF* estimates (see Section 5.3).

The parameters have been grouped according to the context of their use in the model and examples of the underlying data sources are given. In the last part of this section the principles used to select Best Estimate values representing the site, and to determine PDFs representing natural variation and measurement uncertainties are described. All parameters are listed with a short description in Appendix B. References to reports where details on parameter values and the methods used to derive them are also given in Appendix B.

### 3.3.1 Overview of model parameters

#### *Geometries and regolith properties*

The development of the landscape causes changes in the dimensions of discharge areas and determines the succession of ecosystems in the objects (Section 3.2.2). The temporal development of the geometric extension of catchment areas, biosphere objects and compartments within objects, were calculated with a *coupled regolith-lake development model* (RLDM) of Forsmark area /Brydsten and Strömgren 2010/. The outputs from this model included areas of the aquatic and terrestrial compartments, average and maximum depths of the aquatic compartments, and areas of watersheds and sub-catchments. The model also predicted time points for ecosystem transitions, such as the start and completion of lake isolation, the completion of wetland in-growth, and the point in time when the wetland elevation above sea level allows sustainable cultivation.

Five of the compartments in the Radionuclide Model for the biosphere represent regolith layers (Figure 3-1, Figure 3-3).The properties of these compartments (density, porosity and depth) were determined from the site investigation and site descriptive models /Lindborg 2008/. In addition, the depth development of post glacial sediment layers (regoMid and regoUp) was described with the RLDM model.

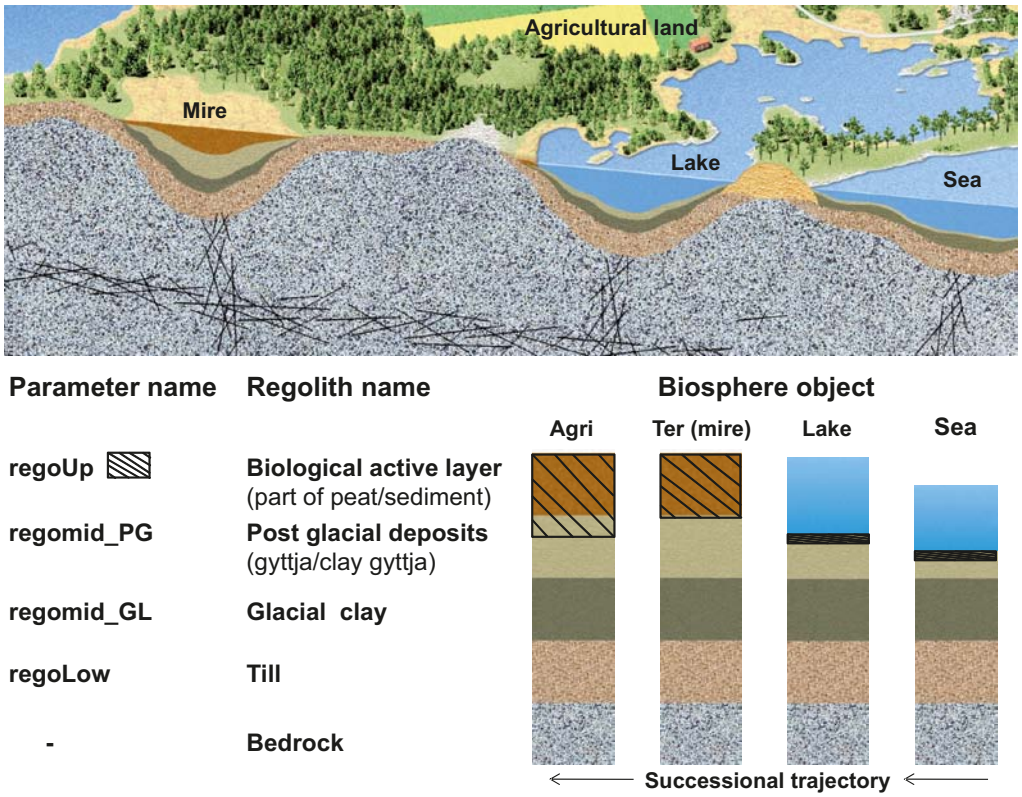


***Figure 3-3.*** *The conceptual model of regolith distributions for different types of biosphere objects. The landscape pictures represent a succession trajectory from sea to a wetland, which is later converted to agricultural land by drainage.*

### *Water exchange and surface hydrology*

In the Radionuclide Model for the biosphere water born transport of radionuclides is assumed to be proportional to the advective water fluxes or to diffusive fluxes, which could be important when surface water fluxes are very low. Horizontal water fluxes during the sea stage were calculated from water residence time in different sea basins. A hydrodynamic model, which used the atmosphere, the surrounding sea and land runoff as external forcing factors was used to predict the water residence time in sea basins as a function of time /Karlsson et al. 2010/.

Parameters describing vertical hydrological fluxes, and horizontal fluxes between the lake and the wetland, were derived from detailed hydrological modelling with MIKE SHE /Bosson et al. 2010/. Water balances obtained for a selection of lake-mire systems obtained from MIKE SHE were translated into the parameter required by the Radionuclide Model for the biosphere to describe vertical water fluxes. A description of how these parameters were derived can be found in /Löfgren 2010/.

Another hydrological parameter required in the Radionuclide Model for the biosphere is the well capacity (yield), used in the model for calculation of radionuclide concentrations in well water. This parameter was derived from data obtained for the Forsmark area as described in /Löfgren 2010/.

### *Distribution and diffusivity coefficients*

The retention of the radionuclides in regolith and on suspended material was calculated with element-specific distribution coefficients ($K_d$). The $K_d$ describes the ratio of equilibrium concentrations in the solid and liquid phase of a model compartment, and parameter values were determined from a combination of site and literature data /Nordén et al. 2010/. Diffusive transport between compartments was calculated with element-specific diffusivity coefficients derived from literature data /Nordén et al. 2010/.

### *Aquatic ecosystems*

Aquatic ecosystems include marine, lake and stream stages of the biosphere objects. Lakes and marine basins were parameterised with site data, i.e. with data from brackish marine basins and oligotrophic hard water lakes at Forsmark today. The range of parameter values were selected to cover changes that may be induced due to altered salinity in the marine basins, and altered nutrient conditions in the oligotrophic lakes /Andersson 2010, Aquilonius 2010/.

Parameters representing sedimentation and resuspension processes in aquatic ecosystems were calculated using the RLDM model. The concentrations of particles in water were assumed to be approximately constant, and were determined from site measurements in sea basins and lakes, respectively.

Biological uptake was calculated from biomass production, assuming that radionuclide uptake is proportional to water concentrations. The parameter values for biomass and productivity were determined from site data, (as a function of the changing water depth predicted by the RLDM). The element-specific proportionality constants (CRs) were determined from a combination of site and literature data /Nordén et al. 2010/. Litter production was assumed to equal biomass production.

The sustainable production of natural food in aquatic ecosystems was determined from site data (fish) and literature (crayfish). Minimum water depths required for production of edible fish and crayfish were determined from literature data.

### *Terrestrial ecosystems*

Terrestrial ecosystems include wetlands and agricultural land. Wetlands were parameterised with data representing forested wetlands at the investigated sites, and parameters for agricultural land were selected to represent present agricultural practice in the region /Löfgren 2010/.

Wetland in-growth was described by a time-dependent parameter from the coupled lake regolith development model. Uptake of radionuclides by wetland vegetation was calculated from biomass production, assuming an uptake proportional to soil (or atmosphere) concentrations. The parameter values for biomass and productivity were determined from site data. The element-specific proportionality constants (CRs) were determined from a combination of site and literature data /Nordén et al. 2010/. Litter production was assumed to equal biomass production. Parameters describing long-term decomposition rate and enrichment of radionuclides in litter were determined from site data.

The sustainable yield of natural food (fungi, berries and game) from the terrestrial ecosystem was determined from site data and literature. The production of crop (cereals, vegetables and root crop), meat and dairy products were determined primarily from regional data, where as other characteristic of the agricultural ecosystem (including e.g. CRs, dust concentrations and irrigation parameters) were based on literature data /Nordén et al. 2010/.

#### *Exchange with the atmosphere*

The main entry point of C-14 into the terrestrial food chain is fixation of carbon from air by primary producers. Therefore, the atmosphere was included as a compartment in the radionuclide model for assessment of C-14. Parameters used to describe gas-exchange between surface waters and the atmosphere were determined from site data and site modelling /Andersson 2010, Aquilonius 2010/. Parameters used to calculate the gas flux from peat and decomposing litter in the wetland, were determined primarily from literature data.

C-14 is exported from the atmosphere by wind exchange. Parameters for wind velocities and height of the mixing layer were derived from site data, whereas the values for the zero displacement height were taken from literature /Nordén et al. 2010/.

#### *Parameters used to assess exposure to humans*

Parameter values that describe habits and characteristics of the exposed individual were primarily collected from the literature. These parameters include the amount of food and water consumed, inhalation rate, and time spent in the contaminated area, as well as dose coefficients for external exposure, inhalation, and ingestion of water and food. In line with international recommendations /ICRP 2006/, fixed, slightly conservative values were chosen for these parameters.

The dose coefficients for exposure take radiation sensitivities of different tissues and organs into account, as well as retention of radionuclides in the human body and exposure from daughter radionuclides (i.e. exposure represents the committed effective dose). As recommended by the ICRP /ICRP 1998/ only dose coefficients for adults were used.

### 3.3.2 Principles for selecting Best Estimate values and Probability Distribution Functions

The extensive site investigations performed by SKB at Forsmark have resulted in a detailed description of the site and its development. Data from this description have been the primary source for parameter values of the radionuclide model.

In the Radionuclide Model for the biosphere, compartments are assumed to be internally homogeneous (Section 3.1), and a temporal resolution of years was considered to be sufficient for assessing life-time dose from long-term releases. Thus, parameters were selected to give a yearly mean representing a compartment on the scale of a sea or lake basins (Section 7 in /Lindborg 2010/ gives a detailed description of the biosphere objects included in the assessment).

Parameter uncertainty refers to the sum of natural variation, (comprising variation due to real and identifiable heterogeneity in nature) and measurement uncertainties (i.e. errors in measurement or limitations in the assessment). Thus PDFs derived from site data reflect the random variation of the typical value between years, or if such data was not available, the random variation between compartments in similar biosphere objects within the study area.

PDFs for parameters were judged to be either log-normal or normal. For a lognormal distribution, the geometric mean and standard deviation were used to describe the best estimate and the variation around the mean whereas the arithmetic mean and standard deviation were used for parameters with a normal distribution. For each parameter, maximum and minimum values were also identified to set limits on the possible range of the parameter value. The possible range includes expected natural variation that is not observed at the site presently, but may historically have existed at the site or is expected in the future under similar climate conditions (e.g. presence/characteristics of species/ communities that are likely to develop on the site, but are not presently observed).

When data were insufficient to estimate a parameter distribution, (e.g. for properties of future site conditions estimated from literature data), the parameter was represented with a uniform distribution. For these parameters, the best estimate corresponded to the arithmetic mean of the min and max values.

In the radionuclide model, distribution coefficients ($K_d$) and concentration ratios (CR) are used to describe radionuclide retention and biological uptake. The Best Estimate value and PDFs for these parameters were calculated from a combination of site and literature data, using Bayesian inference methods /Nordén et al. 2010/. Literature data were primarily retrieved through the EMRAS and ERICA databases /IAEA 2010, Beresford et al. 2007/. When data were missing in these databases, parameter values compiled for previous SKB safety assessments were used /Karlsson and Bergström 2002/. For a few elements, appropriate data were not available from the site or from the open literature. In these cases, data for other biota types or analogue elements were used to derive best estimates and PDFs for model parameters.

## 3.4 Software implementation

The Radonuclide model was implemented in the software package Pandora /Åstrand et al. 2005, Ekström 2011/. Pandora is an extension of the codes Matlab and Simulink (www: The Mathworks Inc). The tool is described in detail in /Ekström 2011/. Below is a brief description of the development, functionality and features of the Pandora tool.

Pandora was developed by Facilia AB for the specific needs of the biosphere modeling, and it has been used by SKB and Posiva OY for the safety assessments of high level waste repositories. Pandora support solution of the systems of ODEs, using numerical methods that are appropriate for solving stiff and non-stiff problems, and has all required functionalities for the biosphere assessments, including: handling of large sets of parameters, handling of time evolving parameters, representation of discrete transitions between states, handling of large number of radionuclides and decay chains, and performing probabilistic simulations using the assessment tool Pandas.

Pandora also simplifies the development of compartment models consisting of large systems of ordinary differential equations and the handling of radionuclide decay chains. The tool comprises a library of Simulink blocks that facilitates the creation of compartment models, a Manager that aids the model building, and a standalone assessment tool called Pandas.

Pandora extends the Simulink graphical user interface to allow the user to easily inspect and modify the conceptual and mathematical models implemented. Since Pandora is integrated with the assessment tool Pandas, it facilitates the performing of sensitivity and uncertainty analyses of the implemented models.

Pandora has been benchmarked, tested and compared with other similar tools /Åstrand et al. 2005, Ekström 2011/. The solutions with the predecessor of Pandora (Tensit) were compared with analytical results, as well as with numerical results obtained with other simulation tools /Jones et al. 2004, 2005/. These comparisons have shown that Pandora provides reliable solutions.

## 3.5 Simulations for derivation of LDF values

The *LDF* and *LDF pulse* values were calculated by performing separate simulations for each biosphere object using the Radionuclide Model for the biosphere. In the simulations for derivation of *LDFs* a unit constant release rate was directed to each biosphere object during the whole simulation period. Indirect contamination by surface water from upstream objects was disregarded. That this simplification is appropriate for the derivation of *LDF* values representing the maximum doses across all biosphere objects, was demonstrated with alternative simulations where a constant unit release rate (1 Bq/y) was applied to each biosphere object (one at a time) and the contamination by surface water in all downstream objects was considered. The results from these alternative simulations are presented in Chapter 5 dedicated to uncertainty analyses. For the derivation of *LDF pulse* values a unit pulse release (1 Bq) of each radionuclide was directed during a short time period to the biosphere object that gave the maximum *LDF*.

### 3.5.1 Simulations for deriving LDFs for long term releases

For each radionuclide, the maximum *LDFs* were derived by first finding the maximum annual dose over time per unit release rate or unit release to a representative individual of the most exposed group in each biosphere object, and thereafter finding the maximum *LDF* across all biosphere objects. This procedure was repeated for all climatic conditions considered (see Section 2.3), using an appropriate simulation period.

The first step in the derivation of *LDF* values was to run the Radionuclide Model for each separate biosphere object and obtain time series of radionuclide amounts (Bq per Bq/y) in each model compartment. In the simulations for radionuclides that decay into radioactive isotopes (see Table 2.1), daughter radionuclides were also included. The time series of radionuclide amounts in different compartments reflect the retention and accumulation of radionuclides in each biosphere object. Figure 3-4 shows a time series of the maximum inventory, across all biosphere objects, of Ra-226 and I-129 in all model compartments and in compartments above the lower regolith. Similar time dynamics of the inventories are observed for other radionuclides. A large part of the amount of a radionuclide retained in a biosphere object is found in the lower regolith compartment, though the fraction of the inventory found in the lower regolith compartment varied between radionuclides. The main variables affecting the retained fraction are the $K_d$ values and half-life of the radionuclides. Hence, it is important that transport and retention processes in the lower regolith compartment are addressed properly in the model. A discussion on this issue is presented in Chapter 5.

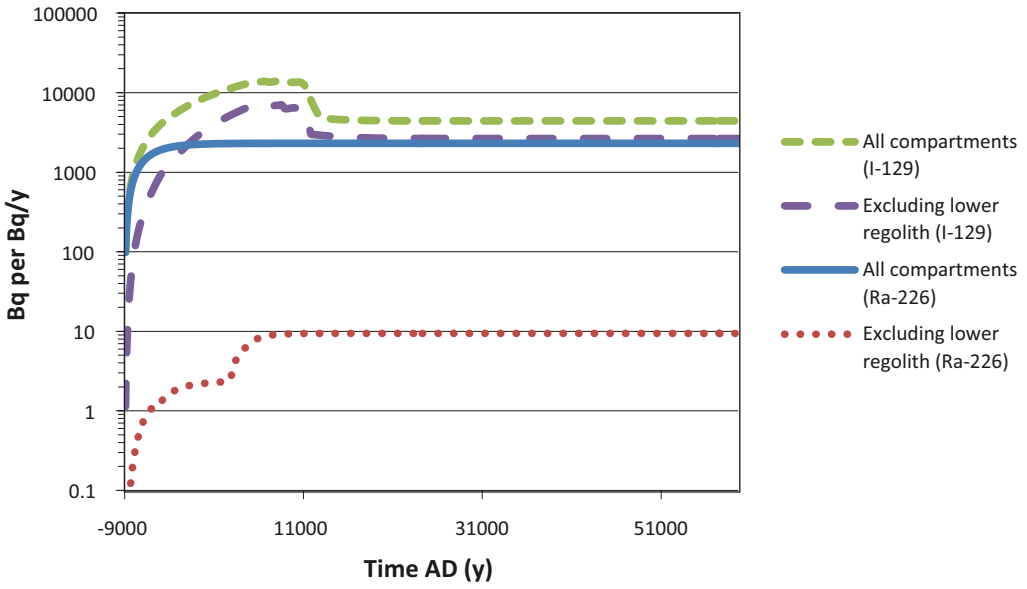


***Figure 3-4.*** *Ra-226 and I-129 inventories in all model compartments including and excluding the lower regolith compartment. Maximum values across all biosphere objects are shown. The values were obtained from deterministic simulations with a constant unit release rate during the interglacial period.*

The second step was to obtain time series of activity concentrations per unit release rate (Bq/kg DW per Bq/y or Bq/m$^3$ per Bq/y) of each radionuclide in different environmental media (water, sediments, air and soil) using the methods explained in Section 3.1.3. The activity concentrations in environmental media were used to calculate concentrations in different types of food consumed by humans (Bq/kgC per Bq/y). Examples of time series of Ra-226 and I-129 activity concentrations in the environmental media and in human food are shown in Figure 3-5, 3-6 and 3-7. In general large differences in concentrations were observed between radionuclides. For example, there is a difference of two orders of magnitude between the I-129 and Ra-226 concentrations in surface water (Figure 3-5). This difference can be explained by the differences in steady-state output of these radionuclides from lower regolith compartment, the difference may have been enhanced by further losses of Ra226 due to radioactive decay, as it passes the terrestrial compartments before reaching the water.

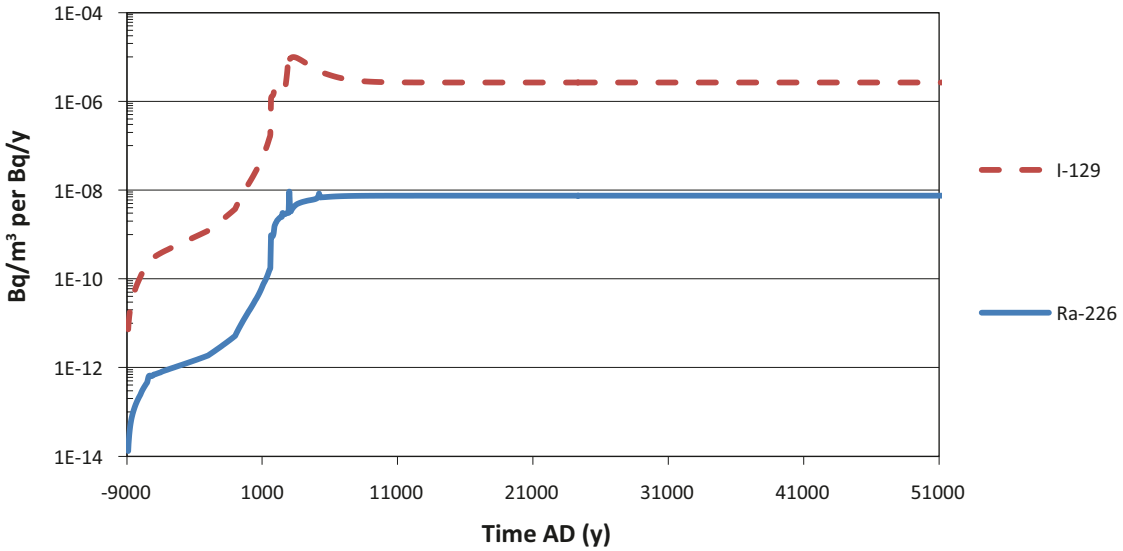


***Figure 3-5.*** *Activity concentrations of Ra-226 and I-129 in surface waters. Maximum values across all biosphere objects are shown. The values were obtained from deterministic simulations with a constant unit release rate during the interglacial period.*

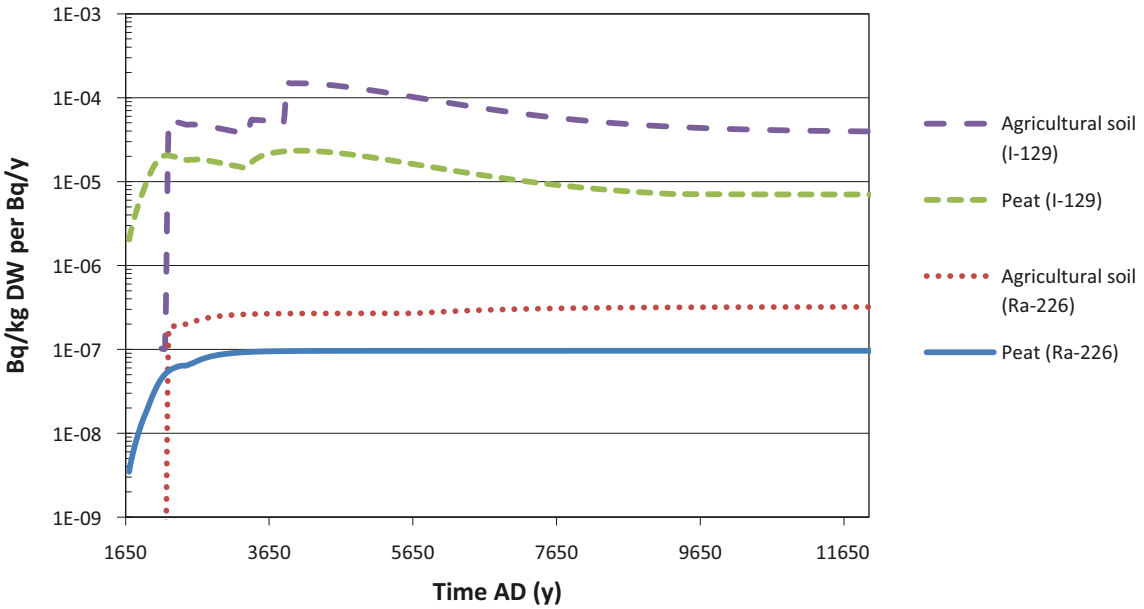


***Figure 3-6.*** *Activity concentrations of Ra-226 and I-129 in the upper layer of the mire and in agricultural soil. Maximum values across all biosphere objects are shown. The values were obtained from deterministic simulations with a constant unit release rate during the interglacial period.*

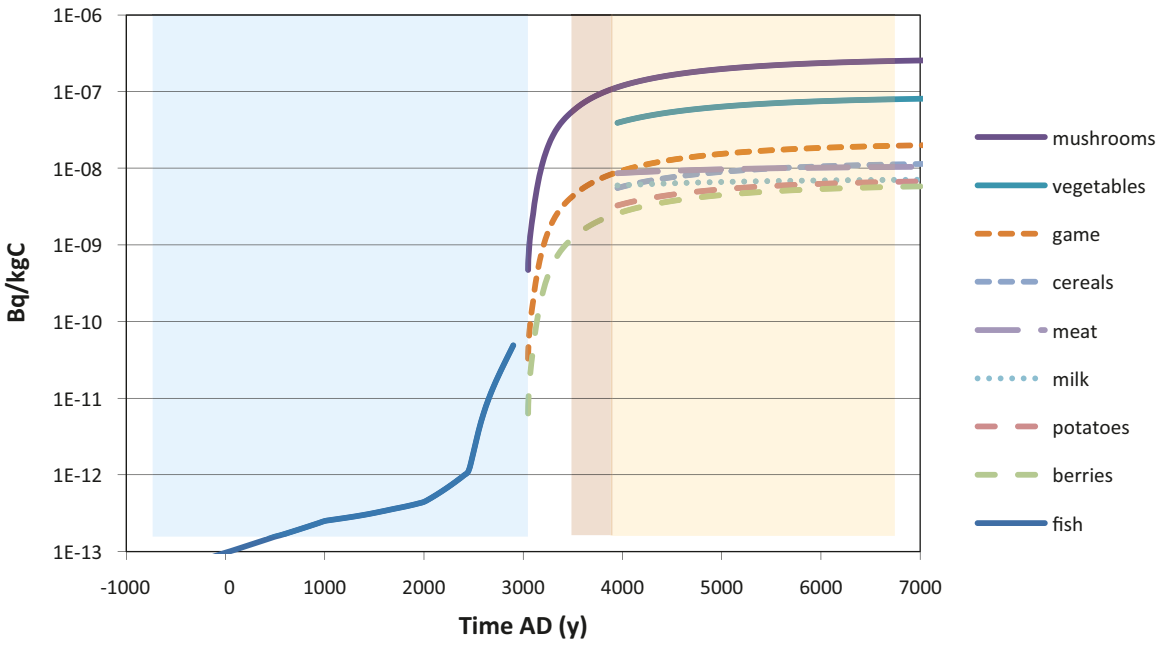


***Figure 3-7.*** *Activity concentrations of Ra-226 in different food resources in biosphere object 121_03 during an interglacial period. This specific object does not have a lake stage, but it transforms directly into a wetland and therefore concentrations in aquatic products are not shown for this stage. Although values of activity concentrations in crayfish and mussels are shown for the Sea stage, these food products do not contributed to the doses, as their productivity in the sea period is insignificant*

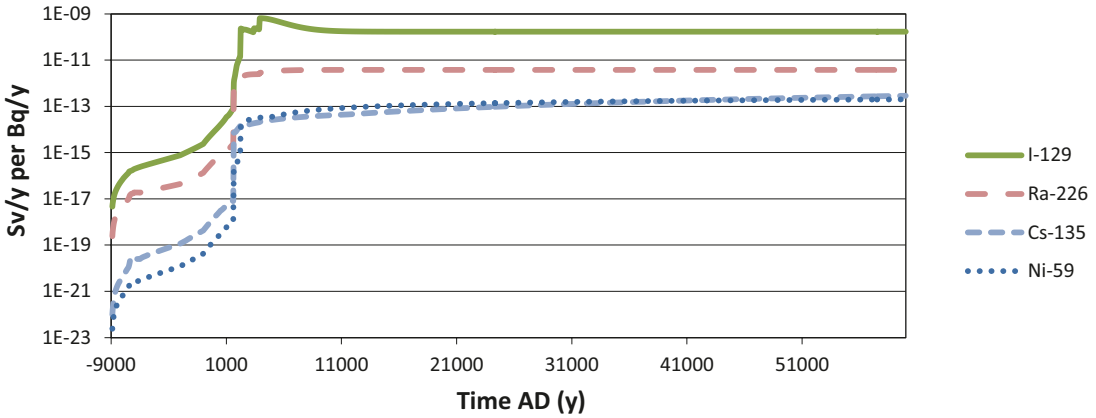


***Figure 3-8.*** *Time series of LDF values for a selection of radionuclides. Maximum values across all biosphere objects are shown.*

### 3.5.2 Simulations for derivation of LDFs for pulse releases

The same model and overall approach for derivation of *LDF* values, as presented above, was applied for derivation of *LDF pulse* values. However, since pulse releases by definition will take place during a short time period, the derivation of *LDF pulse* values was done by performing simulations with a pulse release of 1 Bq to the biosphere object. For each radionuclide these simulations were done for the biosphere object with the highest *LDF*. The duration of the pulse release was set to 1 year and the timing of the pulse that gave the maximum *LDF pulse* was selected (see Chapter 5).

# 4 Values of the Dose Conversion Factors, LDF and LDF pulse

This chapter presents values of the Dose Conversion Factors that are used in assessments of doses resulting from long-term constant releases to the biosphere (*LDF*) and for assessment of doses resulting from pulse releases (*LDF pulse*). The definition of these *LDFs* can be found in Section 2.3. The overall approach for derivation of the *LDF* values used in SR-Site can be found in Section 2.4. The models and methods used for derivation of *LDF* values are described in Chapter 3.

## 4.1 LDF values for long-term releases

The *LDFs* used in SR-Site for assessment of doses resulting from long-term releases have been derived from simulations (3.5.1) for different climate conditions (see Section 2.3). The values obtained are presented in Tables 4-1 and 4-2. The *LDFs* for the interglacial period (Table 4-1) are the ones that were used in SR-Site dose assessments for demonstration of compliance with the risk criterion. The uncertainty analyses presented in Chapter 5 are therefore focused on these *LDFs*.

During the reference glacial cycle, the maximum *LDF* is consistently higher under the interglacial period than under the other climate domains (Table 4-2). For instance, *LDFs* for glacial conditions were below the values for interglacial conditions by two orders of magnitude. The maximum *LDFs* during periglacial conditions were also lower than during temperate conditions, and these results were confirmed by detailed simulations of periglacial conditions (Chapter 5). Hence, the maximum *LDFs* for the interglacial period are also maximum values during the whole reference glacial cycle, and have therefore been used for dose assessments for long-term releases of radionuclides from a future repository.

In the biosphere assessment, the global warming climate case is represented by a 50,000 year extension of temperate conditions. Consequently, radionuclides that do not reach steady state activity concentrations within the initial temperate period (–9000 to 9400 AD) will continue to accumulate during the extended temperate period. However, most radionuclides have approached steady state at 9400 AD, and additional accumulation and associated increase in maximum *LDF* is marginal for radionuclides expected to contribute to dose. Only for two radionuclides, Cs-135 and U-238, *LDFs* were larger (approximately an order of magnitude) in the global warming climate case than under the reference glacial cycle, which can be explained by several factors as discussed in Chapter 5. However, due to the small contribution of Cs-135 and U-238 to the total risk estimate resulting from a long-term release (see Section 13.5.4 in /SKB 2011/), a tenfold increase in the *LDFs* of these nuclides would not affect the final risk estimates significantly.

**Table 4-1. LDFs (Sv/y per Bq/y) for the interglacial period based on the maximum during the period with temperate conditions (from –9000 to 9400 AD). The time when the maximum LDF value was observed, the biosphere object with the maximum LDF, the number of people in the most exposed group (N) and the contribution of different exposure pathways to the LDFs are also shown.**

| Radionuclide | LDF Interglacial | | | | Pathways [%] | | | |
|---|---|---|---|---|---|---|---|---|
| | LDF (Sv/y per Bq/y) | Time AD | N | Object | External | Inhalation | Ingestion Water | Ingestion Food |
| Ac-227 | 8.0E–12 | 4350 | 79 | 121_03 | 0.0 | 0.0 | 100.0 | 0.0 |
| Ag-108m | 7.1E–13 | 9400 | 74 | 125 | 49.1 | 0.0 | 1.2 | 49.7 |
| Am-241 | 1.5E–12 | 9400 | 79 | 121_03 | 0.0 | 0.0 | 99.9 | 0.1 |
| Am-243 | 1.5E–12 | 9400 | 79 | 121_03 | 0.3 | 3.5 | 95.0 | 1.2 |
| C-14 | 5.4E–12 | 2650 | 2 | 118 | 0.0 | 0.0 | 0.0 | 100.0 |
| Ca-41 | 9.9E–14 | 3900 | 79 | 121_03 | 0.0 | 0.0 | 1.4 | 98.6 |
| Cl-36 | 5.8E–13 | 3900 | 79 | 121_03 | 0.0 | 0.0 | 1.2 | 98.8 |
| Cm-244 | 8.7E–13 | 4100 | 79 | 121_03 | 0.0 | 0.0 | 99.9 | 0.1 |
| Cm-245 | 1.6E–12 | 9400 | 79 | 121_03 | 0.4 | 1.2 | 96.7 | 1.8 |
| Cm-246 | 1.6E–12 | 9400 | 79 | 121_03 | 0.0 | 0.7 | 98.2 | 1.1 |
| Cs-135 | 4E–14 | 9400 | 80 | 124 | 0.0 | 0.0 | 18.4 | 81.6 |
| Cs-137 | 1.2E–13 | 4500 | 79 | 121_03 | 0.0 | 0.0 | 79.1 | 20.9 |
| Ho-166m | 5.9E–14 | 9400 | 80 | 124 | 85.3 | 0.0 | 12.3 | 2.4 |
| I-129 | 6.5E–10 | 4050 | 79 | 121_03 | 0.0 | 0.0 | 0.1 | 99.9 |
| Nb-94 | 4E–12 | 9400 | 80 | 124 | 98.0 | 0.0 | 0.2 | 1.8 |
| Ni-59 | 7.4E–14 | 9400 | 79 | 121_03 | 0.0 | 0.0 | 0.6 | 99.4 |
| Ni-63 | 1.2E–15 | 8100 | 79 | 121_03 | 0.0 | 0.0 | 90.1 | 9.9 |
| Np-237 | 4.8E–11 | 3200 | 1 | 118 | 0.0 | 0.1 | 1.0 | 98.9 |
| Pa-231 | 8.1E–12 | 9400 | 79 | 121_03 | 0.3 | 2.0 | 63.8 | 34.0 |
| Pb-210 | 5.1E–12 | 4300 | 79 | 121_03 | 0.0 | 0.0 | 98.9 | 1.1 |
| Pd-107 | 6.7E–15 | 9400 | 79 | 121_03 | 0.0 | 0.0 | 4.0 | 96.0 |
| Po-210 | 8.9E–12 | 3900 | 79 | 121_03 | 0.0 | 0.0 | 98.6 | 1.4 |
| Pu-239 | 1.9E–12 | 9400 | 79 | 121_03 | 0.0 | 5.3 | 93.8 | 0.9 |
| Pu-240 | 1.9E–12 | 9400 | 79 | 121_03 | 0.0 | 3.0 | 96.5 | 0.5 |
| Pu-242 | 1.9E–12 | 9400 | 79 | 121_03 | 0.0 | 6.4 | 92.4 | 1.1 |
| Ra-226 | 3.8E–12 | 9400 | 79 | 121_03 | 0.0 | 0.0 | 54.3 | 45.7 |
| Se-79 | 1.2E–09 | 4750 | 79 | 121_03 | 0.0 | 0.0 | 0.0 | 100.0 |
| Sm-151 | 7.2E–16 | 7100 | 79 | 121_03 | 0.0 | 0.0 | 99.5 | 0.5 |
| Sn-126 | 2.5E–11 | 9400 | 79 | 121_03 | 0.7 | 0.0 | 0.1 | 99.2 |
| Sr-90 | 2.2E–13 | 4450 | 79 | 121_03 | 0.0 | 0.0 | 92.9 | 7.1 |
| Tc-99 | 9E–13 | 2850 | 1 | 118 | 0.0 | 0.0 | 0.3 | 99.7 |
| Th-229 | 3.6E–12 | 9400 | 79 | 121_03 | 0.0 | 0.3 | 98.8 | 0.9 |
| Th-230 | 1.3E–11 | 9400 | 79 | 121_03 | 0.0 | 0.1 | 11.7 | 88.2 |
| Th-232 | 1.7E–12 | 9400 | 79 | 121_03 | 0.0 | 0.8 | 97.1 | 2.1 |
| U-233 | 2.5E–12 | 9400 | 79 | 121_03 | 0.8 | 7.0 | 14.9 | 77.3 |
| U-234 | 3.6E–12 | 9400 | 79 | 121_03 | 0.0 | 0.8 | 9.8 | 89.3 |
| U-235 | 2.8E–12 | 9400 | 79 | 121_03 | 6.1 | 2.2 | 12.4 | 79.3 |
| U-236 | 1.9E–12 | 9400 | 79 | 121_03 | 0.0 | 1.1 | 18.5 | 80.4 |
| U-238 | 1.9E–12 | 9400 | 79 | 121_03 | 0.0 | 1.0 | 17.7 | 81.3 |
| Zr-93 | 2.8E–14 | 9400 | 79 | 121_03 | 0.0 | 0.6 | 28.9 | 70.5 |

**Table 4-2. LDF (Sv/y per Bq/y) for the interglacial, permafrost, glacial and global warming climate conditions covering the period from –9000 to 59600 AD.**

| Radionuclide | LDF (Sv/y per Bq/y) | | | |
|---|---|---|---|---|
| | Interglacial | Global Warming | Permafrost | Glacial |
| Ac-227 | 8.0E–12 | 8.0E–12 | 8.9E–16 | 6.4E–17 |
| Ag-108m | 7.1E–13 | 7.1E–13 | 8.8E–15 | 4.6E–16 |
| Am-241 | 1.5E–12 | 1.5E–12 | 1.1E–14 | 1.6E–17 |
| Am-243 | 1.5E–12 | 1.6E–12 | 2.0E–13 | 1.4E–15 |
| C-14 | 5.4E–12 | 5.4E–12 | 5.4E–12 | 8.5E–13 |
| Ca-41 | 9.9E–14 | 9.9E–14 | 9.3E–15 | 1.9E–16 |
| Cl-36 | 5.8E–13 | 5.8E–13 | 4.4E–13 | 2.2E–17 |
| Cm-244 | 8.7E–13 | 8.7E–13 | 8.1E–19 | 2.2E–20 |
| Cm-245 | 1.6E–12 | 1.6E–12 | 2.2E–14 | 3.6E–16 |
| Cm-246 | 1.6E–12 | 1.6E–12 | 1.6E–14 | 2.1E–16 |
| Cs-135 | 4E–14 | 2.9E–13 | 3.0E–13 | 4.3E–17 |
| Cs-137 | 1.2E–13 | 1.2E–13 | 9.5E–18 | 3.7E–20 |
| Ho-166m | 5.9E–14 | 5.9E–14 | 8.4E–16 | 1.5E–18 |
| I-129 | 6.5E–10 | 6.5E–10 | 2.6E–11 | 1.7E–13 |
| Nb-94 | 4E–12 | 1.2E–11 | 1.1E–13 | 2.1E–17 |
| Ni-59 | 7.4E–14 | 2E–13 | 1.3E–15 | 4E–18 |
| Ni-63 | 1.2E–15 | 1.2E–15 | 6.3E–18 | 1.9E–20 |
| Np-237 | 4.8E–11 | 4.8E–11 | 2.2E–11 | 8.7E–15 |
| Pa-231 | 8.1E–12 | 1.3E–11 | 1.7E–13 | 2.8E–15 |
| Pb-210 | 5.1E–12 | 5.1E–12 | 2.6E–17 | 2.2E–18 |
| Pd-107 | 6.7E–15 | 9.4E–15 | 2.7E–15 | 4.6E–18 |
| Po-210 | 8.9E–12 | 8.9E–12 | 3.1E–20 | 9.3E–21 |
| Pu-239 | 1.9E–12 | 2E–12 | 2.0E–13 | 6.4E–15 |
| Pu-240 | 1.9E–12 | 1.9E–12 | 1.3E–13 | 4.1E–15 |
| Pu-242 | 1.9E–12 | 2.2E–12 | 2.3E–13 | 7.2E–15 |
| Ra-226 | 3.8E–12 | 3.8E–12 | 9.8E–13 | 4.5E–15 |
| Se-79 | 1.2E–09 | 1.2E–09 | 5.8E–11 | 9.6E–13 |
| Sm-151 | 7.2E–16 | 7.2E–16 | 1.0E–20 | 4.6E–22 |
| Sn-126 | 2.5E–11 | 1.1E–10 | 6.1E–13 | 1.6E–14 |
| Sr-90 | 2.2E–13 | 2.2E–13 | 7.2E–17 | 2E–19 |
| Tc-99 | 9E–13 | 9E–13 | 2.8E–13 | 1.6E–15 |
| Th-229 | 3.6E–12 | 3.7E–12 | 7.0E–14 | 9.6E–17 |
| Th-230 | 1.3E–11 | 6.4E–11 | 1.5E–11 | 1.7E–14 |
| Th-232 | 1.7E–12 | 2.6E–12 | 4.5E–13 | 1.2E–16 |
| U-233 | 2.5E–12 | 1.9E–11 | 2.5E–12 | 2E–15 |
| U-234 | 3.6E–12 | 7.1E–11 | 1.1E–11 | 4.5E–15 |
| U-235 | 2.8E–12 | 2E–11 | 1.3E–13 | 5.6E–16 |
| U-236 | 1.9E–12 | 1.1E–11 | 2.9E–14 | 1.9E–17 |
| U-238 | 1.9E–12 | 1.6E–11 | 8.1E–13 | 1E–16 |
| Zr-93 | 2.8E–14 | 1.1E–13 | 6.5E–16 | 8.2E–17 |

## 4.2 LDF values for pulse releases

The *LDF pulse,* used in SR-Site for assessment of doses resulting from pulse releases, have been derived from deterministic simulations (3.5.2), which explore different variants of timing and duration of the pulse releases during temperate climate conditions. The derived *LDF pulse* for radionuclides that can be present in a pulse release are presented in Table 4-3. The effect of the timing and duration of the pulse release on the *LDF pulse* is discussed in Chapter 5.

**Table 4-3. LDFs for pulse releases (Sv/y per Bq) obtained from deterministic simulations for radionuclides that can be present in a pulse release.**

| Radionuclide | LDF pulse |
|---|---|
| Ag-108 | 5.1E–16 |
| Cl-36 | 4.3E–15 |
| Cs-135 | 1.8E–16 |
| I-129 | 5.6E–14 |
| Nb-94 | 3.2E–16 |
| Ni-59 | 9.7E–18 |
| Se-79 | 9.7E–14 |
| Sn-126 | 2.3E–15 |
| Tc-99 | 2.8E–15 |

# 5 Uncertainty analyses

This chapter presents the results from studies that have been carried out for analysis of uncertainties associated with the *LDFs*. To facilitate the discussion the uncertainties have been classified into three types: i) System Uncertainties – arising from our inability to make accurate predictions of the long-term development of the biosphere and the future use of the biosphere by humans (Section 5.1), ii) Model Uncertainties – arising from our necessarily imperfect knowledge of the processes affecting the behavior of radionuclides in the biosphere, which leads to imperfect conceptual models and simplified mathematical representation of the conceptual models (Section 5.2), iii) Parameter Uncertainties – arising from the natural variability of the parameters and from imperfect and insufficient measured data (Section 5.3). In addition, uncertainties associated with errors arising during the numerical integration of the models are also discussed in Section 5.4. The chapter concludes with a comparison of *LDF* values derived here with values derived from early studies (Section 5.5) and with a summary of results from the uncertainty analyses (Section 5.6).

The approach to uncertainty analyses adopted here is consistent with frameworks for analysis of uncertainties applied in disposal programmes worldwide. A study performed within the EC project PAMINA (see /Galson and Khursheed 2007/) has shown that there is a high level of consensus on both how uncertainties considered in performance assessments should be classified and the nature of the uncertainties, although this consensus may be masked by variations in terminology and differences in how uncertainties are treated in various programmes.

The study of the uncertainties has been focused on the effects of uncertainties on the *LDFs* for long-term releases during an interglacial period, referred below as the baseline *LDF*. However, many of the uncertainties associated with *LDFs* for long-term release are shared by the modified *LDF*, i.e. the *LDF for pulse* releases. The major difference between these two *LDF* types is in the timing and duration of the release, which effect has been studied here for both *LDF* types. The effect on the *LDF* values of the system and conceptual uncertainties was studied for those radionuclides that had the highest contribution to the doses. Examples are most frequently drawn from the results of Ra-226 (including daughter nuclides Pb-210 and Po-210) and I-129, and to a lesser extent from Se-79, Np-237, Cs-135, and Cl-36. The first four radionuclides where selected because of their expected effect in long-term release (as indicated by the central corrosion case), where as Cs-135, and Cl-36 are primarily expected to contribute to dose in a pulse release (Section 13.5.4 in /SKB 2011/). The study of parameter uncertainties and the sensitivity analyses were carried out for a larger set of 19 potentially dose contributing radionuclides.

## 5.1 System uncertainties

In this study, system uncertainties refer to uncertainties associated with the development of the biosphere and future human utilization of natural resources. The system uncertainties that have been considered are summarized in Table 5-1, where the source of the uncertainties, the method for their treatment and an evaluation are also presented. System uncertainties have been treated by introducing assumptions in the assessments, some of which are considered cautious and other realistic. The quantification of the effects of system uncertainties has consisted of deriving *LDF* under alternative assumptions and comparing these with the baseline *LDF*. The last column in Table 5-1 shows codes assigned to those uncertainties for which the effect on the *LDFs* was estimated quantitatively. These codes have been used as identifiers of the different uncertainties in figures presented in Section 5.6.

**Table 5-1. Summary of system uncertainties which have been analysed, with a short explanation of the approaches for their treatment and evaluation.**

| Source of uncertainty | Treatment | Evaluation | Code |
|---|---|---|---|
| *Development of the biosphere* | | | |
| State of the biosphere in relation to the timing and duration of the releases | LDFs are peak values over the whole interglacial period.<br>(cautious assumption) | Simulations with different timing and release duration were carried out. | A |
| State of the biosphere in relation to the localization of potential releases in the landscape | Maximum LDF across all biosphere objects selected.<br>(cautious assumption) | Values for all biosphere objects and average values were compared. | B |
| Climate change | Maximum LDF from the interglacial period used for dose calculations during the whole simulation period.<br>(cautious assumption) | Simulations with alternative climate conditions. | C |
| *Human utilization of natural resources* | | | |
| Occupancy of potentially contaminated areas | It is assumed that the representative individual of the most exposed group is exposed 100% of the time to radionuclides in soil (mire) and reduction of external exposure inside buildings is neglected.<br>(cautious assumptions) | Qualitative discussion showing that exposure from occupancy is not underestimated. | |
| Use of well water for drinking | 100% of drinking water demand by humans and cows comes from contaminated surface and well water.<br>(cautious assumption) | Simulation where it is assumed that only surface water is used for drinking. | D |
| Use of well water for short-term irrigation | It is assumed that only contaminated surface water is used for short-term irrigation.<br>(realistic assumption) | Simulations considering short-term irrigation with well water. | E |
| Long-term irrigation | Long-term irrigation with surface is considered bounded by accumulation in mire and short-term irrigation. Use of well water for long term irrigation is considered unlikely.<br>(realistic assumption) | Simulations considering long-term irrigation with contaminated surface water were carried out. | F |
| Use of potentially contaminated areas for food supply | It is assumed that mires are converted to agricultural lands at all times starting from the moment when agriculture is possible. Losses of radionuclides during drainage of mires are neglected. All alternative uses of the land for food production are considered equally likely.<br>(cautious assumption) | Probabilistic simulations to study the effects of alternative uses of the land for food production were carried out. | G |
| Diet of the exposed individuals | It is assumed that the diet is proportional to the production capacity in the biosphere object.<br>(realistic assumption) | Calculations using diet from contemporary food statistics. | |
| Other uses of potentially contaminated areas | It is considered that other uses of the potentially contaminated areas are bounded by the uses considered in the assessment.<br>(realistic assumption) | Qualitative discussion showing that neglecting other potential uses of the land does not lead to underestimation of the doses. | |

### 5.1.1 Development of the biosphere

The assessment of radionuclide releases to the biosphere in a distant future requires that assumptions are made about the development of the biosphere. In this study, it has been assumed that at Forsmark the landscape development during the present ice-free period will give an acceptable representation also of the landscape development during future ice-free periods of repeated glacial cycles /Lindborg 2010/. Geometries of the landscape will change with glacial cycles, as bedrock is eroded and the regolith is reworked by glacial and post-glacial processes. However, the general geometrical patterns are expected to be similar and the identified biosphere objects span a wide range of sizes and positions in the landscape. It is argued that the geometric properties of future objects will be captured in the variation of identified biosphere objects. Nevertheless, there remain large uncertainties

associated with these features and how these can be taken into account in the derivations of *LDF* values. In this section, the approaches for treatment of these uncertainties are described together with an evaluation of their potential effect on the *LDF* values. Another source of uncertainty related to the biosphere development is climate change. In the SR-Site assessment, the uncertainty of future climates has been handled by assuming that a reconstruction of the latest glacial cycle will cover the climatic variations that are expected in the future. Covering all these variations with a single *LDF* value has required that several cautious and simplifying assumptions are introduced in their derivation. In this section these assumptions are discussed and evaluated.

### *Timing and duration of the releases*

In the derivation of *LDF* values for long-term releases the uncertainty associated with the timing and duration of releases reaching biosphere objects has been handled by cautiously assuming that the entire release from the repository will reach each assessed biosphere object during the whole simulation period, i.e. starting from the beginning of the submerged period and until the end of the interglacial period. To evaluate the degree of cautiousness of this assumption three alternative simulations were carried with different starting points of the releases: after the end of the submerged period, after the end of the transitional stage and from the end of the temperate period, i.e. from 9400 AD. Examples of the results of these simulations are presented in Figures 5-1, 5-2 and 5-3 for Ra-226, I-129 and Cs-135, respectively. The simulations showed that the timing and duration of the releases had some effect for some of the studied radionuclides (I-129, Se-79, Cs-135 and Np-237) and practically no effect for other (Ra-226, Cl-36). The degree of cautiousness of the assumption made for derivation of the baseline *LDF* values has been estimated by dividing the baseline *LDF* by the *LDF* obtained for the alternative simulation with releases starting after the submerged period. The following values of this ratio were obtained: 4 for I-129, 3 for Se-79, 2 for Cs-135, 14 for Np-237, 3 for Tc-99 and 1 for both Ra-226 and Cl-36.

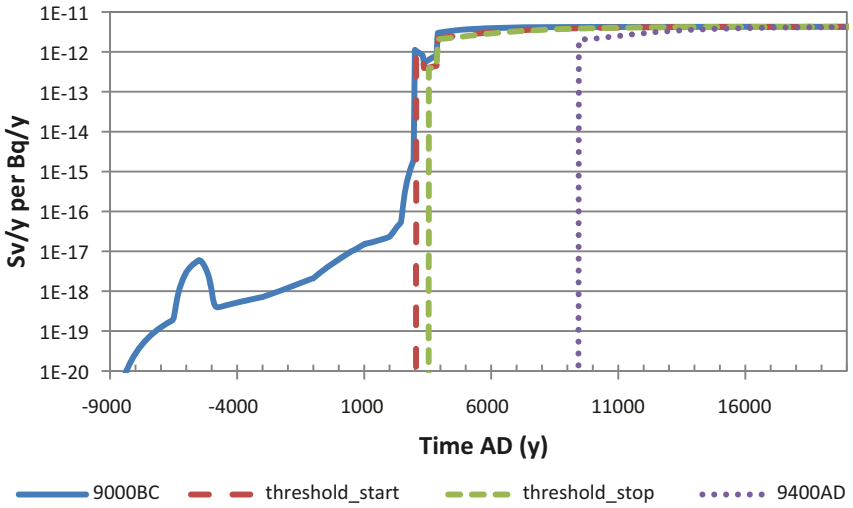


***Figure 5-1.*** *Time series of annual doses per unit release rate obtained from simulations where 1 Bq/y of Ra-226 is released to the biosphere object with the highest LDF (see Table 4-1). Results are presented for four cases with different starting times of the releases; from the start of the submerged period at 9000 BC (used for the derivation of baseline LDFs), after the end of the submerged period (threshold_start), after the end of the transitional stage (threshold_stop) and after the end of the temperate period at 9400 AD.*

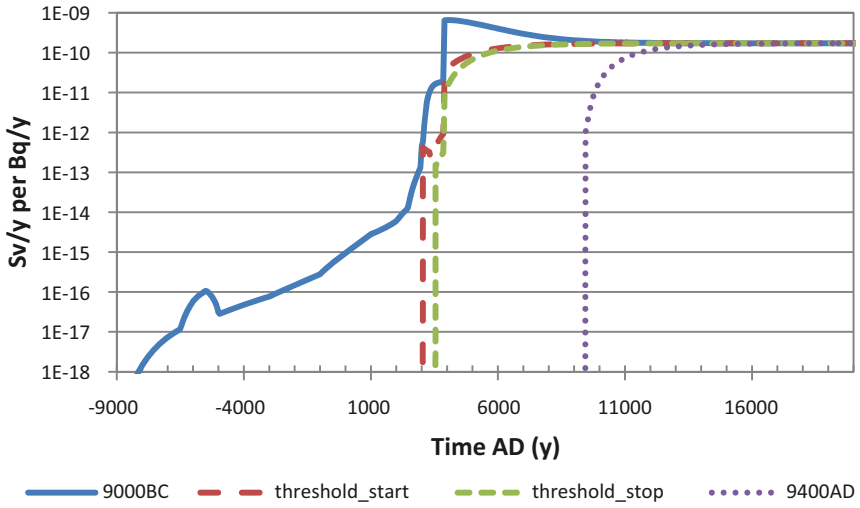


***Figure 5-2.*** *Time series of annual doses per unit release rate obtained from simulations where 1 Bq/y of I-129 is released to the biosphere object with the highest LDF (see Table 4-1). Results are presented for four cases with different starting times of the releases: from the start of the submerged period at 9000 BC (used for the derivation of baseline LDFs), after the end of the submerged period (threshold_start), after the end of the transitional stage (threshold_stop) and after the end of the temperate period at 9400 AD.*

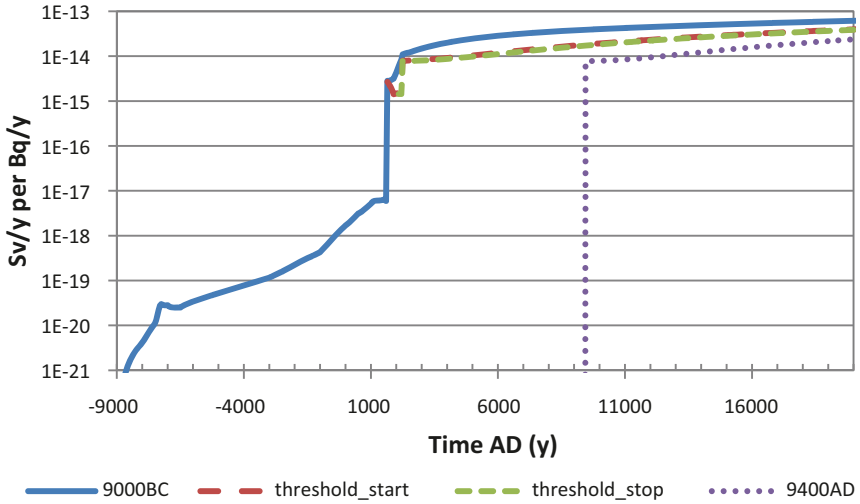


***Figure 5-3.*** *Time series of annual doses per unit release rate obtained from simulations where 1 Bq/y of Cs-135 is released to the biosphere with the highest LDF (see Table 4-1). Results are presented for four cases with different starting times of the releases: from the start of the submerged period at 9000 BC (used for the derivation of baseline LDFs), after the end of the submerged period (threshold_start), after the end of the transitional stage (threshold_stop) and after the end of the temperate period at 9400 AD.*

As explained in Section 3.5.2, the modified *LDFs for pulse* releases were derived by performing simulations with pulse releases of different duration occurring at different points in time and selecting the maximum values obtained from these simulations (values presented in Section 4.2). The same time points were used for all studied radionuclides. Examples of results from these simulations are presented in Figures 5-4 to 5-13. The effect of the timing on the modified *LDF for pulse* releases for pulse releases varied among the considered radionuclides. As it can be seen from Figures 5-4 and 5-5, for I-129 and Se-79 the timing of the pulse release has a limited impact on the values of the modified *LDFs for pulse* releases. In contrast, for highly mobile radionuclides with relative low $K_d$ values, such as Cl-36 and Tc-99, the timing of the releases has a significant effect on the values of the modified *LDFs for pulse* releases (see Figures 5-7 and 5-8). If pulse releases of such poorly retained radionuclides occur during the submerged period, then the resulting doses will be relatively

low, due to the large dilution that would take place in the sea. For Cs-135, which has a relative high $K_d$ in the regolith, the timing of the release is also important (Figure 5-6). For this radionuclide, the contribution from the well to the doses is important and therefore releases during the submerged period, when exposure from wells is not relevant, would result in lower doses. Hence, it can be concluded that, for some radionuclides, using the SR-site values of modified *LDF for pulse* releases, presented in Section 4.2, might result in substantially overestimation of the doses in scenarios where the pulse releases occur during the submerged period.

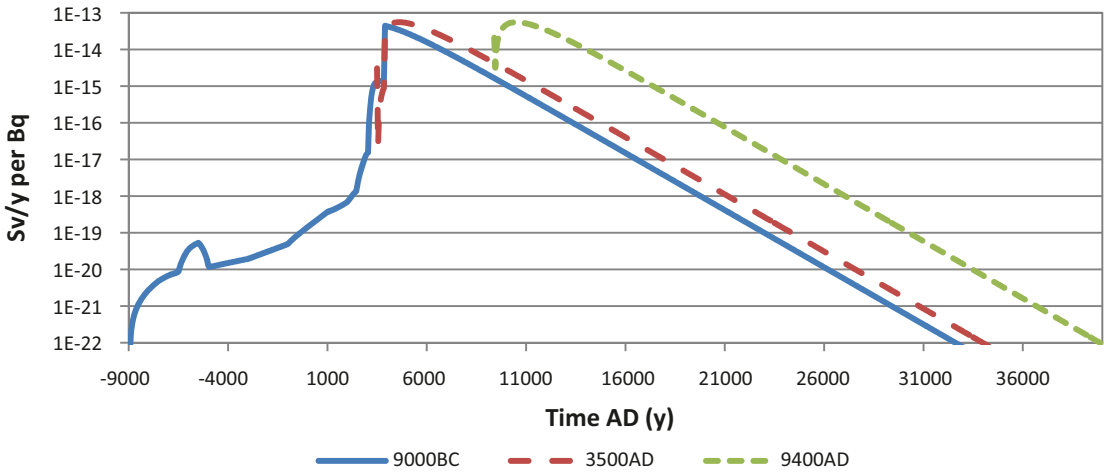


***Figure 5-4.*** *Time series of annual doses per unit release obtained from simulations where 1 Bq of I-129 released to the biosphere object with the highest LDF (see Table 4-1) as a pulse with duration of 50 years. Results are presented for three cases with the pulse release starting at different time points. For all studied radionuclides the peak values of LDF pulse are observed after the transition from sea to land. This is the case even if the pulse release occurs before the transition from sea to land, for example at –9000 AD. In this case the peak values of the LDF pulse are associated with the flush of activity retained in the lower regolith; as result of increase of upward water flow rates during the passage of the coast line.*

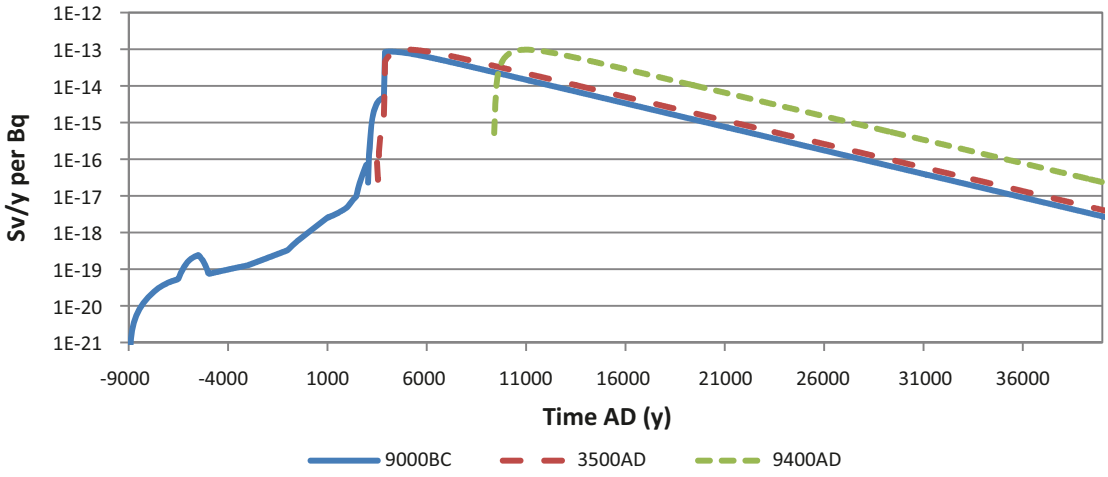


***Figure 5-5.*** *Time series of annual doses per unit release obtained from simulations where 1 Bq of Se-79 released to the biosphere object with the highest LDF (see Table 4-1) as a pulse with duration of 50 years. Results are presented for three cases with the pulse release starting at different time points.*

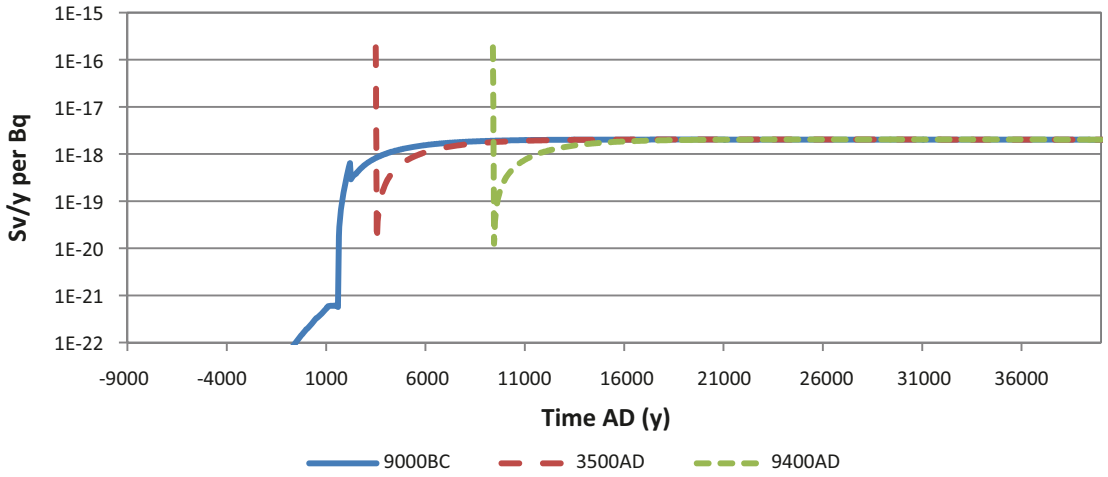


***Figure 5-6.*** *Time series of annual doses per unit release obtained from simulations where 1 Bq of Cs-135 released to the biosphere object with the highest LDF (see Table 4-1) as a pulse with duration of 50 years. Results are presented for three cases with the pulse release starting at different time points. The spikes at the beginning of the last two figures to the right is due to the contribution from the well to the LDF, which is only included only for the first 50 years when the pulse release occurs and can pass a drilled well.*

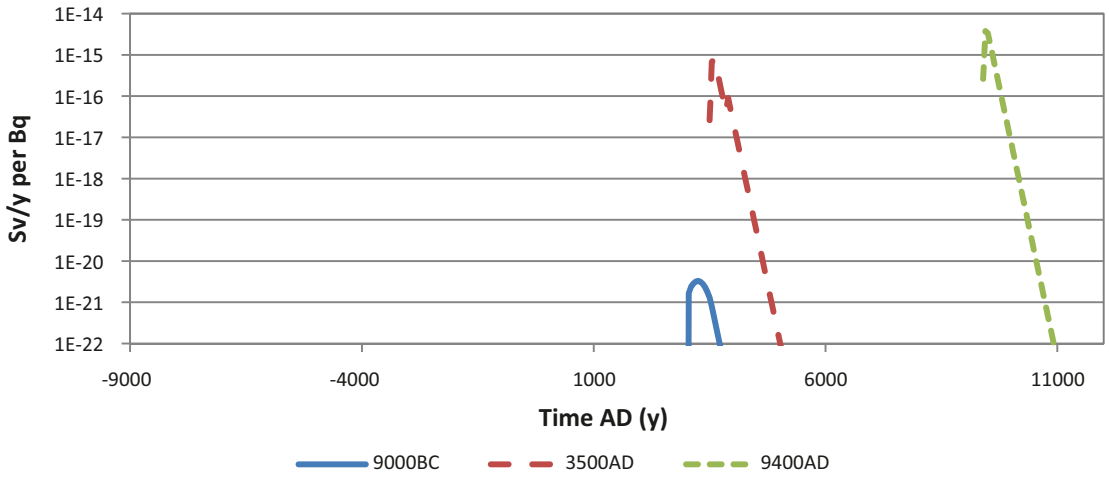


***Figure 5-7.*** *Time series of annual doses per unit release obtained from simulations where 1 Bq of Cl-36 released to the biosphere object with the highest LDF (see Table 4-1) as a pulse with duration of 50 years. Results are presented for three cases with releases starting at different time points.*

The study of the effect of the duration of the pulse on the values of the modified *LDFs* was carried out by performing simulations with different durations of a pulse occurring at year 9400 AD, which is the point in time when pulse releases within an interglacial period result in the highest doses. The effect of the duration of the pulse was different for different studied radionuclides (see Figures 5-8 to 5-11), but the general tendency was that longer the duration of the pulse the lower was the dose, although the differences were marginal for pulse durations ranging from 1 to a few hundred years.

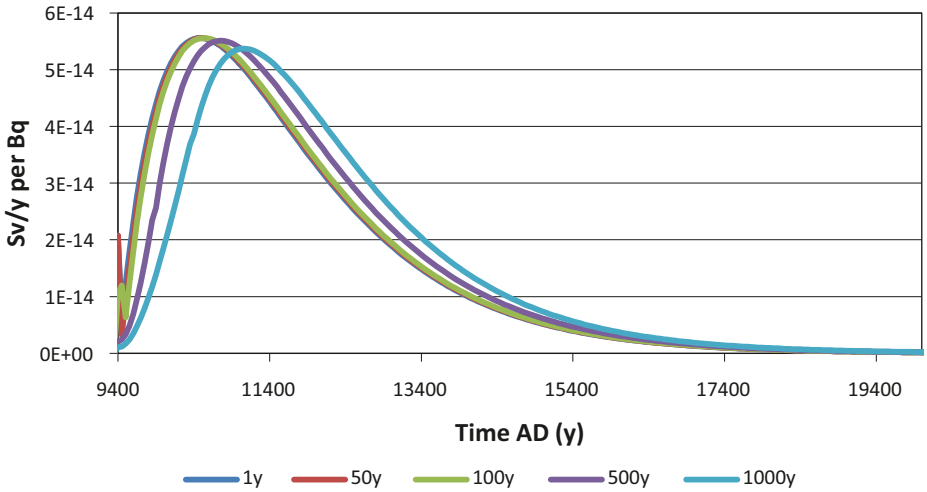


***Figure 5-8.*** *Time series of annual doses per unit release obtained from simulations where 1 Bq of I-129 released at year 9400 AD to the biosphere object with the highest LDF (see Table 4-1) as pulses of different duration (from 1 year to 1,000 years).*

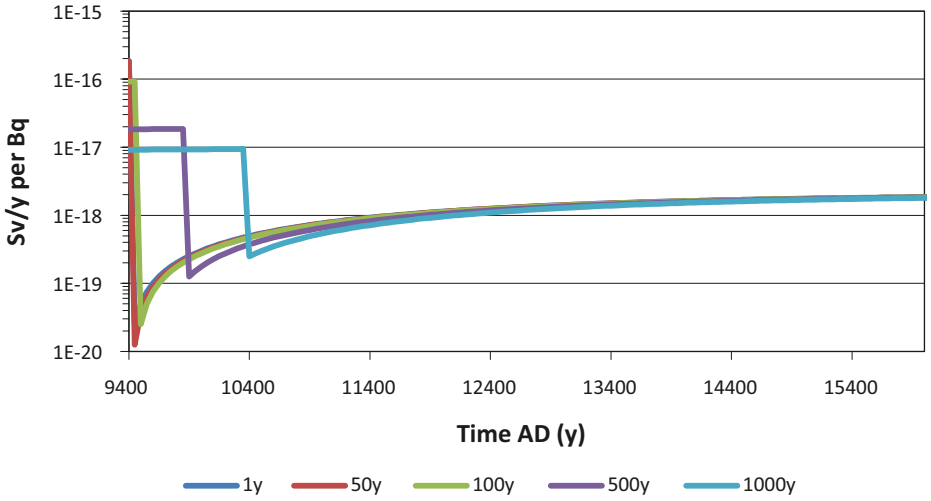


***Figure 5-9.*** *Time series of annual doses per unit release obtained from simulations where 1 Bq of Cs-135 released at year 9400 AD to the biosphere object with the highest LDF (see Table 4-1) as pulses of different durations (from 1 year to 1,000 years).The observed maximum during the pulse release is explained by the contribution from the well during this period. For pulses of longer duration, a build-up phase is observed following the maximum, which is explained by the relatively low mobility of Cs-135 with increase of the time to reach equilibrium levels.*

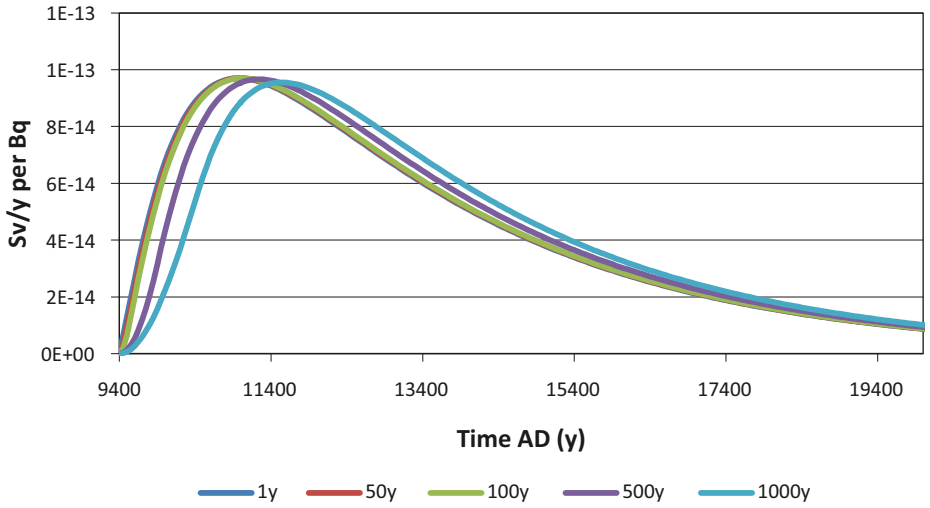


***Figure 5-10.*** *Time series of annual doses per unit release obtained from simulations where 1 Bq of Se-79 released at year 9400 AD to the biosphere object with the highest LDF(see Table 4-1) as pulses of different duration (from 1 year to 1,000 years).*

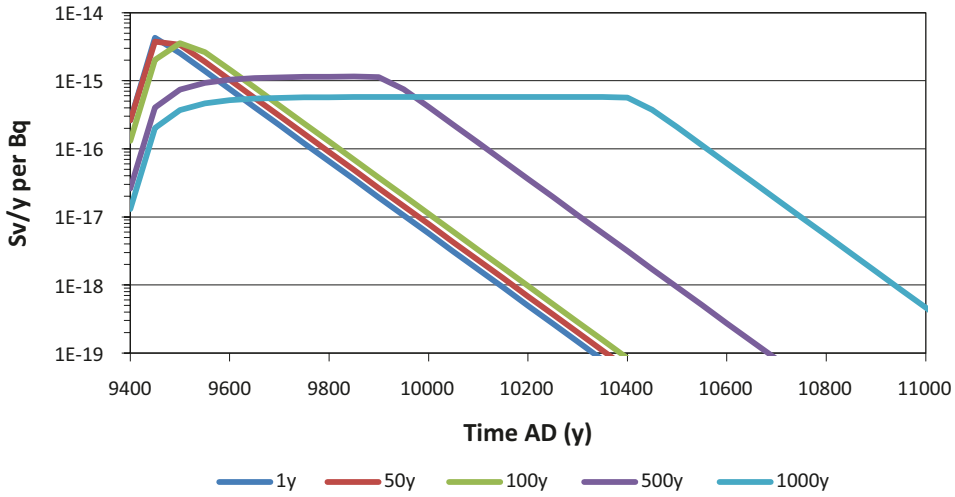


***Figure 5-11.*** *Time series of annual doses per unit release obtained from simulations where 1 Bq of Cl-36 released at year 9400 AD to the biosphere object with the highest LDF (see Table 4-1) as pulses of different durations (from 1 year to 1,000 years).*

### *Localisation of potential releases in the landscape*

In the derivation of baseline *LDF* values for long-term releases, the uncertainty associated with the identification of biosphere objects affected by releases occurring in a distance future has been handled by making the cautious assumption that releases during the whole simulation period are directed to the biosphere object that gives the highest dose (Section 3.5.1). This assumption was applied for each potentially released radionuclide separately. The degree of cautiousness in this assumption was quantified by calculating *LDFs* for the alternative assumption that all identified biosphere objects are equally likely to receive the release, and contrasting these with the baseline *LDFs*.

As shown in Figure 5-12, the *LDF* clearly varies between biosphere objects, and the degree of variation depends on the properties of radionuclides. The difference between the baseline *LDF* and the arithmetic mean value (Figure 5-13) across all landscape objects (excluding object 105) was typically a factor two for radionuclides where drinking water from the well was an important pathway for exposure (e.g. Ra-226). For radionuclides where exposure from food was the dominant pathway, the difference was more pronounced and varied between a factor four (Cl-36) and a factor

nine (I-129). The reason for excluding object 105 in the calculation of the arithmetic mean across all landscape objects was that this object remains under submerged conditions during the whole interglacial period and therefore showed significantly lower *LDF* values for all radionuclides.

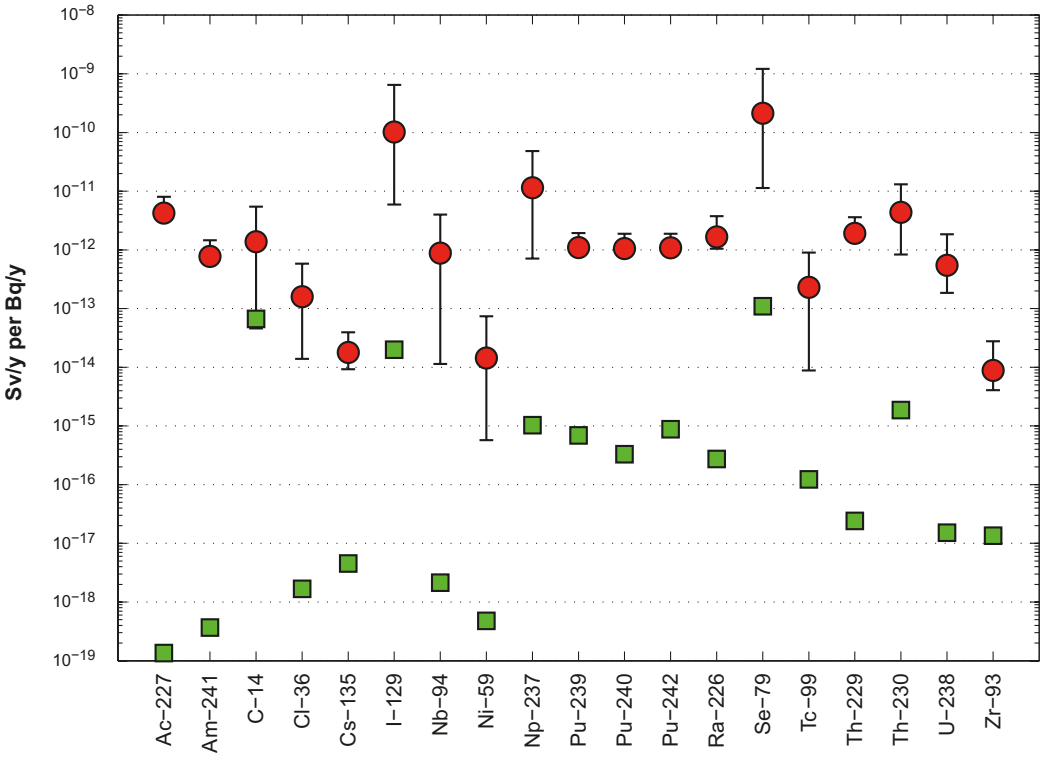


***Figure 5-12.*** *Mean (circles), minimum and maximum LDF values obtained from simulations for the different biosphere objects. The LDF values of object 105 (squares), shown separately, were lower for all radionuclides, since this object remains in the sea stage during the whole simulation period.*

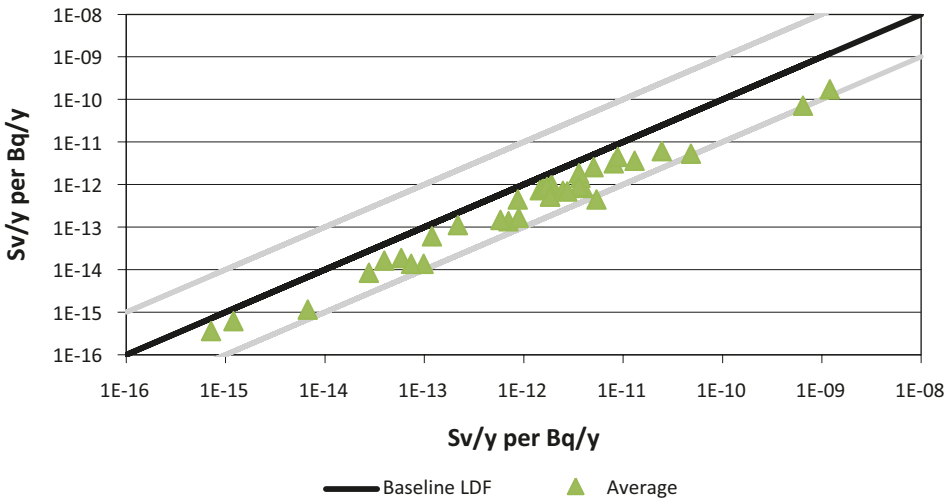


***Figure 5-13.*** *Comparison of baseline LDF values (x-axis) of studied radionuclides against the alternative LDF – arithmetic average of LDFs obtained for different biosphere objects, excluding object 105 (y-axis). The solid line represents a 1:1 relationship between the baseline and alternative LDFs.*

### *Climate change*

In the SR-Site assessment, the uncertainty of future climates has been handled by assuming that a reconstruction of the latest glacial cycle /SKB 2010b/ will cover expected future climatic variations. According to the reference glacial cycle, the initial period of temperate conditions will be followed by a 40,000 year period when temperate and periglacial domains will alternate. For this period a separate *LDF* was calculated assuming that radionuclides from contaminated groundwater would reach all biosphere objects, but that a colder climate would prevent agriculture and the use of well water due to deep permafrost. From these simulations it is concluded that the maximum *LDF* from the period of temperate domain will be a cautious estimate for the entire reference glacial cycle (see Section 2.3).

**Permafrost conditions**

Cold climate and permafrost may influence a number of processes in the biosphere that affect transport, accumulation and exposure. For example permafrost will prevent discharge of deep groundwater to most of the lakes and wetlands in the area. The reduced precipitation and longer periods of frozen conditions result in reduced vertical transport on a yearly basis /Bosson et al. 2010/. The terrestrial vegetation community will change with climate. Primary production will be hampered in a harsher climate, resulting in a reduced rate of in-growth of wetlands into lakes /Brydsten and Strömgren 2010/ and a reduced productivity of natural food stuffs and agricultural crops in the area /Löfgren 2010/. Thus, to evaluate whether the maximum interglacial *LDF* could be exceeded during fluctuating periods of temperate and permafrost conditions, an alternative simulation was carried out. In this simulation a biosphere object having a potential through-talik was simulated allowing key process rates to fluctuate according to the reference glacial cycle.

The first permafrost will appear in Forsmark at around 9400 AD. At this time only two of the biosphere objects will have an open water area that is large enough to prevent permafrost developing beneath the lake /Brydsten and Strömgren 2010/. The lake in biosphere object 114 is likely to receive discharge of deep ground water even during deep permafrost conditions (Figure 5-14) and consequently this object was selected for studying the effect of repeated cycles of permafrost on transport and accumulation of radionuclides.

The periods when the object experiences permafrost were determined from the mean permafrost depth along a transect running from east to west through the Forsmark area /Hartikainen et al. 2010/. For these periods, parameters that describe hydrological fluxes and properties of wetland vegetation and crops were given values representing permafrost conditions (Table 5-2) /Bosson et al. 2010, Löfgren 2010, Andersson 2010/ and the wetland growth rate was reduced by 75% (Figure 5-15) /Brydsten and Strömgren 2010/. The transition between temperate conditions and full permafrost conditions has been estimated to require between 2,000 and 5,000 years for the investigation area /SKB 2010b/. The local catchment area of object 114 makes up a considerable fraction of the model area and thus transition periods flanking permafrost periods were assumed to be 2,000 years. During these periods, all parameters affected by permafrost were assumed to change continuously between temperate and permafrost values (see dotted line in Figure 5-16). Permafrost periods that were shorter than 2,000 years were disregarded in the simulation.

The permafrost depth and area of open water were also used to determine whether the conditions were such as to prevent permafrost from developing under the lake /Brydsten and Strömgren 2010/. According to these predictions, permafrost will develop under the lake in object 114 at 50,000 AD, and consequently for the last 3,000 years of the simulation there is no further release of radionuclides to the object. In addition, it was assumed that a drilled well would not provide water during permafrost conditions.

The simulation of the reference climate with periods of temperate climate between periods of permafrost demonstrated that *LDFs* will be clearly affected by the transitions from colder to warmer climates. The dynamic effects on the *LDF* are primarily caused by changes in hydrological conditions. During permafrost conditions vertical flows from the till (Regolith low) to overlying sediments (Regolith mid) are reduced by a factor ten. For radionuclides with a long half-life this will cause an increase in equilibrium concentrations in the till. The equilibrium concentrations of radionuclides with a short half-life are unaffected by reduced flows from the till, but the export from the till to the

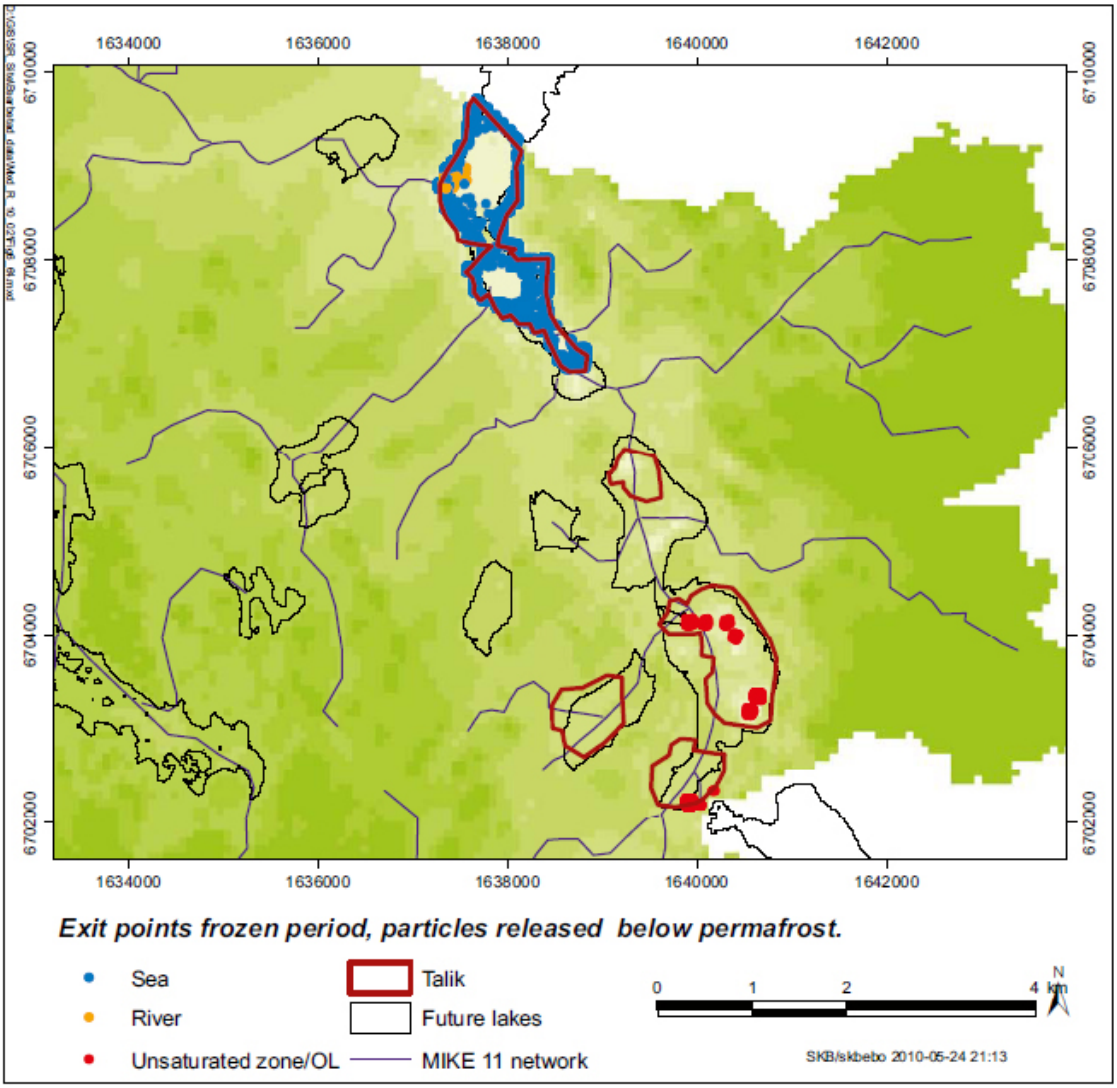


***Figure 5-14.*** *Discharge points during periods of severe permafrost. For the simulation, particles were released below a 240 m permafrost layer. The majority of discharge points are located in a sea-talik (blue points), but there is also some discharge in biosphere object 114 (red points). (Extracted from /Bosson et al. 2010/).*

rest of the biosphere object will be reduced. Once the permafrost period has ended, the hydrological fluxes will gradually increase, flushing radionuclides out of the till as the activity concentration approaches the temperate equilibrium concentration. The effect on different environmental media of repeated build up and flushing in the till will vary with radionuclide properties, and effects on exposure will be modified by dietary shifts caused by changes in conditions for terrestrial and aquatic biota.

The results from the simulations for periglacial conditions are presented in Figures 5-16 to 5-21. The *LDFs* obtained from these alternative simulations could, in some cases, be higher than the *LDF* for object 114 during temperate conditions and in global warming conditions. However, for all studied radionuclides these *LDFs* were lower than the baseline *LDF*, i.e. lower than the maximum across all biosphere objects during the interglacial period. Hence, it is concluded that the use of baseline *LDF* will give a cautious dose estimate even for permafrost conditions.

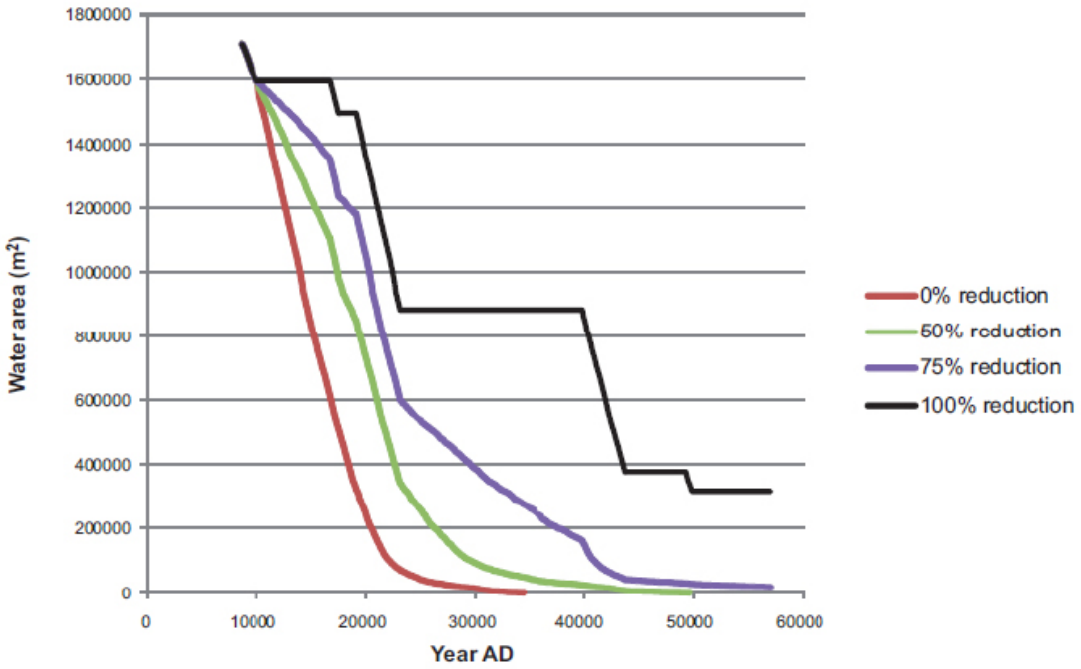


***Figure 5-15.*** *Time variations of the open water area in a biosphere object as a function of the rate of infilling. The red line represents no reduction in vegetation in-growth and sedimentation during permafrost conditions, whereas the black line represents a complete stop of lake infilling during permafrost conditions. For the dose simulation permafrost was assumed to reduce lake infilling by 75%. (Extracted from /Brydsten and Strömgren 2010/.*

**Table 5-2. Parameters in the radionuclide model that were assumed to be affected by permafrost conditions. Parameter values are listed for temperate and permafrost conditions.**

| Parameter | Description | Temperate conditions | Permafrost conditions | Unit |
|---|---|---|---|---|
| *Atmosphere* | | | | |
| conc_C_atmos | The concentration of carbon in the atmosphere | 0.00020 | 0.00011 | kg/m$^3$ |
| *Hydrology* | | | | |
| runoff | The total runoff in the model area | 0.19 | 0.22 | m/y |
| Lake_Aqu_adv_mid_up_norm | Advective flux in the aquatic object between the sediment and the water during lake stage[a] | 0.64 | 0.03 | unitless |
| Lake_fract_Mire | The fraction of the advective flux from the till that goes to deposits under the wetland | 0.98 | 0.33 | unitless |
| Lake_adv_low_mid | The total advective flux from till to glacial and post glacial deposits after the marine phase | 0.044 | 0.0030 | m/y |
| Ter_adv_mid_up_norm | The advective flux from post glacial and glacial deposits to peat[a] | 0.31 | 0.0014 | unitless |
| Flooding_coef | The gross flux from wetland to lake[a] | 1.3 | 1.1 | unitless |
| *Wetland ecosystem* | | | | |
| Ter_biom_pp | The terrestrial biomass of primary producers | 6.0 | 0.82 | kgC/m$^2$ |
| Ter_prodBiom_pp | The productivity of primary producers | 0.081 | 0.099 | kgC/y/kgC |
| Ter_z_roughness | The zero displacement height of vegetation | 1.0 | 0.25 | m |
| Ter_z_mixlay | The height of the mixing layer | 9.5 | 0.90 | m |
| Ter_decomp | The decomposition rate | 0.91 | 0.80 | 1/y |
| frac_C_atmos | The fraction of the decomposed carbon that is leaving as $CO_2$ to the atmosphere | 0.98 | 0.92 | unitless |

| Parameter | Description | Temperate conditions | Permafrost conditions | Unit |
|---|---|---|---|---|
| *Productivity of human food* | | | | |
| prod_edib_cereal | The production of edible cereals | 0.11 | 0.091 | kgC/m²/y |
| prod_edib_tuber | The production of edible root crops | 0.13 | 0.11 | kgC/m²/y |
| prod_fodder | The production of fodder on agricultural land | 0.20 | 0.17 | kgC/m²/y |
| prod_cereal | The production of edible cereals | 0.17 | 0.13 | kgC/m²/y |
| leaf_areaIndex | The ratio of leaf to soil surface area of vegetation | 3.6 | 1.9 | m²/m² |
| prod_edib_fish_Lake | The production of edible fish in the lake | 0.00027 | 3.2E–05 | kgC/m²/y |
| prod_edib_cray_Lake | The production of edible crayfish in the lake | 3.143E–05 | 0 | kgC/m²/y |

a = normalized by the net lateral flux from the mire.

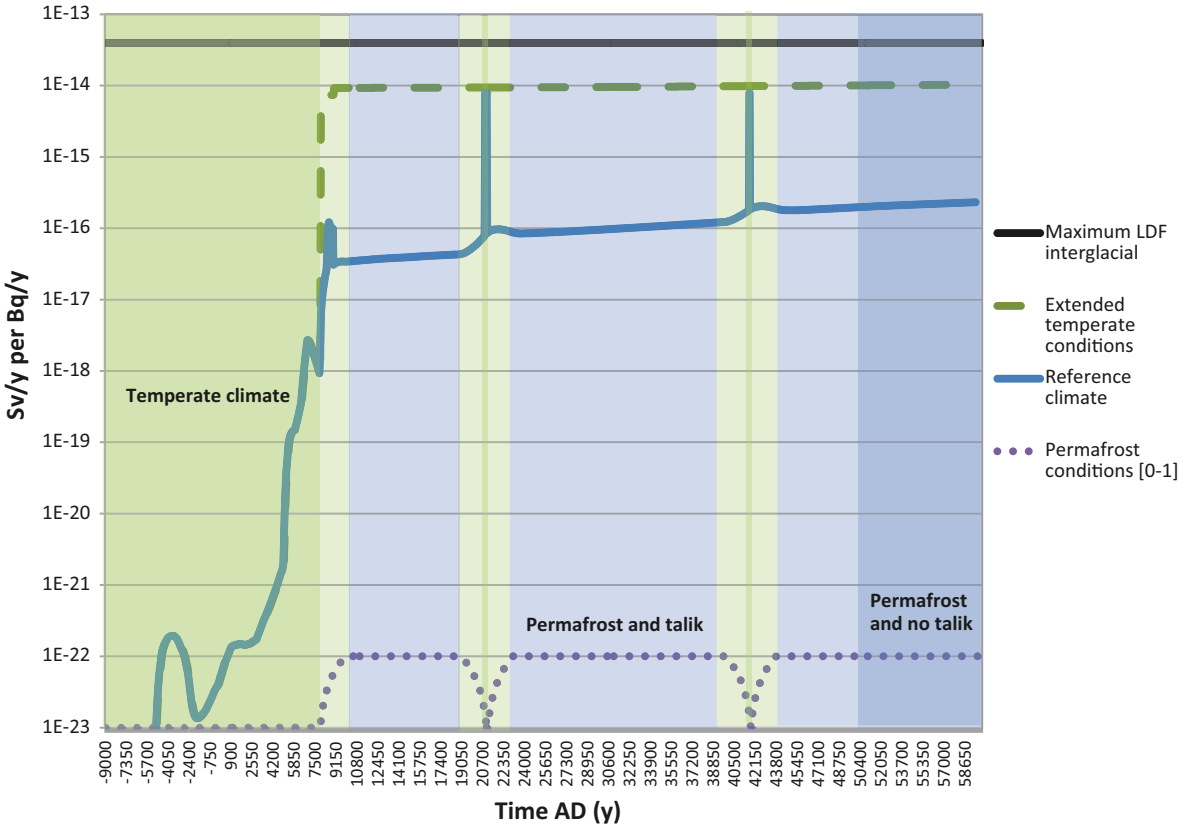


***Figure 5-16.*** *Effect of fluctuating periods of temperate and permafrost conditions on LDF for Cs-135 from simulations for object 114. In the simulation the initial 20 ky interglacial was followed by an interval over which long periods of permafrost are alternated with short periods of temperate climate conditions. The LDF from the simulation (blue line) is compared with the LDF from constant temperate conditions in the object (dashed line) and the maximum LDF over all biosphere objects from interglacial conditions used in the safety assessment (black line). The spikes in the simulated LDF correspond to short periods of temperate conditions when absence of permafrost allowed use of a deep drilled well. Background colour indicate climate condition (green = temperate, blue = permafrost, yellow = transition). In the transition between temperate and permafrost conditions parameters were averaged according to the dotted line.*

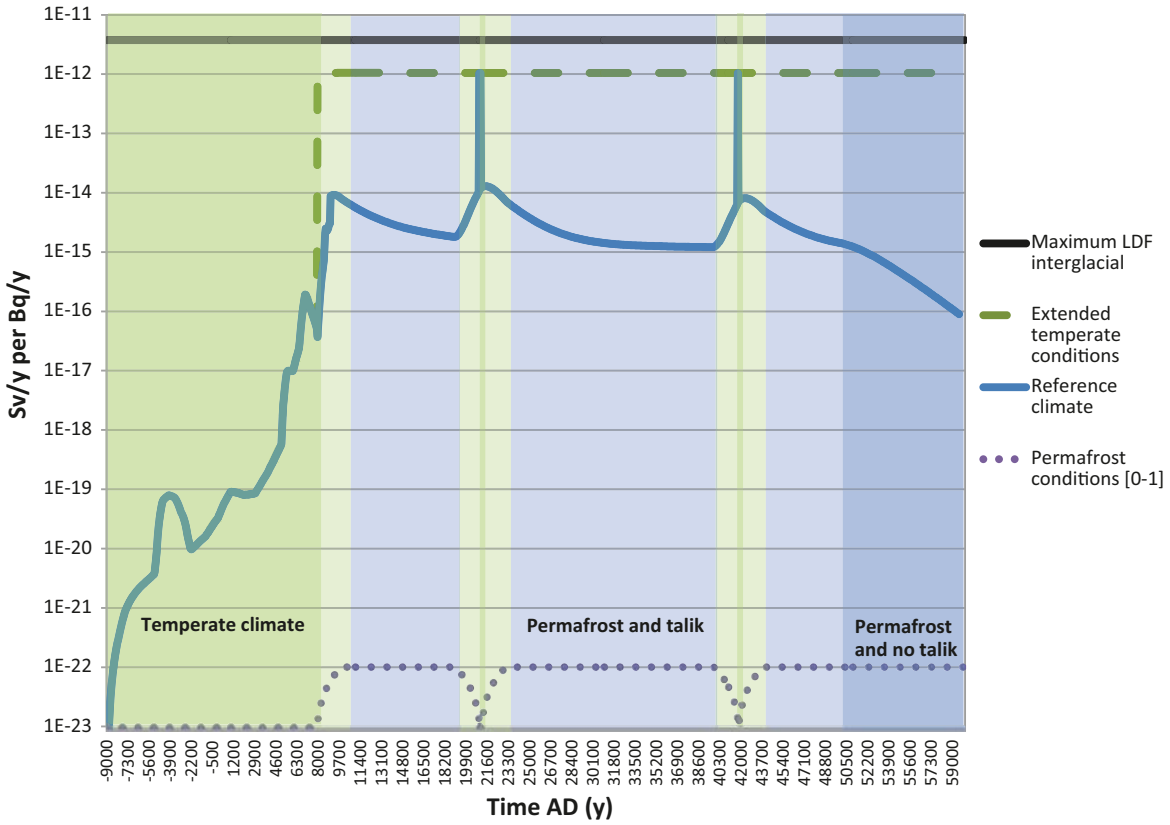


***Figure 5-17.*** *Effect of fluctuating periods of temperate and permafrost conditions on LDF for Ra-226 from simulations for object 114. In the simulation the initial 20 ky interglacial was followed by a period where long periods of permafrost are alternated with short periods of temperate climate conditions. The LDF from the simulation (blue line) is contrasted against LDF from constant temperate conditions in the object (dashed line) and the maximum LDF over all biosphere objects from interglacial conditions used in the safety assessment (black line). The spikes in the simulated LDF correspond to short periods of temperate conditions when absence of permafrost allowed use of a deep drilled well. Background colour indicate climate condition (green = temperate, blue = permafrost, yellow = transition). In the transition between temperate and permafrost conditions parameters were averaged according to the dotted line.*

### Global warming conditions

The temperate domain covers a broad range of mean annual temperatures and precipitation, spanning conditions for a global warming scenario as predicted by for example in /BIOCLIM 2003, Rummukainen 2003, Kjellström et al. 2009/. Conditions characterising global warming have not been assigned a special climate domain or a unique parameterisation in SR-Site surface system modelling. Instead the uncertainty associated with global warming has been handled by calculating the maximum *LDF* for a 40,000 year extension of the initial temperate domain (see Section 4.1). Comparison of these *LDF* values with the baseline *LDF* values shows that for the most dose contributing radionuclides, except for Cs-135, the use of the baseline *LDF* for dose calculations under global warming conditions will not lead to underestimation of the doses. In the case of Cs-135, the maximum *LDF* for global warming conditions was more than one order of magnitude higher than the baseline *LDF*. This is explained by the high retention of this radionuclide in the biosphere objects, leading to continued increase of the *LDFs* during the extended simulation period, i.e. the *LDF* do not reach equilibrium.

It was concluded from this study that these variations have a marginal effect on the *LDFs*. Parameter sensitivity analysis (see Section 5.3.1) showed runoff to be the only parameter that had any quantitatively important effect on *LDF* calculations, among all the parameters that are expected to change substantially during a warmer climate. Moreover, a warmer climate is associated with an increased runoff /Kjellström et al. 2009/ and for the examined radionuclides an increase in runoff was associated with a decrease in *LDF*.

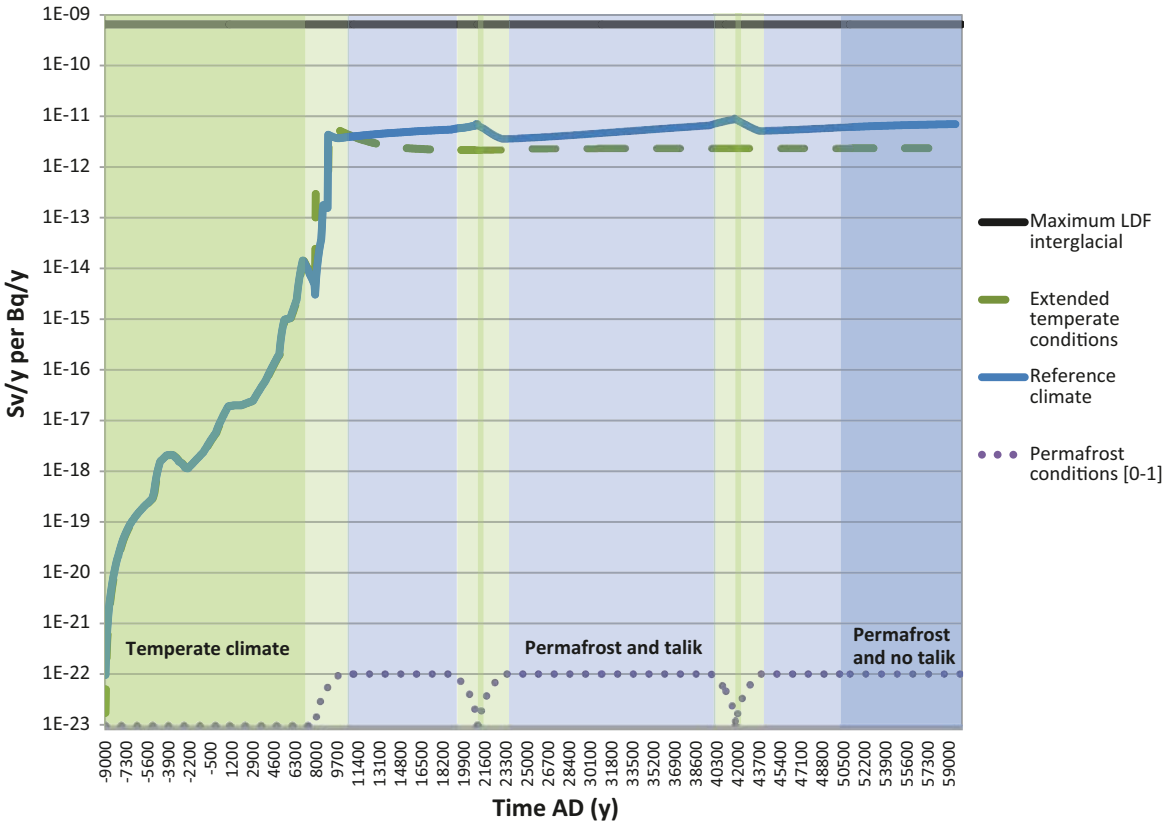


***Figure 5-18.*** *Effect of fluctuating periods of temperate and permafrost conditions on LDF for I-129 from simulations for object 114. In the simulation the initial 20 ky interglacial was followed by a period where long periods of permafrost are alternated with short periods of temperate climate conditions. The LDF from the simulation (blue line) is contrasted against LDF from constant temperate conditions in the object (dashed line) and the maximum LDF over all biosphere objects from interglacial conditions used in the safety assessment (black line). The spikes in the simulated LDF correspond to short periods of temperate conditions when absence of permafrost allowed use of a deep drilled well. Background colour indicate climate condition (green = temperate, blue = permafrost, yellow = transition). In the transition between temperate and permafrost conditions parameters were averaged according to the dotted line.*

### 5.1.2 Human utilization of natural resourses

#### *Occupancy of potentially contaminated areas*

The uncertainties with respect to the degree that future humans will inhabit contaminated areas and the extent to which they will be dependent of the natural resources in the object has been handled by cautious assumptions. Below follows a discussion on why the assumption that a representative individual of the most exposed group spend all of her/his time in the contaminated area, and get her/his full supply of food and water from the biosphere object is a cautious assumption in a cultural or landscape use perspective.

When agriculture is not possible in a biosphere object, (due to frequent salt water intrusions), most lakes and wetlands will support no more than one or a few individuals. Non-agricultural communities existing in the past or today are typically non-stationary, and it is hard to see why future inhabitants of such cultures would restrict their foraging for food to one isolated lake with a surrounding wetland in the Forsmark area. In addition, during the terrestrial phase the production from most biosphere objects could only support a fraction of the yearly energy demand of a family sized group. It is possible that a family group or a small community living in the coastal area can be fully supported by the fish production corresponding to the size of the sea basin of a biosphere object. However, these groups would be catching fish primarily from migrating stocks. Consequently, it is likely that individuals that feed only on natural food would obtain only a fraction of their diet from the most highly contaminated discharge area, and thus contaminated food would be diluted considerably.

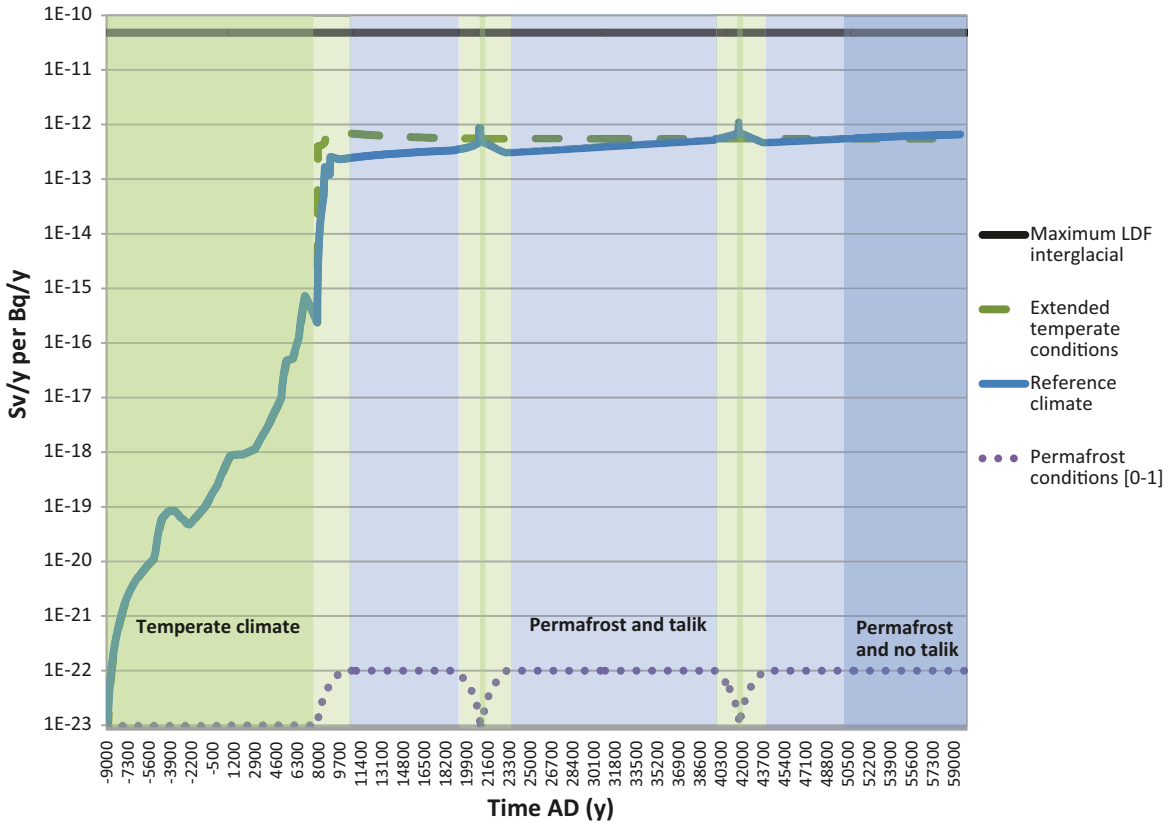


***Figure 5-19.*** *Effect of fluctuating periods of temperate and permafrost conditions on LDF for Np-237 from simulations for object 114. In the simulation the initial 20 ky interglacial was followed by a period where long periods of permafrost are alternated with short periods of temperate climate conditions. The LDF from the simulation (blue line) is contrasted against LDF from constant temperate conditions in the object (dashed line) and the maximum LDF over all biosphere objects from interglacial conditions used in the safety assessment (black line). The spikes in the simulated LDF correspond to short periods of temperate conditions when absence of permafrost allowed use of a deep drilled well. Background colour indicate climate condition (green = temperate, blue = permafrost, yellow = transition). In the transition between temperate and permafrost conditions parameters were averaged according to the dotted line.*

Sustainable agricultural is made possible only for a period of 50–100 years on drained organic soils, that might provide the only arable land in several biosphere objects /Lindborg 2010/. In contrast, the thick and partly continuous layers of clay and sand in the central parts of Öregrundsgrepen can be sustainably cultivated for thousands of years. Thus, a more realistic scenario for a future self-supporting society in the area is that the mainly low contaminated central parts of Öregrundsgrepen will be intensively cultivated and contribute the major part of the food consumed, even to the most exposed group. Some of the small biosphere objects may occasionally be cultivated and may then complement the food produced in the more suitable agricultural areas in Öregrundsgrepen, but most likely the biosphere objects will primarily be utilised for extensive collection of naturally produced food. Thus, it is concluded that the assumption of a representative individual of the most exposed group spends all his or her time in the contaminated area and gets his/her full supply of food and water from this biosphere object seems improbable given the availability of non-contaminated land in the future landscape and the organisation of present and historical societies.

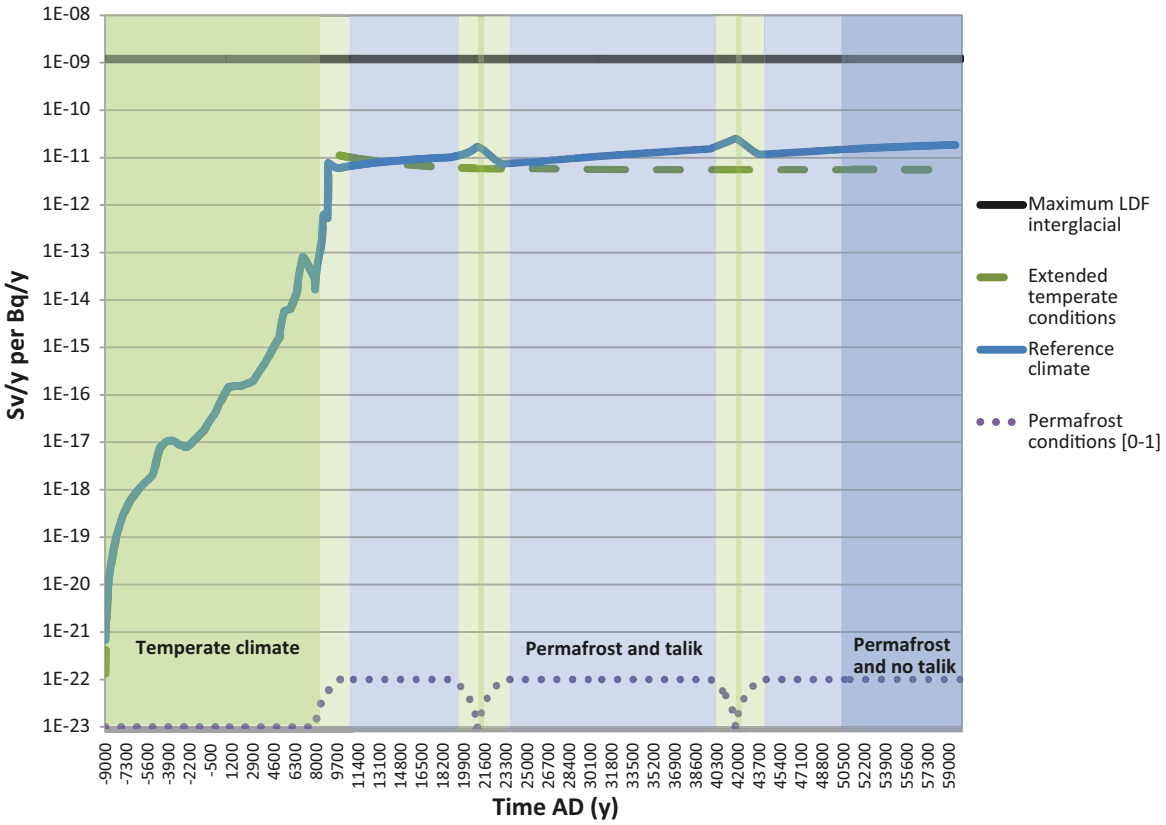


***Figure 5-20.*** *Effect of fluctuating periods of temperate and permafrost conditions on LDF for Se-79 from simulations for object 114. In the simulation the initial 20 ky interglacial was followed by a period where long periods of permafrost are alternated with short periods of temperate climate conditions. The LDF from the simulation (blue line) is contrasted against LDF from constant temperate conditions in the object (dashed line) and the maximum LDF over all biosphere objects from interglacial conditions used in the safety assessment (black line). The spikes in the simulated LDF correspond to short periods of temperate conditions when absence of permafrost allowed use of a deep drilled well. Background colour indicate climate condition (green = temperate, blue = permafrost, yellow = transition). In the transition between temperate and permafrost conditions parameters were averaged according to the dotted line.*

### Indoor exposures

Exposures from radionuclides in the environment can also take place during occupancy of indoor areas. In this case, the most important exposure pathways are external irradiation from radionuclides in the surrounding environments and inhalation of radionuclides in the indoor atmosphere. Indoor external exposures are normally lower than outdoor exposures, since buildings provide shielding against radiation emitted by radionuclides in the outside environment. The use of radioactively contaminated materials for construction of houses could in some cases lead to increased external exposures indoors. An example of relevance for this study is the use of potentially contaminated peat from mires as material for construction of houses. In the derivation of baseline *LDF* values external doses have been calculated with a dose coefficient derived under the assumption that the contaminants are homogeneously distributed in an infinite volume, with infinite surface area and depth. Hence, dose obtained with these coefficients can be expected to give cautious estimates of indoor doses in situations when radionuclides are found in construction materials at the same concentration levels as in the peat.

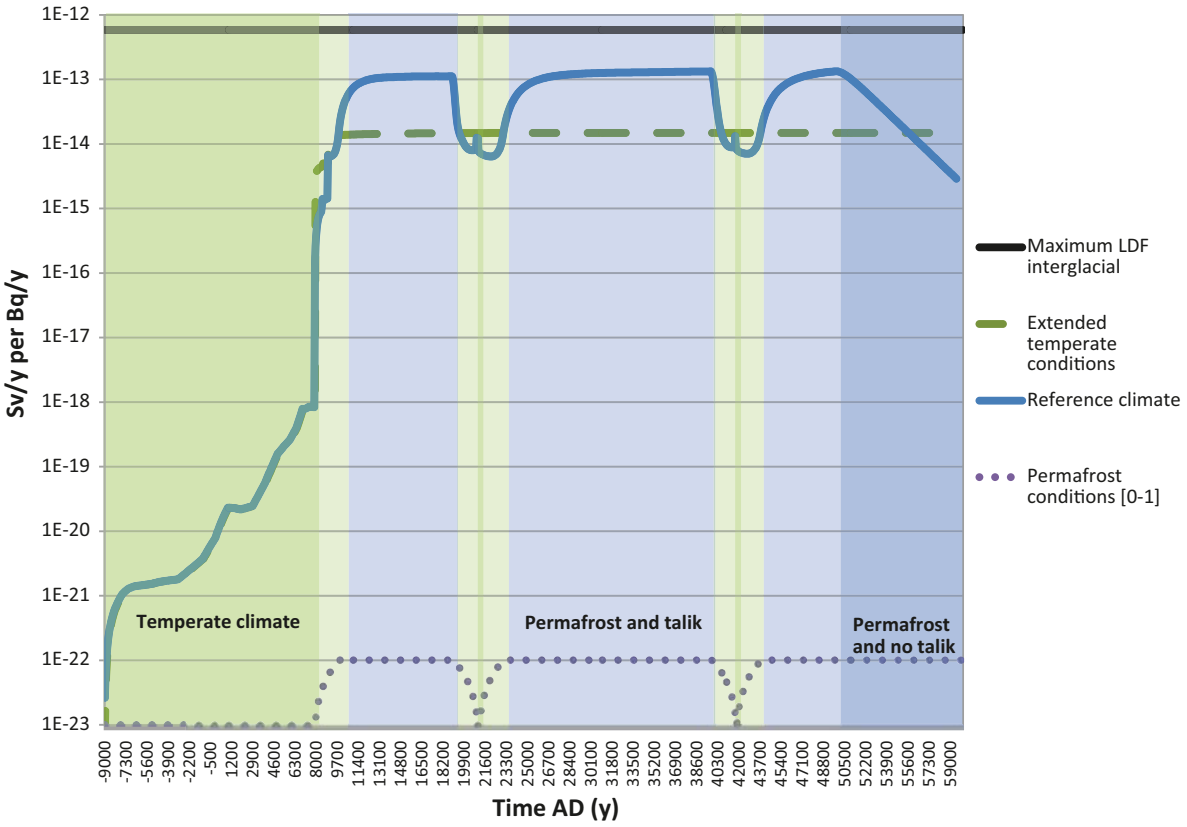


***Figure 5-21.*** *Effect of fluctuating periods of temperate and permafrost conditions on LDF for Cl-36 from simulations for object 114. In the simulation the initial 20 ky interglacial was followed by a period where long periods of permafrost are alternated with short periods of temperate climate conditions. The LDF from the simulation (blue line) is contrasted against LDF from constant temperate conditions in the object (dashed line) and the maximum LDF over all biosphere objects from interglacial conditions used in the safety assessment (black line). The spikes in the simulated LDF correspond to short periods of temperate conditions when absence of permafrost allowed use of a deep drilled well. Background colour indicate climate condition (green = temperate, blue = permafrost, yellow = transition). In the transition between temperate and permafrost conditions parameters were averaged according to the dotted line.*

Radionuclides with important dose contributions from inhalation, such as Pu, are often found in air attached to dust particles. Dust loads are normally lower indoors than outdoors and therefore indoor air concentrations of these radionuclides and the corresponding inhalation doses will be also lower. Some radionuclides can be found in the environment in gas form. Radon is an example of a gas that can penetrate buildings and in some cases accumulate in areas with deficient ventilation. Radon is an important contributor to background doses in many regions of the word, due to high inhalation doses received by people living in houses with high Radon concentrations. Although, it should be recognised that doses from Radon inhalation could have a potential impact on *LDFs* for Ra-226, these have not been included in the derivation of baseline *LDFs*. It has been considered that in conditions where doses from "repository originated" Radon could be important, these will be outset by much higher doses from "natural" Radon. There are other "repository originated" radionuclides that could also be present in gas form, e.g. C-14, I-129 and Se-79. Doses from these radionuclides from inhalation outdoors of dust have been included in the derivation of baseline *LDFs*, although they show a very small contribution to the *LDF* values. Gas releases of these radionuclides occurring outdoors will interact with dust particles in air and with different surfaces to a larger degree than radon, which is an inert gas. This reduces the likelihood that of penetration into building and that they will accumulate in the indoor air. Hence, it can be concluded that the contribution of indoor inhalation doses to the total doses will also be small. Hence, it has been concluded that the approach for calculation of inhalation doses that was used in the derivation of baseline *LDF* values, i.e. considering exposures outdoors during 100% of the time; does not lead to significant underestimation of the *LDF* values. The treatment and evaluation of uncertainties associated with gas releases is discussed in Section 5.2.3.

### *Use of well water water for drinking*

The potential contribution to exposure from wells contaminated by radionuclide releases has been evaluated by assuming that all radionuclide releases are intercepted by a well drilled in the bedrock. The activity concentration in the well water has been calculated by dividing the release rate (1 Bq/year) to the biosphere by the well capacity, assuming that the release is completely captured by the wells annual recharge. The release into the well is made independently of the release into the biosphere object of 1 Bq/year. This handling is cautious as compared to assuming that the release either would transect a well or reach a biosphere object (as assumed in previous biosphere assessments). The overestimation of the doses will be pronounced for radionuclides with important contributions to the doses, from ingestion of water and food. However, the effect of this cautious handling on *LDF* calculations will not exceed a factor two, as compared to a more realistic handling.

The uncertainty of what type of water source will be used for drinking in the contaminated area has been handled by assuming that it is equally likely that humans and livestock will use surface water and water from the well affected by the release. The degree of cautiousness in this assumption was quantified by calculating *LDF* values for the alternative assumption that no release would reach a drilled well. This simulation has shown that for short-lived radionuclides (half-life < 100 years) the well water consumption was the dominating exposure pathway by two or more orders of magnitude. For longer lived radionuclides the well was a less important pathway for exposure (Figure 5-22). Among them, the highest contribution from consumption of well water was observed for Am-241 and Th-229, which have relatively short half lives in comparison with the other long-lived radionuclides considered. From this comparison, it was concluded that for radionuclides expected to contribute to dose, Ra-226 was the only radionuclide to be affected by the handling of the uncertainty associated with the use of contaminated well water. For Ra-226 the *LDF* decreased by a factor two when consumption of contaminated well water was disregarded.

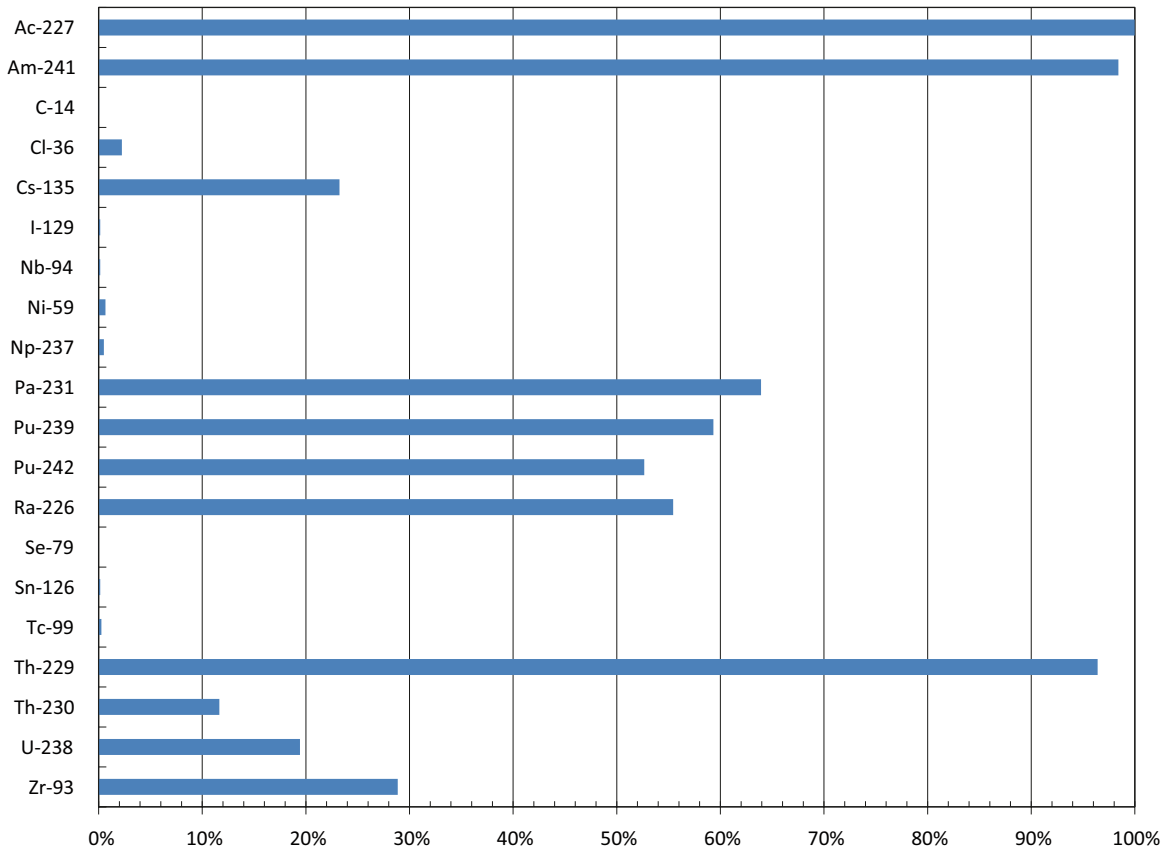


***Figure 5-22.*** *Estimated contribution (in %) to the baseline LDF values of doses from consumption of well water.*

### *Use of well water for short-term irrigation*

In the Forsmark area, stream or lake water will be readily available in most biosphere objects and drainage water can be stored for periods of drought. Irrigation with well water is therefore considered to be unlikely in the area /Löfgren 2010/, and consequently it was assumed for *LDF* calculations, that vegetables are only irrigated with contaminated surface water. However, as irrigation with water from a drilled well cannot be totally excluded, this uncertainty was examined by calculating *LDF* values under the alternative assumption that well and surface water are equally likely to be used for irrigation.

Irrigation by well water increased activity concentrations in vegetables somewhat for most examined radionuclides, but the effects on the *LDFs* of radionuclides expected to contribute to dose was typically below a factor two (Figure 5-23). From this comparison it was clear that the handling of the uncertainty associated with the use of well water for irrigation did not affect the *LDF* values for these radionuclides, with the exception of Ra-226. For Ra-226, the *LDF* increased by a factor two when well water was considered for irrigation.

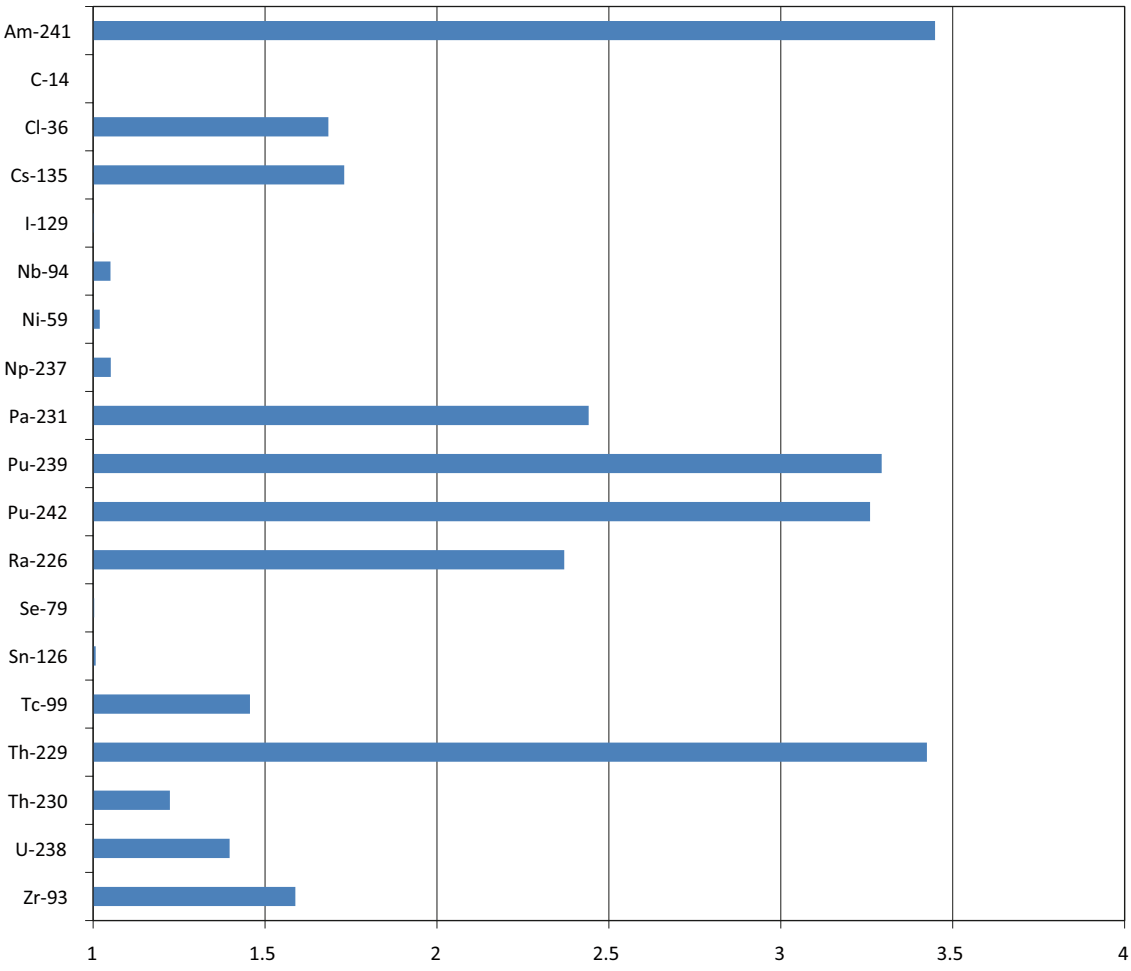


***Figure 5-23.*** *Ratio between LDF values obtained under the assumption that surface and well water contribute equally to short term irrigation and the baseline LDF values, which only consider irrigation with surface water.*

### *Long-term irrigation*

Use of organic soils that originate from drained wetlands in the Forsmark area is expected to be productive for agriculture only during a limited time (50–100 years), and consequently long-term use of arable land has not been considered in the *LDF* calculations. However, future shallow wetlands of Öresundsgrepen can probably be drained relatively easily, and the underlying minerogenic deposits can be sustainably cultivated for thousands of years.

An alternative simulation was conducted under the assumption that initially uncontaminated deposits of glacial and post-glacial clay in Öresundsgrepen were cultivated and irrigated for 10,000 years with contaminated surface water. Figure 5-24 shows the ratio between the maximum value of concentration in vegetables when long-term irrigation is considered and the concentration in vegetables obtained from simulations for derivation of the baseline *LDF* values. The results show that activity concentrations in vegetables were typically two orders of magnitude lower than those resulting from draining and cultivating a wetland in an adjacent contaminated discharge area. That is, the accumulation of radionuclides in the wetland is much higher than accumulation resulting from long term irrigation. It was concluded from these simulations that the consequences of disregarding contamination through long-term irrigation were insignificant.

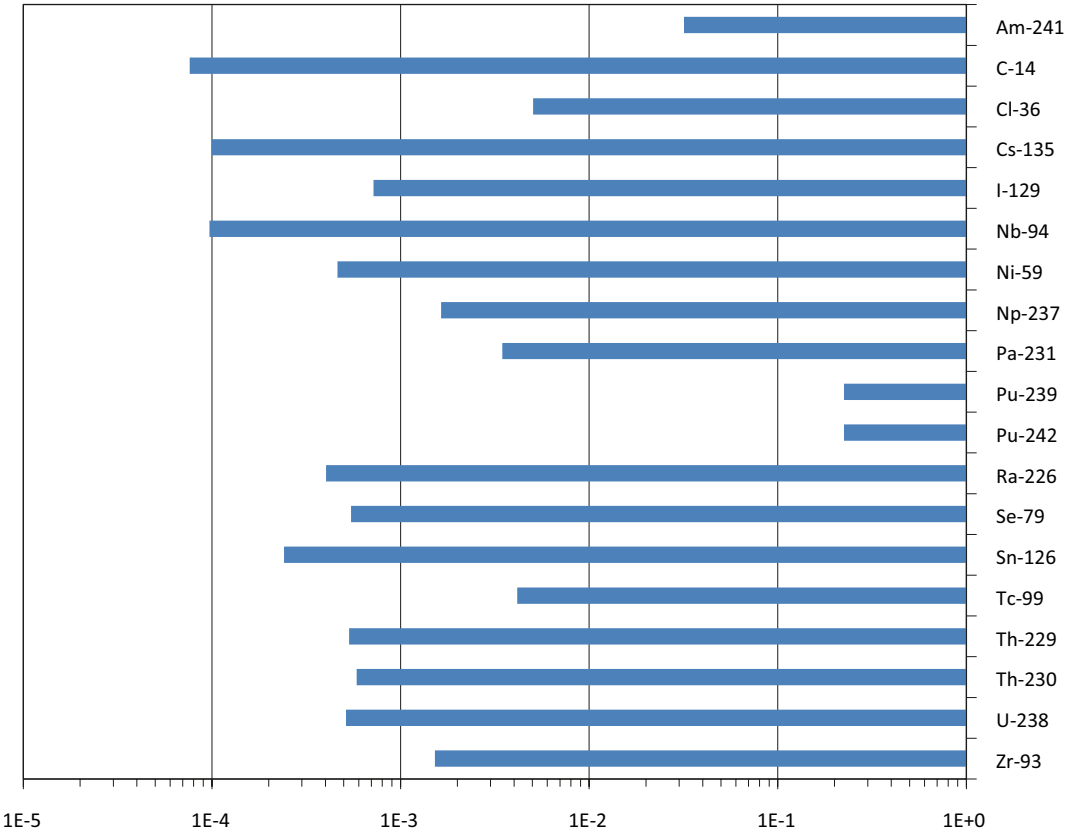


***Figure 5-24.*** *Ratio of the concentration in vegetables obtained for the case when long-term irrigation with surface water is considered to the concentration in vegetables used in the derivation of baseline LDF values.*

### *Use of potentially contaminated areas for food supply*

In the derivation of baseline *LDF* values no specific dietary composition has been pre-defined for calculation of doses from food ingestion. Instead, it has been assumed that future human inhabitants will maximally utilize all available food sources in a biosphere object, and that the contribution of food types to the diet is proportional to the production capacity of the food types. The uncertainty associated with the use of contaminated terrestrial areas for food supply has been handled by assigning an equal probability to all land uses considered possible. Consequently, the diet during periods when agriculture is possible will be dominated by root crops, cereals and vegetables, with minor contributions from meat, milk and natural food (Table 5-3).

The effect of uncertainty with respect to human land use on *LDF* values was examined by two probabilistic simulations. In the first simulation the human diet implicitly used in the calculations, was varied between iterations in the Monte Carlo simulations. This was done by varying the productivity of the different food types using PDFs that reflect uncertainty in their values and by a random allocation of the terrestrial land for production of different agricultural crops and natural food. Monte Carlo simulations were carried out under the constraint that probabilities of different uses of the land should sum to one. In the second simulation, in addition to the variation of the implicit diet, the activity concentrations in different food types were also varied using samples generated from Monte Carlo simulations for the study of parameter uncertainties (see Section 5.3).

Examples of results obtained from these simulations are shown in Figures 5-25, 5-26 and 5-27 for Ra-226, I-129 and Cs-135, respectively. The simulations showed that the uncertainty in estimates of food ingestion doses is dominated by the uncertainty in radionuclide activity concentrations in different diet components. The contribution of this uncertainty was an order of magnitude larger than the contribution from uncertainty in the implicit diet. The later uncertainty is caused by uncertainty in the land use and in the productivity of different food types. Consequently, uncertainty with respect to human diet had a small relative effect on dose from food ingestion, and the differences between deterministic calculations for derivation of baseline *LDF* values and the expected value from including uncertainty with respect to land use and productivity was within a factor two. It was concluded from these simulations that the handling of the uncertainty with respect to human land use and productivity of food types had no significant influence on the *LDFs*.

**Table 5-3. Productivity of food items considered in the calculations of food ingestion doses and relative contribution to the total production of food are presented for two situations: i) the terrestrial area is not used for agriculture and ii) different uses of the land for food production, including agriculture are equally likely. A typical contemporary diet derived from food statistics is also presented for comparison.**

| | Production | | | Diet from food statistic | |
|---|---|---|---|---|---|
| | Productivity ($kgC\ m^{-2}\ y^{-1}$) | Relative | | ($kgFW\ y^{-1}$) | |
| | | Without agriculture[a] | With agriculture[a] | | Relative |
| Milk | 0.030 | | 7.2% | 115[b] | 12% |
| Meat | 0.001 | | 0.3% | 72 | 14% |
| Vegetables | 0.135 | | 33% | 51 | 3% |
| Tuber | 0.127 | | 31% | 84 | 14% |
| Cereal | 0.114 | | 28% | 71 | 45% |
| Fruit | | | | 23.5 | 2% |
| Fish | $2.7 \cdot 10^{-4}$ | 47.9% | 0.3% | 27 | 4% |
| Crayfish | $3.1 \cdot 10^{-5}$ | 5.7% | 0.04% | 1.7 | 0.2% |
| Berries | $1.3 \cdot 10^{-4}$ | 22.9% | 0.03% | 4.25 | 0.4% |
| Mushrooms | $1.2 \cdot 10^{-4}$ | 22.0% | 0.03% | 1.3 | 0% |
| Game | $8.3 \cdot 10^{-6}$ | 1.5% | 0.002% | 25 | 5% |

[a] equal land and lake area assumed,
[b] unit is litre per year.

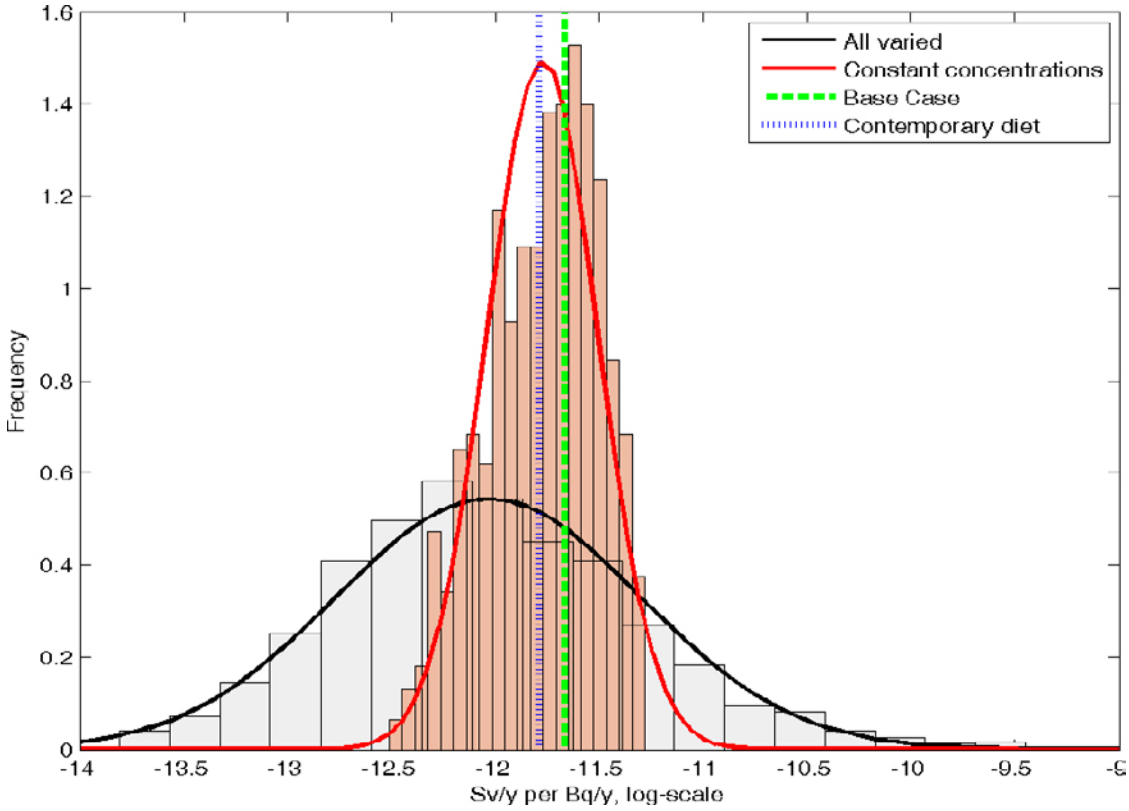


***Figure 5-25.*** *Distribution of Ra-226 (and daughter radionuclide) doses from food ingestion obtained from probabilistic simulations for two cases: (a) the concentrations in foods are kept constant in the simulations, whereas the productivity of different foods and the use of the land are varied probabilistically and (b) all variables used in the food dose calculations (concentrations in food, productivity of the foods and use of the land) are varied in the simulations. The vertical blue line shows the deterministic values obtained in the derivation of baseline LDF values and green vertical lines shows the values obtained when a pre-defined dietary composition is assumed.*

### *Diet of potentially exposed individuals*

The baseline *LDFs* used in SR-Site were also contrasted against the dose from ingestion of contaminated food that would result if a diet derived from contemporary Swedish food statistics (Table 5-3) is used in the dose calculations. Examples of results from these calculations are shown in Figures 5-25, 5-26 and 5-27. The differences in *LDFs* for nuclides expected to contribute to dose was typically within a factor two. However, for Np-237, which gave peak exposure from natural foods, the baseline *LDF* was an order of magnitude larger than the *LDF* from the alternative diet. The reason for this is that in the calculation of baseline *LDFs* the contribution from natural foods was not diluted by uncontaminated agricultural products.

### *Other uses of potentially contaminated areas*

In the derivation of *LDFs* a maximal use of potentially contaminated areas has been assumed. External irradiation and inhalation doses have been calculated to individuals that stay 100% of the time in the terrestrial part of the most contaminated objects, where exposure by these pathways are the highest. Hence, it can be concluded that the calculations done will bound other occupancy-elated uses of the contaminated biosphere objects, i.e. those uses that can lead to additional exposures by external irradiation and inhalation. Examples of occupancy-related uses of biosphere objects are: recreational activities like sunbathing and fishing, work related activities such as farming and construction works, etc. Doses from food and water ingestion have also been calculated under cautious assumptions (see above) regarding the extent by which potentially affected areas and resources are used. Moreover, all potential dose contributors to these doses have been considered. Hence, it can be

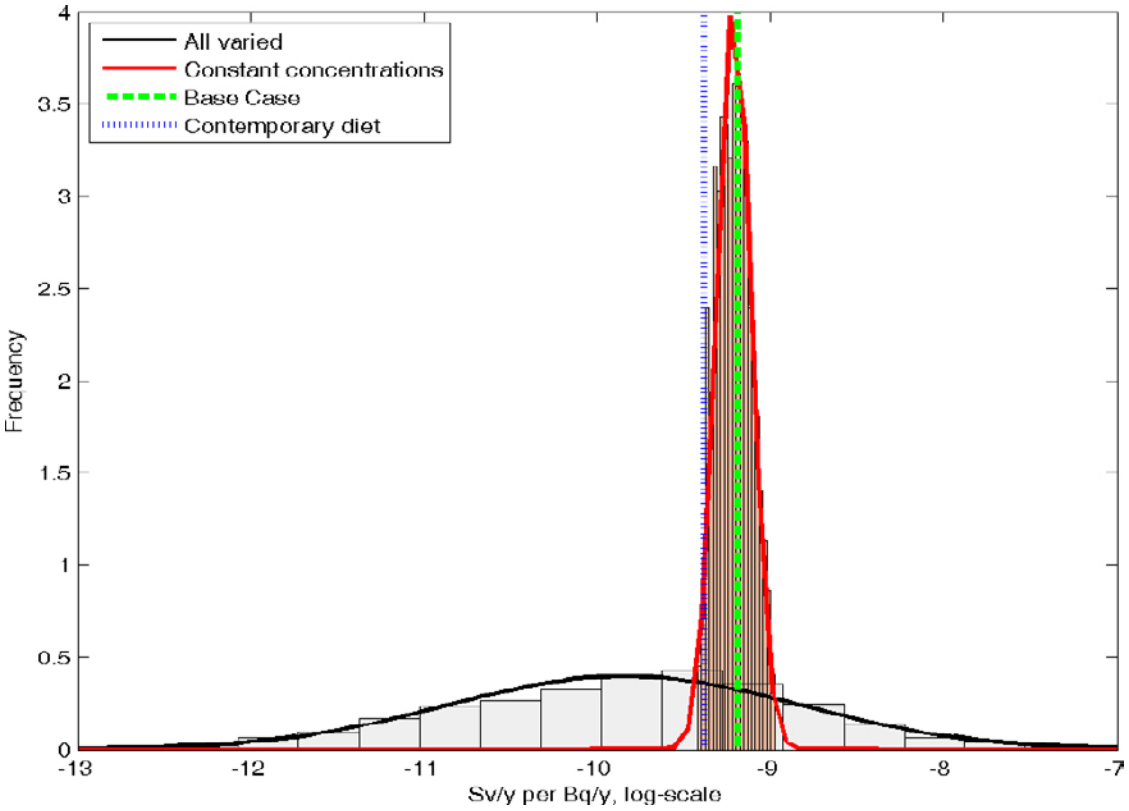


***Figure 5-26.*** *Distribution of I-129 doses from food ingestion obtained from probabilistic simulations for two cases: (a) the concentrations in foods are kept constant in the simulations, whereas the productivity of different foods and the use of the land are varied probabilistically and (b) all variables used in the food dose calculations (concentrations in food, productivity of the foods and use of the land) are varied in the simulations. The vertical blue line shows the deterministic values obtained in the derivation of baseline LDF values and green vertical lines shows the values obtained when a pre-defined dietary composition is assumed.*

stated that in the derivation of baseline *LDF* values all exposure pathways have been considered and in most cases treated cautiously. Therefore, it is reasonable to expect that the derived baseline *LDFs* will cover a large variety of possible uses of the biosphere objects. Additional uses of potentially contaminated objects that could be of interest are those that lead to increases of radionuclide concentration in environmental media. An example is the use of peat from the mires as combustible, which could lead to increased radionuclide concentrations in air due to gas releases. However, studies of this use of the biosphere objects, performed in previous safety assessments /SKB 1999/, have shown that the contribution to human exposure from all related exposure pathways is insignificant in comparison with other uses of the object.

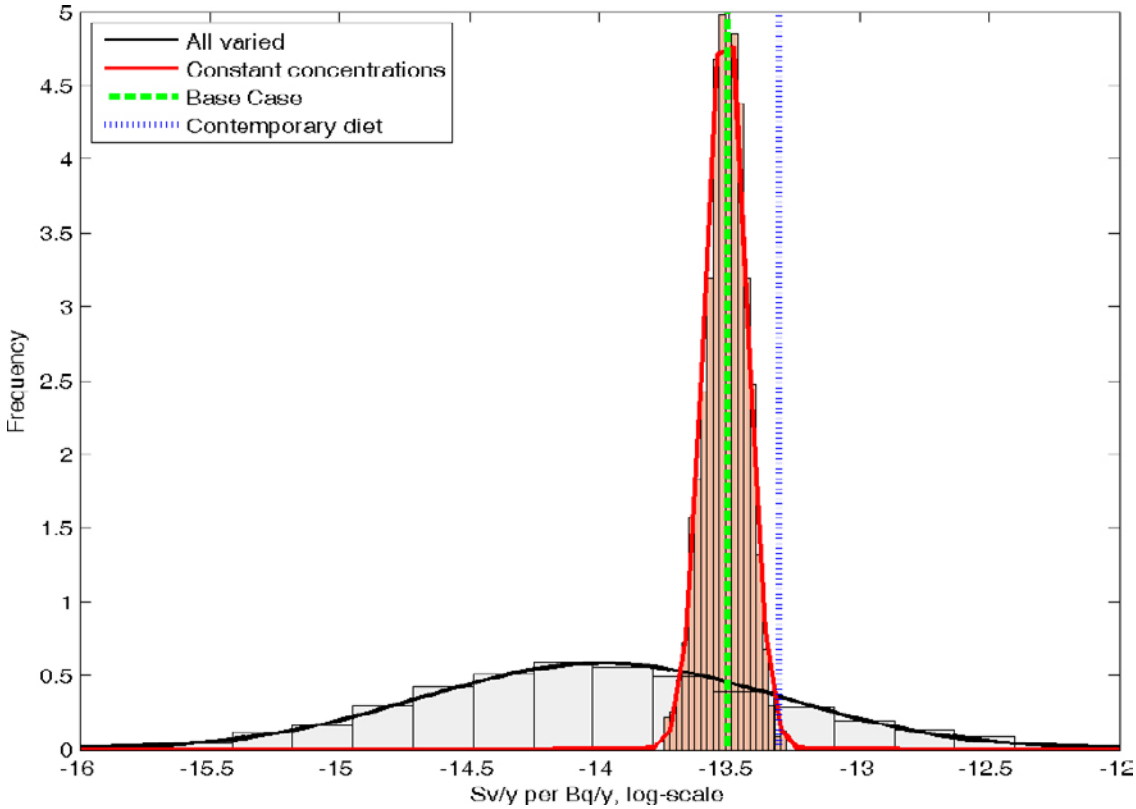


***Figure 5-27.*** *Distribution of Cs-135 doses from food ingestion obtained from probabilistic simulations for two cases: (a) the concentrations in foods are kept constant in the simulations, whereas the productivity of different foods and the use of the land are varied probabilistically and (b) all variables used in the food dose calculations (concentrations in food, productivity of the foods and use of the land) are varied in the simulations. The vertical blue line shows the deterministic values obtained in the derivation of baseline LDF values and green vertical lines shows the values obtained when a pre-defined diet composition is assumed.*

## 5.2 Model uncertainties

Model uncertainty is defined in this report as the collective uncertainty present in Radionuclide Model for the biosphere, excluding parameter uncertainty which is discussed in Section 5.3 and numerical uncertainty in the integration of the models, which is discussed in Section 5.4. Sources of model uncertainty are those assumptions, approximations or choices made during model development and application for which reasonable alternative solutions may exist /Hansen 2010/. In this study, evaluation of model uncertainty has comprised both quantitative and qualitative analyses of the assumptions made for handling different uncertainties. The quantitative analyses have consisted of performing simulations with alternative assumptions and models to derive alternative *LDF* values which are then compared with the baseline *LDF* values. A list of the uncertainties considered is provided in Table 5-4, where the approach adopted for their treatment and evaluation is also provided. The last column in this table shows codes assigned to those uncertainties that were evaluated quantitatively. These codes have been used as identifiers of the different uncertainties in figures presented in Section 5.6.

**Table 5-4. Summary of studied model uncertainties and supporting assessments for their evaluation.**

| Source of uncertainty | Treatment | Evaluation | Code* |
|---|---|---|---|
| *Model discretisation* | | | |
| Size of the biosphere objects | The size of biosphere objects equals the size of sea/lake basin. Basin 121 divided into three biosphere objects.<br>(cautious assumption) | Simulations with basin 121 as one biosphere object. | H |
| Discretisation of the lower regolith | The lower regolith compartment is represented by a single compartment.<br>(cautious assumption) | Simulations with a finer discretisation of the lower regolith. | I |
| Disregarding contamination from upstream objects | The approach applied for calculating the LDF values disregards the contamination from upstream objects.<br>(simplifying assumption) | Simulations with the whole landscape model, i.e. considering all biosphere objects. | J |
| *Vertical transport and retention of radionuclides in the regolith* | | | |
| Representation of diffusion | Vertical transport by advection and diffusion considered.<br>(simplifying assumption) | Simulations disregarding diffusion. | K |
| Representation of advective transport from the lower regolith | In the simulations advective transport increases from sea to lake/terrestrial stages.<br>(simplifying assumption) | Simulations assuming constant high advection.<br>Simulations assuming constant low advection. | L<br>M |
| Limitations of the $K_d$ approach | Distribution coefficients ($K_d$) to model the retention of radionuclides.<br>In the deterministic simulations the same $K_d$ values were used for different organic and inorganic regolith layers.<br>(simplifying assumption) | In the probabilistic simulations the $K_d$ values of different layers were treated as distinct parameters. | |
| | It is assumed that sorption of radionuclides is reversible and is rapid compared to flow rates.<br>(simplifying assumption) | Qualitative discussion on the limitations of the $K_d$ approach. | |
| *Uptake of radionuclides by biota* | | | |
| Limitations of the CR approach | Concentration ratios are used to calculation radionuclide transfer to biota.<br>Except for C-14, it is assumed that radionuclides are taken up by the vegetation from the soil, i.e. uptake from air is neglected.<br>(cautious assumption) | Qualitative discussion on the limitations of the CR approach. | |
| | It is assumed that there is linear relationship between the radionuclide concentrations in soil and in the plant.<br>(simplifying assumption) | | |

* Uncertainties that were evaluated quantitatively.

### 5.2.1 Model discretisation

Several characteristics of the biosphere objects (including area of sub-catchment, timing of emergence from the sea and depth of regolith layers) affect the transport and accumulation of radionuclides. Some of these are related to the size of the object. For example, the steady state activity concentration in surface water is primarily determined by the watershed area of the object, and the steady state concentration in the wetland peat is primarily determined by the object sub-catchment area.

The biosphere objects that yield the highest environmental activity concentrations are objects with small sub-catchment areas and no inflow of surface water from upstream watersheds (Figure 5-28). These objects can typically support around 80 individuals from agriculture, and the most extreme object has a small sub-catchment area (0.24 $km^2$) that is only three times as large as the lake/wetland area. In theory smaller biosphere objects, with smaller sub-catchments, could sustainably support a group of approximately 10–20 individuals. However, a thorough analysis of the Forsmark landscape failed to identify any potential discharge area (biosphere object) with a sub-catchment area less than 0.24 $km^2$ that is likely to persistently receive releases from the repository /Lindborg 2010/.

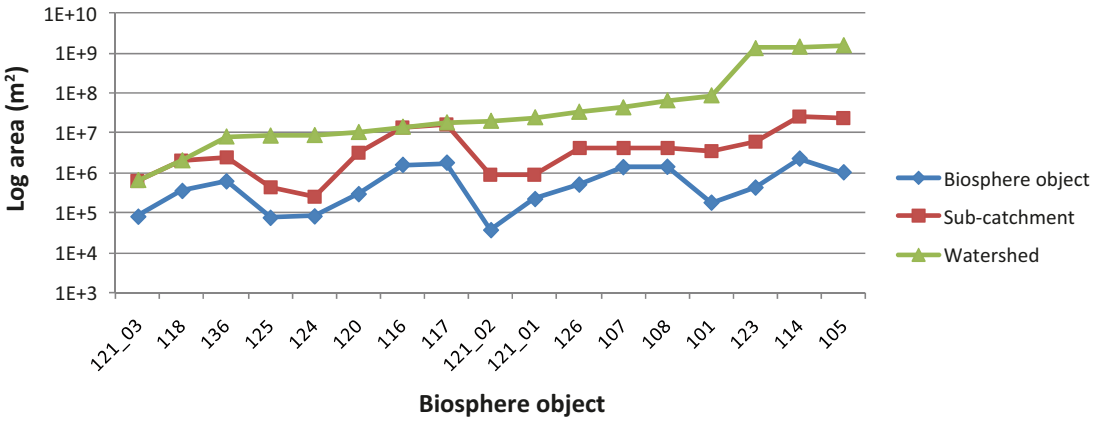


***Figure 5-28.*** *Areas of the biosphere objects and of their sub-catchment and watershed. Objects are sorted in ascending order of the watershed area.*

The basin of one of the biosphere objects (121), initially identified during the development of the landscape model /Lindborg 2010/, was partitioned into three separate biosphere objects in order to be able to represent direct radionuclide releases into a stream or a wetland, without going through a lake stage. These three sub-divided objects were included in the derivation of baseline *LDF* values. One of these objects, 121_3, turned out to be small with respect to both area of the sub-catchment and watershed. Thus, to examine the effect of the subdivision of object 121 on the *LDF* values, an alternative simulation was performed where object 121 was kept undivided and an alternative *LDF* was obtained from this simulation. A comparison of the baseline *LDF* with the alternative *LDF* is shown in Figure 5-29. The *LDF* of most radionuclides was lower when the undivided object 121 was used. However, as several other small biosphere objects were included in the assessment and the contribution from the well is independent of the size of the objects, the effect of the sub-division of object 121 on the maximum *LDF* was small. Among radionuclides expected to contribute to the dose, only I-129 and Se-79 were significantly affected by the sub-division of object 121 (by a factor two and three respectively).

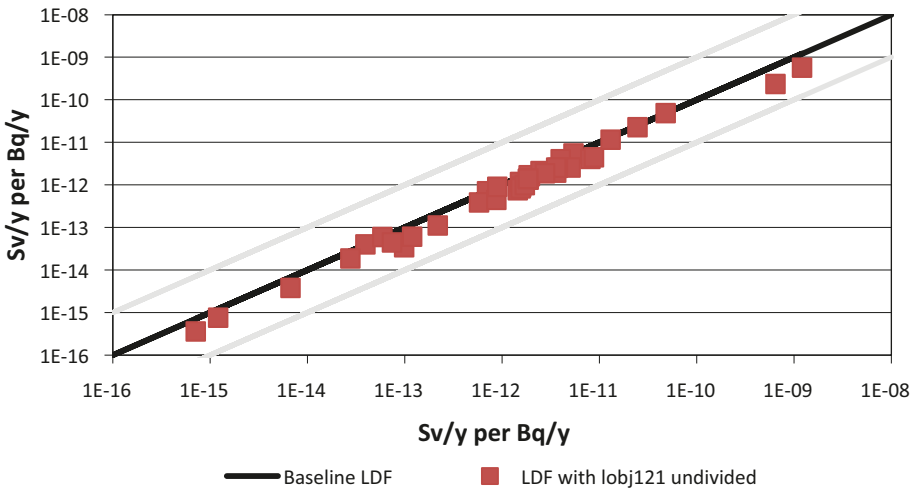


***Figure 5-29.*** *Comparison of baseline LDFs for the studied radionuclides with the alternative LDFs obtained from simulations with the undivided object 121. The solid line represents a 1:1 relationship between the baseline and alternative LDFs.*

### *Discretisation of the lower regolith*

In the Radionuclide Model for the biosphere the lower regolith is represented by a single compartment, which will tend to produce earlier breakthrough and more dispersion than if the lower regolith is represented as multiple compartments. To examine the effect of dilution and dispersion in the lower regolith on the *LDFs*, a supporting simulation was carried out using an alternative version of the Radionuclide Model with a finer discretisation of the lower regolith compartment, i.e. the regolith compartment was split into several compartments stacked on top of each other. All other settings and assumptions in the simulation were the same as in the simulation for derivation of baseline *LDF* values.

Examples of results from this analysis are presented in Figure 5-30, which shows the ratio between the *LDFs* obtained with the alternative Radionuclide Model and the baseline *LDF* values. The *LDFs* for low and moderate sorbing radionuclides, such as Cl-36, Tc-99, I-129, Np-237 and Se-79, were not significantly affected by the finer discretisation. The *LDFs* of more highly sorbing radionuclides, such as Ra-226 and Cs-135, also did not show significant differences from baseline *LDFs*. For these radionuclides, the exposure by ingestion of contaminated well water had an important contribution to the alternative *LDF* values. As it can be seen from comparing Figures 5-31 and 5-22, the well contribution is much higher on the alternative than on the baseline *LDFs*. This compensates the reducing effect on the *LDFs* of a finer discretisation of the regolith. Hence, from these supporting simulations it can be concluded that a finer discretisation of the lower regolith compartment did not result in *LDFs* that are significantly different from the baseline *LDFs*. Moreover, for radionuclides with the highest effects from a finer discretisation, the single-compartment representation lead to cautious baseline *LDF* estimates; e.g. the alternative *LDF* of Cs-135 obtained with a finer discretisation was a factor of five lower than the baseline *LDF*.

### *Disregarding contamination from upstream biosphere objects*

The *LDF* were derived from simulations where a constant release rate was applied to each biosphere object during the whole simulation period; disregarding the effect on downstream objects. This was considered an appropriate approximation for finding maximum doses in the landscape over the simulation period. An alternative simulation was carried out confirm that this way of derivation of *LDF* values does not lead to their underestimation. In the alternative simulation the releases were directed to each of the objects during the whole simulation period and *LDF* values were calculated for the receptor object and all other objects in the landscape. Such a simulation was repeated as many times as there are biosphere objects in the landscape model; with a different biosphere object being the receptor of the releases in each repetition.

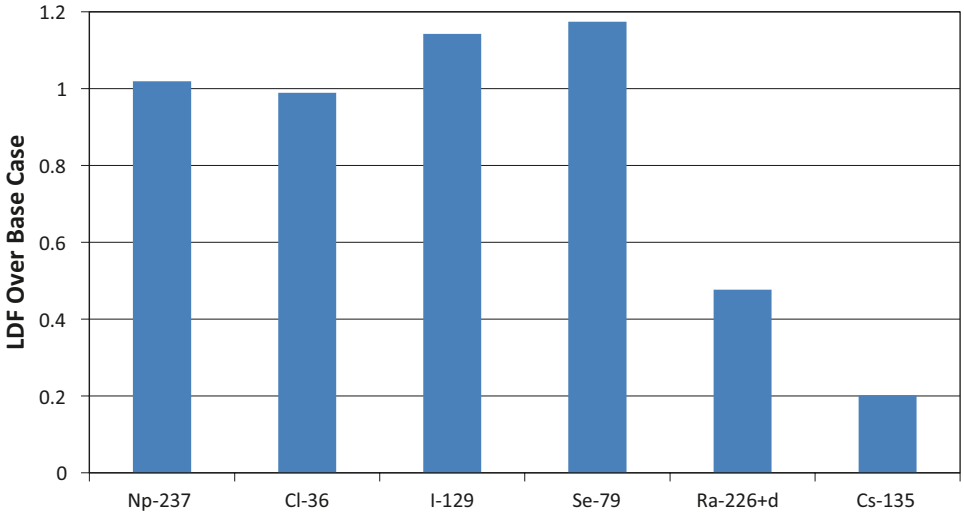


***Figure 5-30.*** *Ratio of LDF values obtained for the case with a finer discretisation of the lower regolith compartment to the baseline LDF values.*

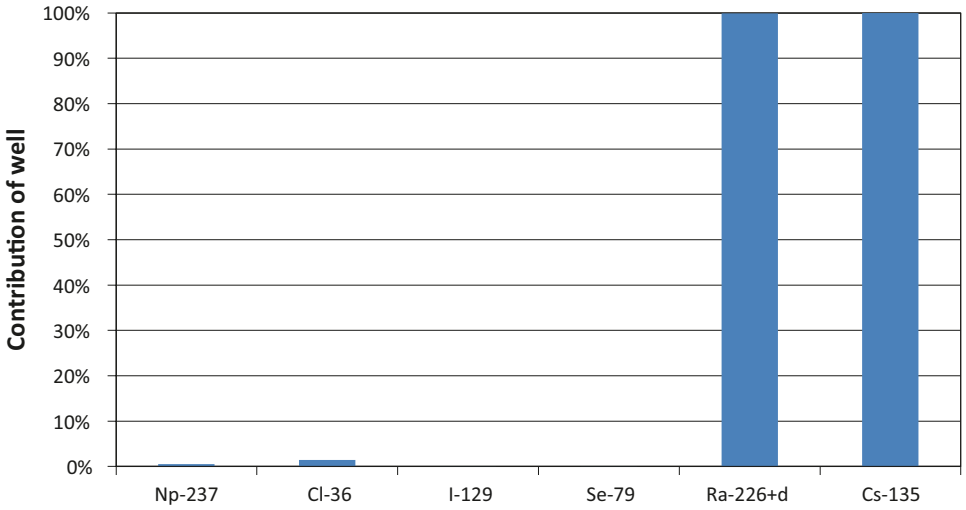


***Figure 5-31.*** *Estimated contribution of the well to the LDF values obtained with a finer discretisation of the lower regolith compartment.*

Figure 5-32 presents an example of the simulation results for the case of constant unit release rates directed to object 136 during the whole interglacial period. It can be seen that the *LDF* for object 136 is higher than the *LDF* for downstream objects. The same pattern of results has been obtained from simulations when other objects in the landscape are receptors of releases from the geosphere.

The alternative simulations also showed that, for some biosphere objects, releasing to their upstream objects may give higher *LDFs* than when releasing to these objects. To see if this could have an impact on the final *LDFs,* the maximum *LDF* over time and across all objects in the landscape was also extracted. This means that each simulation with releases to an object gave a maximum *LDF* value across all objects in the landscape. Then, the maximum *LDF* from all these simulations was found and compared with the baseline *LDF*. The comparison showed that these were identical. From these simulations it was concluded that considering direct release to separate biosphere object and taking the maximum across all objects, will give a realistic or cautious *LDF*, as compared to results with more complex models where all objects and connections are explicitly modelled.

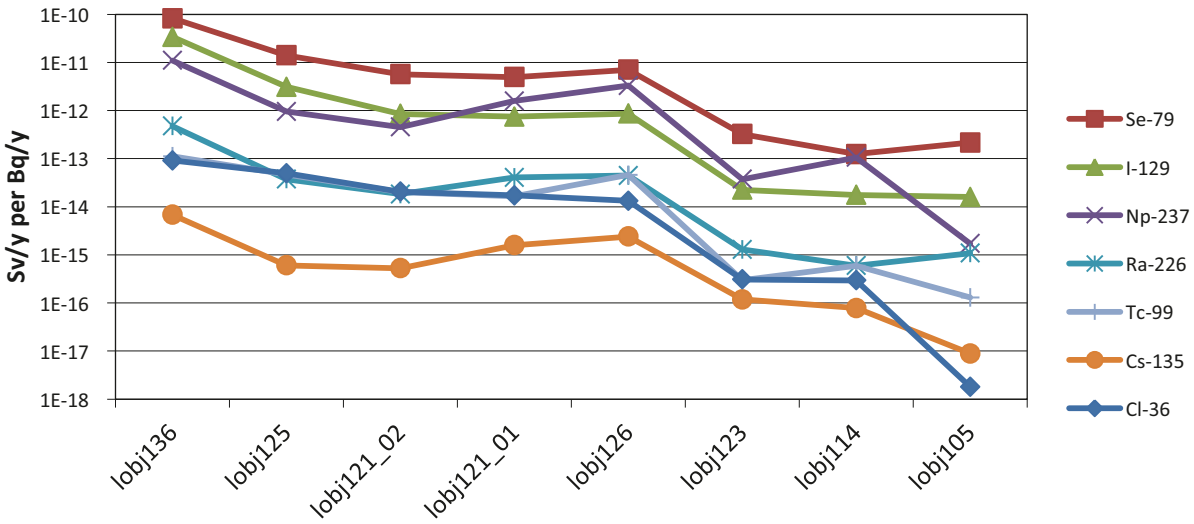


***Figure 5-32.*** *LDFs obtained for different interconnected objects in the same chain. Radionuclides were released at a constant rate to the lower regolith of biosphere object 136. Biosphere objects downstream were contaminated through surface water. LDFs are maximum values from an interglacial period. Biosphere objects appear in the same order as in the chain from left to right.*

### 5.2.2 Transport and retention of radionuclides

#### *Representation of diffusion*

In the Radionuclide Model for the biosphere the vertical transport of radionuclides in the regolith is driven by advection and diffusion. There are uncertainties associated with the description of diffusion in situations when vertical water fluxes vary both in time and space. To quantify the relative contribution of diffusion to the vertical transport of radionuclides and how it affected the *LDF* estimates, simulations with an alternative model disregarding diffusion were carried out (by setting diffusion coefficients to zero). Results from this analysis (Figure 5-33) showed *LDFs* to be insensitive to the consideration of diffusion in the model and the difference between *LDFs* including or excluding diffusion was within a factor two. Therefore, it is concluded that uncertainties associated with the representation of diffusion in the radionuclide model has no significant effect on the *LDFs*.

#### *Representation of advective transport from the lower regolith*

In the simulations for derivation of *LDFs* a constant unit radionuclide release rate is applied to the lower regolith during the whole simulation period. At the same time, it is assumed that the upward water flow rate from the lower regolith increases by a factor of five when biosphere objects are transformed from sea basins into lakes or mires. This increased flow rate will be associated with a proportional decrease in the steady state inventory of long-lived radionuclides in the lower regolith. Thus, in the model, radionuclides may potentially be flushed out from the lower regolith when the biosphere object is under transgression.

However, groundwater flow and transport from the geosphere to the biosphere is also expected to change when the site develops from submerged to terrestrial conditions. For example, in the MARFA flow transport simulation, that illustrates the effect of varying flow conditions on final risk estimates, the flow scaling factor for submerged conditions is a factor of five smaller than the corresponding factor for terrestrial temperate conditions. No effects from flushing of radionuclides would be expected if this change in release rate to the biosphere was factored in to the biosphere simulations.

To evaluate to what extend a potential flush of radionuclides accumulated in the lower regolith, associated with the coastline passage, can affect the *LDF* values, two alternative simulations were carried out. In one simulation a constant lower value of the flow rate from the lower regolith (corresponding to water flow rate in the sea stage) was used. In the other simulation a constant higher value of the flow rate from the lower regolith (corresponding to water flow rates in the terrestrial stage) was used. In both these simulations the flow rates were kept constant during the whole simulation period and therefore the flush of radionuclides accumulated in the regolith will not occur.

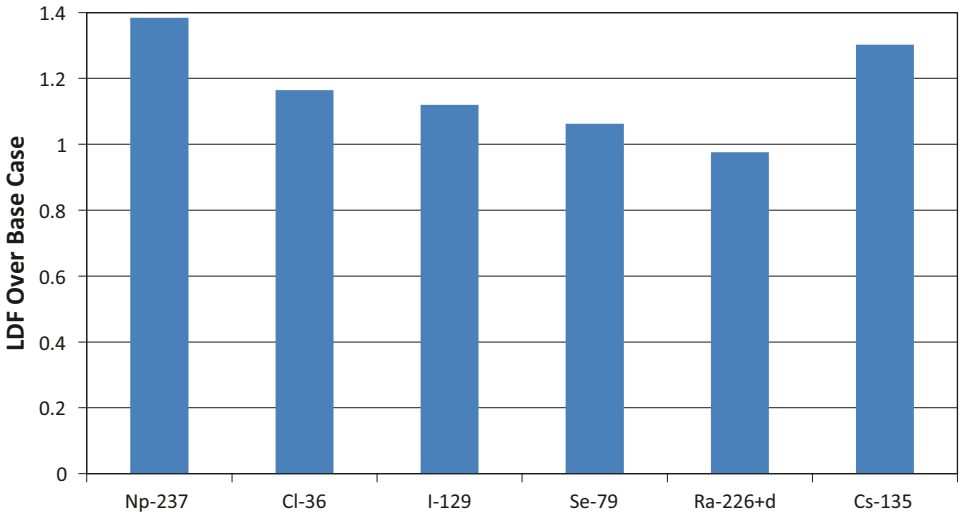


***Figure 5-33.*** *Ratio of LDF values obtained for the case when diffusive transport is not included in the Radionuclide Model to the baseline LDF values.*

These simulations also allowed studying the sensitivity of the *LDFs* to the values of upward flow rates from the lower regolith. Results from these simulations are presented in Figures 5-34 and 5-35, which show the ratio between the *LDFs* obtained from these simulations and the baseline *LDFs*. The alternative simulations showed that variations in upward water flow rates from the lower regolith had a limited effect on *LDF* calculations. Of nuclides expected to contribute to dose, Cs-135 was the only one to be significantly affected by the alternative parameterisation. For this radionuclide, the baseline *LDF* was a factor of two larger, than the values obtained for a low constant flow rate. Thus, it was concluded that the uncertainty in variation of flow rates from the lower regolith, associated with coastline passage, did not have a significantly effect on the *LDFs*.

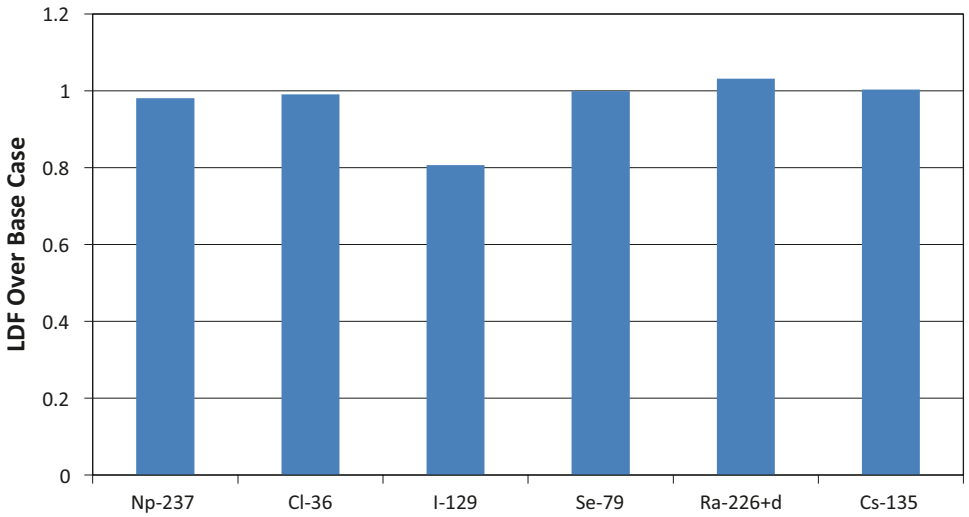


***Figure 5-34.*** *Ratio between LDF values obtained from simulations with constant high water flow rates from the lower regolith and the baseline LDF values.*

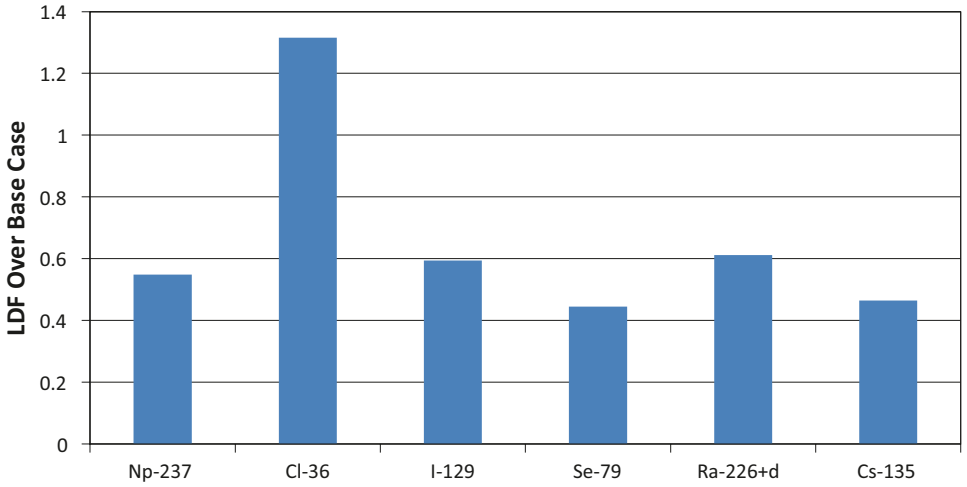


***Figure 5-35.*** *Ratio between LDF values obtained from simulations with constant low water flow rates from the lower regolith and the baseline LDF values.*

### *Limitations of the $K_d$ approach*

In the Radionuclide Model for the biosphere, the retention of radionuclides in the regolith and their partition between suspended particles and the soluble phase in surface waters is modelled using distribution coefficients ($K_d$s). This is currently the most widely used approach for modelling these types of processes in performance assessments of repositories. One reason for this is the mathematical simplicity of the $K_d$ approach. Any model used for simulation of the transport of water can be easily modified to model the transport of elements and radionuclides, by introducing a retardation factor expressed as a function of the $K_d$. At the same time, experimental determinations of $K_d$ values are also relatively easy to perform, which can explain that numerous $K_d$ values have been reported in the literature covering a wide range of conditions.

Measurement or estimation techniques of $K_d$, whether based on laboratory measurements or field observations, do not consider explicitly the chemical and physical processes that may be responsible for the partitioning of an element between mobile and immobile phases. The partitioning, as measured by a $K_d$ value, is generally considered to involve a reversible sorption process, even though the elements of interest may also undergo partitioning due to other processes like precipitation, matrix diffusion, biological uptake, chemical reactions and other processes. The $K_d$s used in the Radionuclide Model for the biosphere should account implicitly for all these processes, since they are not otherwise explicitly considered in the model. This results that $K_d$s are commonly associated with large uncertainty.

Hence, a main disadvantage of the $K_d$ approach is that $K_d$ values usually show large variation. The fact that different measurement methods can give very different $K_d$ values for the same conditions /IAEA 2010/ also contributes to large variation in $K_d$ values reported in the literature. This lack of robustness of the $K_d$s makes it difficult to select representative $K_d$ values for a given assessment context. To handle this situation, site-specific $K_d$ values have been obtained for the SR-Site assessment. These values are representative of the biosphere conditions at Forsmark, taking into account expected spatial and temporal variability within the time frame of the assessments. Furthermore, whenever possible, the site-specific values have been combined with literature data using Bayesian updating methods. The rationale for using Bayesian methods is to complement the site data with other available information, for example literature data, so that selected PDFs better cover the relevant rank of variation of the $K_d$s. Although the site data has been in many cases sufficient to obtain representative BE values, the number of samples are in most cases too few for giving, on their own, a good characterisation of the variation in the $K_d$ distribution (determined by the Geometric Standard Deviation, GSD, of the distribution). The effect of applying the Bayesian updating methods is that larger GSDs have been assigned to the distributions, than if these had been obtained from the site data alone. Large values of the GSD of the PDFs were also assumed when site data were not available and the distributions had to be derived from literature data. The use of PDFs with overestimated GSD values in the probabilistic simulations will result in overestimation of the effects of the uncertainties with respect to these parameters and the sensitivity of the *LDFs* to the uncertainty in the parameters, i.e. it will lead to cautious estimates.

One consequence of the large variability inherent to $K_d$s is that relatively large data sets are required for deriving representative BE values and PDFs. During the site investigation program site data of $K_d$ for different regolith layers have been collected. This data was not, however, sufficient to derive representative $K_d$ values for each of the regolith layers included in the Radionuclide Model for the biosphere /Nordén et al. 2010/. Instead, the same BE values and PDFs had to be assigned to the different organic layers of the regolith (Ter_regoMid, Ter_regoUp, Aqu_regoMid and Aqu_regoUp). It is, however, recognised that chemical conditions in these layers are different /Tröjbom and Nordén 2010/ and therefore differences in $K_d$ are to be expected. To study the effect of this source of uncertainty, the $K_d$ of the different layers were treated as distinct parameters in the probabilistic simulations. This means that although the same PDF was used for the $K_d$ of these layers, distinct samples were drawn for each layer during the Monte Carlo simulations. Hence, the probabilistically derived distributions of *LDFs* take into account variations in $K_d$ between different regolith layers.

### 5.2.3 Transfer of radionuclides to biota

In the Radionuclide Model for the biosphere radionuclide concentrations in biota are calculated using Concentration Ratios (CR) that relate the elements concentrations in different media (soil, water, animal feed) to the concentrations in biota (see Section 3.1.3). The main advantage of the CR approach is its simplicity. CRs are relatively easy to measure and have actually been measured and reported in the literature for a wide range of environmental conditions. Their main disadvantage of using this approach in the assessment lies in the large variation of the CRs. The CR approach relies on the assumption that element concentration in the biota is proportional to the total element concentration in the relevant environmental media, which is not always the case /Sheppard and Evenden 1988/. The element concentrations in biota are often related to the concentration of bioavailable fraction of the element in the relevant media, rather than to the total element concentration. The bioavailable fractions will depend on many factors and processes and this translates into a large variation in the CR obtained for different sites and conditions.

For the SR-Site assessments BE values and PDFs of several of the CRs included in the model have been derived by combining data collected from the site with literature data, using Bayesian methods /Nordén et al. 2010/. For some of the CRs, when site data were not available, these were either derived from the literature data alone or using a kinetic-allometric model /Nordén 2010/. It is considered that the selected BE values and PDFs are representative of the biosphere conditions at Forsmark, taking into account spatial and temporal variability within the time frame of the assessments. However, the variation in the selected PDFs is, in many cases much larger, than the "natural" variation that can be expected within the spatial and time frames of the assessment. This overestimation of the CR variation will translate in overestimation of the *LDF* uncertainties and sensitivity of the *LDFs* to uncertainty in CRs obtained from probabilistic simulations (see Section 5.3.1).

Another factor that has to be taken into account is that there might be strong negative correlations between CRs and $K_d$s of an element in nature. For example, negative correlation between the CRs from soil to plants and $K_d$s in soil have been reported /Sheppard and Evenden 1988, Sheppard 1989/. Correlations between CR and $K_d$ have not been taken into account in the probabilistic simulations carried out in the SR-Site assessment (see Section 5.3.1). This may have resulted in overestimations of the *LDFs* uncertainties due to parameter uncertainty (Section 5.3).

Another potential problem is that in some circumstances the CR approach could give large overestimation of concentrations in biota. For example, for elements with large soil-to-plant CRs, the predicted radionuclide inventory in plants (calculated by multiplying the radionuclide concentrations in plants by the plant biomass) could be larger than the radionuclide inventory in soil. This seems to be the case with the concentrations of Se-79 in terrestrial plants used in derivation of baseline *LDFs*. For example, if calculated concentrations in vegetables are multiplied by the biomass of vegetables the resulting inventory is larger than the inventory in soil. This means that the *LDFs* are probably overestimated. A perspective on the calculated *LDFs* can be offered by conducting the following simple calculation. If we assume that the whole release rate of 1 Bq/y, is ingested by individuals from the most exposed group (79 individuals is the size of the most exposed group corresponding to the *LDF* for Se-79, Table 4-1 in Section 4.1), then an average individual from this group would receive a dose of 3.7E–11 Sv/year (dose coefficient for ingestion, 2.9E–9, divided by 79) which can be compared with the *LDF* for the interglacial period in Table 4-1 (1.2E–9 Sv/year).

## 5.3 Parameter uncertainties and sensitivity analysis

In the study of the effect of parameter uncertainty on the SR-Site *LDFs* the parameters were divided into three categories: i) time-independent parameters considered to be certain, ii) time-independent parameters with uncertain values, and iii) time-dependent parameters. The methods used for treatment and evaluation of the parameter uncertainties were different among these categories. Parameters that fall into the first category are those that represent habits and properties of the exposed individuals, such as inhalation rates, water ingestion rates food ingestion rates and dose coefficients. These parameters were assigned constant values, corresponding to the values recommended for Reference Man and therefore effects of their uncertainty on *LDF* values were not studied. All other time-independent parameters were considered to fall into the second category and

the effect of their uncertainty on the *LDF* values was studied by performing probabilistic simulations using Monte Carlo methods (see Section 5.3.1). For these parameters, sensitivity analyses were also carried out using results from the probabilistic simulations. The effect on the *LDF* values of the uncertainty in time-dependent parameters could not be studied by Monte Carlo simulations, since these variables are strongly correlated with each other. Instead, the uncertainty evaluation was carried out by performing a series of alternative deterministic simulations where these parameters were co-varied as a group (see Section 5.3.2). The *LDF* values obtained from these simulations were then compared with the baseline *LDF* values.

### 5.3.1 Analyses for time-independent parameters

The approach for quantification of the effect on *LDF* values of uncertainties in time-independent parameters consisted of propagating uncertainties in the parameter distributions through the model to obtain probability distribution functions of the *LDFs*. The propagation of the uncertainties was carried out by performing probabilistic simulations using the Monte Carlo method with Latin Hypercube sampling. For each studied radionuclide, 1,000 simulations were carried out for the biosphere object that showed the highest baseline *LDF*. In these simulations correlations between parameters were not taken into account.

The values for each of the studied time-independent parameter required for the probabilistic simulations were obtained by drawing independent samples from the Probability Distribution Functions (PDF) of each parameter. For the sampling, all PDFs were assumed to be bounded between the 1st and 99th percentiles. The derivation of PDFs for the different parameters was carried out as described in Section 3.3.2. In the case of element-specific parameters, such as Concentration Ratios (CR) and Distribution Coefficients ($K_d$), Bayesian Updating methods were applied to obtain probability distributions that represent a compromise between the available generic and site-specific data.

Each Monte Carlo simulation resulted in a time series of *LDF* values. That is, in total 1,000 individual *LDF* time series were obtained for each radionuclide. These time series were processed together to obtain time series of different statistics, such as median, mean and different percentiles of the *LDFs*. Figures 5-36 and 5-37 show examples of time series of different statistics of the *LDFs* obtained from probabilistic simulations for Ra-226 (including daughters) and I-129, respectively. To estimate the ranges of uncertainty of the baseline *LDFs* distributions were derived for the time point when the time series of the median from the probabilistic simulations reached its peak value. Examples of histograms of these distributions are shown in Figures 5-38 and 5-39 for Ra-226 and I-129, respectively. It can be seen from these figures that these distributions were approximately lognormal, which was also the case for other studied radionuclides. Statistics of the derived *LDF* distributions for all studied radionuclides are presented in Table 5-5.

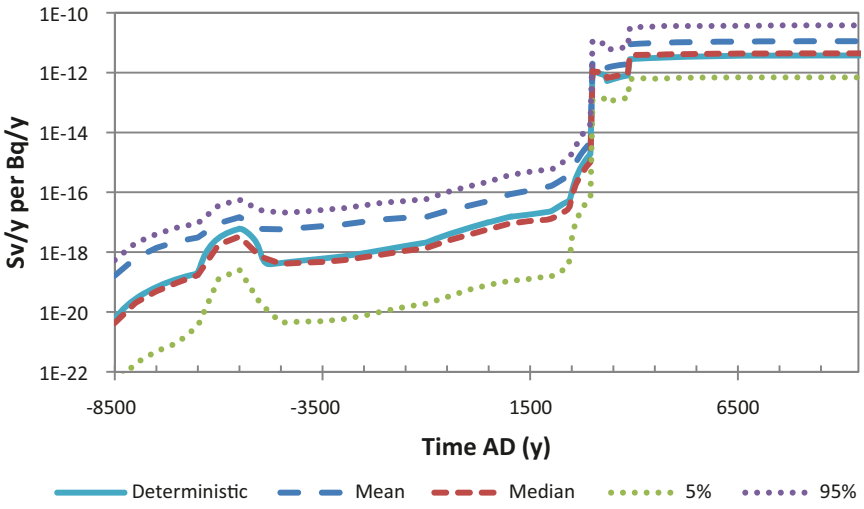


***Figure 5-36.*** *Evolution of the LDF in time for Ra-226, showing the effect of uncertain parameters. The deterministic LDF values are also shown for comparison.*

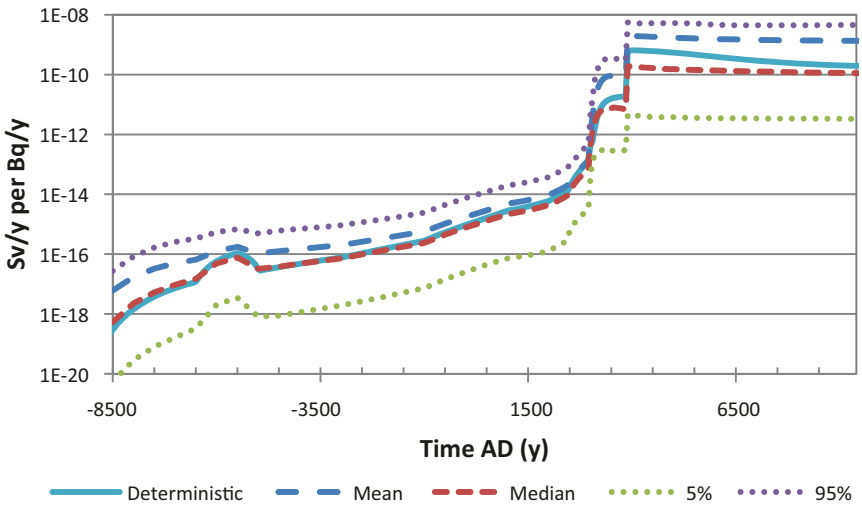


***Figure 5-37.*** *Evolution of the LDF in time for I-129, showing the effect of uncertain parameters. The deterministic LDF values are also shown for comparison.*

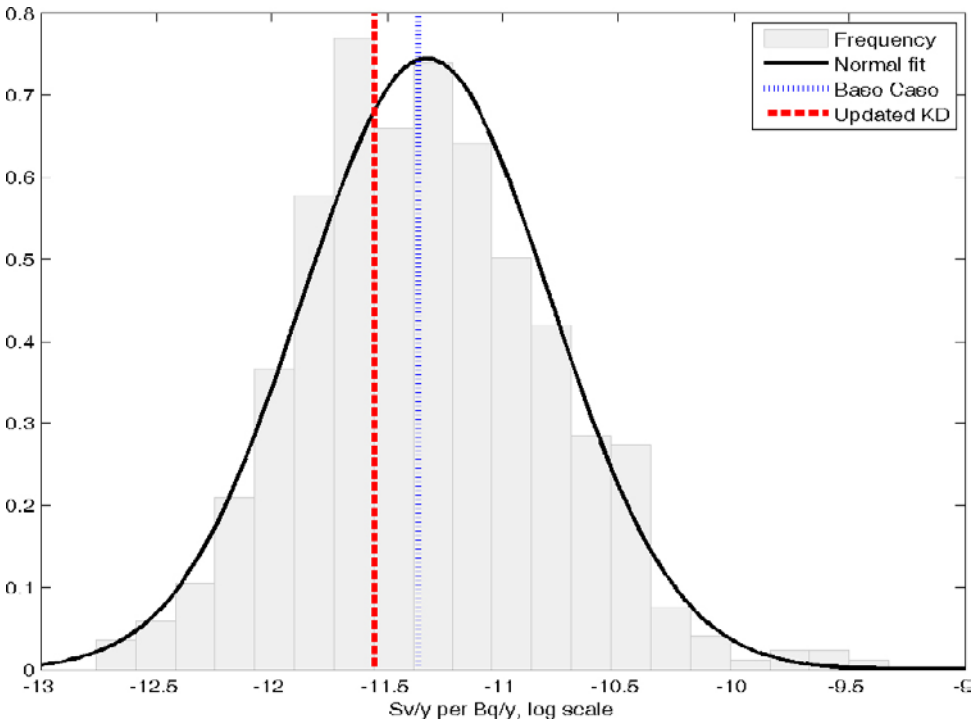


***Figure 5-38.*** *Distribution of the logarithm of LDF values for Ra-226 at the time of the peak of the median values from probabilistic simulations. The histogram shows the frequency of different values obtained from the simulations. The curve represents the best fit to a normal distribution of the logarithm of the LDF values. The vertical lines represent the values obtained from two deterministic simulations: i) using $K_d$ values derived from literature data only, ii) using $K_d$ values derived from literature and site data using Bayesian methods.*

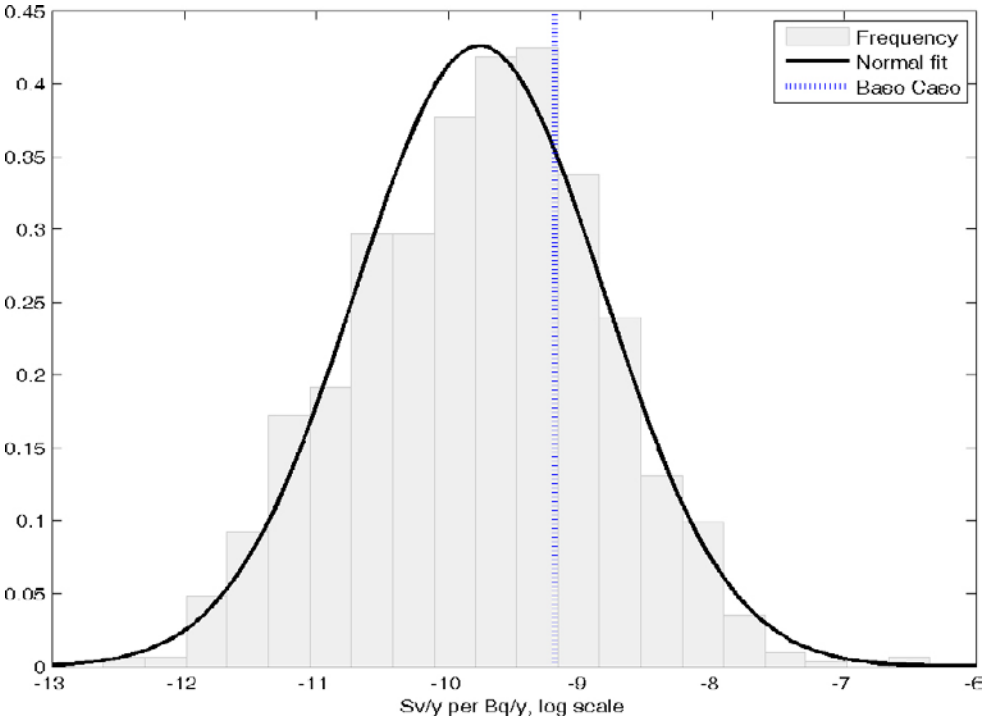


***Figure 5-39.*** *Distribution of the logarithm of LDF values for I-129 at the time of the peak of the median values from probabilistic simulations. The histogram shows the frequency of different values obtained from the simulations. The curve represents the best fit to a normal distribution of the logarithm of the LDF values. The vertical line represents the value obtained from deterministic simulation.*

**Table 5-5. Baseline LDF values (Sv/y per Bq/y) obtained from deterministic simulations and different statistics obtained from probabilistic simulations for the point in time when the median reaches its peak value. For Ra-226, Th-230 and U-238 the contribution from daughter radionuclides is included.**

| Radionuclide | Deterministic | Mean | Median | 5% | 95% |
|---|---|---|---|---|---|
| Am-241 | 1.46E–12 | 1.74E–12 | 7.29E–13 | 7.61E–14 | 7.12E–12 |
| C-14 | 5.44E–12 | 8.05E–12 | 6.91E–12 | 3.35E–12 | 1.63E–11 |
| Cl-36 | 5.84E–13 | 2.12E–12 | 6.01E–13 | 6.00E–14 | 7.86E–12 |
| Cs-135 | 3.96E–14 | 5.37E–14 | 2.50E–14 | 3.94E–15 | 1.92E–13 |
| I-129 | 6.46E–10 | 2.00E–09 | 1.92E–10 | 4.62E–12 | 5.52E–09 |
| Nb-94 | 4.00E–12 | 1.44E–12 | 3.99E–13 | 3.08E–14 | 6.66E–12 |
| Ni-59 | 7.39E–14 | 2.35E–13 | 3.75E–14 | 1.44E–15 | 1.05E–12 |
| Np-237 | 4.83E–11 | 7.84E–11 | 2.57E–11 | 2.71E–12 | 2.88E–10 |
| Pa-231 | 8.10E–12 | 1.75E–11 | 1.02E–11 | 1.67E–12 | 5.86E–11 |
| Pu-239 | 1.94E–12 | 3.21E–12 | 1.38E–12 | 1.80E–13 | 1.10E–11 |
| Pu-242 | 1.89E–12 | 3.33E–12 | 1.39E–12 | 1.83E–13 | 1.11E–11 |
| Ra-226 | 3.75E–12 | 1.12E–11 | 4.38E–12 | 6.89E–13 | 3.77E–11 |
| Se-79 | 1.21E–09 | 8.62E–10 | 3.88E–10 | 2.00E–11 | 3.18E–09 |
| Sn-126 | 2.47E–11 | 5.18E–11 | 2.48E–11 | 2.89E–12 | 1.95E–10 |
| Tc-99 | 8.98E–13 | 3.03E–11 | 6.91E–13 | 2.41E–14 | 7.79E–11 |
| Th-229 | 3.61E–12 | 4.76E–12 | 2.08E–12 | 2.57E–13 | 1.85E–11 |
| Th-230 | 1.31E–11 | 1.29E–10 | 1.76E–11 | 1.85E–12 | 4.36E–10 |
| U-238 | 1.85E–12 | 2.04E–11 | 3.35E–12 | 4.41E–13 | 7.47E–11 |
| Zr-93 | 2.77E–14 | 3.89E–13 | 6.21E–14 | 5.08E–15 | 1.32E–12 |

Several statistics obtained from the probabilistic results have been compared with the deterministic baseline *LDF* estimates (Figure 5-40). These comparisons show that, for all studied radionuclides, except for Nb-94, the baseline *LDFs* are within 1st and 3rd quartiles of the probabilistic results and are close to the median (50th percentile) of the probabilistic simulations. Hence, it can be concluded that the baseline *LDF*s obtained from the deterministic simulations provide a reasonably good measure of the central tendency of *LDFs*, i.e. the typical outcome when parameter uncertainties are considered.

It is also interesting to compare the baseline *LDF* values with the arithmetic means obtained from the probabilistic simulations. The arithmetic mean values are the expected values of the *LDFs* taking into account parameter uncertainties and are the appropriate measure to be used in estimations of expected doses and the risk for a representative individual of the most exposed group. For all radionuclides, the arithmetic means were higher than the median value, which was expected since the distributions are approximately lognormal. Moreover, for all studied radionuclides, except for Nb-94 and Se-79, the arithmetic means were also higher than the baseline *LDFs*. The differences are, however, relatively small (within a factor of three) for most radionuclides, including those that are expected to contribute the most to the doses and the risk (Ra-226, I-129, Se-79, Cs-135, Np-237 and Cl-36). However, for a few radionuclides (Tc-99, Th-230, U-238 and Zr-93) the arithmetic means of the probabilistic *LDF* distributions were about one order of magnitude higher than the baseline *LDFs*.

To be able to judge the significance of the differences between the baseline and the mean of the *LDFs* from the distributions derived with Monte Carlo simulations, one has to take into consideration the limitations of the probabilistic simulations that have been carried out in this study. Though a great effort has been put into the process of deriving meaningful PDFs for the model parameters, site-specific data were in some cases insufficient. This has resulted in several PDFs reflecting the large span of values reported in the literature; rather than the natural variations expected for the site.

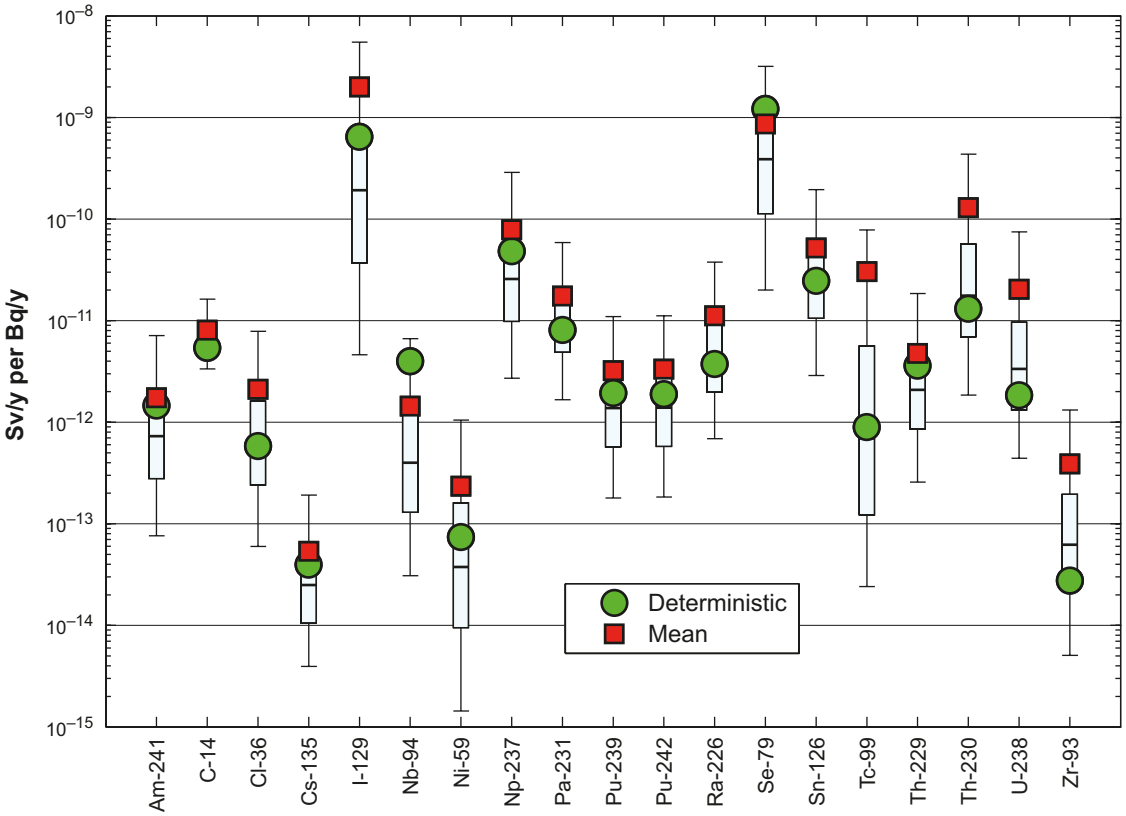


***Figure 5-40.*** *Variation in LDF values obtained from probabilistic simulations. This figure shows the distribution of LDF values at the time when the median of the probabilistic output reaches its peak. The mean, median, 5 percentile, 25 percentile, 75 percentile and 95 percentile from the probabilistic simulations are shown. The deterministic LDF value is also shown for comparison.*

The effect of using such PDFs has been that for some radionuclides the generated distributions of *LDF* values are long-tailed and have large standard deviations. This may have caused an overestimation of some of the arithmetic means, since the sampling was not designed to give precise estimates in presence of long-tailed distributions. Moreover, the Monte Carlo sampling did not incorporate dependence between parameters (for example negative correlations between CR values for plants and $K_d$ values for soil) and consideration of other constraints to avoid samples with very unlikely combination of parameter values. This may have also resulted in excessively broad *LDF* distributions.

Despite the above-mentioned limitations of the probabilistic simulations, the differences between deterministic *LDFs* and expected *LDF* values from the probabilistic simulations give a good indication of the potential impact of parameter uncertainties on the results. Thus, if the final risk estimates are close to the regulatory limits, as compared with differences between the baseline *LDF* and the expected value from probabilistic simulations, then it might be reasonable to make efforts to reduce the parameter uncertainty for dose-contributing radionuclides.

### *Sensitivity analyses*

The Monte Carlo simulations described above were also used for sensitivity analysis. The aim of the sensitivity analysis was to rank the model parameters by their relative effect on the calculated *LDF* values. The results were focused on *LDF* variation with respect to the uncertainty of individual parameters (i.e. not with respect to variations of fixed or proportional size), and thus the sensitivity analyses identified parameters where most benefit would be gained from reducing uncertainties by improving understanding and collecting additional site data.

The sensitivity analysis consisted of computing the First Order Sensitivity Index (FOSI) and the Standardized Regression Coefficients (SRC) using the samples generated from the Monte Carlo simulations. The SCRs are a measure of the importance of the different parameters for a given output, which is obtained from fitting the model predictions for the output to a linear first order polynomial /Saltelli et al. 2000/ dependency with the studied input parameters. The higher the SRC for a parameter, the higher effect on the output. A positive SRC value indicates that the input and the output move in the same direction, whereas a negative SRC indicates that they move in opposite directions. The FOSI is a measure of the contribution of input parameters to the variance of the outputs, obtained by sensitivity analyses methods based on variance decomposition /Saltelli et al. 2000/. The FOSIs consider the first order contribution to the variance of the output, i.e. contributions from interactions with other parameters are not taken into account. The sensitivity analyses were carried out using the software-package Eikos /Ekström and Broed 2006/.

Both sensitivity measures, i.e. the SRCs and FOSIs, were calculated for untransformed inputs and outputs, as well as for their ranks and logarithms. The results with untransformed data showed a poor explanation of the observed variation in *LDF* values, as evidenced by low values of the coefficients of determination ($R^2$). On the contrary, the results with ranked and logarithmic data showed a good explanation of the variation in *LDF* values, i.e. the coefficients of determination were close to 1. Hence, the sensitivity analyses presented here are based on the result obtained from logarithmic data.

Selected results from the sensitivity analysis are presented in Figures 5-41 to 5-45 for Ra-226 and I-129 and in Appendix C for the most dose-contributing radionuclides. Three types of plots summarizing results from the sensitivity analyses are presented:

- A plot with the values of the First Order Sensitivity Indexes as function of time, where the coefficients of determination ($R^2$) from the calculated Standardized Regression Coefficients are also presented.
- A tornado plot with the values of Standardized Rank regression Coefficients showing the effect of different model parameters on the maximum *LDF* values, i.e. the *LDF* value at the time point when the median from the probabilistic simulations reaches its maximum value.
- A bar plot with the values of the First Order Sensitivity Indexes showing the contribution in percent of the individual contribution of the different model parameters to the variance of the maximum *LDFs*, i.e. the *LDF* at the time point when the median from the probabilistic simulations reaches its maximum value.

It is evident from the plots with the First Order Sensitivity Indexes as function of time that the relative contribution of the uncertainty of different parameters to the uncertainty of the *LDF* values varied with time, owing to the temporal development that is experienced by the biosphere objects. This is expected because the major pathway for exposure is ingestion of contaminated food and water for most examined radionuclides, and the processes determining food and water concentrations are different between the sea and lake/terrestrial stages. For example, uncertainty in the properties of regolith layers and fish productivity caused the majority of uncertainty in the *LDF* values during the sea stage for Ra-226. This is contrasted to uncertainty in well capacity and parameters describing plant uptake dominating *LDF* uncertainty during the terrestrial stage (Figure 5-41).

For assessing the exposure of human inhabitants to potential releases to the biosphere, the maximum *LDF* values obtained from deterministic simulations (baseline *LDFs*) have been used (see Chapter 4). It has been assumed here that the sensitivity results obtained for the point in time when the median *LDF* from the probabilistic simulations reaches its maximum value are representative of the parameter sensitivity of baseline *LDFs*. Indeed, for the studied radionuclides the maximum *LDFs* from the deterministic and probabilistic simulations are observed at approximately the same time point.

As a rule, parameter uncertainty associated with the dominant exposure pathway, which varied between radionuclides, was the major source of *LDF* uncertainty. Consequently, the relative importance of parameters for *LDF* uncertainty also varied between radionuclides.

For Ra-226 uncertainty in well capacity explains 48% of *LDF* uncertainty due to the relatively high contribution of ingestion of well water to the *LDF*. The corresponding numbers for the CR of Ra-226 and its daughter Pb-210 are around 6% and 20%, respectively (Figure 5-46). In addition, uncertainty in the parameter describing retention in the lowest regolith layer (Kd_regolow) explains an additional 5% of *LDF* uncertainty. The standardized regression coefficients indicate both the magnitude and direction of the effects of a parameter on *LDF*. Thus as expected, the *LDF* for Ra-226 would decrease with an increase in well capacity or in the $K_d$ for the low regolith layer, and increase with an increased CR for vegetables (see wellCapac, kD_regoLow[Ra-226], cR_soilToVegetab[Pb-210] and cR_soilToVegetab[Ra-226] in Figure 5-45).

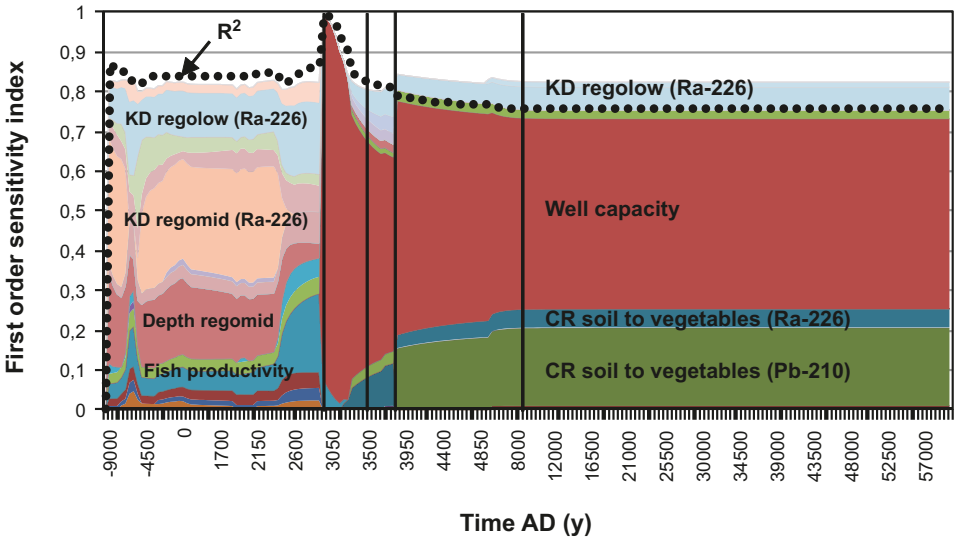


***Figure 5-41.*** *Time series of the first-order sensitivity indexes of the LDF for Ra-226 obtained from probabilistic simulations. The dotted line shows the coefficient of determination ($R^2$) from the calculated standardized regression coefficients for the logarithm of the input data and the results.*

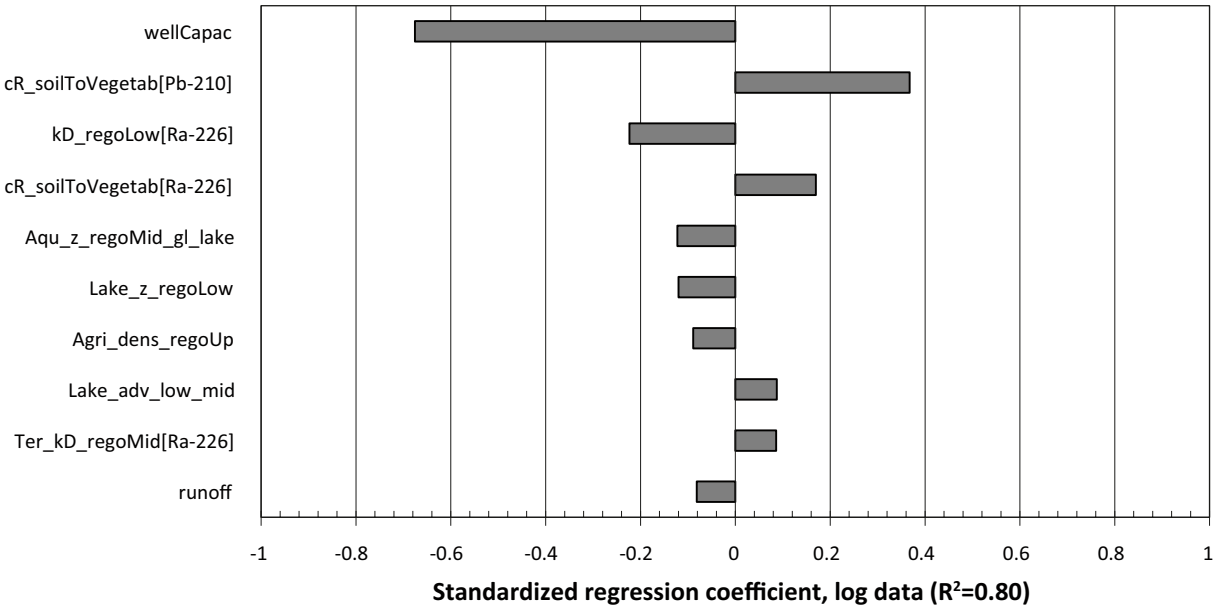


***Figure 5-42.*** *Standardized rank regression coefficients of the maximum LDF for Ra-226 obtained from probabilistic simulations.*

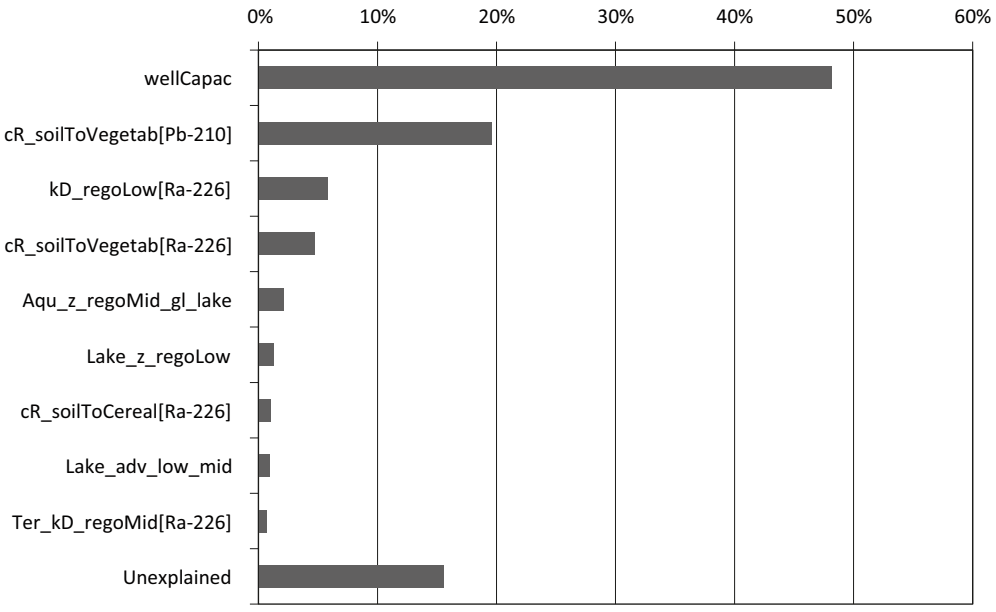


***Figure 5-43.*** *First-order sensitivity indexes of the maximum LDF for Ra-226 obtained from probabilistic simulations.*

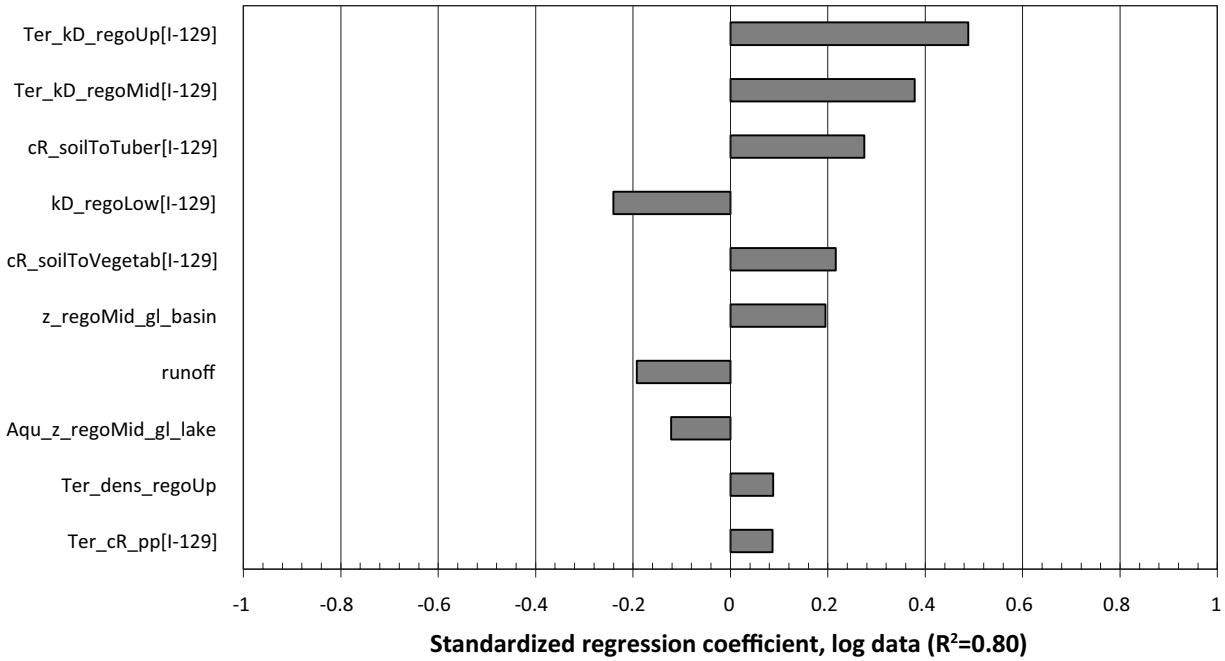


***Figure 5-44.*** *Standardized rank regression coefficients of the maximum LDF for I-129 obtained from probabilistic simulations.*

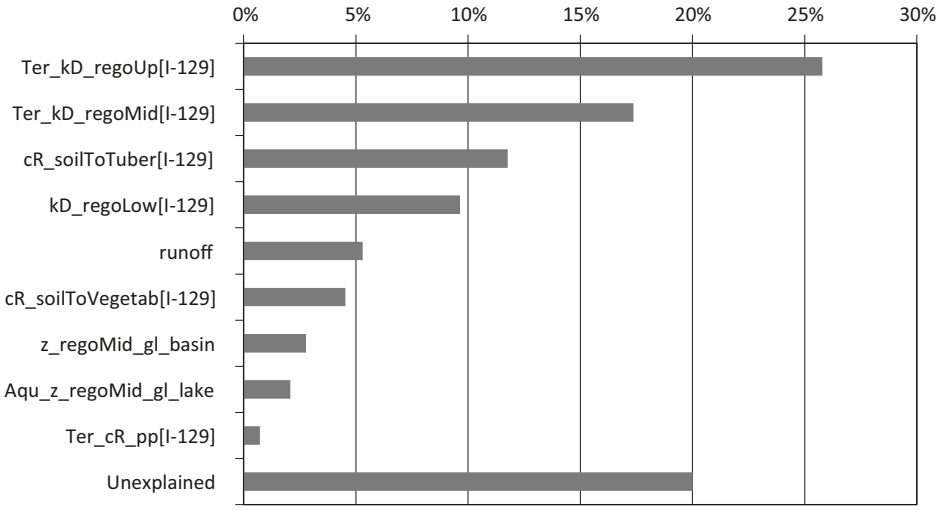


***Figure 5-45.*** *First order sensitivity indexes of the maximum LDF for I-129 obtained from probabilistic simulations.*

For I-129 the uncertainty in the well capacity has no effect on the uncertainty of the *LDF*. For this radionuclide, the parameters with the highest contribution to the *LDF* uncertainty are the $K_d$ for the upper and middle regolith and the CR from soil to tubers (Ter_kD_regoUp[I-129], Ter_kD_regoMid[I-129] and cR_soilToTuber[I-129] in Figures 5-47 and 5-48) with a positive effect and the $K_d$ for the lower regolith (kD_regoLow[I-129] in Figures 5-47 and 5-48) with a negative effect. As can be seen from Figure 5-48, around 20% of the variance of the *LDFs* for I-129 cannot be explained by the uncertainty of the individual parameters and is classified as unexplained. This could be a result of non-monotonic relationships between the parameters and the *LDFs* or of interactions between the parameters. In this case, it can be expected that a negative correlation between the $K_d$ in the upper regolith layers and the CR will have an impact on the *LDFs*.

For the studied radionuclides, the percentage of unexplained variability varied between 10% and 20% and the coefficients of determination were relatively high. This is comparable with the contribution to the variance in *LDFs* of the most sensitive parameters, which varied between 10% and 35% depending on the radionuclide. Hence, the effect on the *LDF* uncertainties of interactions between parameters may be as high as the effect from individual parameters.

Although there are differences between radionuclides, uncertainty in parameters that describe retention in regolith layers ($K_d$) and uptake by biota (CR) explained a large fraction of *LDF* uncertainty for all radionuclides. An increase in CRs and in $K_d$ for the upper and the mid regolith layers was always associated with an increase in *LDF*, whereas an increase in $K_d$ for the lowest regolith layer was associated with a decrease in *LDF*. The primary reason for the large impact of uncertainty in $K_d$ and CR values on the *LDF* uncertainty, was that the distributions of these parameters were typically very wide. The distributions of these parameters were generally estimated from combining site and literature data which covered a broad range of environments. Systematic variations due to, for example, climate, and geographical location, type of ecosystem or measurement technique were not addressed in the process of combining literature and site data. Hence, the derived PDFs for these parameters are likely to overestimate the natural variation to be expected at the site /Tröjbom and Nordén 2010/. It can, therefore, be expected that uncertainty in the *LDFs* could be significantly reduced if the uncertainties in these parameters could be reduced to reflect natural variation on the site. It may also be possible to reduce uncertainties for some radionuclides by describing plant uptake by alternative modelling approaches that are less sensitive to parameter uncertainties.

### 5.3.2 Analyses for time depended parameters

Time-dependent parameters in the models are those related to dimensions of the compartments of the biosphere objects, such as depth of different layers, areas, the biomass and biomass production, the growth of the mire, gas uptake and release, etc. These parameters are strongly correlated to each other and in time and therefore probabilistic methods for uncertainty and sensitivity analyses could not be directly applied. Instead, their effect on the uncertainty in the *LDF* values was studied by performing alternative simulations, where these parameters were systematically varied.

Two sets of alternative simulations were carried out. One of the sets consisted of systematically varying some of the parameters, giving a low or high value to the each of the parameters, and keeping all other parameter at the Best Estimate value used in the derivation of baseline *LDF* values. The following alternative simulations were considered in this set:

- Small biomass – the biomass of primary producers was given a smaller value during the whole simulation period.
- Large biomass – the biomass of primary producers was given a larger value during the whole simulation period.
- Small production – the production of primary producers was given a smaller value during the whole simulation period.
- Large production – the production of primary producers was given a larger value during the whole simulation period.
- Low gas uptake – the gas uptake in the terrestrial and aquatic parts of the biosphere object was given a smaller value during the whole simulation period.

- High gas uptake – the gas uptake in the terrestrial and aquatic parts of the biosphere object was given a larger value during the whole simulation period.
- Higher water retention – the residence time of water in the objects during the sea stage was given a higher value.
- Lower water retention – the residence time of water in the objects during the sea stage was given a lower value.

The results for this set of alternative simulations are presented in Figure 5-46. In general, for the potentially dose-contributing radionuclides relatively small differences, within a factor of about 2, were observed between the *LDF* obtained from the alternative simulations and the baseline *LDF*. The largest differences were observed for radionuclides (C-14, Np-237, Pu-239 and Pu-242) with a relatively high contribution to the *LDF* values from ingestion of aquatic foods.

A second set of alternative simulations was carried out to investigate the potential impact on the *LDF* values of time-dependent parameters related to the predicted landscape development. These simulations consisted of systematically varying key process rates in the coupled regolith-lake development model, i.e. sedimentation and in-growth rate in sea basins and lakes. A total of 12 alternative landscape development variants were considered, by increasing or decreasing the values of rates one or three driving processes with 10%, as compare to the values used to derive baseline *LDFs* (see Chapter 5 in /Brydsten and Strömgren 2010/ for details). The results from this set of simulations are presented in Figure 5-47. It is evident from this figure that the variations of parameters related to predicted landscape development have a very limited effect on the *LDF* values. Moreover, the observed relative variation in *LDFs* is smaller than the relative variation in key process rates, i.e. the response of the *LDF* to these variations is sub-linear.

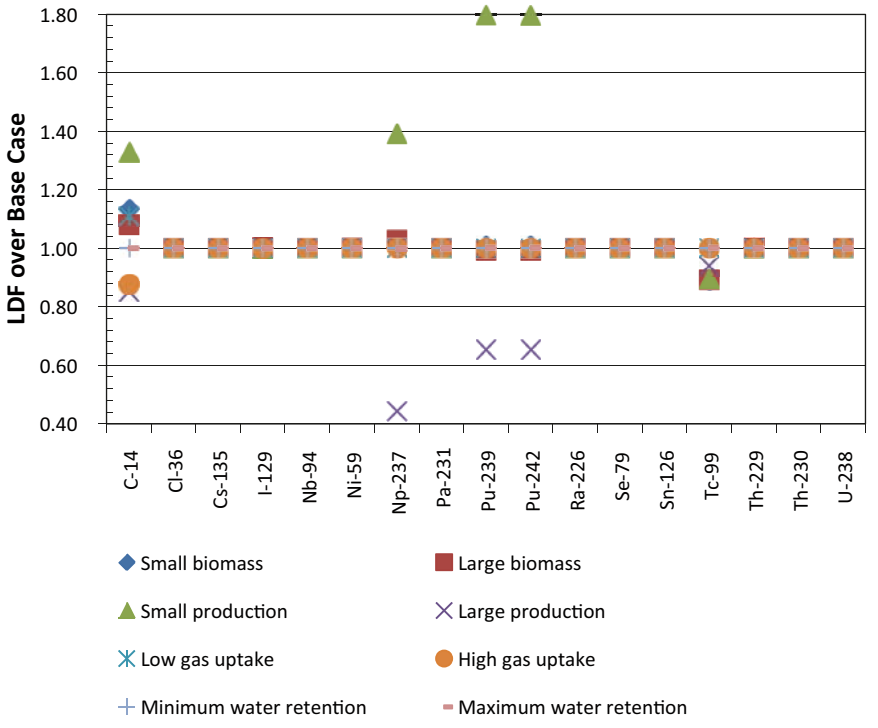


***Figure 5-46.*** *Ratio between the LDFs and the baseline LDFs obtained for the first set of alternative simulations to investigate the impact of time dependent parameters: biomass, biomass production, gas uptake, water retention time in sea objects*

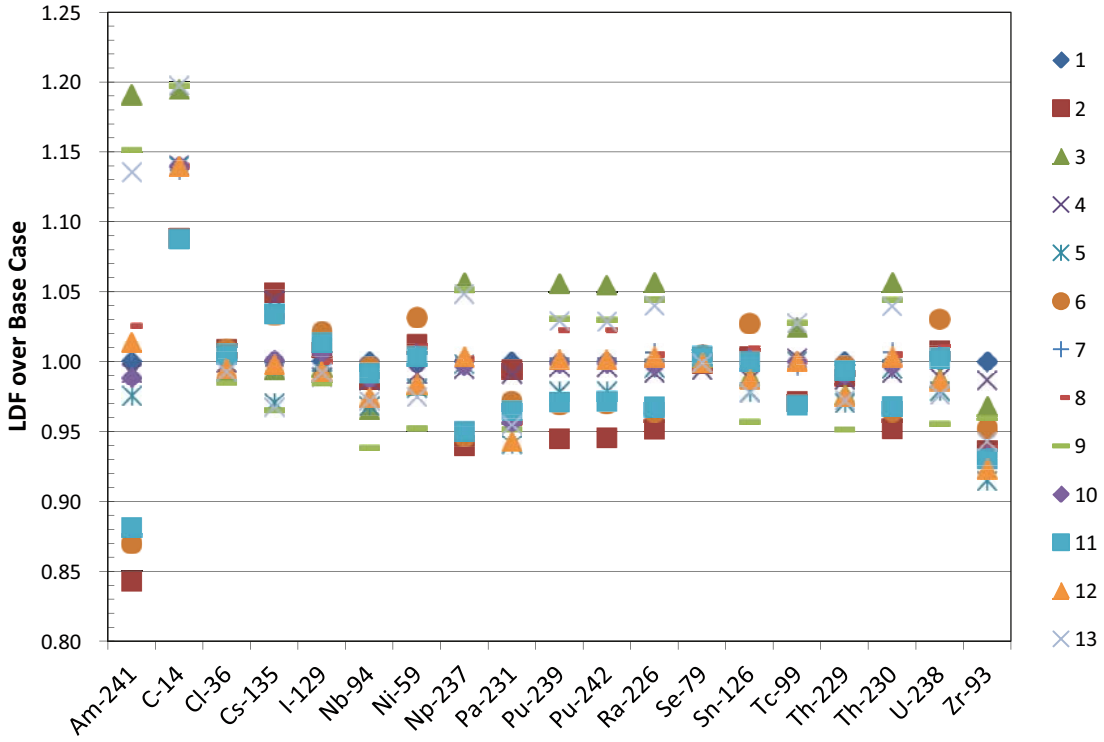


***Figure 5-47.*** *Ratio between the LDFs and the baseline LDFs obtained for the second set of alternative simulations to investigate the impact of time-dependent parameters related to the predicted landscape development*

## 5.4 Uncertainties due to numerical approximations

In simulations for derivation of *LDF* values, numerical methods have been applied for the time integration of the Radionuclide Model for the biosphere. The deterministic simulations were carried out using the Pandora tool /Ekström 2011/, which relies on the Matlab toolbox Simulink[1] for the numerical integration. Simulink is used in many fields for solution of numerical problems. It is a reliable tool which includes a selection of well-established numerical methods. In this particular assessment the solver ode15s /Shampine and Reichelt 1997/ was used. This is an implicit multistep-solver of variable order (1–5), which gives stable and precise solutions for most systems of ordinary differential equations, including systems with stiff problems.

The probabilistic simulations where carried out with the Ecolego software[2], using an independent implementation of the same numerical method used in the ode15s solver, based on the description of the method given in /Shampine and Reichelt 1997/ and /Shampine at al. 1999/. A comparison of the numerical integration of the model with Ecolego and Pandora was performed by repeating the deterministic simulation for derivation of *LDF* values in Ecolego and comparing with the values obtained with Pandora. For all radionuclides and biosphere objects the *LDF* obtained with both tools were practically identical, with observed differences of less than 1%.

[1] Mathworks Inc, 2011. Simulink – Simulation and model-based design. [Online]. Available at: http://www.mathworks.com/products/simulink/. [11 March 2011].

[2] Facilia AB, 2011. Ecolego. [Online]. Available at: http://ecolego.facilia.se/. [11 March 2011].

## 5.5 Comparison with early studies

The method used for calculating landscape dose factors in SR-Site has been updated in several important ways since the last two biosphere assessments of a deep repository: SR-Can /SKB 2006/ and SR 97 /SKB 1999/. Data from the site have been used to modify parameters from values used in the past, with improved justification for the values used in the present assessment. The maximum values of the ecosystem-specific dose conversion factors (EDF) used in SR 97 /SKB 1999/ were systematically higher than the *LDFs* calculated in the present assessment, with exception of a few radionuclides, e.g. C-14 (Figure 5-48). These differences are attributable to important methodological differences between the two assessments, including the delineation of sub-catchments, assumptions on where a release will reach discharge areas and enter the ecosystems, as well as differences in the approach to evaluating the well. Moreover, in the SR 97 assessment generic parameter values were used in most cases, whereas site-specific data obtained during the site investigation programme have been broadly applied in the SR-Site assessment.

The methodology applied in SR-Site is based on that developed in SR-Can, but has been updated in several important ways taking into account comments and recommendations from the regulatory authority and independent reviewers. An important difference between the biosphere assessments in SR-Site and SR-Can is that in SR-Site site specific parameters were used to a much larger extend than in SR-Can. This is particularly relevant for the CRs and $K_d$s, which in SR-Can where totally based on generic data, whereas in SR-Site many were estimated using site data /Nordén et al. 2010/. As shown by the sensitivity and uncertainty analyses (see Section 5.3.1), the *LDFs* are highly sensitive to the $K_d$s and CR. Hence, large differences can be expected between *LDF* values from SR-Site and SR-Can; due alone from differences in the $K_d$ and CR values used in these assessments.

Figure 5-49 shows a comparison between the SR-Can *LDFs* values with values obtained from simulations with the SR-Site Radionuclide Model for the biosphere. In these simulations it has been assumed, as in SR-Can, that the radionuclide releases are distributed between biosphere objects in the landscape in proportion to estimated release fractions to different objects at different time points. No general tendency can be observed in Figure 5-49 of the *LDFs* from SR-Can being higher or lower than the *LDF* obtained from these simulations. The most likely reason for this is that for some radionuclides the use of updated $K_d$ and CR values has led to increases and for other to decreases in *LDFs*. So, comparison of numerical values of the *LDFs* from SR-Site and SR-Can is not

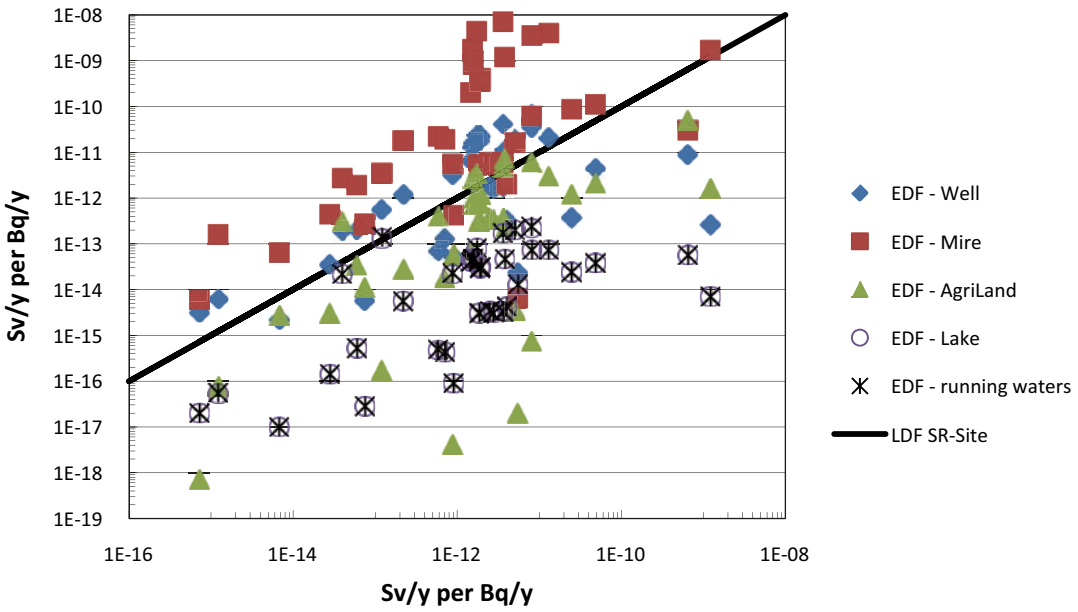


***Figure 5-48.*** *Baseline LDFs from SR-Site for different radionuclides compared with the corresponding Ecosystem Dose Factors (EDF) reported from SR-97. The solid line represents a 1:1 relationship between the baseline LDFs and the EDFs.*

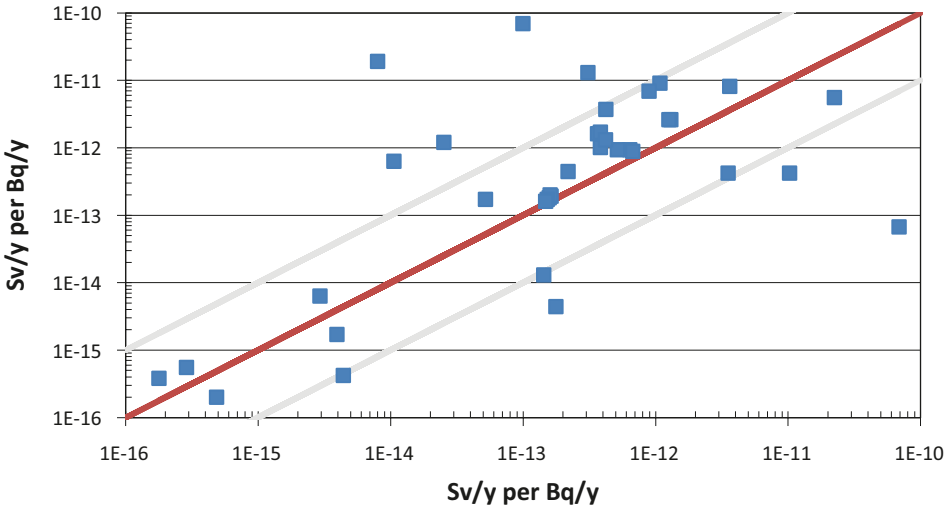


***Figure 5-49.*** *LDF values for different radionuclides reported in SR-Can compared with the corresponding LDF values derived in the SR-Site project with a similar method to that used in SR-Can, but applying updated models and parameter values. The solid line represents a 1:1 relationship between the baseline LDFs and the EDFs.*

very meaningful. However, a general pattern observed is that for those radionuclides for which consumption of contaminated food is the dominant pathway of exposure, the SR-Site *LDFs* are typically an order of magnitude higher than the SR-Can *LDFs*. However, the activity concentration in well water was calculated in a similar way in the two assessments (though the exposure from the well was not combined with other pathways in SR-Can), and consequently *LDF* values for radionuclides where drinking water is the dominant pathway are similar in the two assessments.

A main conceptual difference between SR-Can and SR-Site approaches for derivation of the *LDFs* is that in SR-Can it was assumed that the releases were distributed over the whole landscape, whereas in SR-Site it is assumed that all releases will reach the discharge area (biosphere object), where they will cause maximum exposure. The impact of this difference in approaches has been indirectly addressed by the analysis of uncertainties associated with the localization of potential releases in the landscape presented in Section 5.1.1. From this analysis it can be inferred that SR-Site *LDFs* should be higher or similar to SR-Can *LDFs*, everything else being equal apart from this difference in approaches.

There are other differences between the biosphere assessments in SR-Site and SR-Can, mainly related to improvements in the Radionuclide Model for the biosphere that have been done for the SR-Site assessment. Examples of improvements implemented in the SR-Site model are: the transition between ecosystem types has been described as a continuous process, the radionuclide transport in quaternary deposits (lower layer of the regolith) has been explicitly considered, contributions from the well have been integrated in the model and calculation of food ingestion doses have been improved by including more food types.

## 5.6 Summary of uncertainty analyses

In this chapter, the contribution of different sources of uncertainty to the uncertainty of the *LDFs* has been examined. To facilitate the discussions the different sources of uncertainty have been divided into three categories: system uncertainties, model uncertainties and parameter uncertainties. Several sources of uncertainty have been evaluated quantitatively by performing additional deterministic simulations using alternative assumptions, models and parameter values, and by performing Monte-Carlo simulations. The significance of some of the uncertainties has been evaluating qualitatively by discussion the reasonableness of the assumptions made and the limitations of the modelling approached applied.

The results from quantitative evaluation of different sources of uncertainty are summarized in Figures 5-50–5-55. These figures show *LDFs* obtained from alternative deterministic simulations done for evaluating each specific source of uncertainty, denoted with the codes from A to G (see Table 5-1) for the system uncertainties and with the codes from H to M (see Table 5-4) for the model uncertainties. The figures also show different statistics of *LDFs* obtained from the probabilistic simulations: the median, the mean value, the 5, 25, 75 and 95 percentiles. The horizontal line represents the *LDFs* obtained from deterministic simulations, i.e. the *LDF* that was used for dose assessments in the SR-Site. Values below this line indicate that the treatment of the uncertainty has led to cautious *LDF* estimates and values above the line indicate that the use of baseline *LDF* values might lead to underestimation of doses under specific conditions; depending on the corresponding source of uncertainty. Several conclusions can be drawn from the examination of these figures:

- The *LDFs* obtained from the simulations to evaluate system and model uncertainties are, in most cases, within the 5th and 95th and in many case between the 25th and 75th percentiles from the probabilistic simulations. This indicates that the overall uncertainty of the *LDF* is dominated by the parameter uncertainty. The only exception was the effect of uncertainty related for climate change for Cs-135 (code C in Figure 5-54). The results in this case indicate that for this radionuclide *LDFs* for a global warming scenario might be higher than the baseline *LDF* and the 95th percentile from the probabilistic simulations (see discussion of this source of uncertainty in Section 5.1.1).
- Most of the performed evaluations of system and model uncertainties indicate that the use of baseline *LDF* would lead to cautious or realistic estimates. An exception to this was the evaluation of uncertainty from climate change for Cs-135 (code C in Figure 5-54). However, in SR-Site this has been handled by calculating a separate *LDF* for the global warming climate alternative (Table 4-2). Another exception is the uncertainty in the *LDF* values for Ra-226 associated with the use of well water for irrigation (code E in Figure 5-50) which is discussed in Section 5.1.2.
- The degree of cautiousness in the approaches for treatment of system and model uncertainties has been moderate, as evidenced by small differences between the alternative and baseline *LDFs*. The sources of uncertainties that have been treated most cautiously are those related to the timing and localization of the releases (codes A and B) discussed in Section 5.1.1 and the discretisation of the regolith (code I) discussed in Section 5.2.1. The degree of cautiousness varied between radionuclides, but since the alternative *LDFs* were within the interval from the probabilistic simulations, it can be concluded that the treatment of these uncertainties was not over-conservative.
- The expected values from the probabilistic simulations were systematically somewhat higher than the *LDFs* used in the safety assessment, although the difference varied between radionuclides.

The effects of parameter uncertainties on *LDF* calculations were assessed with both systematic (for time dependent parameters) and random variation (for time independent parameters) of model parameters. It was concluded from these assessments that uncertainties in time dependent parameters, for example parameters that represented landscape development, had a limited effect on the uncertainty of the *LDF* estimates. From the results of the Monte Carlo simulations it is evident that uncertainty in time independent parameters had a significant contribution to the uncertainty in *LDFs*. Moreover, the expected values from the probabilistic simulations were systematically higher than the baseline *LDF* values used in the safety assessment. It should, however, be taken into account that though a great effort was put into the process to derive meaningful PDFs (see Section 3.3.2), information from the site was occasionally insufficient, resulting in PDFs reflecting a wide span reported in the literature, rather than the variation expected for the site, taking into account expected spatial and time variability within the time frame of the assessments. Moreover, the Monte-Carlo sampling did not incorporate correlations between parameters (e.g. a negative correlation between CR for plants and $K_d$ for soil). Nevertheless, the difference between deterministic calculations and expected values from the probabilistic simulations gives a good indication of the potential impact of parameter uncertainties. Thus, if the final risk estimates are close to the regulatory limits, (as compared to difference between *LDFs* and the expected value from the Monte-Carlo simulation), it would be reasonable to make an effort to reduce the parameter uncertainty of dose-contributing radionuclides.

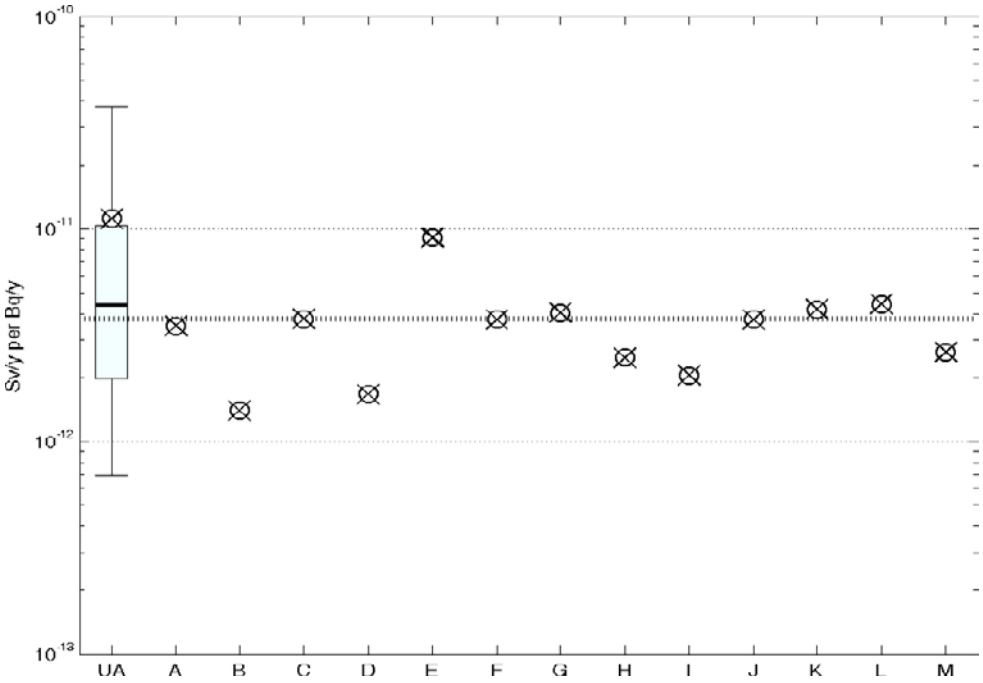


***Figure 5-50.*** *Results from uncertainty analyses of the LDF for Ra-226.The circles with codes from A to G (see Table 5-1) show LDF values obtained from simulations for evaluation of system uncertainties. The circles with codes from H to M (see Table 5-4) show LDF values obtained from simulations for evaluation of model uncertainties. The whisker plot on the left shows the 5th, 25th, 50th, 75th, 95th and mean value (circle) of the LDFs obtained from the probabilistic simulations.*

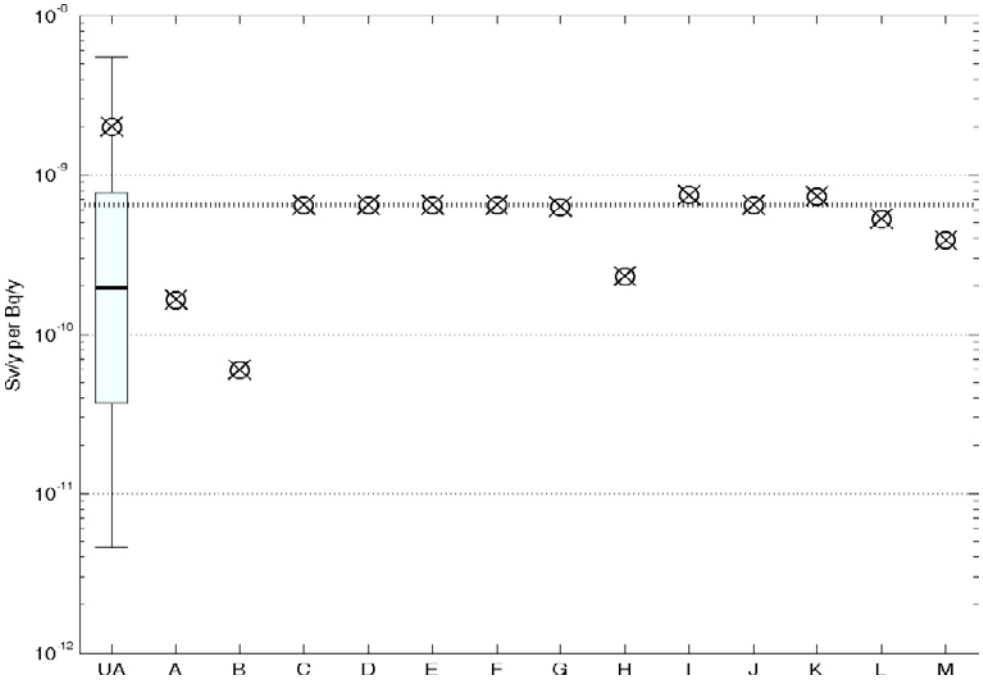


***Figure 5-51.*** *Results from uncertainty analyses of the LDF for I-129.The circles with codes from A to G (see Table 5-1) show LDF values obtained from simulations for evaluation of system uncertainties. The circles with codes from H to M (see Table 5-4) show LDF values obtained from simulations for evaluation of model uncertainties. The whisker plot on the left shows the 5th, 25th, 50th, 75th, 95th and mean value (circle) of the LDFs obtained from the probabilistic simulations.*

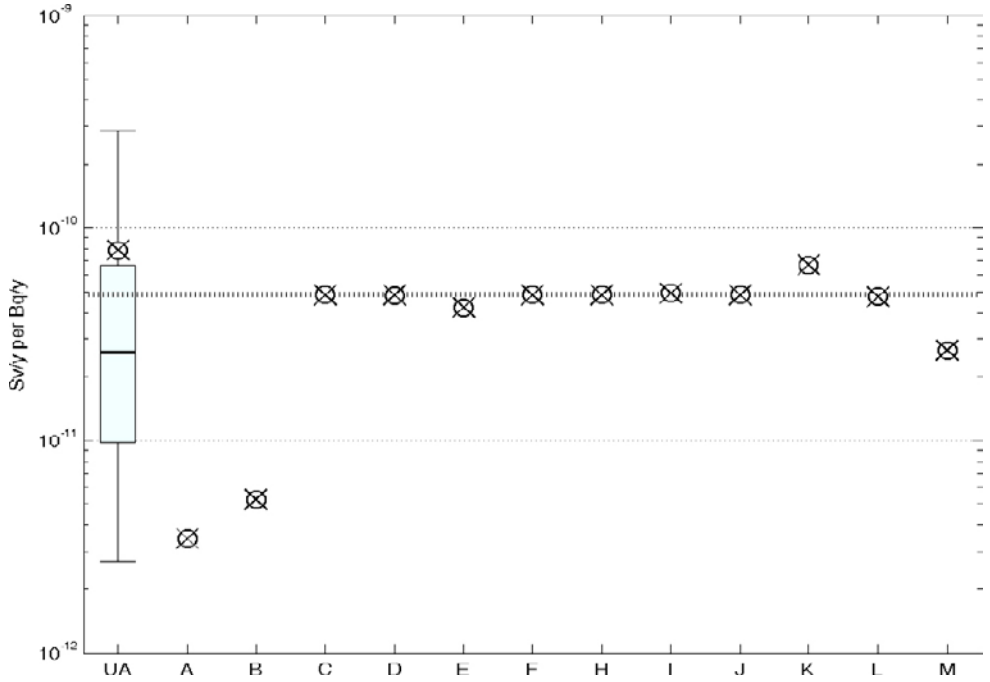


***Figure 5-52.*** *Results from uncertainty analyses of the LDF for Np-237.The circles with codes from A to G (see Table 5-1) show LDF values obtained from simulations for evaluation of system uncertainties. The circles with codes from H to M (see Table 5-4) show LDF values obtained from simulations for evaluation of model uncertainties. The whisker plot on the left shows the 5th, 25th, 50th, 75th, 95th and mean value (circle) of the LDFs obtained from the probabilistic simulations.*

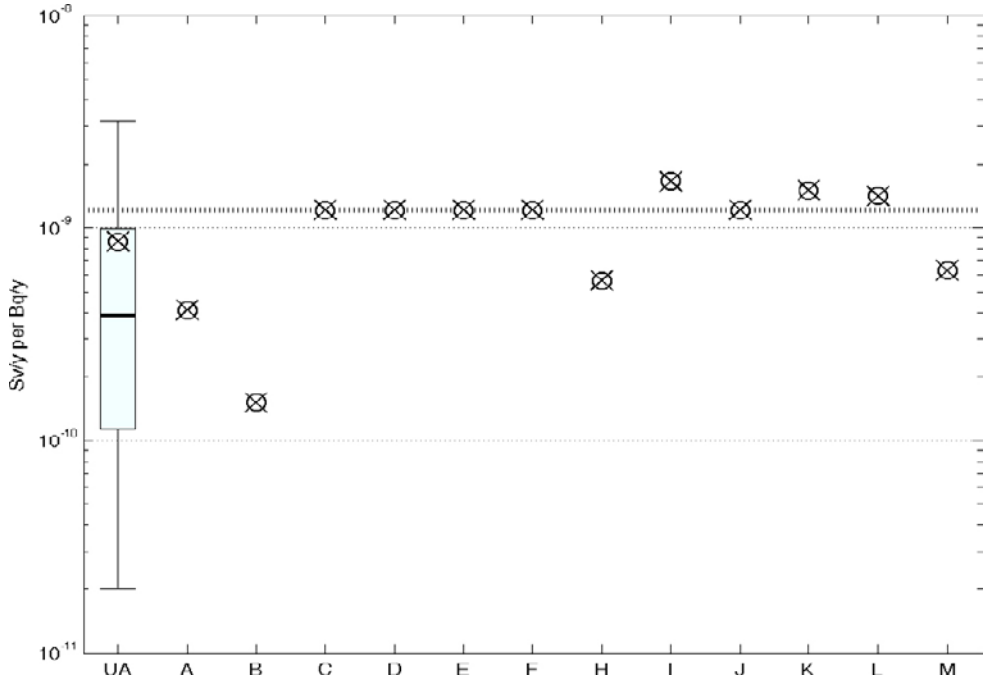


***Figure 5-53.*** *Results from uncertainty analyses of the LDF for Se-79.The circles with codes from A to G (see Table 5-1) show LDF values obtained from simulations for evaluation of system uncertainties. The circles with codes from H to M (see Table 5-4) show LDF values obtained from simulations for evaluation of model uncertainties. The whisker plot on the left shows the 5th, 25th, 50th, 75th, 95th and mean value (circle) of the LDFs obtained from the probabilistic simulations.*

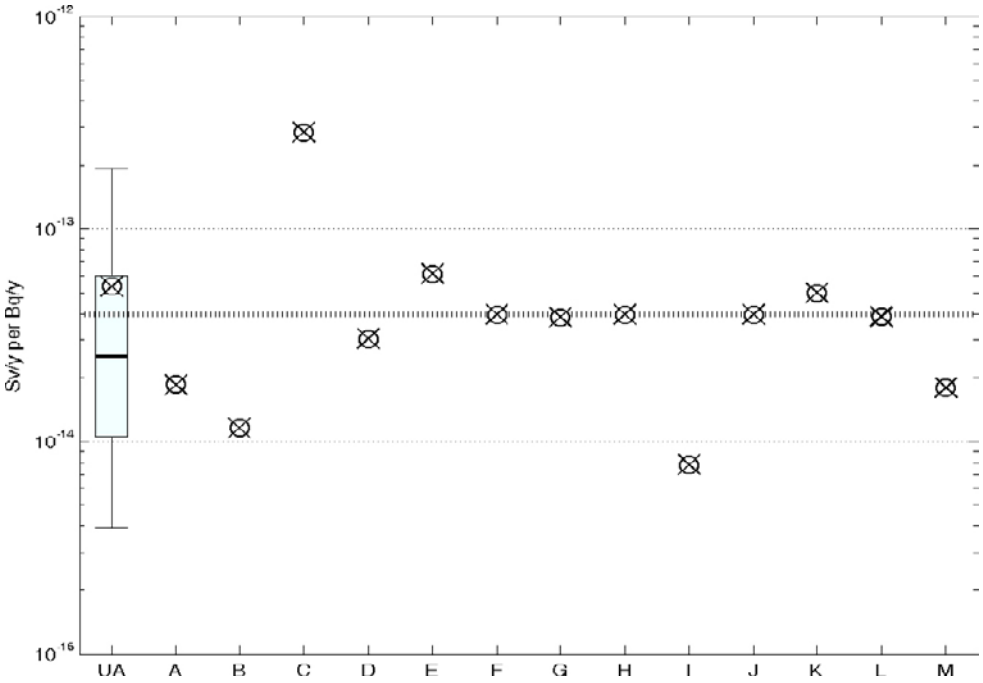


***Figure 5-54.*** *Results from uncertainty analyses of the LDF for Cs-135.The circles with codes from A to G (see Table 5-1) show LDF values obtained from simulations for evaluation of system uncertainties. The circles with codes from H to M (see Table 5-4) show LDF values obtained from simulations for evaluation of model uncertainties. The whisker plot on the left shows the 5th, 25th, 50th, 75th, 95th and mean value (circle) of the LDFs obtained from the probabilistic simulations.*

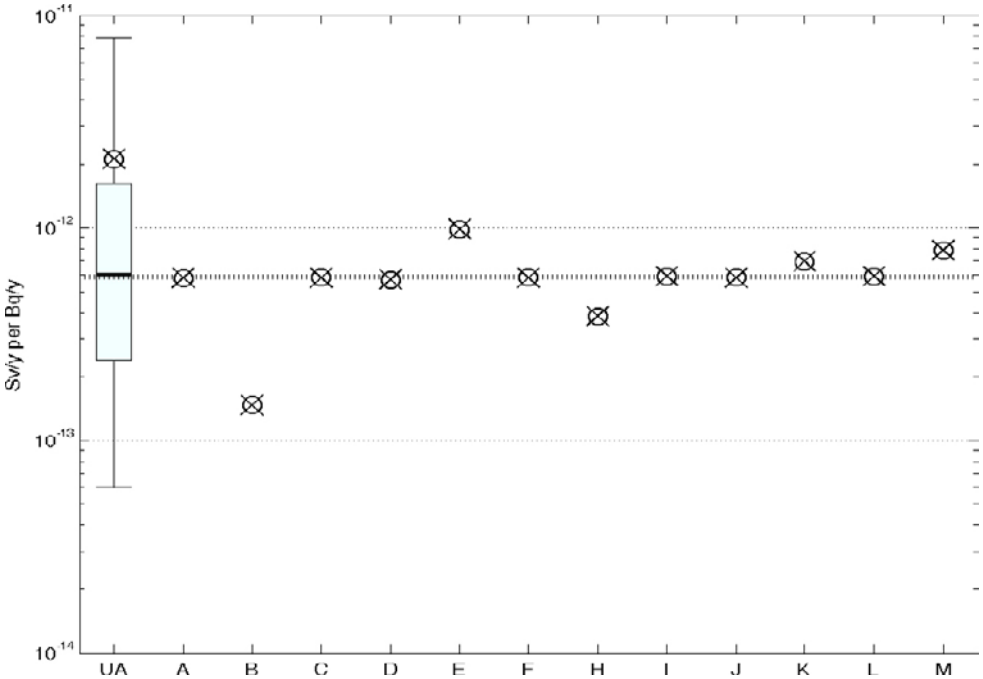


***Figure 5-55.*** *Results from uncertainty analyses of the LDF for Cl-36.The circles with codes from A to G (see Table 5-1) show LDF values obtained from simulations for evaluation of system uncertainties. The circles with codes from H to M (see Table 5-4) show LDF values obtained from simulations for evaluation of model uncertainties. The whisker plot on the left shows the 5th, 25th, 50th, 75th, 95th and mean value (circle) of the LDFs obtained from the probabilistic simulations.*

Extensive analyses were carried out to characterise which parameters have a strong influence on the assessment endpoint. The sensitivity analyses demonstrated that the influence of individual parameters on *LDF* values varied between radionuclides and depended on the development of the landscape. The analyses highlighted that a large proportion of *LDF* uncertainty can be attributed to parameters describing the partitioning of radionuclides between the solid and liquid phases (i.e. $K_d$) and biological uptake (i.e. CR). For most radionuclides, a combination of generic and site data was used to estimate these parameters, indicating the potential benefit of additional site measurements that would cover systematic natural variation and reduce measurement errors. Alternatively, *LDF* uncertainty could be reduced by describing uptake of radionuclides with models that are less sensitive to parameter uncertainties.

The philosophy of the biosphere assessment has been to make estimations of landscape dose conversion factors as realistic as possible, based on the knowledge of present-day conditions at Forsmark and of the past and expected future development of the site. From the summary of quantitative effects of system and model uncertainties, it is evident that the handling of these types of uncertainties has been balanced for the examined radionuclides. However, the overall handling of system and model uncertainties tended to be cautious, due the adopted approach for handling uncertainties associated to where a potential release from the repository would reach the biosphere and for how long it could affect a specific discharge area.

A representative individual of the most exposed group is assumed spend a lifetime in the discharge area where the environmental concentrations lead to the highest dose, and to get his or her full supply of food and water from the contaminated area. A fairly large sized group of individuals (> 40) can be sustainably supported by agriculture from a transformed wetland in any of the biosphere objects. However, the assumption that a representative individual of the most exposed group should be totally dependent on resources from a small area seems improbable given the availability of non-contaminated land in the future landscape and the organisation of present and historical societies. Though no attempt has been made to quantify a reasonable degree of dilution that would result from the consumption of non-contaminated food and water due to e.g. trading or migration, the assumptions as to the behaviour of future human inhabitants are inherently cautious.

# 6 Conclusions

In this report two types of Dose Conversion Factors have been derived: i) a Landscape Dose Conversion Factor that is applicable to continuous long-term releases at a constant rate (*LDF*), and ii) a Landscape Dose Conversion Factor for pulse releases that is applicable to a radionuclide release that reaches the biosphere in a pulse within years to hundreds of years (*LDF pulse*). In SR-Site, these Dose Factors are multiplied with modelled release rates or pulse releases from the geosphere to obtain estimates of the annual doses to a representative individual of the most exposed group. The dose estimates obtained for different release scenarios are used to assess compliance with the regulatory risk criterion.

The *LDFs* were calculated for three different periods of the reference glacial cycle; the period of submerged conditions following the deglaciation, the temperate period, and a prolonged period of periglacial conditions. Additionally, *LDFs* were calculated for the global warming climate case. The *LDF pulse* was only derived for temperate climate conditions.

The *LDFs* and *LDF pulse* were obtained from deterministic simulations with the Radionuclide Model for the biosphere, using Best Estimated values for the model parameters. The assumptions made for these deterministic simulations are the combined result of process understanding, the most precise description of the site available and reasonable assumptions about the use of natural resources by future human inhabitants of potentially affected areas. Thus, the *LDF* and *LDF pulse* can be considered as Best Estimate values, which can be used in calculations of Best Estimate values of doses to a representative individual of the most exposed group from potential releases from a future repository.

A systematic analysis of the effects of system, model and parameter uncertainties on the *LDFs* has been carried out. The overall handling of system and model uncertainties tended to be cautious, due the adopted approach for handling uncertainties associated to where a potential release from the repository would reach the biosphere and for how long it could affect a specific discharge area. The uncertainty has shown that the use of the derived *LDF* would lead to moderately cautious dose estimates, although the degree of cautiousness varied between radionuclides. The effects of parameter uncertainties on *LDF* calculations were assessed with both systematic (for time dependent parameters) and random variation (for time independent parameters) of model parameters. It was concluded from these assessments that uncertainties in time dependent parameters, for example parameters that represented landscape development, had a limited effect on the uncertainty of the *LDF* estimates. However, from the results of the Monte Carlo simulations it is evident that uncertainty in time independent parameters had a significant contribution to the uncertainty in *LDFs*.

Thus, taken together we are confident that the maximum *LDFs* used in SR-Site are robust estimates for the most exposed group, reflecting process understanding and the most precise description of the site available. Nevertheless, it is recognised that there is a potential to reduce uncertainties, in particular with respect to processes describing the partitioning of radionuclides between the solid and liquid phases (i.e. $K_d$) and biological uptake (i.e. CR). Thus, if the final risk estimates are close to the regulatory limits, it would be reasonable to make an effort to reduce the uncertainty associated with these processes at least for dose-contributing radionuclides.

# 7 References

SKB's (Svensk Kärnbränslehantering AB) publications can be found at www.skb.se/publications.


**Andersson E (ed), 2010.** The limnic ecosystems at Forsmark and Laxemar-Simpevarp. SR-Site Biosphere. SKB TR-10-02, Svensk Kärnbränslehantering AB.

**Aquilonius K (ed), 2010.** The marine ecosystems at Forsmark and Laxemar-Simpevarp. SR-Site Biosphere. SKB TR-10-03, Svensk Kärnbränslehantering AB.

**Avila R, 2006.** Model of the long-term transfer of radionuclides in forests. SKB TR-06-08, Svensk Kärnbränslehantering AB.

**Avila R, Bergström U, 2006.** Methodology for calculation of doses to man and implementation in Pandora. SKB R-06-68, Svensk Kärnbränslehantering AB.

**Avila R, Pröhl G, 2008.** Models used in the SFR 1, SAR-08 and KBS-3H safety assessments for calculation of $^{14}C$ doses. SKB R-08-16, Svensk Kärnbränslehantering AB.

**Beresford N A, Brown J, Copplestone D, Garnier-Laplace J, Howard B, Larsson C M, Oughton D, Pröhl G, Zinger I (eds), 2007.** D-ERICA: An integrated approach to the assessment and management of environmental risk from ionising radiation. Description of purpose, methodology and application. EC contract number FI6R-CT-2004-508847, European Commission, Brussels.

**Bergström U, Nordlinder S, Aggeryd I, 1999.** Models for dose assessments. Modules for various biosphere types. SKB TR-99-14, Svensk Kärnbränslehantering AB.

**BIOCLIM, 2003.** Deliverable D7. Continuous climate evolution scenarios over western Europe (1,000 km scale). Work package 2: Simulation of the future evolution of the biosphere system using the hierarchical strategy. Châtenay-Malabry: Agence nationale pour la gestion des déchets radioactifs (ANDRA).

**Bosson E, Sassner M, Sabel U, Gustafsson L-G, 2010.** Modelling of present and future hydrology and solute transport at Forsmark. SR-Site Biosphere. SKB R-10-02, Svensk Kärnbränslehantering AB.

**Brunberg A-K, Carlsson T, Blomqvist P, Brydsten L, Strömgren M, 2004.** Forsmark site investigation. Identification of catchments, lake-related drainage parameters and lake habitats. SKB P-04-25, Svensk Kärnbränslehantering AB.

**Brydsten L, 2006.** A model for landscape development in terms of shoreline displacement, sediment dynamics, lake formation, and lake choke-up processes. SKB TR-06-40, Svensk Kärnbränslehantering AB.

**Brydsten L, Strömgren M, 2004.** Digital elevation models for site investigation programme in Forsmark. Site description version 1.2. SKB R-04-70, Svensk Kärnbränslehantering AB.

**Brydsten L, Strömgren M, 2010.** A coupled regolith-lake development model applied to the Forsmark site. SKB TR-10-56, Svensk Kärnbränslehantering AB.

**Ekström P-A, 2011.** Pandora – a simulation tool for safety assessments. Technical description and user's guide. SR-Site Biosphere. SKB R-11-01, Svensk Kärnbränslehantering AB.

**Ekström P-A, Broed R, 2006.** Sensitivity analysis methods and a biosphere test case implemented in EIKOS. Posiva Working Report 2006-31, Posiva Oy, Finland.

**Eriksson S, Sellei C, Wallström K, 1977.** The structure of the plankton community of the Öregrundsgrepen (southwest Bothnian Sea). Helgoländer Wissenschaftliche Meeresuntersuchungen, 30, pp 582–597.

**Galson D A, Khursheed A, 2007.** The treatment of uncertainty in performance assessment and safety case development: state-of-the art overview. PAMINA Milestone Report M1.2.1, European Commission.

**Hansen C, 2010.** PAMINA (Preformance Assessment Methodologies in Application to Guide the Development of the Safety Case). Treatment of model uncertainty deliverable: D2.2.B.4 Version 1, Sandia National Laboratory.

**Hartikainen J, Kouhia R, Wallroth T, 2010.** Permafrost simulations at Forsmark using a numerical 2D thermo-hydro-chemical model. SKB TR-09-17, Svensk Kärnbränslehantering AB.

**Hedenström A, Sohlenius G, 2008.** Description of the regolith at Forsmark. Site descriptive modelling, SDM-Site Forsmark. SKB R-08-04, Svensk Kärnbränslehantering AB.

**Hedenström A, Sohlenius G, Strömgren M, Brydsten L, Nyman H, 2008.** Depth and stratigraphy of regolith at Forsmark. Site desprictive modelling, SDM-Site Forsmark. SKB R-08-07, Svensk Kärnbränslehantering AB.

**IAEA, 2010.** Handbook of parameter values for the prediction of radionuclide transfer to humans in terrestrial and freshwater environments. IAEA Technical Reports Series 472, International Atomic Energy Agency, Vienna.

**ICRP, 1991.** 1990 Recommendations of the International Commission on Radiological Protection. Oxford: Pergamon. (ICRP Publication 60; Annals of the ICRP 21)

**ICRP, 1998.** Radiation protection recommendations as applied to the disposal of long-lived solid radioactive waste. Oxford: Pergamon. (ICRP Publication 81; Annals of the ICRP 28)

**ICRP, 2006.** Assessing dose of the representative person for the purpose of radiation protection of the public, and the optimisation of radiological protection: broadening the process. Oxford: Pergamon. (ICRP Publication 101; Annals of the ICRP 36)

**Johansson P-O, 2008.** Description of surface hydrology and near-surface hydrogeology at Forsmark. Site descriptive modelling, SDM-Site Forsmark. SKB R-08-08, Svensk Kärnbränslehantering AB.

**Jones J, Vahlund F, Kautsky U, 2004.** Tensit – a novel probabilistic simulation tool for safety assessments. Tests and verifications using biosphere models. SKB TR-04-07, Svensk Kärnbränslehantering AB.

**Jones J, Kautsky U, Vahlund F, 2005.** Tensit – a simulation tool for nuclide transport, risk and dose calculations. Radioprotection, 40, Suppl. 1, pp S933–S938.

**Jonsell B, Jonsell L, 1995.** Floran i Hållnäs socken (Vasculan plants in the parish of Hållnäs, N Uppland, Sweden) (in Swedish). Svensk Botanisk Tidskrift, 89, pp 257–312.

**Joyce S, Simpson T, Hartley L, Applegate D, Hoek J, Jackson P, Swan D, Marsic N, Follin S, 2010.** Groundwater flow modelling of periods with temperate climate conditions – Forsmark. SKB R-09-20, Svensk Kärnbränslehantering AB.

**Karlsson A, Eriksson C, Borell Lövstedt C, Liungman O, Engqvist A, 2010.** High-resolution hydrodynamic modelling of the marine environment at Forsmark between 6500 BC and 9000 AD. SKB R-10-09, Svensk Kärnbränslehantering AB.

**Karlsson S, Bergström U, 2000.** Dose rate estimates for the Olkiluoto site using the biospheric models of SR 97. Posiva Working Report 2000-20, Posiva Oy, Finland.

**Kjellström E, Strandberg G, Brandefelt J, Näslund J-O, Smith B, Wohlfarth B, 2009.** Climate conditions in Sweden in a 100,000 year time perspective. SKB TR-09-04, Svensk Kärnbränslehantering AB.

**Lindborg T (ed), 2008.** Surface system Forsmark. Site descriptive modelling, SDM-Site Forsmark. SKB R-08-11, Svensk Kärnbränslehantering AB.

**Lindborg T (ed), 2010.** Landscape Forsmark – data, methodology and results for SR-Site. SKB TR-10-05, Svensk Kärnbränslehantering AB.

**Löfgren A (ed), 2010.** The terrestrial ecosystems at Forsmark and Laxemar-Simpevarp. SR-Site Biosphere. SKB TR-10-01, Svensk Kärnbränslehantering AB.

**Miliander S, Punakivi M, Kyläkorpi L, Rydgren B, 2004.** Human population and activities in Forsmark. Site description. SKB R-04-10, Svensk Kärnbränslehantering AB.

**Nordén S, Avila R, de la Cruz I, Stenberg K, Grolander S, 2010.** Element-specific and constant parameters used for dose calculations in SR-Site. SKB TR-10-07, Svensk Kärnbränslehantering AB.

**Rummukainen M, 2003.** The Swedish regional climate modeling program, SWECLIM, 1996–2003: final report. Norrköping: Sveriges meteorologiska och hydrologiska institut (Swedish Meteorological and Hydrological Institute). (SMHI reports. Meteorology and Climatology 104)

**Saltelli A, Chan K, Scott M (eds), 2000.** Sensitivity analysis. Chichester: Wiley.

**Shampine L F, Reichelt M W, 1997.** The MATLAB ODE suite. SIAM Journal on Scientific Computing, 18, pp 1–22.

**Shampine L F, Reichelt M W, Kierzenka J A, 1999.** Solving Index-1 DAEs in MATLAB and Simulink. SIAM Review, 41, pp 538–552.

**Sheppard S C, Evenden W G, 1988.** The assumption of linearity in soil and plant concentration ratios: an experimental evaluation. Journal of Environmental Radioactivity, 7, pp 221–247.

**Sheppard S C, Sheppard M I, 1989.** Impact of correlations on stochastic estimates of soil contamination and plant uptake. Health Physics 57: 653–657.

**SKB, 1999.** Deep repository for spent nuclear fuel. SR 97 – Post-closure safety. Main report – Vol. I, Vol. II and Summary. SKB TR-99-06, Svensk Kärnbränslehantering AB.

**SKB, 2006.** Long-term safety for KBS-3 repositories at Forsmark and Laxemar – a first evaluation. Main report of the SR-Can project. SKB TR-06-09, Svensk Kärnbränslehantering AB.

**SKB, 2008.** Site description of Forsmark at completion of the site investigation phase. SDM-Site Forsmark. SKB TR-08-05, Svensk Kärnbränslehantering AB.

**SKB, 2009.** Site description of Laxemar at completion of the site investigation phase. SDM-Site Laxemar. SKB TR-09-01, Svensk Kärnbränslehantering AB.

**SKB, 2010a.** Biosphere analyses for the safety assessment SR-Site – synthesis and summary of results. SKB TR-10-09, Svensk Kärnbränslehantering AB.

**SKB, 2010b.** Climate and climate-related issues for the safety assessment SR-Site. SKB TR-10-49, Svensk Kärnbränslehantering AB.

**Sonesten L, 2005.** Chemical characteristics of surface waters in the Forsmark area. Evaluation of data from lakes, streams, and coastal sites. SKB R-05-41, Svensk Kärnbränslehantering AB.

**SKB, 2011.** Long-term safety for the final repository for spent nuclear fuel at Forsmark. Main report of the SR-Site project. SKB TR-11-01, Svensk Kärnbränslehantering AB.

**SSM, 2008a.** Strålsäkerhetsmyndighetens föreskrifter och allmänna råd om säkerhet vid slutförvaring av kärnämne och kärnavfall (The Swedish Radiation Safety Authority's Regulations concerning safety in connection with the disposal of nuclear material and nuclear waste) (in Swedish). Stockholm: Strålsäkerhetsmyndigheten (Swedish Radiation Safety Authority). (SSMFS 2008:21)

**SSM, 2008b.** Strålsäkerhetsmyndighetens föreskrifter och allmänna råd om skydd av människors hälsa och miljön vid slutligt omhändertagande av använt kärnbränsle och kärnavfall (The Swedish Radiation Safety Authority's Regulations on the protection of human health and the environment in connection with the final management of spent nuclear fuel and nuclear waste) (in Swedish). Stockholm: Strålsäkerhetsmyndigheten (Swedish Radiation Safety Authority). (SSMFS 2008:37)

**Strömgren M, Brydsten L, 2008.** Digital elevation models of Forsmark. Site descriptive modelling, SDM-Site Forsmark. SKB R-08-62, Svensk Kärnbränslehantering AB.

**Torudd J, 2010.** Long term radiological effects on plants and animals of a deep geological repository. SR-Site Biosphere. SKB TR-10-08, Svensk Kärnbränslehantering AB.

**Tröjbom M, Nordén S, 2010.** Chemistry data from surface ecosystems in Forsmark and Laxemar-Simpevarp. Site specific data used for estimation of CR and $K_d$ values in SR-Site. SKB R-10-28, Svensk Kärnbränslehantering AB.

**Tröjbom M, Söderbäck B, 2006.** Chemical characteristics of surface systems in the Forsmark area. Visualisation and statistical evaluation of data from shallow groundwater, precipitation, and regolith. SKB R-06-19, Svensk Kärnbränslehantering AB.

**Tröjbom M, Söderbäck B, Johansson P-O, 2007.** Hydrochemistry in surface water and shallow groundwater. Site descriptive modelling, SDM-Site Forsmark. SKB R-07-55, Svensk Kärnbränslehantering AB.

**Tröjbom M, Söderbäck B, Kalinowski B, 2008.** Hydrochemistry of surface water and shallow groundwater. Site descriptive modelling, SDM-Site Laxemar. SKB R-08-46, Svensk Kärnbränslehantering AB.

**Åstrand P-G, Broed R, Jones J, 2005.** Pandora technical description and user guide. Posiva Working Report 2005-64, Posiva Oy, Finland.

# Appendix A

## Equations in the Radionuclide Model for the biosphere

In this Appendix the equations included in the Radionuclide Model for the biosphere are presented. Firstly, a model overview is given including the conceptual model, the differential equations and the transfer rate coefficients; secondly a report generated by the software tool Ecolego is presented including all the detailed equations used in the model.

### *Model overview*

The Radionuclide Model for the biosphere is a compartment model consisting of a System of 10 Ordinary Differential Equations (ODEs). Each ODE represents the rate of change of the radionuclide inventory (Bq) in a model compartment, as a function of the radionuclide fluxes (Bq/y) from and to this compartment, and of radioactive decay and in-growth of progeny. The ODE of a compartment (*k*) has the following general form:

$$\frac{dA^j_k}{dt} = F^j_{\text{out to k}} - F^j_{\text{k to out}} + \sum_i F^j_{\text{i to k}} - \sum_i F^j_{\text{k to i}} - \lambda^j \cdot A^j_k + \text{ingrowth}^j$$

$$F^j_{\text{k to out}} = TC^j_{k\ to\ out} \cdot A^j_k$$

$$F^j_{\text{i to k}} = TC^j_{i\ to\ k} \cdot A^j_i$$

$$F^j_{\text{k to i}} = TC^j_{k\ to\ i} \cdot A^j_k$$

where,

$A^j_k$ is in inventory of the *j-th* radionuclide in compartment k (Bq).

$\lambda^j$ is the decay constant for the *j-th* radionuclide (year$^{-1}$).

Ingrowth $^j$ is the in-growth of the *j-th* radionuclide from decay of the parents (Bq·year$^{-1}$).

$F^j_{\text{out to k}}$ is the inflow of the *j-th* radionuclide from outside the system to *k-th* compartment (Bq·year$^{-1}$).

$F_{\text{k to out}}$ is the outflow of the *j-th* radionuclide from *k-th* compartment out from the system (Bq·year$^{-1}$).

$F^j_{\text{i to k}}$ is the flux of the *j-th* radionuclide from *i-th* to *k-th* compartment (Bq·year$^{-1}$).

$F^j_{\text{k to i}}$ is the flux of the *j-th* radionuclide from *k-th* to *i-th* compartment (Bq·year$^{-1}$).

$TC^j_{\text{k to out}}$ is the transfer rate coefficient of the *j-th* radionuclide from *k-th* compartment out from the system (year$^{-1}$).

$TC^j_{\text{k to i}}$ is the transfer rate coefficient of the *j-th* radionuclide from *k-th* to *i-th* compartment (year$^{-1}$).

$TC^j_{\text{i to k}}$ is the transfer rate coefficient rate of the *j-th* radionuclide from *i-th* to *k-th* compartment (year$^{-1}$).

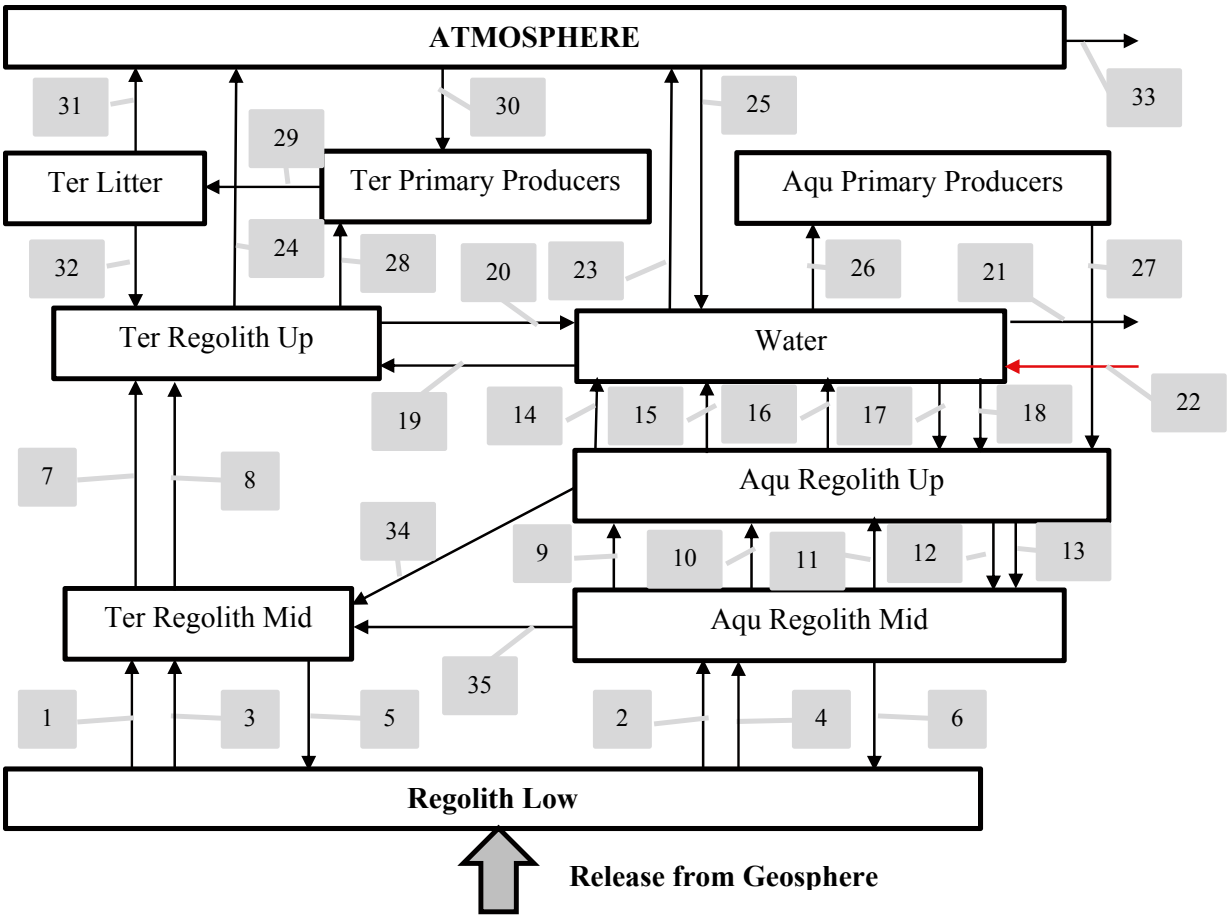


***Figure A-1.*** *Conceptual representation of the Radionuclide Model for the biosphere. The boxes represent model compartments and the black arrows represent radionuclide fluxes calculated with Transfer Rate Coefficients. The red arrow represents inflows with surface waters from adjacent biosphere objects.*

### *Transfer rate coefficients (TC)*

The transfer rate coefficients, *TC*, represent the fraction of the inventory in one compartment that is transferred to other compartments and out from the biosphere object. The different fluxes included in the model are represented with arrows in Figure A-1.

The parameters used in the equations of *TCs* are listed in Appendix B and are shown below in **bold**.

**Regolith_Low to Ter_Regolith_ Mid and Aqu_ Regolith_ Mid**

1 The equation for the *TC* of the *j-th* radionuclide from Regolith_Low to Ter_Regolith_Mid by advection (arrow 1 in Figure A-1) is:

$$TC^j = adv\_low\_mid \cdot \frac{fract\_Mire}{z\_regoLow \cdot \boldsymbol{poro\_regoLow} \cdot R^j\_regoLow}$$

where,

*adv_low_mid* (m/y) equals ***Sea_adv_low_mid*** for time < ***threshold_start***

*adv_low_mid* (m/y) equals ***Lake_adv_low_mid*** for time > ***threshold_stop***

*adv_low_mid* (m/y) is calculated with a linear equation going from ***Sea_adv_low_mid*** to ***Lake_adv_low_mid*** for times between ***threshold_start*** and ***threshold_stop***

*fract_Mire* (unitless) equals zero for time < ***threshold_start***

*fract_Mire* (unitless) equals ***Lake_fract_Mire*** for time > ***threshold_stop***

*fract_Mire* (unitless) is calculated with a linear equation going from zero to ***Lake_fract_Mire*** for times between ***threshold_start*** and ***threshold_stop***

*z_regoLow* (m) equals ***Sea_z_regoLow*** for time < ***threshold_start***

*z_regoLow* (m) equals ***Lake_z_regoLow*** for time > ***threshold_stop***

*z_regoLow* (m) is calculated with a linear equation going from ***Sea_z_regoLow*** to ***Lake_z_regoLow*** for times between ***threshold_start*** and ***threshold_stop***

$R^j\_regoLow$ (unitless) is the retardation factor for the *j-th* radionuclide in the *Regolith_Low* compartment

$$R^j\_regoLow = 1.0 + \boldsymbol{kD\_regoLow^j} \cdot \frac{\boldsymbol{dens\_regoLow}}{\boldsymbol{poro\_regoLow}}$$

2 The equation for the *TC* of the *j-th* radionuclide from Regolith_Low to Aqu_Regolith_Mid by advection (arrow 2 in Figure A-1) is:

$$TC^j = adv\_low\_mid \cdot \frac{1 - fract\_Mire}{z\_regoLow \cdot \boldsymbol{poro\_regoLow} \cdot R^j\_regoLow}$$

3 The equation for the *TC* of the *j-th* radionuclide from Regolith_Low to Ter_Regolith_Mid by diffusion (arrow 3 in Figure A-1) is:

$$TC^j = 2.0 \cdot \frac{\boldsymbol{diffcoef^j}}{z\_regoLow^2 \cdot R^j\_regoLow} \cdot \frac{\boldsymbol{Ter\_area\_obj}}{\boldsymbol{Ter\_area\_obj} + \boldsymbol{Aqu\_area\_obj}}$$

4 The equation for the *TC* of the *j-th* radionuclide from Regolith_Low to Aqu_Regolith_Mid by diffusion (arrow 4 in Figure A-1) is:

$$TC^j = 2.0 \cdot \frac{\boldsymbol{diffcoef^j}}{z\_regoLow^2 \cdot R^j\_regoLow} \cdot \frac{\boldsymbol{Aqu\_area\_obj}}{\boldsymbol{Ter\_area\_obj + Aqu\_area\_obj}}$$

**Ter_Regolith_ Mid and Aqu_ Regolith_ Mid to Regolith_Low**

5 The equation for the *TC* of the *j-th* radionuclide from Ter_Regolith_Mid to Regolith_Low by diffusion (arrow 5 in Figure A-1) is:

$$TC^j = 2.0 \cdot \frac{\boldsymbol{diffcoef^j}}{Ter\_z\_regoMid^2 \cdot R^j\_Ter\_regoMid}$$

where,

*Ter_z_regoMid* (m) is the sum of ***Ter_z_regoMid_pg*** and ***Aqu_z_regoMid_gl_lake***

$R^j$*_Ter_regoMid* (unitless) is the retardation factor for the *j-th* radionuclide in the *Ter_Regolith_Mid* compartment

$$R^j\_Ter\_regoMid = 1.0 + \boldsymbol{Ter\_kD\_regoMid^j} \cdot \frac{Ter\_dens\_regoMid}{Ter\_poro\_regoMid}$$

$$Ter\_dens\_regoMid = \frac{\boldsymbol{Ter\_z\_regoMid\_pg \cdot Ter\_dens\_regoMid\_pg + z\_rego\_Mid\_gl\_basin \cdot Ter\_dens\_regoMid\_gl}}{Ter\_z\_regoMid}$$

$$Ter\_poro\_regoMid = \frac{\boldsymbol{Ter\_z\_regoMid\_pg \cdot Ter\_poro\_regoMid\_pg + z\_rego\_Mid\_gl\_basin \cdot Ter\_poro\_regoMid\_gl}}{Ter\_z\_regoMid}$$

6 The equation for the *TC* of the *j-th* radionuclide from Aqu_Regolith_Mid to Regolith_Low by diffusion (arrow 6 in Figure A-1) is:

$$TC^j = 2.0 \cdot \frac{\boldsymbol{diffcoef^j}}{Aqu\_z\_regoMid^2 \cdot R^j\_Aqu\_regoMid}$$

where,

*Aqu_z_regoMid* (m) is the sum of ***Agu_z_regoMid_pg*** and *Aqu_z_regoMid_gl*

*Aqu_z_regoMid_gl* (m) equals ***z_regoMid_gl_basin*** for time < ***threshold_start***

*Aqu_z_regoMid_gl* (m) equals ***Aqu_z_regoMid_gl_lake*** for time > ***threshold_stop***

*Aqu_z_regoMid*_gl (m) is calculated with a linear equation going from ***z_regoMid_gl_basin*** to ***Aqu_z_regoMid_gl_lake*** for times between ***threshold_start*** and ***threshold_stop***

$R^j$ *_Aqu_regoMid* (unitless) is the retardation factor for the *j-th* radionuclide in the *Ter_Regolith_Mid* compartment

$$R^j\_Aqu\_regoMid = 1.0 + Aqu\_kD\_regoMid^j \cdot \frac{Aqu\_dens\_regoMid}{Aqu\_poro\_regoMid}$$

where,

*Aqu_kD_regoMid*$^j$ (m$^3$/kg dw) equals ***Sea_kD_regoMid*** for time < ***threshold_start***

*Aqu_kD_regoMid*$^j$ (m$^3$/kg dw) equals ***Lake_kD_regoMid*** for time > ***threshold_stop***

*Aqu_kD_regoMid*$^j$ (m$^3$/kg dw) is calculated with a linear equation going from ***Sea_kD_regoMid*** to ***Lake_kD_regoMid*** for times between ***threshold_start*** and ***threshold_stop***

$$Aqu\_dens\_regoMid = \frac{\boldsymbol{Aqu\_z\_regoMid\_pg} \cdot \boldsymbol{Aqu\_dens\_regoMid\_pg} + Aqu\_z\_rego\_Mid\_gl \cdot \boldsymbol{Aqu\_dens\_regoMid\_gl}}{Aqu\_z\_regoMid}$$

$$Aqu\_poro\_regoMid = \frac{\boldsymbol{Aqu\_z\_regoMid\_pg} \cdot \boldsymbol{Aqu\_poro\_regoMid\_pg} + Aqu\_z\_rego\_Mid\_gl \cdot \boldsymbol{Aqu\_poro\_regoMid\_gl}}{Aqu\_z\_regoMid}$$

**Ter_Regolith_Mid to Ter_Regolith_Up**

7 The equation for the *TC* of the *j-th* radionuclide from Ter_Regolith_Mid to Ter_Regolith_Up by advection (arrow 7 in Figure A-1) is:

$$TC^j = \frac{\boldsymbol{area\_subcatch} \cdot \boldsymbol{runoff} \cdot \boldsymbol{Ter\_adv\_mid\_up\_norm}}{\boldsymbol{Ter\_area\_obj} \cdot Ter\_z\_regoMid \cdot Ter\_poro\_regoMid \cdot R^j\_Ter\_regoMid}$$

8 The equation for the *TC* of the *j-th* radionuclide from Ter_Regolith_Mid to Ter_Regolith_Up by diffusion (arrow 8 in Figure A-1) is:

$$TC^j = 2.0 \cdot \frac{\boldsymbol{diffcoef^j}}{Ter\_z\_regoMid^2 \cdot R^j\_Ter\_regoMid}$$

**Aqu_Regolith_Mid to Aqu_Regolith_Up**

9 The equation for the *TC* of the *j-th* radionuclide from Aqu_Regolith_Mid to Aqu_Regolith_Up by advection (arrow 9 in Figure A-1) is:

$$TC^j = \frac{\boldsymbol{area\_subcatch} \cdot \boldsymbol{runoff} \cdot Aqu\_adv\_mid\_up\_norm}{\boldsymbol{Aqu\_area\_object} \cdot Aqu\_z\_regoMid \cdot Aqu\_poro\_regoMid.R^j\_Aqu\_regoMid}$$

$$+\frac{adv\_low\_mid \cdot (1 - fract\_Mire) \cdot (\boldsymbol{Ter\_area\_object} + \boldsymbol{Aqu\_area\_object})}{\boldsymbol{Aqu\_area\_object} \cdot Aqu\_z\_regoMid \cdot Aqu\_poro\_regoMid \cdot R^j\_Aqu\_regoMid}$$

where,

*Aqu_adv_mid_up_norm* (unitless) equals zero for time < ***threshold_start***

*Aqu_adv_mid_up_norm* (unitless) equals ***Lake_Aqu_adv_mid_up_norm*** for time > ***threshold_stop***

*Aqu_adv_mid_up_norm* (unitless) is calculated with a linear equation going from zero to ***Lake_Aqu_adv_mid_up_norm*** for times between ***threshold_start*** and ***threshold_stop***

10 The equation for the *TC* of the *j-th* radionuclide from Aqu_Regolith_Mid to Aqu_Regolith_Up by diffusion (arrow 10 in Figure A-1) is:

$$TC^j = 2.0 \cdot \frac{\boldsymbol{diffcoef^j}}{Aqu\_z\_regoMid^2 \cdot R^j\_Aqu\_regoMid}$$

11 The equation for the *TC* of the *j-th* radionuclide from Aqu_Regolith_Mid to Aqu_Regolith_Up by erosion of sediments (arrow 11 in Figure A-1) is:

$$TC^j = -\frac{\boldsymbol{growth\_rego}}{Aqu\_z\_regoMid}$$

*If* ***growth_rego*** *is negative and zero otherwise*

**Aqu_Regolith_Up to Aqu_Regolith_Mid**

12 The equation for the *TC* of the *j-th* radionuclide from Aqu_Regolith_Up to Aqu_Regolith_Mid by advection (arrow 12 in Figure A-1) is:

$$TC^j = \frac{\boldsymbol{area\_subcatch} \cdot \boldsymbol{runoff} \cdot Aqu\_adv\_mid\_up\_norm}{\boldsymbol{Aqu\_area\_object} \cdot Aqu\_z\_regoUp \cdot \boldsymbol{Aqu\_poro\_regoUp} \cdot R^j\_Aqu\_regoUp}$$

where,

*Aqu_z_regoUp* (m) equals ***Sea_z_regoUp*** for time < ***threshold_start***

*Aqu_z_regoUp* (m) equals ***Lake_z_regoUp*** for time > ***threshold_stop***

*Aqu_z_regoUp* (m) is calculated with a linear equation going from ***Sea_z_regoUp*** to ***Lake_z_regoUp*** for times between ***threshold_start*** and ***threshold_stop***

$R^j$*_Aqu_regoUp* (unitless) is the is the retardation factor for the *j-th* radionuclide in the *Aqu_Regolith_Up* compartment

$$R^j\_Aqu\_regoUp = 1.0 + Aqu\_kD\_regoUp^j \cdot \frac{\boldsymbol{Aqu\_dens\_regoUp}}{\boldsymbol{Aqu\_poro\_regoUp}}$$

where,

*Aqu_kD_regoUp*$^j$ (m$^3$/kg dw) equals ***Sea_kD_regoUp*** for time < ***threshold_start***

*Aqu_kD_regoUp*$^j$ (m$^3$/kg dw) equals ***Lake_kD_regoUp*** for time > ***threshold_stop***

*Aqu_kD_regoUp*$^j$ (m$^3$/kg dw) is calculated with a linear equation going from ***Sea_kD_regoUp*** to ***Lake_kD_regoUp*** for times between ***threshold_start*** and ***threshold_stop***

13 The equation for the *TC* of the *j-th* radionuclide from Aqu_Regolith_Up to Aqu_Regolith_Mid by sedimentation (arrow 13 in Figure A-1) is:

$$TC^j = \frac{\boldsymbol{growth\_rego}}{Aqu\_z\_regoMid}$$

*If* ***growth_rego*** *is positive and zero otherwise*

**Aqu_Regolith_Up to Water**

14 The equation for the *TC* of the *j-th* radionuclide from Aqu_Regolith_Up to Water by advection (arrow 14 in Figure A-1) is:

$$TC^j = \frac{\boldsymbol{area\_subcatch}\cdot\boldsymbol{runoff}\cdot Aqu\_adv\_mid\_up\_norm}{\boldsymbol{Aqu\_area\_object}\cdot Aqu\_z\_regoUp\cdot\boldsymbol{Aqu\_poro\_regoUp}\cdot R^j\_Aqu\_regoUp} + \frac{adv\_low\_mid\cdot(1-fract\_Mire)\cdot(\boldsymbol{Ter\_area\_object}+\boldsymbol{Aqu\_area\_object})}{\boldsymbol{Aqu\_area\_object}\cdot Aqu\_z\_regoUp\cdot\boldsymbol{Aqu\_poro\_regoUp}\cdot R^j\_Aqu\_regoUp}$$

15 The equation for the *TC* of the *j-th* radionuclide from Aqu_Regolith_Up to Water by diffusion (arrow 15 in Figure A-1) is:

$$TC^j = 2.0 \cdot \frac{\boldsymbol{diffcoef}^j}{Aqu\_z\_regoUp^2 \cdot R^j\_Aqu\_regoUp}$$

16 The equation for the *TC* of the *j-th* radionuclide from Aqu_Regolith_Up to Water by resuspension (arrow 16 in Figure A-1) is:

$$TC^j = \boldsymbol{res\_rate} \cdot \frac{Aqu\_kD\_regoUp}{Aqu\_z\_regoUp \cdot \boldsymbol{Aqu\_poro\_regoUp} \cdot R^j\_Aqu\_regoUp}$$

**Water to Aqu_Regolith_Up**

17 The equation for the *TC* of the *j-th* radionuclide from Water to Aqu_Regolith_Up by advection (arrow 17 in Figure A-1) is:

$$TC^j = \frac{\boldsymbol{area\_subcatch} \cdot \boldsymbol{runoff} \cdot Aqu\_adv\_mid\_up\_norm}{\boldsymbol{Aqu\_area\_object} \cdot \boldsymbol{depth\_aver} \cdot R^j\_Water}$$

where,

$R^j\_Water$ (unitless) is the is the retardation factor for the *j-th* radionuclide in the *WATER compartment*

$$R^j_{Water} = 1.0 + kD\_PM^j \cdot Aqu\_conc\_PM^j$$

where,

$kD\_PM^j$ ($m^3$/kg dw) equals ***Sea_kD_PM*** for time < ***threshold_start***

$kD\_PM^j$ ($m^3$/kg dw) equals ***Lake_kD_PM*** for time > ***threshold_stop***

$kD\_PM^j$ ($m^3$/kg dw) is calculated with a linear equation going from ***Sea_kD_PM*** to ***Lake_kD_PM*** for times between ***threshold_start*** and ***threshold_stop***

$Aqu\_conc\_PM^j$ (kg dw /$m^3$) equals ***Sea_conc_PM*** for time < ***threshold_start***

$Aqu\_conc\_PM^j$ (kg dw /$m^3$) equals ***Lake_conc_PM*** for time > ***threshold_stop***

$Aqu\_conc\_PM^j$ (kg dw /$m^3$) is calculated with a linear equation going from ***Sea_conc_PM*** to ***Lake_conc_PM*** for times between ***threshold_start*** and ***threshold_stop***

18 The equation for the *TC* of the *j-th* radionuclide from Water to Aqu_Regolith_Up by sedimentation (arrow 18 in Figure A-1) is:

$$TC^j = \boldsymbol{sed\_rate} \cdot \frac{kD\_PM^j}{\boldsymbol{depth\_aver} \,.\, R^j\_Water}$$

**Water to Ter_Regolith_Up**

19 The equation for the *TC* of the *j-th* radionuclide from Water to Ter_Regolith_Up by advection (arrow 19 in Figure A-1) is:

$$TC^j = \frac{\boldsymbol{Flooding\_coef} \cdot \boldsymbol{area\_subcatch} \cdot \boldsymbol{runoff}}{\boldsymbol{depth\_aver} \cdot \boldsymbol{Aqu\_area\_obj}}$$

**Ter_Regolith_Up to Water**

20 The equation for the *TC* of the *j-th* radionuclide from Ter_Regolith_Up to Water by advection (arrow 20 in Figure A-1) is:

$$TC^j = \frac{\boldsymbol{area\_subcatch} \cdot \boldsymbol{runoff} + \boldsymbol{Flooding\_coef} \cdot \boldsymbol{area\_subcatch} \cdot \boldsymbol{runoff}}{\boldsymbol{Ter\_area\_obj} \cdot \boldsymbol{Ter\_poro\_regoUp} \cdot \boldsymbol{Ter\_z\_regoUp} \cdot R^j\_Ter\_regoUp}$$

where,

$R^j\_Ter\_regoUp$ (unitless) is the is the retardation factor for the *j-th* radionuclide in the *Ter_Regolith_Up* compartment

$$R^j\_Ter\_regoUp = 1.0 + \boldsymbol{Ter\_kD\_regoUp^j} \cdot \frac{\boldsymbol{Ter\_dens\_regoUp}}{\boldsymbol{Ter\_poro\_regoUp}}$$

**Water to downstream biosphere objects**

21 The equation for the *TC* of the *j-th* radionuclide from Water to downstream biosphere objects by advection (arrow 21 in Figure A-1) is:

For time < ***threshold_start***

$$TC^j = \frac{1.0}{\boldsymbol{wat\_ret}}$$

For time ≥ ***threshold_start***

$$TC^j = \frac{\boldsymbol{area\_wshed} \cdot \boldsymbol{runoff}}{\boldsymbol{depth\_aver} \cdot \boldsymbol{Aqu\_area\_obj}}$$

**Backflux to Water during Sea stage**

22 The equation for the *back flux* of the *j-th* radionuclide to the WATER compartment from a connected Sea object *X* (arrow 22 in Figure A-1) is:

$$TC^j = \frac{\boldsymbol{depth\_aver} \cdot \boldsymbol{Aqu\_area\_object}}{\boldsymbol{depth\_aver\_X} \cdot \boldsymbol{Aqu\_aver\_X} \cdot \boldsymbol{wat\_ret}}$$

This *TC* is multiplied by the radionuclide inventory in the WATER compartment of the Sea object *X* to obtain the flux to the WATER compartment of the biosphere object of interest.

**Water to Atmosphere**

23 The equation for the *TC* of C-14 from Water to Atmosphere by gas exchange (arrow 23 in Figure A-1) is:

$$TC = \frac{\boldsymbol{Aqu\_degass\_C}}{Aqu\_conc\_DIC \cdot \boldsymbol{depth\_aver}}$$

where,

*Aqu_conc_DIC* (kgC/m$^3$) equals ***Sea_conc_DIC*** for time < ***threshold_start***

*Aqu_conc_DIC* (kgC/m$^3$)) equals ***Lake_conc_DIC*** for time > ***threshold_stop***

*Aqu_conc_DIC* (kgC/m$^3$) is calculated with a linear equation going from ***Sea_conc_DIC*** to ***Lake_conc_DIC*** for times between ***threshold_start*** and ***threshold_stop***

**Ter_Regolith Up to Atmosphere**

24 The equation for the *TC* of C-14 from Ter_Regolith_Up to Atmosphere by gas exchange (arrow 24 in Figure A-1) is:

$$TC = \frac{\boldsymbol{Ter\_degass\_C}}{\boldsymbol{Ter\_z\_regoUp} \cdot \boldsymbol{Ter\_conc\_C\_regoUp}}$$

**Atmosphere to Water**

25 The equation for the *TC* of C-14 from Atmosphere to Water by gas exchange (arrow 25 in Figure A-1) is:

$$TC = \frac{\boldsymbol{gasUptake\_C}}{\boldsymbol{conc\_C\_atmos} \cdot \boldsymbol{Ter\_z\_mixlay}}$$

**Water to Aqu_Primary_Producers**

26 The equation for the *TC* of the *j-th* radionuclide (except C-14) from Water to Aqu_Primary_Producers (arrow 26 in Figure A-1) is:

$$TC = \frac{\begin{array}{l}\boldsymbol{Aqu\_prod\_pp\_plank} \cdot \boldsymbol{Aqu\_biom\_pp\_plank} \cdot cR\_pp\_plank^{j} + \boldsymbol{Aqu\_prod\_pp\_ubent} \cdot \boldsymbol{Aqu\_biom\_pp\_ubent} \cdot cR\_pp\_ubent \\ + \boldsymbol{Aqu\_prod\_pp\_macro} \cdot \boldsymbol{Aqu\_biom\_pp\_macro} \cdot cR\_pp\_macro\end{array}}{\boldsymbol{depth\_aver} \cdot R^{j}\_Water}$$

where,

$cR\_pp\_plank^{j}$ ($m^3$/kgC) equals ***Sea_cR_pp_plank*** for time < ***threshold_start***

$cR\_pp\_plank^{j}$ ($m^3$/kgC) equals ***Lake_ cR_pp_plank*** for time > ***threshold_stop***

$cR\_pp\_plank^{j}$ ($m^3$/kgC) is calculated with a linear equation going from ***Sea_cR_pp_plank*** to ***Lake_ cR_pp_plank*** for times between ***threshold_start*** and ***threshold_stop***

$cR\_pp\_ubent^{j}$ ($m^3$/kgC) equals ***Sea_cR_pp_ubent*** for time < ***threshold_start***

$cR\_pp\_ubent^{j}$ ($m^3$/kgC) equals ***Lake_ cR_pp_ubent*** for time > ***threshold_stop***

$cR\_pp\_ubent^{j}$ ($m^3$/kgC) is calculated with a linear equation going from ***Sea_cR_pp_ubent*** to ***Lake_ cR_pp_ubent*** for times between ***threshold_start*** and ***threshold_stop***

$cR\_pp\_macro^{j}$ ($m^3$/kgC) equals ***Sea_cR_pp_macro*** for time < ***threshold_start***

$cR\_pp\_macro^{j}$ ($m^3$/kgC) equals ***Lake_ cR_pp_macro*** for time > ***threshold_stop***

$cR\_pp\_macro^{j}$ ($m^3$/kgC) is calculated with a linear equation going from ***Sea_cR_pp_macro*** to ***Lake_ cR_pp_macro*** for times between ***threshold_start*** and ***threshold_stop***

26 The equation for the *TC* of C-14 from Water to Aqu_Primary_Producers (arrow 26 in Figure A-1) is:

$$TC = \frac{\boldsymbol{Aqu\_prod\_pp\_plank} \cdot \boldsymbol{Aqu\_biom\_pp\_plank} + \boldsymbol{Aqu\_prod\_pp\_ubent} \cdot \boldsymbol{Aqu\_biom\_pp\_ubent} + \boldsymbol{Aqu\_prod\_pp\_macro} \cdot \boldsymbol{Aqu\_biom\_pp\_macro}}{\boldsymbol{depth\_aver} \cdot Aqu\_conc\_DIC \cdot R\_Water}$$

where,

*Aqu_conc_DIC* (kgC/ $m^3$) equals ***Sea_conc_DIC*** for time < ***threshold_start***

*Aqu_conc_DIC* (kgC/ $m^3$) equals ***Lake_conc_DIC*** for time > ***threshold_stop***

*Aqu_conc_DIC* (kgC/ $m^3$) is calculated with a linear equation going from ***Sea_conc_DIC*** to ***Lake_ conc_DIC*** for times between ***threshold_start*** and ***threshold_stop***

**Aqu_Primary_Producers to Aqu_regolith_Up**

27 The equation for the *TC* of the *j-th* radionuclide from Aqu_Primary_Producers to Aqu_Regolith_Up (arrow 27 in Figure A-1) is:

$$TC = \frac{\boldsymbol{Aqu\_prod\_pp\_plank} \cdot \boldsymbol{Aqu\_biom\_pp\_plank} + \boldsymbol{Aqu\_prod\_pp\_ubent} \cdot \boldsymbol{Aqu\_biom\_pp\_ubent} + \boldsymbol{Aqu\_prod\_pp\_macro} \cdot \boldsymbol{Aqu\_biom\_pp\_macro}}{\boldsymbol{Aqu\_biom\_pp\_plank} + \boldsymbol{Aqu\_biom\_pp\_ubent} + \boldsymbol{Aqu\_biom\_pp\_macro}}$$

**Ter_Regolith_Up to Ter_Primary_Producers**

28 The equation for the *TC* of the *j-th* radionuclide (except C-14) from Ter_Regolith Up to Ter_Primary_Producers (arrow 28 in Figure A-1) is:

$$TC^j = \frac{\boldsymbol{Ter\_Biom\_pp} \cdot \boldsymbol{Ter\_prodBiomass\_pp} \cdot \boldsymbol{Ter\_cR\_pp}}{\boldsymbol{Ter\_z\_regoUp} \cdot \boldsymbol{Ter\_dens\_regoUp}}$$

**Ter_Primary_Producers to Ter_Litter**

29 The equation for the *TC* of the *j-th* radionuclide from Ter_Primary_Producers to Ter_Litter (arrow 29 in Figure A-1) is:

$$TC^j = \boldsymbol{Ter\_prodBiom\_pp}$$

**Atmosphere to Ter_Primary_Producers**

30 The equation for the *TC* of C-14 from Atmosphere to Ter_Primary_Producers (arrow 30 in Figure A-1) is:

$$TC = \frac{\boldsymbol{Ter\_prodBiom\_pp} \cdot \boldsymbol{Ter\_biom\_pp}}{\boldsymbol{Ter\_z\_mixlay} \cdot \boldsymbol{conc\_C\_atmos}}$$

**Ter_Litter to Atmosphere**

31 The equation for the *TC* of C-14 from Ter_Litter to Atmosphere (arrow 31 in Figure A-1) is:

$$TC = \boldsymbol{Ter\_decomp} \cdot \boldsymbol{frac\_C\_atmos}$$

**Ter_Litter to Ter_Regolith Up**

32 The equation for the *TC* of the *j-th* radionuclide (except C-14) from Ter_Litter to Ter_Regolith Up by decomposition (arrow 32 in Figure A-1) is:

$$TC^j = \boldsymbol{Ter\_decomp} \cdot \boldsymbol{Ter\_df\_decomp^j}$$

32 The equation for the *TC* of C-14 from Ter_Litter to Ter_Regolith Up by decomposition (arrow 32 in Figure A-1) is:

$$TC = \boldsymbol{Ter\_decomp} \cdot (\mathbf{1.0} - \boldsymbol{frac\_C\_atmos})$$

**Atmosphere out from the biosphere object**

33 The equation for the *TC* of C-14 from Atmosphere out from the biosphere object (arrow 33 in Figure A-1) is:

$$TC = \frac{\boldsymbol{vel\_wind}}{log\left(\frac{10.0}{\boldsymbol{Ter\_z\_roughness}}\right)} \cdot \frac{\boldsymbol{Ter\_z\_mixlay}}{\boldsymbol{Ter\_z\_mixlay} - \boldsymbol{Ter\_z\_roughness}} \cdot log\left(\frac{\boldsymbol{Ter\_z\_mixlay}}{\boldsymbol{Ter\_z\_roughness}}\right) - \frac{1}{sqrt\left(\frac{\boldsymbol{Ter\_area\_obj}}{pi}\right)}$$

**Aqu_Regolith_Mid and Aqu_Regolith_Up to Ter_Regolith Mid**

34 35 The equation for the *TC* of the *j-th* radionuclide from Aqu_Regolith_Mid and Aqu_Regolith_Up to Ter_Regolith Mid due to the wetland growth (arrows 34 and 35 in Figure A-1) is:

$$TC^j = \boldsymbol{Ter\_growth\_rego}$$

# 1 Model description generated by Ecolego

## 1.1 Interaction Matrix

| | | | | | |
|---|---|---|---|---|---|
| Source | Import<br>Release Regolith Low | | | | 1 |
| | Biosphere object | Mire Dowstream<br>Outflow Sea<br>Outflow Downstream | | Export | 2 |
| | Backflow | Object 10 | outflow | | 3 |
| | | Backflow | Object 1 | outflow | 4 |
| | | | | Sink | 5 |
| 1 | 2 | 3 | 4 | 5 | |

| **Import** | Transfer |
|---|---|
| **Equation** | **Unit** |
| Import from upstream object. | Bq year $^{-1}$ |

| **Release_Regolith_Low** | Transfer |
|---|---|
| **Equation** | **Unit** |
| Release of radionuclides from the bedrock. | Bq year $^{-1}$ |

## 1.2 Biosphere object

### *Interaction Matrix*

| | | | | | | | | | | |
|---|---|---|---|---|---|---|---|---|---|---|
| ATMOSPHERE | Assimilation Mire | | | | Assimilation Lake | | | | | 1 |
| | Ter PRIMARY PRODUCERS | Excess | | | | | | | | 2 |
| Respiration | | Ter LITTER | Decomposition | | | | | | | 3 |
| Mire Degassing | Mire Uptake | | Ter REGOLITH UP | | Mire Lake | | | | | 4 |
| | | | Mire Adv mid up<br>Mire Diff mid up | Ter REGOLITH MID | | | | | Diff midMire low | 5 |
| Lake Degassing | | | flooding | | Aqu WATER | Lake uptake | Adv water up<br>Sedimentation | | | 6 |
| | | | | | | Aqu PRIMARY PRODUCERS | Lake Litter | | | 7 |
| | | | | Mire ingrowth up | Resuspension<br>Adv up water<br>Diff up water | | Aqu REGOLITH UP | NedSed<br>Lake Adv up mid | | 8 |
| | | | | Mire ingrowth mid | | | UpSed<br>Lake Adv mid up<br>Lake Diff mid up | Aqu REGOLITH MID | Diff midLake low | 9 |
| | | | | Adv low midMire<br>Diff low midMire | | | | Adv low midLake<br>Diff low midLake | REGOLITH LOW | 10 |
| 1 | 2 | 3 | 4 | 5 | 6 | 7 | 8 | 9 | 10 | |

**ATMOSPHERE**

Compartment

The lower part of the atmosphere (the troposphere) where released radionuclides are fully mixed (only relevant for C-14).

| Differential equation | Unit |
|---|---|
| d ATMOSPHERE /dt = -λ · ATMOSPHERE + Ter_LITTER · Respiration + Ter_REGOLITH_UP · Mire_Degassing + Aqu_WATER · Lake_Degassing - ATMOSPHERE · Assimilation_Mire - ATMOSPHERE · Export - ATMOSPHERE · Assimilation_Lake + ingrowth | Bq |

### Assimilation_Lake

Transfer rate coefficient corresponding to the assimilation of radionuclides in the WATER compartment by gas uptake (only relevant for C-14)

Transfer Coefficient

| Equation | Unit |
|---|---|
| if ( have_water AND switcherC )<br>  gasUptake_C / ( conc_C_atmos · Ter_z_mixlay )<br>else<br>  0.0<br>end | year $^{-1}$ |

### have_water

True (1) if object has a water part at a time point. False (0) otherwise.

Expression

| Equation | Unit |
|---|---|
| if ( switcherRiver OR (1.0 - time_GE_threshold_end ))<br>  1.0<br>else<br>  0.0<br>end | unitless |

### time_GE_threshold_end

True (1) for times after the time point when ingrowth of wetland stops. False (0) otherwise.

Expression

| Equation | Unit |
|---|---|
| if (time >= threshold_end )<br>  1.0<br>else<br>  0.0<br>end | unitless |

### Assimilation_Mire

Transfer rate coefficient corresponding to the assimilation rate of C-14 by primary producers

Transfer Coefficient

| Equation | Unit |
|---|---|
| if ( time_GE_threshold_start AND switcherC )<br>  Ter_prodBiom_pp · Ter_biom_pp / conc_C_atmos / Ter_z_mixlay<br>else<br>  0.0<br>end | year $^{-1}$ |

### time_GE_threshold_start

Expression

True (1) for times after the time point when isolation of the bay starts (the bay will become a lake). False (0) otherwise.

| Equation | Unit |
|---|---|
| if (time >= threshold_start )<br>  1.0<br>else<br>  0.0<br>end | unitless |

### Export

Transfer Coefficient

Transfer rate coefficient corresponding to the export of radionuclides from the biosphere object with lateral wind.

| Equation | Unit |
|---|---|
| vel_wind / log(10.0 / Ter_z_roughness ) · ( Ter_z_mixlay / ( Ter_z_mixlay - Ter_z_roughness ) · log( Ter_z_mixlay / Ter_z_roughness ) - 1.0) / sqrt( Ter_area_obj / pi) | year $^{-1}$ |

### Lake_Degassing

Transfer Coefficient

Transfer rate coefficient corresponding to the loss of radionuclides from the WATER compartment by degassing (only relevant for C-14)

| Equation | Unit |
|---|---|
| if ( have_water AND switcherC )<br>  Aqu_degass_C / ( Aqu_conc_DIC · depth_aver )<br>else<br>  0.0<br>end | year $^{-1}$ |

### Aqu_conc_DIC

Expression

Concentration of Dissolved Inorganic Carbon in lake/river or sea water

| Equation | Unit |
|---|---|
| Lake_conc_DIC + ( Sea_conc_DIC - Lake_conc_DIC ) · threshold_sea_lake | kg C/m $^{3}$ |

### threshold_sea_lake

Expression

1 during the sea period: i.e. before threshold_start
0 during the terrestrial period: i.e. after threshold_stop
linearly decreasing from 1 to 0 for times between threshold_start and threshold_stop

| Equation | Unit |
|---|---|
| if (time < threshold_start )<br>  1.0<br>else<br>  if ( time_G_threshold_stop )<br>  0.0<br>  else<br>  ( threshold_stop - time) / ( threshold_stop - threshold_start )<br>  end<br>end | unitless |

### time_G_threshold_stop

Expression

True (1) for times after the time point when the isolation of the bay has ended (the bay will become a lake). False (0) otherwise.

| Equation | Unit |
|---|---|
| if (time > threshold_stop )<br>  1.0<br>else<br>  0.0<br>end | unitless |

### Mire_Degassing

Transfer Coefficient

Transfer rate coefficient corresponding to the loss of radionuclides from the Ter_regoUp compartment due to degassing (only relevant for C-14)

| Equation | Unit |
|---|---|
| if ( time_GE_threshold_start AND switcherC )<br>  Ter_degass_C / ( Ter_z_regoUp · Ter_conc_C_regoUp )<br>else<br>  0.0<br>end | year $^{-1}$ |

### Respiration

Transfer rate coefficient corresponding to the loss of radionuclides to the atmosphere from the Litter compartment driven by respiration (only relevant for C-14)

Transfer Coefficient

| Equation | Unit |
|---|---|
| if ( time_GE_threshold_start AND switcherC )<br>  Ter_decomp · frac_C_atmos<br>else<br>  0.0<br>end | year $^{-1}$ |

### Ter_PRIMARY_PRODUCERS

Terrestrial primary producers.

Compartment

| Differential equation | Unit |
|---|---|
| d Ter_PRIMARY_PRODUCERS /dt = -λ · Ter_PRIMARY_PRODUCERS + ATMOSPHERE · Assimilation_Mire + Ter_REGOLITH_UP · Mire_Uptake - Ter_PRIMARY_PRODUCERS · Excess + ingrowth | Bq |

### Excess

Transfer rate coefficient from primary producers to the Litter compartment.

Transfer Coefficient

| Equation | Unit |
|---|---|
| Ter_prodBiom_pp | year $^{-1}$ |

### Mire_Uptake

Transfer rate coefficient corresponding to the root uptake of radionuclides (except for C-14) by primary producers

Transfer Coefficient

| Equation | Unit |
|---|---|
| if ( switcherC )<br>  0.0<br>else<br>  Ter_biom_pp · Ter_prodBiom_pp · Ter_cR_pp / ( Ter_z_regoUp · Ter_dens_regoUp )<br>end | year $^{-1}$ |

### Ter_LITTER

Compartment

Dead plant material overlying the regolith

| Differential equation | Unit |
|---|---|
| d Ter_LITTER /dt = -λ · Ter_LITTER + Ter_PRIMARY_PRODUCERS · Excess - Ter_LITTER · Decomposition - Ter_LITTER · Respiration + ingrowth | Bq |

### Decomposition

Transfer Coefficient

Transfer rate coefficient from the litter compartment by decomposition.

| Equation | Unit |
|---|---|
| if ( switcherC )<br>  Ter_decomp · (1.0 - frac_C_atmos )<br>else<br>  Ter_decomp · Ter_df_decomp<br>end | year $^{-1}$ |

### Ter_REGOLITH_UP

Compartment

The upper part of the terrestrial regolith which has the highest biological activity, like the peat in a wetland, or the plowing depth of in cultivated land.

| Differential equation | Unit |
|---|---|
| d Ter_REGOLITH_UP /dt = -λ · Ter_REGOLITH_UP + Ter_LITTER · Decomposition + Ter_REGOLITH_MID · Mire_Adv_mid_up + Ter_REGOLITH_MID · Mire_Diff_mid_up + Aqu_WATER · flooding - Ter_REGOLITH_UP · Mire_Uptake - Ter_REGOLITH_UP · Mire_Degassing - Ter_REGOLITH_UP · Mire_Lake - Ter_REGOLITH_UP · Mire_Dowstream + ingrowth | Bq |

### Mire_Adv_mid_up

Transfer Coefficient

Advective transfer rate coefficient between the compartments Ter_regoMid and Ter_regoUp.

| Equation | Unit |
|---|---|
| area_subcatch · runoff · Ter_adv_mid_up_norm / ( Ter_area_obj · Ter_z_regoMid · Ter_poro_regoMid · Ter_R_regoMid ) | year $^{-1}$ |

### Ter_R_regoMid

Expression

Retention coefficient of the Ter_regoMid compartment

| Equation | Unit |
|---|---|
| 1.0 + Ter_kD_regoMid · Ter_dens_regoMid / Ter_poro_regoMid | unitless |

### Ter_dens_regoMid

Expression

Density of the Ter_regoMid compartment

| Equation | Unit |
|---|---|
| ( Ter_z_regoMid_pg · Ter_dens_regoMid_pg + z_regoMid_gl_basin · Ter_dens_regoMid_gl ) / Ter_z_regoMid | kg DW/m $^{3}$ |

### Ter_z_regoMid

Expression

Thickness of the Ter_regoMid compartment.

| Equation | Unit |
|---|---|
| if (( Aqu_z_regoMid_gl_lake + Ter_z_regoMid_pg ) = 0.0)<br>  1.0<br>else<br>  Aqu_z_regoMid_gl_lake + Ter_z_regoMid_pg<br>end | m |

### Ter_poro_regoMid

Expression

Porosity of the Ter_regoMid compartment.

| Equation | Unit |
|---|---|
| ( Ter_z_regoMid_pg · Ter_poro_regoMid_pg + z_regoMid_gl_basin · Ter_poro_regoMid_gl ) / Ter_z_regoMid | m $^{3}$ /m $^{3}$ |

### Mire_Diff_mid_up

Transfer Coefficient

Diffusive transfer rate coefficient between the compartments Ter_regoMid and Ter_regoUp.

| Equation | Unit |
|---|---|
| if ( time_GE_threshold_start )<br>  2.0 · diffcoef / ( Ter_z_regoMid ^ 2.0 · Ter_R_regoMid )<br>else<br>  0.0<br>end | year $^{-1}$ |

### Mire_Dowstream

Transfer Coefficient

Transfer rate coefficient corresponding to the downstream transport from the compartment Ter_regoUp by surface runoff.

| Equation | Unit |
|---|---|
| if ( have_water )<br>  0.0<br>else<br>  area_subcatch · runoff / ( Ter_area_obj · Ter_poro_regoUp · Ter_z_regoUp · Ter_R_regoUp )<br>end | year $^{-1}$ |

### Ter_R_regoUp

Expression

Retardation factor of the Ter_regoUp compartment

| Equation | Unit |
|---|---|
| 1.0 + Ter_kD_regoUp · Ter_dens_regoUp / Ter_poro_regoUp | unitless |

### Mire_Lake

Transfer Coefficient

Transfer rate coefficient from the Ter_regoUp compartment to the WATER compartment during the lake stage.

| Equation | Unit |
|---|---|
| if ( have_water AND time_GE_threshold_start )<br>  area_subcatch · runoff · (1.0 + Flooding_coef ) / ( Ter_area_obj · Ter_poro_regoUp · Ter_z_regoUp · Ter_R_regoUp )<br>else<br>  0.0<br>end | year $^{-1}$ |

### Flooding

Transfer Coefficient

Transfer rate coefficient from the WATER compartment to the Ter_regoUp compartment by flooding.

| Equation | Unit |
|---|---|
| if ( have_water AND time_GE_threshold_start )<br>  Flooding_coef · area_subcatch · runoff / ( depth_aver · Aqu_area_obj )<br>else<br>  0.0<br>end | year $^{-1}$ |

### Ter_REGOLITH_MID

Compartment

The middle part of the terrestrial regolith, containing glacial and postglacial fine material, i.e. sediments formed in a former seabed / lake bottom environment.

| Differential equation | Unit |
|---|---|
| d Ter_REGOLITH_MID /dt = -λ · Ter_REGOLITH_MID + REGOLITH_LOW · Adv_low_midMire + REGOLITH_LOW · Diff_low_midMire + Aqu_REGOLITH_MID · Mire_ingrowth_mid + Aqu_REGOLITH_UP · Mire_ingrowth_up - Ter_REGOLITH_MID · Diff_midMire_low - Ter_REGOLITH_MID · Mire_Adv_mid_up - Ter_REGOLITH_MID · Mire_Diff_mid_up + ingrowth | Bq |

### Adv_low_midMire

Transfer Coefficient

Advective transfer rate coefficient from the regoLow compartment to the Ter_regoMid compartment.

| Equation | Unit |
|---|---|
| Adv_low_mid · fract_Mire / ( z_regoLow · poro_regoLow · R_regoLow ) | year $^{-1}$ |

### Adv_low_mid

Expression

Advective velocity in the regoLow compartment.

| Equation | Unit |
|---|---|
| Lake_adv_low_mid + ( Sea_adv_low_mid - Lake_adv_low_mid ) · threshold_sea_lake | m/year |

### R_regoLow

Expression

Retardation factor of the regoLow compartment

| Equation | Unit |
|---|---|
| 1.0 + kD_regoLow · dens_regoLow / poro_regoLow | unitless |

### fract_Mire

fraction of the upward water flux from the regolith_low compartment that goes to the terrestrial part of the object

Expression

| Equation | Unit |
|---|---|
| if ( have_water )<br>  Lake_fract_Mire · (1.0 - threshold_sea_lake )<br>else<br>  1.0<br>end | unitless |

### z_regoLow

Thickness of the regoLow compartment.

Expression

| Equation | Unit |
|---|---|
| Lake_z_regoLow + ( Sea_z_regoLow - Lake_z_regoLow ) · threshold_sea_lake | m |

### Diff_low_midMire

Diffusive transfer rate coefficient from the regoLow compartment to the Ter_regoMid compartment.

Transfer Coefficient

| Equation | Unit |
|---|---|
| if ( time_GE_threshold_start )<br>  2.0 · diffcoef / ( z_regoLow ^ 2.0 · R_regoLow ) · Ter_area_obj / area_obj<br>else<br>  0.0<br>end | year $^{-1}$ |

### area_obj

Total area of the biosphere object.

Expression

| Equation | Unit |
|---|---|
| if ( time_GE_threshold_start )<br>  Ter_area_obj + Aqu_area_obj<br>else<br>  Aqu_area_obj<br>end | m $^{2}$ |

### Diff_midMire_low

Transfer Coefficient

Diffusive transfer rate coefficient from the Ter_regolith_Mid compartment to the regolith_Low compartment.

| Equation | Unit |
|---|---|
| 2.0 · diffcoef / ( Ter_z_regoMid ^ 2.0 · Ter_R_regoMid ) | year $^{-1}$ |

### Mire_ingrowth_mid

Transfer Coefficient

Transfer rate coefficient from the Aqu_regoolith_Mid compartment to the Ter_regoMid compartment by ingrowth of the mire

| Equation | Unit |
|---|---|
| if ( time_GE_threshold_start )<br>  Ter_growth_rego<br>else<br>  0.0<br>end | year $^{-1}$ |

### Mire_ingrowth_up

Transfer Coefficient

Transfer rate coefficient from the Aqu_regolith_Up compartment to the Ter_regoMid compartment by ingrowth of the mire

| Equation | Unit |
|---|---|
| if ( time_GE_threshold_start )<br>  Ter_growth_rego<br>else<br>  0.0<br>end | year $^{-1}$ |

### Aqu_WATER

Compartment

The surface water (stream, lake, or sea water).

| Differential equation | Unit |
|---|---|
| d Aqu_WATER /dt = -λ • Aqu_WATER + Import + ATMOSPHERE • Assimilation_Lake + Ter_REGOLITH_UP • Mire_Lake + Aqu_REGOLITH_UP • Resuspension + Aqu_REGOLITH_UP • Adv_up_water + Aqu_REGOLITH_UP • Diff_up_water + Aqu_WATER • Backflow - Aqu_WATER • Lake_Degassing - Aqu_WATER • flooding - Aqu_WATER • Adv_water_up - Aqu_WATER • Sedimentation - Aqu_WATER • Lake_uptake - Aqu_WATER • Outflow_Sea - Aqu_WATER • Outflow_Downstream + ingrowth | Bq |

### Adv_up_water

Transfer Coefficient

Advective transfer rate coefficient from the Agu_regolith_Up compartment to the WATER compartment.

| Equation | Unit |
|---|---|
| area_subcatch • runoff • Aqu_adv_mid_up_norm / ( Aqu_area_obj • Aqu_z_regoUp • Aqu_poro_regoUp • Aqu_R_regoUp ) + area_obj • Adv_low_mid • (1.0 - fract_Mire ) / ( Aqu_area_obj • Aqu_z_regoUp • Aqu_poro_regoUp • Aqu_R_regoUp ) | year $^{-1}$ |

### Aqu_R_regoUp

Expression

Retardation factor of the Aqu_regolith_Up compartment.

| Equation | Unit |
|---|---|
| 1.0 + Aqu_kD_regoUp • Aqu_dens_regoUp / Aqu_poro_regoUp | unitless |

### Aqu_kD_regoUp

Expression

Kd value of the Aqu_regolith_Up compartment.

| Equation | Unit |
|---|---|
| Lake_kD_regoUp + ( Sea_kD_regoUp - Lake_kD_regoUp ) • threshold_sea_lake | m $^{3}$ /kg DW |

### Aqu_adv_mid_up_norm

Expression

Normalized advective transfer rate coefficient from the Aqu_regolith_Mid compartment to the Aqu_regolith_Up compartment.

| Equation | Unit |
|---|---|
| Lake_Aqu_adv_mid_up_norm • (1.0 - threshold_sea_lake ) | unitless |

### Aqu_z_regoUp

Expression

Thickness of the Aqu_regolith_Up compartment.

| Equation | Unit |
|---|---|
| Lake_z_regoUp + ( Sea_z_regoUp - Lake_z_regoUp ) • threshold_sea_lake | m |

### Adv_water_up

Transfer Coefficient

Advective transfer rate coefficient from the Aqu_regolith_Up compartment to the WATER compartment.

| Equation | Unit |
|---|---|
| area_subcatch • runoff • Aqu_adv_mid_up_norm / ( Aqu_area_obj • depth_aver • R_water ) | year $^{-1}$ |

### R_water

Expression

Retardation factor of the WATER compartment.

| Equation | Unit |
|---|---|
| 1.0 + kD_PM • Aqu_conc_PM | unitless |

### Aqu_conc_PM

Expression

Concentration of suspended particular matter in the WATER compartment.

| Equation | Unit |
|---|---|
| Lake_conc_PM + ( Sea_conc_PM - Lake_conc_PM ) • threshold_sea_lake | kg DW/m $^{3}$ |

### kD_PM

Expression

Kd value for suspended particular matter in the WATER compartment.

| Equation | Unit |
|---|---|
| Lake_kD_PM + ( Sea_kD_PM - Lake_kD_PM ) • threshold_sea_lake | m $^{3}$ /kg DW |

### Diff_up_water

Transfer Coefficient

Diffusive transfer rate coefficient from the Ter_regolith_Up compartment to the WATER compartment.

| Equation | Unit |
|---|---|
| 2.0 • diffcoef / ( Aqu_z_regoUp ^ 2.0 • Aqu_R_regoUp ) | year $^{-1}$ |

### Lake_uptake

Transfer rate coefficient corresponding to the uptake of C-14 by aquatic primary producers.

Transfer Coefficient

| Equation | Unit |
|---|---|
| if ( switcherC )<br><br>( Aqu_prod_pp_plank • Aqu_biom_pp_plank + Aqu_prod_pp_ubent • Aqu_biom_pp_ubent + Aqu_prod_pp_macro • Aqu_biom_pp_macro ) / ( Aqu_conc_DIC • depth_aver • R_water )<br><br>Else<br><br>Aqu_TC_pp / R_water<br><br>end | year $^{-1}$ |

### Aqu_TC_pp

Transfer rate coefficient corresponding to the uptake of radionuclides (except for C-14) by aquatic primary producers

Expression

| Equation | Unit |
|---|---|
| ( Aqu_prod_pp_plank • Aqu_biom_pp_plank • cR_pp_plank + Aqu_prod_pp_ubent • Aqu_biom_pp_ubent • cR_pp_ubent + Aqu_prod_pp_macro • Aqu_biom_pp_macro • cR_pp_macro ) / depth_aver | year $^{-1}$ |

### cR_pp_macro

Concentration Ratio for macro algae.

Expression

| Equation | Unit |
|---|---|
| Lake_cR_pp_macro + ( Sea_cR_pp_macro - Lake_cR_pp_macro ) • threshold_sea_lake | m $^{3}$ /kg C |

### cR_pp_plank

Concentration Ratio for plankton.

Expression

| Equation | Unit |
|---|---|
| Lake_cR_pp_plank + ( Sea_cR_pp_plank - Lake_cR_pp_plank ) • threshold_sea_lake | m $^{3}$ /kg C |

### cR_pp_ubent

Expression

Concentration Ratio for benthic primary producers.

| Equation | Unit |
|---|---|
| Lake_cR_pp_ubent + ( Sea_cR_pp_ubent - Lake_cR_pp_ubent ) • threshold_sea_lake | $m^3$ /kg C |

### Outflow_Downstream

Transfer Coefficient

Transfer rate coefficient corresponding to the transport from the WATER compartment by surface runoff

| Equation | Unit |
|---|---|
| if ( have_water AND time_GE_threshold_start )<br>  area_wshed • runoff / ( depth_aver • Aqu_area_obj )<br>else<br>  0.0<br>end | $year^{-1}$ |

### Outflow_Sea

Transfer Coefficient

Transfer rate coefficient corresponding to the transport from the WATER compartment to object 10 during the Sea period.

| Equation | Unit |
|---|---|
| if ( is_sea )<br>  1.0 / wat_ret<br>else<br>  0.0<br>end | $year^{-1}$ |

### is_sea

Expression

True (1) for times before the time point when isolation of the bay starts (the bay will become a lake). False (0) otherwise.

| Equation | Unit |
|---|---|
| if ( time_GE_threshold_start )<br>  0.0<br>else<br>  1.0<br>end | unitless |

**Resuspension**

Transfer rate coefficient from the Aqu_regolith_Up compartment to the WATER compartment by resuspension.

Transfer Coefficient

| Equation | Unit |
|---|---|
| res_rate · Aqu_kD_regoUp / ( Aqu_z_regoUp · Aqu_poro_regoUp · Aqu_R_regoUp ) | year $^{-1}$ |

**Sedimentation**

Transfer rate coefficient from the WATER compartment to the Aqu_regolith_Up compartment by sedimentation.

Transfer Coefficient

| Equation | Unit |
|---|---|
| sed_rate · kD_PM / ( depth_aver · R_water ) | year $^{-1}$ |

**Aqu_PRIMARY_PRODUCERS**

The biotic community in aquatic habitats, comprising both primary producers and consumers

Compartment

| Differential equation | Unit |
|---|---|
| d Aqu_PRIMARY_PRODUCERS /dt = -λ · Aqu_PRIMARY_PRODUCERS + Aqu_WATER · Lake_uptake - Aqu_PRIMARY_PRODUCERS · Lake_Litter + ingrowth | Bq |

**Lake_Litter**

Transfer rate coefficient from the aquatic primary producers to the Aqu_regolith_Up compartment

Transfer Coefficient

| Equation | Unit |
|---|---|
| ( Aqu_prod_pp_plank · Aqu_biom_pp_plank + Aqu_prod_pp_ubent · Aqu_biom_pp_ubent + Aqu_prod_pp_macro · Aqu_biom_pp_macro ) / Aqu_biom_pp | year $^{-1}$ |

**Aqu_biom_pp**

Biomass of aquatic primary producers.

Expression

| Equation | Unit |
|---|---|
| Aqu_biom_pp_macro + Aqu_biom_pp_plank + Aqu_biom_pp_ubent | kg C/m $^{2}$ |

## Aqu_REGOLITH_UP

The part of the aquatic regolith with highest biological activity, comprising ca 5-10 cm of the upper aquatic sediments where resuspension and bioturbation can maintain an oxidizing environment.

Compartment

| Differential equation | Unit |
|---|---|
| d Aqu_REGOLITH_UP /dt = -λ • Aqu_REGOLITH_UP + Aqu_REGOLITH_MID • UpSed + Aqu_REGOLITH_MID • Lake_Adv_mid_up + Aqu_REGOLITH_MID • Lake_Diff_mid_up + Aqu_PRIMARY_PRODUCERS • Lake_Litter + Aqu_WATER • Adv_water_up + Aqu_WATER • Sedimentation - Aqu_REGOLITH_UP • Mire_ingrowth_up - Aqu_REGOLITH_UP • NedSed - Aqu_REGOLITH_UP • Lake_Adv_up_mid - Aqu_REGOLITH_UP • Resuspension - Aqu_REGOLITH_UP • Adv_up_water - Aqu_REGOLITH_UP • Diff_up_water + ingrowth | Bq |

## Lake_Adv_mid_up

Advective transfer rate coefficient from the Aqu_regolith_Up compartment to the Aqu_regolith_Mid compartment.

Transfer Coefficient

| Equation | Unit |
|---|---|
| if ( have_water )<br><br>( area_subcatch • runoff • Aqu_adv_mid_up_norm + (1.0 - fract_Mire ) • area_obj • Adv_low_mid ) / ( Aqu_area_obj • Aqu_z_regoMid • Aqu_poro_regoMid • Aqu_R_regoMid )<br>else<br>0.0<br>end | year $^{-1}$ |

## Aqu_R_regoMid

Retardation factor of the Aqu_regolith_Mid compartment.

Expression

| Equation | Unit |
|---|---|
| 1.0 + Aqu_kD_regoMid • Aqu_dens_regoMid / Aqu_poro_regoMid | unitless |

## Aqu_dens_regoMid

Density of the Aqu_regolith_Mid compartment.

Expression

| Equation | Unit |
|---|---|
| ( Aqu_z_regoMid_pg • Aqu_dens_regoMid_pg + Aqu_z_regoMid_gl • Aqu_dens_regoMid_gl ) / Aqu_z_regoMid | kg DW/m $^{3}$ |

### Aqu_z_regoMid

Expression

Thickness of the Aqu_regolith_Mid compartment.

| Equation | Unit |
|---|---|
| Aqu_z_regoMid_pg + Aqu_z_regoMid_gl | m |

### Aqu_z_regoMid_gl

Expression

Thickness of the glacial clay component of the Aqu_regolith_Mid compartment

| Equation | Unit |
|---|---|
| Aqu_z_regoMid_gl_lake + ( z_regoMid_gl_basin - Aqu_z_regoMid_gl_lake ) · threshold_sea_lake | m |

### Aqu_z_regoMid_pg

Expression

Thickness of the post-glacial clay component of the Aqu_regolith_Mid compartment

| Equation | Unit |
|---|---|
| max( Aqu_z_rego_pg - Aqu_z_regoUp , 0.0) | m |

### Aqu_kD_regoMid

Expression

Kd values of the Aqu_regolith_Mid compartment.

| Equation | Unit |
|---|---|
| Lake_kD_regoMid + ( Sea_kD_regoMid - Lake_kD_regoMid ) · threshold_sea_lake | $m^3$ /kg DW |

### Aqu_poro_regoMid

Expression

Porosity of the Aqu_regolith_Mid compartment.

| Equation | Unit |
|---|---|
| ( Aqu_z_regoMid_pg · Aqu_poro_regoMid_pg + Aqu_z_regoMid_gl · Aqu_poro_regoMid_gl ) / Aqu_z_regoMid | $m^3$ /$m^3$ |

### Lake_Adv_up_mid

Advective transfer rate coefficient from the Aqu_regolith_Up compartment to the Aqu_regolith_Mid compartment.

Transfer Coefficient

| Equation | Unit |
|---|---|
| area_subcatch · runoff · Aqu_adv_mid_up_norm / ( Aqu_area_obj · Aqu_z_regoUp · Aqu_poro_regoUp · Aqu_R_regoUp ) | year $^{-1}$ |

### Lake_Diff_mid_up

Diffusive transfer rate coefficient from the Aqu_regolith_Up compartment to the Aqu_regolith_Mid compartment.

Transfer Coefficient

| Equation | Unit |
|---|---|
| if ( have_water )<br>  2.0 · diffcoef / ( Aqu_z_regoMid ^ 2.0 · Aqu_R_regoMid )<br>else<br>  0.0<br>end | year $^{-1}$ |

### NedSed

Transfer rate coefficient from the Aqu_regolith_Up compartment to the Aqu_regolith_Mid compartment due to sediment growth when there is positive net sedimentation.

Transfer Coefficient

| Equation | Unit |
|---|---|
| if ( growth_rego > 0.0)<br>  growth_rego / Aqu_z_regoUp<br>else<br>  0.0<br>end | year $^{-1}$ |

### UpSed

Transfer rate coefficient from the Aqu_regolith_Mid compartment to the Aqu_regolith_Up compartment due to reduction of sediment thickness when there is negative net sedimentation.

Transfer Coefficient

| Equation | Unit |
|---|---|
| if ( growth_rego < 0.0 AND have_water )<br>  - growth_rego / Aqu_z_regoMid<br>else<br>  0.0<br>end | year $^{-1}$ |

### Aqu_REGOLITH_MID

Compartment

The middle part of the regolith in the aquatic part of biosphere objects, usually consisting of glacial and postglacial clay and gyttja.

| Differential equation | Unit |
|---|---|
| d Aqu_REGOLITH_MID /dt = -λ · Aqu_REGOLITH_MID + REGOLITH_LOW · Adv_low_midLake + REGOLITH_LOW · Diff_low_midLake + Aqu_REGOLITH_UP · NedSed + Aqu_REGOLITH_UP · Lake_Adv_up_mid - Aqu_REGOLITH_MID · Mire_ingrowth_mid - Aqu_REGOLITH_MID · Diff_midLake_low - Aqu_REGOLITH_MID · UpSed - Aqu_REGOLITH_MID · Lake_Adv_mid_up - Aqu_REGOLITH_MID · Lake_Diff_mid_up + ingrowth | Bq |

### Adv_low_midLake

Transfer Coefficient

Advective transfer rate coefficient from the regoLow compartment to the Aqu_regolith_Mid compartment.

| Equation | Unit |
|---|---|
| if ( have_water )<br>  Adv_low_mid · (1.0 - fract_Mire ) / ( z_regoLow · poro_regoLow · R_regoLow )<br>else<br>  0.0<br>end | year $^{-1}$ |

### Diff_low_midLake

Transfer Coefficient

Diffusive transfer rate coefficient from the regoLow compartment t the Aqu_regolith_Mid compartment.

| Equation | Unit |
|---|---|
| if ( have_water )<br>  2.0 · diffcoef / ( z_regoLow ^ 2.0 · R_regoLow ) · Aqu_area_obj / area_obj<br>else<br>  0.0<br>end | year $^{-1}$ |

### Diff_midLake_low

Transfer Coefficient

Diffusive transfer rate coefficient between from the Aqu_regolith_Mid compartment to the regoLow compartment.

| Equation | Unit |
|---|---|
| if ( have_water )<br>  2.0 · diffcoef / ( Aqu_z_regoMid ^ 2.0 · Aqu_R_regoMid )<br>else<br>  0.0<br>end | year $^{-1}$ |

**REGOLITH_LOW** — Compartment

The lower part of the regolith overlying the bedrock primarily composed of glacial till.

| Differential equation | Unit |
|---|---|
| d REGOLITH_LOW /dt = -λ · REGOLITH_LOW + Release_Regolith_Low + Ter_REGOLITH_MID · Diff_midMire_low + Aqu_REGOLITH_MID · Diff_midLake_low - REGOLITH_LOW · Adv_low_midMire - REGOLITH_LOW · Diff_low_midMire - REGOLITH_LOW · Adv_low_midLake - REGOLITH_LOW · Diff_low_midLake + ingrowth | Bq |

### 1.2.1 Concentration

**conc_Aqu_PRIMARY_PRODUCER** — Expression

Radionuclide concentration in aquatic primary producers.

| Equation | Unit |
|---|---|
| if ( have_water )<br>  Aqu_PRIMARY_PRODUCERS / ( Aqu_biom_pp · Aqu_area_obj )<br>else<br>  0.0<br>end | Bq/kg C |

**conc_ATMOSPHERE** — Expression

Radionuclide concentration in the ATMOSHERE compartment (only relevant for C-14)

| Equation | Unit |
|---|---|
| ATMOSPHERE / ( Ter_z_mixlay · Ter_area_obj) + conc_Ter_REGOLITH_UP · Ter_conc_Dust | $Bq/m^3$ |

**conc_Ter_PRIMARY_PRODUCER** — Expression

Radionuclide concentration in the Ter_PRIMARY_PRODUCERS compartment.

| Equation | Unit |
|---|---|
| Ter_PRIMARY_PRODUCERS / ( Ter_biom_pp • Ter_area_obj ) | Bq/kg C |

### conc_Ter_REGOLITH_UP

Expression

Radionuclide concentration in the Ter_regoUp compartment.

| Equation | Unit |
|---|---|
| Ter_REGOLITH_UP / ( Ter_area_obj • Ter_z_regoUp • Ter_dens_regoUp ) | Bq/kg DW |

### conc_WATER_Aqu

Expression

Radionuclide concentration in the WATER compartment.

| Equation | Unit |
|---|---|
| if ( have_water )<br>  Aqu_WATER / ( Aqu_area_obj • depth_aver • R_water )<br>else<br>  0.0<br>end | Bq/m $^3$ |

### time_GE_threshold_agriculture

Expression

True (1) for times after the time point when the wetland is 2 m above sea level. False (0) otherwise.

| Equation | Unit |
|---|---|
| if (time >= threshold_agriculture )<br>  1.0<br>else<br>  0.0<br>end | unitless |

### time_GE_threshold_stop

Expression

True (1) for times after the time point when the isolation of the bay has concluded. False (0) otherwise.

| Equation | Unit |
|---|---|
| if (time >= threshold_stop )<br>  1.0<br>else<br>  0.0<br>end | unitless |

### conc_SOIL_Agric

Expression

Radionuclide concentration in the agricultural soil.

| Equation | Unit |
|---|---|
| if ( time_GE_threshold_agriculture )<br>conc_SOIL_Agric_IC · conc_SOIL_Agric_exp + conc_SOIL_Agric_irrig · (1.0 - conc_SOIL_Agric_exp ) / ( lambda + conc_SOIL_Agric_runoffRate )<br>else<br>0.0<br>end | Bq/kg DW |

### conc_SOIL_Agric_IC

Expression

Initial radionuclide concentration in the agricultural soil.

| Equation | Unit |
|---|---|
| ( Ter_LITTER + Ter_REGOLITH_UP + Agri_z_regoUp / Ter_z_regoMid · Ter_REGOLITH_MID ) / ( Ter_area_obj · Agri_z_regoUp · Agri_dens_regoUp ) | Bq/kg DW |

### conc_SOIL_Agric_exp

Expression

Intermedial equation used in the equation of radionuclide concentration in agricultural soil.

| Equation | Unit |
|---|---|
| (1.0 - exp( - ( lambda + conc_SOIL_Agric_runoffRate ) · AverTime )) / (( lambda + conc_SOIL_Agric_runoffRate ) · AverTime ) | unitless |

### conc_SOIL_Agric_runoffRate

Expression

Transfer rate coefficient corresponding to the transport from the agricultural soil by surface runoff.

| Equation | Unit |
|---|---|
| runoff / ( Agri_z_regoUp · Agri_poro_regoUp · Agri_R_regoUp ) | year $^{-1}$ |

### Agri_R_regoUp

Expression

Retardation factor of the agricultural soil

| Equation | Unit |
|---|---|
| 1.0 + Ter_kD_regoUp · Agri_dens_regoUp / Agri_poro_regoUp | unitless |

### Lambda

Expression

Decay rate constant.

| Equation | Unit |
|---|---|
| log(2.0) / halflife | year $^{-1}$ |

### conc_SOIL_Agric_irrig

Expression

Radionuclide concentration in agricultural soil resulting from irrigation

| Equation | Unit |
|---|---|
| vol_irrig · conc_WATER_irrig / ( Agri_z_regoUp · Agri_dens_regoUp ) | Bq/(kg DW year) |

### conc_WATER_irrig

Expression

Radionuclide concentration in irrigation water.

| Equation | Unit |
|---|---|
| conc_WATER_Lake | Bq/m $^{3}$ |

### conc_WATER_Lake

Expression

Radionuclide concentration in the WATER compartment during the lake period.

| Equation | Unit |
|---|---|
| if ( time_GE_threshold_stop )<br>  conc_WATER_Aqu<br>else<br>  0.0<br>end | Bq/m $^{3}$ |

### conc_ATMOSPHERE_Agricultural

Expression

Radionuclide concentration in the atmospheric air above the agricultural soil.

| Equation | Unit |
|---|---|
| conc_SOIL_Agric · Agri_conc_Dust | Bq/m $^{3}$ |

### conc_WATER_Well

Expression

Radionuclide concentration in well water.

| Equation | Unit |
|---|---|
| if ( time_GE_threshold_start )<br>  release / wellCapac<br>else<br>  0.0<br>end | Bq/m $^{3}$ |

### conc_WATER

Expression

Radionuclide concentration in drinking water.

| Equation | Unit |
|---|---|
| if ( have_water )<br>  ( conc_WATER_Lake + conc_WATER_Well ) / 2.0<br>else<br>  conc_WATER_Well<br>end | Bq/m $^{3}$ |

### conc_SOIL_Mire

Expression

Radionuclide concentration in the Ter_regoUp compartment

| Equation | Unit |
|---|---|
| if ( time_GE_threshold_start )<br>  conc_Ter_REGOLITH_UP<br>else<br>  0.0<br>end | Bq/kg DW |

### conc_crayfish

Expression

Radionuclide concentration in crayfish.

| Equation | Unit |
|---|---|
| if ( switcherC )<br>  conc_Aqu_PRIMARY_PRODUCER<br>else<br>  conc_WATER_Aqu · cR_crayfish<br>end | Bq/kg C |

### cR_crayfish

Expression

Concentration Ratio for limnic crayfish.

| Equation | Unit |
|---|---|
| cR_watToCray_Lake · (1.0 - threshold_sea_lake ) | $m^3$ /kg C |

### conc_fish

Expression

Radionuclide concentration in fish.

| Equation | Unit |
|---|---|
| if ( switcherC )<br>  conc_Aqu_PRIMARY_PRODUCER<br>else<br>  conc_WATER_Aqu · cR_fish<br>end | Bq/kg C |

### cR_fish

Expression

Concentration Ratio for fish.

| Equation | Unit |
|---|---|
| cR_watToFish_Lake + ( cR_watToFish_Sea - cR_watToFish_Lake ) · threshold_sea_lake | $m^3$ /kg C |

### prod_edib_crayfish

Expression

Production of edible crayfish.

| Equation | Unit |
|---|---|
| prod_edib_cray_Lake · (1.0 - threshold_sea_lake ) | kg C/($m^2$ year) |

### prod_edib_fish

Expression

Production of edible fish.

| Equation | Unit |
|---|---|
| prod_edib_fish_Lake + ( prod_edib_fish_Sea - prod_edib_fish_Lake ) · threshold_sea_lake | kg C/($m^2$ year) |

### conc_Herbiv

Expression

Radionuclide concentration in terrestrial herbivores.

| Equation | Unit |
|---|---|
| if ( switcherC )<br>  conc_Ter_PRIMARY_PRODUCER<br>else<br>  conc_Diet_Herbiv · cR_foodToHerbiv<br>end | Bq/kg C |

### conc_Diet_Herbiv

Expression

Radionuclide concentration in the diet of terrestrial herbivores.

| Equation | Unit |
|---|---|
| frac_mush_Herbiv · conc_mushrooms + (1.0 - frac_mush_Herbiv ) · conc_Ter_PRIMARY_PRODUCER | Bq/kg C |

### conc_mushrooms

Expression

Radionuclide concentration in mushrooms.

| Equation | Unit |
|---|---|
| if ( switcherC )<br>  conc_Ter_PRIMARY_PRODUCER<br>else<br>  conc_Ter_REGOLITH_UP · cR_soilToMush<br>end | Bq/kg C |

### conc_vegetables

Expression

Radionuclide concentration in cultivated vegetables.

| Equation | Unit |
|---|---|
| if ( switcherC )<br>  conc_Ter_PRIMARY_PRODUCER<br>else<br>  conc_SOIL_Agric · cR_soilToVegetab + conc_WATER_irrig · numb_irrig · leaf_areaIndex · leaf_StoreCapac · coefRetent / prod_edib_vegetab<br>end | Bq/kg C |

### conc_meat

Expression

Radionuclide concentration in cow meat.

| Equation | Unit |
|---|---|
| if ( switcherC )<br>  conc_Ter_PRIMARY_PRODUCER<br>else<br>  ( conc_WATER • ingRate_water_meat + conc_SOIL_Agric • ingRate_soil_Cow + conc_SOIL_Agric • Ter_cR_pp • ingRate_food_meat ) • tC_cowMeat / conc_C_meat<br>end | Bq/kg C |

### conc_milk

Expression

Radionuclide concentration in cow milk.

| Equation | Unit |
|---|---|
| if ( switcherC )<br>  conc_Ter_PRIMARY_PRODUCER<br>else<br>  ( conc_WATER • ingRate_water_milk + conc_SOIL_Agric • ingRate_soil_Cow + conc_SOIL_Agric • Ter_cR_pp • ingRate_food_milk ) • tC_cowMilk / ( densMilk • conc_C_milk )<br>end | Bq/kg C |

### conc_roots

Expression

Radionuclide concentration in root crops (tubers).

| Equation | Unit |
|---|---|
| if ( switcherC )<br>  conc_Ter_PRIMARY_PRODUCER<br>else<br>  conc_SOIL_Agric · cR_soilToTuber<br>end | Bq/kg C |

### conc_cereals

Expression

Radionuclide concentration in cereals.

| Equation | Unit |
|---|---|
| if ( switcherC )<br>  conc_Ter_PRIMARY_PRODUCER<br>else<br>  conc_SOIL_Agric · cR_soilToCereal<br>end | Bq/kg C |

### 1.2.2 Dose

**LDF**

Expression

Landscape Dose Conversion Factor.

| Equation | Unit |
|---|---|
| Dose_ext + Dose_inh + Dose_ing_WATER + Dose_ing_Total | Sv/year |

**Dose_ext**

Expression

Annual effective dose from external irradiation.

| Equation | Unit |
|---|---|
| if ( time_GE_threshold_agriculture )<br>(16.0 / 24.0 · Dose_external_Mire + 8.0 / 24.0 · Dose_external_Agric ) · min(1.0, N )<br>else<br>Dose_external_Mire · min(1.0, N )<br>end | Sv/year |

**Dose_external_Agric**

Expression

Annual effective dose from external irradiation in agricultural areas.

| Equation | Unit |
|---|---|
| conc_SOIL_Agric · Agri_dens_regoUp · expTime · dosCoef_ext | Sv/year |

**Dose_external_Mire**

Expression

Annual effective dose from external irradiation in wetland areas.

| Equation | Unit |
|---|---|
| conc_SOIL_Mire · Ter_dens_regoUp · expTime · dosCoef_ext | Sv/year |

**N**

Expression

Number of individuals in the most exposed group.

| Equation | Unit |
|---|---|
| Production_Total / ingRate_C | unitless |

**Dose_inh**

Expression

Annual effective dose from inhalation.

| Equation | Unit |
|---|---|
| if ( time_GE_threshold_agriculture )<br>(16.0 / 24.0 · Dose_inh_Mire + 8.0 / 24.0 · Dose_inh_Agric ) · min(1.0, N )<br>else<br>Dose_inh_Mire · min(1.0, N )<br>end | Sv/year |

**Dose_inh_Agric**

Expression

Annual effective dose from inhalation in agricultural areas.

| Equation | Unit |
|---|---|
| conc_ATMOSPHERE_Agricultural · inhalRate · expTime · dosCoef_inhal | Sv/year |

**Dose_inh_Mire**

Expression

Annual effective dose from inhalation in wetland areas.

| Equation | Unit |
|---|---|
| conc_ATMOSPHERE · inhalRate · expTime · dosCoef_inhal | Sv/year |

**LDF_perm**

Expression

Landscape Dose Conversion Factors during the permafrost period

| Equation | Unit |
|---|---|
| Dose_ext_perm + Dose_inh_perm + Dose_ing_WATER_perm + Dose_ing_Total_perm | Sv/year |

**Dose_ext_perm**

Expression

Annual effective dose from external irradiation during the permafrost period.

| Equation | Unit |
|---|---|
| Dose_external_Mire · min(1.0, N_perm ) | Sv/year |

**N_perm**

Expression

Number of individuals in the most exposed group during the permafrost period.

| Equation | Unit |
|---|---|
| Production_Total_perm / ingRate_C | unitless |

**Dose_inh_perm**

Expression

Annual effective dose by inhalation during the permafrost period.

| Equation | Unit |
|---|---|
| Dose_inh_Mire · min(1.0, N_perm ) | Sv/year |

**LDF_ter_limnic**

Expression

Landscape Dose Conversion Factor for the terrestrial/limnic period.

| Equation | Unit |
|---|---|
| if ( time_GE_threshold_agriculture )<br>  LDF_interglacial<br>else<br>  0.0<br>end | Sv/year |

**LDF_interglacial**

Expression

Landscape Dose Conversion Factor for the interglacial period (base case).

| Equation | Unit |
|---|---|
| if (time <= interglacial_stop )<br>  LDF<br>else<br>  0.0<br>end | Sv/year |

### LDF_marine_trans

Expression

Landscape Dose Conversion Factor for the marine/transitional period.

| Equation | Unit |
|---|---|
| if ( time_GE_threshold_agriculture )<br>  0.0<br>else<br>  LDF<br>end | Sv/year |

### LDF_greenhouse

Expression

Landscape Dose Conversion Factor for the greenhouse climate variant.

| Equation | Unit |
|---|---|
| if (time <= greenhouse_stop )<br>  LDF<br>else<br>  0.0<br>end | Sv/year |

### LDF_permafrost

Expression

Landscape Dose Conversion Factor for the prolonged permafrost variant.

| Equation | Unit |
|---|---|
| if (time <= greenhouse_stop )<br>  LDF_perm<br>else<br>  0.0<br>end | Sv/year |

### LDF_glacial

Expression

Landscape Dose Conversion Factor for the glacial period.

| Equation | Unit |
|---|---|
| if (time < threshold_start )<br>  LDF<br>else<br>  0.0<br>end | Sv/year |

### Production_Cereals

Production of cereals in the biosphere object assuming that one fifth of the terrestrial area is used for production of cereals.

Expression

| Equation | Unit |
|---|---|
| if ( time_GE_threshold_agriculture )<br>  prod_edib_cereal · Ter_area_obj / 5.0<br>else<br>  0.0<br>end | kg C/year |

### Production_Roots

Production of root crops (tubers) in the biosphere object assuming that one fifth of the terrestrial area is used for production of root crops (tubers).

Expression

| Equation | Unit |
|---|---|
| if ( time_GE_threshold_agriculture )<br>  prod_edib_tuber · Ter_area_obj / 5.0<br>else<br>  0.0<br>end | kg C/year |

### Production_Vegetables

Production of vegetables in the biosphere object assuming that one fifth of the terrestrial area is used for production of vegetables.

Expression

| Equation | Unit |
|---|---|
| if ( time_GE_threshold_agriculture )<br>  prod_edib_vegetab · Ter_area_obj / 5.0<br>else<br>  0.0<br>end | kg C/year |

### Production_Milk

Production of milk in the biosphere object assuming that one fifth of the terrestrial area is used for production of fodder.

Expression

| Equation | Unit |
|---|---|
| if ( time_GE_threshold_agriculture )<br>  prod_edib_milk · prod_fodder · Ter_area_obj / 5.0<br>else<br>  0.0<br>end | kg C/year |

### Production_Game

Production of game in the biosphere object assuming that all terrestrial area is a forest before agriculture is possible and that one fifth of the terrestrial area is forest when agriculture is possible.

Expression

| Equation | Unit |
|---|---|
| if ( time_GE_threshold_agriculture )<br>  prod_edib_game · Ter_area_obj / 5.0<br>else<br>  if ( time_GE_threshold_start )<br>  prod_edib_game · Ter_area_obj<br>  else<br>  0.0<br>  end<br>end | kg C/year |

### Production_Meat

Production of meat in the biosphere object assuming that one fifth of the terrestrial area is used for production of fodder.

Expression

| Equation | Unit |
|---|---|
| if ( time_GE_threshold_agriculture )<br>  prod_edib_meat · prod_fodder · Ter_area_obj / 5.0<br>else<br>  0.0<br>end | kg C/year |

### Production_Mushrooms

Production of mushrooms in the biosphere object assuming that all terrestrial area is a forest before agriculture is possible and that one fifth of the terrestrial area is forest when agriculture is possible.

Expression

| Equation | Unit |
|---|---|
| if ( time_GE_threshold_agriculture )<br>  prod_edib_mush · Ter_area_obj / 5.0<br>else<br>  if ( time_GE_threshold_start )<br>  prod_edib_mush · Ter_area_obj<br>  else<br>  0.0<br>  end<br>end | kg C/year |

### Production_Berries

Expression

Production of berries in the biosphere object assuming that all terrestrial area is a forest before agriculture is possible and that one fifth of the terrestrial area is forest when agriculture is possible.

| Equation |
|---|
| if ( time_GE_threshold_agriculture )<br>  prod_edib_berry · Ter_area_obj / 5.0<br>else<br>  if ( time_GE_threshold_start )<br>  prod_edib_berry · Ter_area_obj<br>  else<br>  0.0<br>  end<br>end |

### Production_Fish

Expression

Production of fish in the biosphere object in periods when the water depth is sufficient for fish production.

| Equation | Unit |
|---|---|
| if ( depth_max >= z_min_prod_edib_fish_Lake )<br>  prod_edib_fish · Aqu_area_obj<br>else<br>  0.0<br>end | kg C/year |

### Production_Crayfish

Expression

Production of crayfish in the biosphere object in periods when the water depth is sufficient for crayfish production.

| Equation | Unit |
|---|---|
| if ( depth_aver >= z_min_prod_edib_crayfish_Lake )<br>  prod_edib_crayfish · Aqu_area_obj<br>else<br>  0.0<br>end | kg C/year |

**Production_Total**

Expression

Total production of food in the biosphere object.

| Equation | Unit |
|---|---|
| ( Production_Berries + Production_Game + Production_Mushrooms ) + ( Production_Cereals + Production_Meat + Production_Milk + Production_Vegetables + Production_Roots ) + ( Production_Crayfish + Production_Fish ) | kg C/year |

**Production_Total_perm**

Expression

Total production of food in the biosphere object during the permafrost period.

| Equation | Unit |
|---|---|
| Production_Berries + Production_Game + Production_Mushrooms + Production_Fish | kg C/year |

**Dose_ing_Fish_perm**

Expression

Annual effective dose from fish ingestion during the permafrost period

| Equation | Unit |
|---|---|
| ingFoodConstant_perm · conc_fish · Fraction_in_Diet_Fish_perm | Sv/year |

**ingFoodConstant_perm**

Expression

Intermedial equation used to shorten ingestion dose equation for the permafrost period.

| Equation | Unit |
|---|---|
| ingRate_C · dosCoef_ing_food · min(1.0, N_perm ) | kg C<br>Sv/(year Bq) |

**Dose_ing_Berries_perm**

Expression

Annual effective dose from ingestion of berries during the permafrost period.

| Equation | Unit |
|---|---|
| ingFoodConstant_perm · conc_Ter_PRIMARY_PRODUCER · Fraction_in_Diet_Berries_perm | Sv/year |

**Dose_ing_Mushrooms_perm**

Expression

Annual effective dose from ingestion of mushrooms during the permafrost period.

| Equation | Unit |
|---|---|
| ingFoodConstant_perm · conc_mushrooms · Fraction_in_Diet_Mushrooms_perm | Sv/year |

**Dose_ing_Game_perm**

Expression

Annual effective dose from ingestion of game during the permafrost period.

| Equation | Unit |
|---|---|
| ingFoodConstant_perm · conc_Herbiv · Fraction_in_Diet_Game_perm | Sv/year |

**Dose_ing_Cereals**

Expression

Annual effective dose from ingestion of cereals.

| Equation | Unit |
|---|---|
| ingFoodConstant · conc_cereals · Fraction_in_diet_Cereals | Sv/year |

**ingFoodConstant**

Expression

Intermedial equation used to shorten ingestion dose equation.

| Equation | Unit |
|---|---|
| ingRate_C · dosCoef_ing_food · min(1.0, N ) | kg C<br>Sv/(year Bq) |

**Dose_ing_Roots**

Expression

Annual effective dose from ingestion of root crops.

| Equation | Unit |
|---|---|
| ingFoodConstant · conc_roots · Fraction_in_Diet_Roots | Sv/year |

**Dose_ing_Vegetables**

Expression

Annual effective dose from ingestion of vegetables.

| Equation | Unit |
|---|---|
| ingFoodConstant · conc_vegetables · Fraction_in_Diet_Vegetables | Sv/year |

**Dose_ing_Milk**

Expression

Annual effective dose from ingestion of cow milk.

| Equation | Unit |
|---|---|
| ingFoodConstant · conc_milk · Fraction_in_Diet_Milk | Sv/year |

**Dose_ing_Meat**

Expression

Annual effective dose from ingestion of cow meat.

| Equation | Unit |
|---|---|
| ingFoodConstant · conc_meat · Fraction_in_Diet_Meat | Sv/year |

**Dose_ing_Game**

Expression

Annual effective dose from ingestion of game meat.

| Equation | Unit |
|---|---|
| ingFoodConstant · conc_Herbiv · Fraction_in_Diet_Game | Sv/year |

**Dose_ing_Mushrooms**

Expression

Annual effective dose from ingestion of mushrooms.

| Equation | Unit |
|---|---|
| ingFoodConstant · conc_mushrooms · Fraction_in_Diet_Mushrooms | Sv/year |

**Dose_ing_Berries**

Expression

Annual effective dose from ingestion of berries.

| Equation | Unit |
|---|---|
| ingFoodConstant · conc_Ter_PRIMARY_PRODUCER · Fraction_in_Diet_Berries | Sv/year |

**Dose_ing_Fish**

Expression

Annual effective dose from ingestion of fish.

| Equation | Unit |
|---|---|
| ingFoodConstant · conc_fish · Fraction_in_Diet_Fish | Sv/year |

**Dose_ing_Crayfish**

Expression

Annual effective dose from ingestion of crayfish.

| Equation | Unit |
|---|---|
| ingFoodConstant · conc_crayfish · Fraction_in_Diet_Crayfish | Sv/year |

**Dose_ing_Total**

Expression

Total annual effective dose from food ingestion

| Equation | Unit |
|---|---|
| ( Dose_ing_Berries + Dose_ing_Mushrooms + Dose_ing_Game ) + ( Dose_ing_Meat + Dose_ing_Milk + Dose_ing_Roots + Dose_ing_Vegetables + Dose_ing_Cereals ) + ( Dose_ing_Crayfish + Dose_ing_Fish ) | Sv/year |

**Dose_ing_WATER_perm**

Expression

Annual effective dose from ingestion of water during the permafrost period.

| Equation | Unit |
|---|---|
| ingRate_wat · dosCoef_ing_water · min(1.0, N_perm ) · conc_WATER_Lake | Sv/year |

**Dose_ing_WATER**

Expression

Annual effective dose from ingestion of water

| Equation | Unit |
|---|---|
| ingRate_wat · dosCoef_ing_water · min(1.0, N ) · conc_WATER | Sv/year |

**Dose_ing_Total_perm**

Expression

Total annual effective dose from food ingestion during the permafrost period.

| Equation | Unit |
|---|---|
| Dose_ing_Berries_perm + Dose_ing_Game_perm + Dose_ing_Mushrooms_perm + Dose_ing_Fish_perm | Sv/year |

**Fraction_in_Diet_Fish_perm**

Expression

Fraction of fish in the diet during the permafrost period.

| Equation | Unit |
|---|---|
| Production_Fish / Production_Total_perm | unitless |

**Fraction_in_Diet_Berries_perm**

Expression

Fraction of berries in the diet during the permafrost period.

| Equation | Unit |
|---|---|
| Production_Berries / Production_Total_perm | unitless |

**Fraction_in_Diet_Mushrooms_perm**

Expression

Fraction of mushrooms in the diet during the permafrost period.

| Equation | Unit |
|---|---|
| Production_Mushrooms / Production_Total_perm | unitless |

**Fraction_in_Diet_Game_perm**

Expression

Fraction of game in the diet during the permafrost period.

| Equation | Unit |
|---|---|
| Production_Game / Production_Total_perm | unitless |

**Fraction_in_diet_Cereals**

Expression

Fraction of cereals in the diet.

| Equation | Unit |
|---|---|
| Production_Cereals / Production_Total | unitless |

**Fraction_in_Diet_Roots**

Expression

Fraction of roots in the diet.

| Equation | Unit |
|---|---|
| Production_Roots / Production_Total | unitless |

**Fraction_in_Diet_Vegetables**

Expression

Fraction of vegetables in the diet.

| Equation | Unit |
|---|---|
| Production_Vegetables / Production_Total | unitless |

**Fraction_in_Diet_Milk**

Expression

Fraction of milk in the diet.

| Equation | Unit |
|---|---|
| Production_Milk / Production_Total | unitless |

**Fraction_in_Diet_Meat**

Expression

Fraction of meat in the diet.

| Equation | Unit |
|---|---|
| Production_Meat / Production_Total | unitless |

**Fraction_in_Diet_Game**

Expression

Fraction of game meat in the diet.

| Equation | Unit |
|---|---|
| Production_Game / Production_Total | unitless |

**Fraction_in_Diet_Mushrooms**

Expression

Fraction of mushrooms in the diet.

| Equation | Unit |
|---|---|
| Production_Mushrooms / Production_Total | unitless |

**Fraction_in_Diet_Berries**

Expression

Fraction of berries in the diet.

| Equation | Unit |
|---|---|
| Production_Berries / Production_Total | unitless |

**Fraction_in_Diet_Fish**

Expression

Fraction of fish in the diet.

| Equation | Unit |
|---|---|
| Production_Fish / Production_Total | unitless |

| **Fraction_in_Diet_Crayfish**<br>Fraction of crayfish in the diet. | Expression |
|---|---|

| Equation | Unit |
|---|---|
| Production_Crayfish / Production_Total | unitless |

### 1.2.3 Activity concentrations used for dose to Biota assessmetns

***Marine***

| **ActivityConcentrationWater**<br>Radionuclide concentration in water used to calculate doses to marine biota. | Expression |
|---|---|

| Equation | Unit |
|---|---|
| if ( is_sea )<br>  conc_WATER_Aqu · 0.0010<br>else<br>  0.0<br>end | Bq/L |

| **ActivityConcentrationSediment_up**<br>Radionuclide concentration in the Aqu_regolith_Up compartment used to calculate doses to marine biota. | Expression |
|---|---|

| Equation | Unit |
|---|---|
| if ( is_sea )<br>  Aqu_REGOLITH_UP / ( Aqu_area_obj · Aqu_z_regoUp · Aqu_dens_regoUp )<br>else<br>  0.0<br>end | Bq/(kg DW) |

| **ActivityConcentrationSediment_mid**<br>Radionuclide concentration in the Aqu_regolith_Mid compartment used to calculate doses to marine biota. | Expression |
|---|---|

| Equation | Unit |
|---|---|
| if ( is_sea )<br>  Aqu_REGOLITH_MID / ( Aqu_area_obj · Aqu_z_regoMid · Aqu_dens_regoMid )<br>else<br>  0.0<br>end | Bq/(kg DW) |

### *FreshWater*

**ActivityConcentrationWater**

Expression

Radionuclide concentration in water used to calculate doses to freshwater biota.

| Equation | Unit |
|---|---|
| if ( time_GE_threshold_start AND switcherRiver )<br>  conc_WATER_Aqu · 0.0010<br>else<br>  0.0<br>end | Bq/L |

**ActivityConcentrationSediment_up**

Expression

Radionuclide concentration in the Aqu_regolith_Up compartment used to calculate doses to freshwater biota.

| Equation | Unit |
|---|---|
| if ( time_GE_threshold_start AND switcherRiver )<br>  Aqu_REGOLITH_UP / ( Aqu_area_obj · Aqu_z_regoUp · Aqu_dens_regoUp )<br>else<br>  0.0<br>end | Bq/(kg DW) |

**ActivityConcentrationSediment_mid**

Expression

Radionuclide concentration in the Aqu_regolith_Mid compartment used to calculate doses to freshwater biota.

| Equation | Unit |
|---|---|
| if ( time_GE_threshold_start AND switcherRiver )<br>  Aqu_REGOLITH_MID / ( Aqu_area_obj · Aqu_z_regoMid · Aqu_dens_regoMid )<br>else<br>  0.0<br>end | Bq/m $^{2}$ |

### *Terrestrial*

**ActivityConcentrationSoil**

Expression

Radionuclide concentration in soil used to calculate doses to terrestrial biota.

| Equation | Unit |
|---|---|
| conc_Ter_REGOLITH_UP | Bq/(kg DW) |

| **ActivityConcentrationAir**<br>Radionuclide concentration in air used to calculate doses to terrestrial biota. | Expression |
|---|---|
| **Equation** | **Unit** |
| conc_ATMOSPHERE | Bq/m $^{3}$ |

## 1.3 Object 10 (Grepen)

| **Aqu_WATER**<br>The surface water (sea water). | Compartment |
|---|---|
| **Differential equation** | **Unit** |
| d Aqu_WATER /dt = -λ • Aqu_WATER + Aqu_WATER • Outflow_Sea + Aqu_WATER • Outflow_Downstream + Aqu_WATER • Backflow + Ter_REGOLITH_UP • Mire_Dowstream - Aqu_WATER • outflow - Aqu_WATER • Backflow + ingrowth | Bq |

| **Backflow**<br>Radionuclide transfer rate coefficient corresponding to the transport from object 10 to the WATER compartment during the Sea period | Transfer Coefficient |
|---|---|
| **Equation** | **Unit** |
| if ( is_sea )<br>depth_aver · Aqu_area_obj / ( depth_aver · Aqu_area_obj ) / wat_ret<br>else<br>0.0<br>end | year $^{-1}$ |

| **Outflow**<br>Radionuclide transfer rate coefficient corresponding to the transport from object 10 to object 1. | Transfer Coefficient |
|---|---|
| **Equation** | **Unit** |
| 1.0 / wat_ret | year $^{-1}$ |

## 1.4 Object 1 (Baltic Sea)

**Aqu_WATER** — Compartment

The surface water (sea water).

| Differential equation | Unit |
|---|---|
| d Aqu_WATER /dt = -λ · Aqu_WATER + Aqu_WATER · outflow - Aqu_WATER · outflow - Aqu_WATER · Backflow + ingrowth | Bq |

**Backflow** — Transfer Coefficient

Radionuclide transfer rate coefficient corresponding to the transport from object 1 object 10

| Equation | Unit |
|---|---|
| ( depth_aver · Aqu_area_obj ) / ( depth_aver · Aqu_area_obj ) / wat_ret | $year^{-1}$ |

**Outflow** — Transfer Coefficient

Radionuclide transfer rate coefficient corresponding to the transport from object 1 out from the system (Atlantic Ocean).

| Equation | Unit |
|---|---|
| 1.0 / wat_ret | $year^{-1}$ |

# Appendix B

## Overview of model parameters

This appendix presents an overview of the parameters used in the Radionuclide Model for the biosphere described in Section 3.1 and Appendix A. The parameters have been classified into different types: Radionuclide specific (different values are given for different radionuclides), Element specific (different values are given for different elements), Object specific (different values are given for different biosphere objects), Time series (different values are given for different time points), Site specific (the same value has been given for all biosphere objects base on site data), Generic (the same value has been given for all biosphere objects base on generic data).

| Parmeter Name | Description | Unit | Type | Report |
|---|---|---|---|---|
| *Physical constant* | | | | |
| Half_life | Radionuclide half-life. | year | Nuclide specific | TR-10-07 |
| *Landscape geometry* | | | | |
| Aqu_area_obj | Water area in the lake basin. | $m^2$ | Object Specific (Time Series) | TR-10-05 |
| area_subcatch | Area of the subcatchment. | $m^2$ | Object Specific | TR-10-05 |
| area_wshed | Watershed area. | $m^2$ | Object Specific (Time Series) | TR-10-05 |
| depth_aver | Average water depth. | m | Object Specific (Time Series) | TR-10-05 |
| depth_max | Maximum water depth. | m | Object Specific (Time Series) | TR-10-05 |
| res_rate | Resuspension rate. | kg DW/ ($m^2$year) | Object Specific (Time Series) | TR-10-05 |
| sed_rate | Sedimentation rate. | kg DW/ ($m^2$year) | Object Specific (Time Series) | TR-10-05 |
| Ter_area_obj | Area with peat in the lake basin. | $m^2$ | Object Specific (Time Series) | TR-10-05 |
| Ter_growth_rego | Growth of wetland relative water area. | $m^2$/ ($m^2$year) | Object Specific (Time Series) | TR-10-05 |
| threshold_agriculture | Point in time when wetland is 2 m above sea level. | year | Object Specific | TR-10-05 |
| threshold_end | Point in time when ingrowth of wetland stops. | year | Object Specific | TR-10-05 |
| threshold_start | Point in time when lake isolation starts. | year | Object Specific | TR-10-05 |
| threshold_stop | Point in time when lake isolation is completed. | year | Object Specific | TR-10-05 |
| *Regolith* | | | | |
| Agri_dens_regoUp | Density of the agricultural upper regolith layer. | kg DW/ $m^3$ | Site Specific | TR-10-01 |
| Agri_poro_regoUp | Porosity of the agricultural upper regolith layer. | $m^3$/ $m^3$ | Site Specific | TR-10-01 |
| Agri_z_regoUp | Depth of the agricultural upper regolith layer. | m | Generic | TR-10-01 |
| Aqu_dens_regoMid_gl | Density of glacial clay in the middle layer of the regolith. | kg DW/$m^3$ | Site Specific | TR-10-02 TR-10-03 |
| Aqu_dens_regoMid_pg | Density of the postglacial sediments in aquatic middle layer of regolith. | kg DW/ $m^3$ | Site Specific | TR-10-02 TR-10-03 |
| Aqu_dens_regoUp | Density of the aquatic upper layer of the regolith. | kg DW/$m^3$ | Site Specific | TR-10-02 TR-10-03 |
| Aqu_poro_regoMid_gl | Porosity of the glacial clay in aquatic middle regolith layer. | $m^3$/$m^3$ | Site Specific | TR-10-02 TR-10-03 |
| Aqu_poro_regoMid_pg | Porosity of postglacial sediments in aquatic middle regolith layer. | $m^3$/$m^3$ | Site Specific | TR-10-02 TR-10-03 |
| Aqu_poro_regoUp | Porosity of the aquatic upper regolith layer. | $m^3$/$m^3$ | Site Specific | TR-10-02 TR-10-03 |
| Aqu_z_regoMid_gl_lake | Average depth of glacial deposits in lake. | m | Object Specific | TR-10-05 |
| Aqu_z_rego_pg | Depth of aquatic postglacial sediments under sea, lake or stream. | m | Object Specific (Time Series) | TR-10-05 |

| Parmeter Name | Description | Unit | Type | Report |
|---|---|---|---|---|
| dens_regoLow | Density of the lower regolith layer (till). | kg DW/$m^3$ | Site Specific | TR-10-01, TR-10-02, TR-10-03 |
| growth_rego | Average accumulation rate of sediment calculated for lake and marine bottoms. | m/year | Object Specific (Time Series) | TR-10-05 |
| Lake_z_regoLow | Depth of the lower regolith (till) in the lake/ terrestrial stage. | m | Object Specific | TR-10-05 |
| Lake_z_regoUp | Depth of the upper regolith layer in the lake basin. | m | Site Specific | TR-10-02 |
| poro_regoLow | Porosit of the lower regolith layer (till). | $m^3/m^3$ | Site Specific | TR-10-01, TR-10-02, TR-10-03 |
| Sea_z_regoLow | Average depth of glacial till in sea basin. | m | Object Specific | TR-10-05 |
| Sea_z_regoUp | Depth of the upper regolith layer in sea. | m | Site Specific | TR-10-03 |
| Ter_dens_regoMid_gl | Density of the glacial clay in terrestrial middle regolith layer. | kg DW/$m^3$ | Site Specific | TR-10-01 |
| Ter_dens_regoMid_pg | Density of the postglacial clay in terrestrial middle regolith layer. | kg DW/$m^3$ | Site Specific | TR-10-01 |
| Ter_dens_regoUp | Density of the terrestrial upper regolith layer (peat). | kg DW/$m^3$ | Site Specific | TR-10-01 |
| Ter_poro_regoMid_gl | Porosity of the glacial clay in terrestrial middle regolith layer. | $m^3/m^3$ | Site Specific | TR-10-01 |
| Ter_poro_regoMid_pg | Porosity of the post glacial clay in terrestrial middle regolith layer. | $m^3/m^3$ | Site Specific | TR-10-01 |
| Ter_poro_regoUp | Porosity of the terrestrial upper regolith layer (peat). | $m^3/m^3$ | Site Specific | TR-10-01 |
| Ter_z_regoMid_pg | Depth of the post glacial clay in terrestrial middle regolith layer (covered by peat). | m | Object Specific (Time Series) | TR-10-05 |
| Ter_z_regoUp | Depth of the terrestrial upper regolith layer (peat). | m | Object Specific (Time Series) | TR-10-05 |
| z_regoMid_gl_basin | Depth of the glacial clay of the aquatic middle layer in the sea basin. | m | Object Specific | TR-10-05 |
| *Aquatic ecosystem* | | | | |
| Aqu_biom_pp_macro | Biomass of macroflora and macrofauna (macroalgae, macrophytes, benthic macro-fauna) in lake. | kg C/$m^2$ | Object Specific (Time Series) | TR-10-02, TR-10-03 |
| Aqu_biom_pp_plank | Biomass of pelagic biota (i.e. phytoplankton bacterioplankton, zooplankton and fish) in lake. | kg C/$m^2$ | Object Specific (Time Series) | TR-10-02, TR-10-03 |
| Aqu_biom_pp_ubent | Biomass of microphytobenthos and benthic bacteria in lake. | kg C/$m^2$ | Object Specific (Time Series) | TR-10-02, TR-10-03 |
| Aqu_degass_C | Carbon degassing rate. Release of carbon from lake water surface to atmosphere. | kg C/ ($m^2$year) | Object Specific (Time Series) | TR-10-02, TR-10-03 |
| Aqu_prod_pp_macro | Net productivity of the benthic macrocom-munity, i.e. the net primary production minus respiration of macrofauna and flora, in lake. | $year^{-1}$ | Object Specific (Time Series) | TR-10-02, TR-10-03 |
| Aqu_prod_pp_plank | Net productivity of the pelagic community, i.e. net primary production by phytoplankton minus respiration by zooplankton, bacterio-plankton, and fish, in lake. | $year^{-1}$ | Object Specific (Time Series) | TR-10-02, TR-10-03 |
| Aqu_prod_pp_ubent | Net productivity of the benthic microscopic community, i.e. net primary production by microphytobenthos minus respiration by benthic bacteria in lake. | $year^{-1}$ | Object Specific (Time Series) | TR-10-02, TR-10-03 |
| gasUptake_C | Uptake of carbon from atmosphere to lake water (mainly $CO_2$). | kg C/ ($m^2$year) | Object Specific (Time Series) | TR-10-02, TR-10-03 |
| Lake_conc_DIC | Concentration of dissolved inorganic carbon in lake water. | kg C/$m^3$ | Site Specific | TR-10-02 |
| Lake_conc_PM | Concentration of particulate matter in lake water. | kg DW/$m^3$ | Site Specific | TR-10-02 |
| prod_edib_cray_Lake | Production of edible crayfish in the lake. | kg C/ ($m^2$year) | Site Specific | TR-10-02 |
| prod_edib_fish_Lake | Production of edible fish in the lake. | kg C/ ($m^2$year) | Site Specific | TR-10-02 |

| Parmeter Name | Description | Unit | Type | Report |
|---|---|---|---|---|
| prod_edib_fish_Sea | Production of edible fish in the sea. | kg C/ ($m^2$year) | Site Specific | TR-10-03 |
| Sea_conc_DIC | Concentration of dissolved inorganic carbon in sea water. | kg C/$m^3$ | Site Specific | TR-10-03 |
| Sea_conc_PM | Concentration of particulate matter in sea water. | kg DW/$m^3$ | Site Specific | TR-10-03 |
| z_min_prod_edib_crayfish_Lake | Minimum lake depth for crayfish production. | m | Site Specific | TR-10-02 |
| z_min_prod_edib_fish_Lake | Minimum lake depth for production of edible fish. | m | Site Specific | TR-10-02 |
| *Terrestrial Ecosystem* | | | | |
| conc_C_atmos | Concentration of carbon in the atmosphere above the terrestrial ecosystem. | kg C/$m^3$ | Generic | TR-10-01 |
| frac_C_atmos | Fraction of decomposed carbon that is mineralised (leaving as $CO_2$ to the atmosphere). | – | Site Specific | TR-10-01 |
| frac_mush_Herbiv | Fraction of mushrooms in the diet of terrestrial herbivores. | – | Generic | TR-10-01 |
| prod_edib_berry | Production of edible berries. | kg C/ ($m^2$year) | Site Specific | TR-10-01 |
| prod_edib_game | Production of edible game meat. | kg C/ ($m^2$year) | Site Specific | TR-10-01 |
| prod_edib_mush | Production of edible mushrooms. | kg C/ ($m^2$year) | Site Specific | TR-10-01 |
| Ter_biom_pp | Biomass of terrestrial primary producers. | kg C/$m^2$ | Site Specific | TR-10-01 |
| Ter_conc_C_regoUp | Concentration of dissolved inorganic carbon in the upper terrestrial regolith (peat). | kg C/$m^3$ | Site Specific | TR-10-01 |
| Ter_conc_Dust | Concentration of dust in air. | kg DW/$m^3$ | Generic | TR-10-01 |
| Ter_decomp | Decomposition rate. | 1/year | Site Specific | TR-10-01 |
| Ter_degass_C | Degassing rate of dissolved inorganic carbon in the terrestrial ecosystem. | kg C/ $m^2$ year | Site Specific | TR-10-01 |
| Ter_prodBiom_pp | Net primary production per unit biomass in the terrestrial ecosystem. | kg C/(kg C year) | Site Specific | TR-10-01 |
| Ter_z_mixlay | Height of the mixing layer in the terrestrial ecosystem. | m | Site Specific | TR-10-01 |
| Ter_z_roughness | Height above ground below which the wind speed is zero due to vegetation. | m | Generic | TR-10-01 |
| vel_wind | Wind velocity. | m/year | Site Specific | TR-10-01 |
| Agri_conc_Dust | Concentration of dust in the atmosphere on agricultural land. | kg DW/$m^3$ | Generic | TR-10-01 |
| conc_C_meat | Concentration of carbon in meat. | kg C/kg FW | Generic | TR-10-07 |
| conc_C_milk | Concentration of carbon in milk. | kg C/kg FW | Generic | TR-10-07 |
| densMilk | Density of the milk. | kg FW/l | Generic | TR-10-07 |
| ingRate_food_meat | Fodder ingestion rate for meat cattle. | kg C/d | Generic | TR-10-07 |
| ingRate_food_milk | Fodder ingestion rate for milk producing cattle. | kg C/d | Generic | TR-10-07 |
| ingRate_soil_Cow | Soil ingestion rate for cattle. | kg DW/d | Generic | TR-10-07 |
| ingRate_water_meat | Water ingestion rate for meat cattle. | $m^3$/d | Generic | TR-10-07 |
| ingRate_water_milk | Water ingestion rate for milk producing cattle. | $m^3$/d | Generic | TR-10-07 |
| leaf_areaIndex | Ratio of total upper leaf surface of vegetation divided by the surface area of the land on which the vegetation grows. | $m^2$/ $m^2$ | Generic | TR-10-01 |
| leaf_StoreCapac | Storage capacity of intercepted water on leaf surface. | $m^3$/ $m^2$ | Generic | TR-10-01 |
| numb_irrig | Number of irrigation events. | $year^{-1}$ | Generic | TR-10-01 |
| prod_edib_cereal | Production of edible cereals. | kg C/ ($m^2$year) | Site Specific | TR-10-01 |
| prod_edib_meat | Production of edible meat (relative fodder consumption). | kg C/kg C | Site Specific | TR-10-01 |
| prod_edib_milk | Production of edible milk (relative fodder consumption). | kg C/kg C | Site Specific | TR-10-01 |
| prod_edib_tuber | Production of edible root crop, e.g. potato. | kg C/ ($m^2$year) | Site Specific | TR-10-01 |
| prod_edib_vegetab | Production of edible vegetables. | kg C/ ($m^2$year) | Site Specific | TR-10-01 |
| prod_fodder | Production of fodder on agricultural land. | kg C/ ($m^2$year) | Site Specific | TR-10-01 |
| vol_irrig | Volume of irrigation water used each year. | m/year | Generic | TR-10-01 |

| Parmeter Name | Description | Unit | Type | Report |
|---|---|---|---|---|
| *Surface Hydrology and water exchange* | | | | |
| Flooding_coef | Gross lateral flux of water from lake/stream to wetland, normalised by the net lateral flux from wetland to lake/stream. | unitless or ($m^3$/year)/ ($m^3$/year) | Site Specific | TR-10-01, TR-10-02 |
| Lake_adv_low_mid | Total advective flux from regoLow (till) to regoMid (glacial and post glacial deposits) for the lake/terrestrial stage. | m/year | Site Specific | TR-10-01, TR-10-02 |
| Lake_Aqu_adv_mid_up_norm | Advective flux in the aquatic object between the sediment and the water during lake stage, normalised by the net lateral advective flux from wetland to lake/stream. | – | Site Specific | TR-10-02 |
| Lake_fract_Mire | Fraction of the upward flux from regoLow (till) that is directed to the terrestrial part of the biosphere object. | – | Site Specific | TR-10-01, TR-10-02 |
| runoff | Total annual runoff. | m/year | Site Specific | TR-10-01, TR-10-02, TR-10-03 |
| Sea_adv_low_mid | Total advective flux from regoLow (till) to regoMid (glacial and post glacial deposits) for the sea stage. | m/year | Site Specific | TR-10-03 |
| Ter_adv_mid_up_norm | The advective flux from regoMid (glacial and post glacial deposits) to regoUp (peat) in the terrestrial ecosystem. normalised by the net lateral flux from terrestrial ecosystem to lake/stream. | – | Site Specific | TR-10-01, TR-10-02 |
| wat_ret | Average water retention time in the sea basin. | year | Object Specific (Time Series) | TR-10-03 |
| wellCapac | The water volume capacity of a well. | $m^3$/year | Site Specific | TR-10-01 |
| *Distribution coefficients and diffusivity* | | | | |
| kD_regoLow | Distribution coefficient for lower regolith layer (till). | $m^3$/kg DW | Element Specific | TR-10-07 |
| Lake_kD_PM | Distribution coefficient for particulate matter in lake/stream. | $m^3$/kg DW | Element Specific | TR-10-07 |
| Lake_kD_regoMid | Distribution coefficient for particulate matter in lake/stream. | $m^3$/kg DW | Element Specific | TR-10-07 |
| Lake_kD_regoUp | Distribution coefficient for the middle regolith layer in lake/stream. | $m^3$/kg DW | Element Specific | TR-10-07 |
| Sea_kD_PM | Distribution coefficient for particulate matter in sea. | $m^3$/kg DW | Element Specific | TR-10-07 |
| Sea_kD_regoMid | Distribution coefficient for the middle regolith layer in sea (glacial clay and post glacial sediments combined). | $m^3$/kg DW | Element Specific | TR-10-07 |
| Sea_kD_regoUp | Distribution coefficient for the upper regolith layer in sea. | $m^3$/kg DW | Element Specific | TR-10-07 |
| Ter_kD_regoMid | Distribution coefficient for the terrestrial middle regolith layer (glacial clay and post glacial sediments combined). | $m^3$/kg DW | Element Specific | TR-10-07 |
| Ter_kD_regoUp | Distribution coefficient for the terrestrial upper regolith layer (peat). | $m^3$/kg DW | Element Specific | TR-10-07 |
| diffcoef | Diffusion coefficient. | $m^2$/year | Element Specific | TR-10-07 |
| *Concentration ratios, retention and release* | | | | |
| cR_foodToHerbiv | Concentration ratio from food to terrestrial herbivores. | kg C/kg C | Element Specific | TR-10-07 |
| cR_soilToCereal | Concentration ratio from soil to cereals. | kg DW/kg C | Element Specific | TR-10-07 |
| cR_soilToMush | Concentration ratio from soil to mushrooms. | kg DW/kg C | Element Specific | TR-10-07 |
| cR_soilToTuber | Concentration ratio from soil to tubers. | kg DW/kg C | Element Specific | TR-10-07 |
| cR_soilToVegetab | Concentration ratio from soil to vegetables. | kg DW/kg C | Element Specific | TR-10-07 |
| cR_watToCray_Lake | Concentration ratio from water to crustacean in the lake. | $m^3$/kg C | Element Specific | TR-10-07 |
| cR_watToFish_Lake | Concentration ratio from water to fish in the lake. | $m^3$/kg C | Element Specific | TR-10-07 |
| cR_watToFish_Sea | Concentration ratio from water to fish in the sea. | $m^3$/kg C | Element Specific | TR-10-07 |

| Parmeter Name | Description | Unit | Type | Report |
|---|---|---|---|---|
| Lake_cR_pp_macro | Concentration ratio from water to macrophytes/macroalgae in lake/stream. | $m^3$/kg C | Element Specific | TR-10-07 |
| Lake_cR_pp_plank | Concentration ratio from water to macrophytes/macroalgae in lake/stream. | $m^3$/kg C | Element Specific | TR-10-07 |
| Lake_cR_pp_ubent | Concentration ratio from water to phytoplankton in lake/stream. | $m^3$/kg C | Element Specific | TR-10-07 |
| Sea_cR_pp_macro | Concentration ratio from water to macrophytes/macroalgae in sea. | $m^3$/kg C | Element Specific | TR-10-07 |
| Sea_cR_pp_plank | Concentration ratio from water to phytoplankton in sea. | $m^3$/kg C | Element Specific | TR-10-07 |
| Sea_cR_pp_ubent | Concentration ratio from water to microphytobenthos in sea. | $m^3$/kg C | Element Specific | TR-10-07 |
| tC_cowMeat | Transfer coefficient from intake of radionuclides in fodder and water to cow meat. | d/kg FW | Element Specific | TR-10-07 |
| tC_cowMilk | Transfer coefficient from intake of radionuclides in fodder and water to cow milk. | d/l | Element Specific | TR-10-07 |
| Ter_cR_pp | Concentration ratio for terrestrial primary producers. | kg DW/kg C | Element Specific | TR-10-07 |
| coefRetent | Fraction of leaf intercepted radionuclides that is adsorbed to edible parts of vegetables during irrigation. | – | Element Specific | TR-10-07 |
| Ter_df_decomp | Discrimination factor during decomposition. | – | Element Specific | TR-10-07 |
| *Human characteristics* | | | | |
| AverTime | The time interval over which concentration in agricultural soil is averaged over. | y | Generic | TR-10-07 |
| expTime | Time spent outdoor (time for exposure from external radiation). | h/year | Generic | TR-10-07 |
| ingRate_C | Human food ingestion rate. | kg C/year | Generic | TR-10-07 |
| ingRate_wat | Human water ingestion rate. | $m^3$/year | Generic | TR-10-07 |
| inhalRate | Human inhalation rate of volume air. | $m^3$/h | Generic | TR-10-07 |
| *Dose coefficients* | | | | |
| dosCoef_ext | Dose coefficient from external exposure. | (Sv/h)/(Bq/$m^3$) | Element Specific | TR-10-07 |
| dosCoef_ing_food | Dose coefficient from ingestion of food. | Sv/Bq | Element Specific | TR-10-07 |
| dosCoef_ing_water | Dose coefficient from ingestion of water. | Sv/Bq | Element Specific | TR-10-07 |
| dosCoef_inhal | Dose coefficient from inhalation. | Sv/Bq | Element Specific | TR-10-07 |

# Appendix C

## Results from sensitivity and uncertainty analyses

This appendix presents, for a selection of radionuclides, two tornado plots with results from sensitivity analysis. In one plot values of Standardized Regression Coefficients (SRC) are presented. The SRC are a measure of the importance of the different parameters for a given output, which is obtained from fitting the model predictions for the output to a linear first order polynomial /Saltelli et al. 2000/ dependency with the studied input parameters. The higher the SRC for a parameter, the higher is effect on the output. A positive SRC value indicates that the input and the output move in the same direction, whereas a negative SRC indicates that they move in opposite directions. In the other plot values of the First Order Sensitivity Indeces (FOSI) are presented. The FOSI is a measure of the contribution of input parameters to the variance of the outputs, obtained from applying sensitivity analyses methods based on variance decomposition /Saltelli et al. 2000/. The FOSIs consider the first order contribution to the variance of the output, i.e. contributions from interactions with other parameters are not taken into account. The SRCs and FOSI presented in the plots were obtained using logarithms of input and outputs.

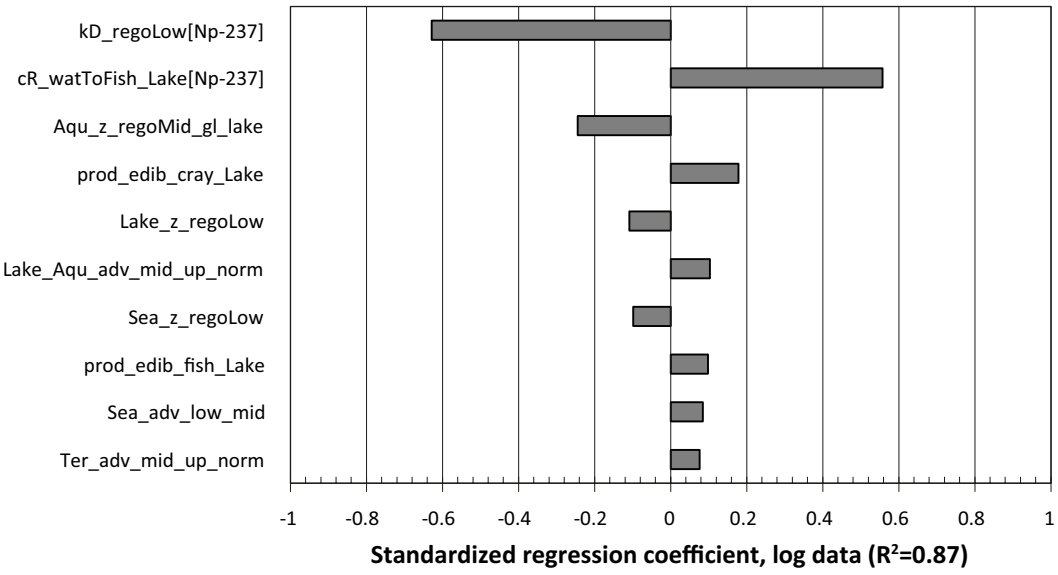


***Figure C-1.*** *Standardized rank regression coefficients of the maximum LDF for Np-237 obtained from probabilistic simulations.*

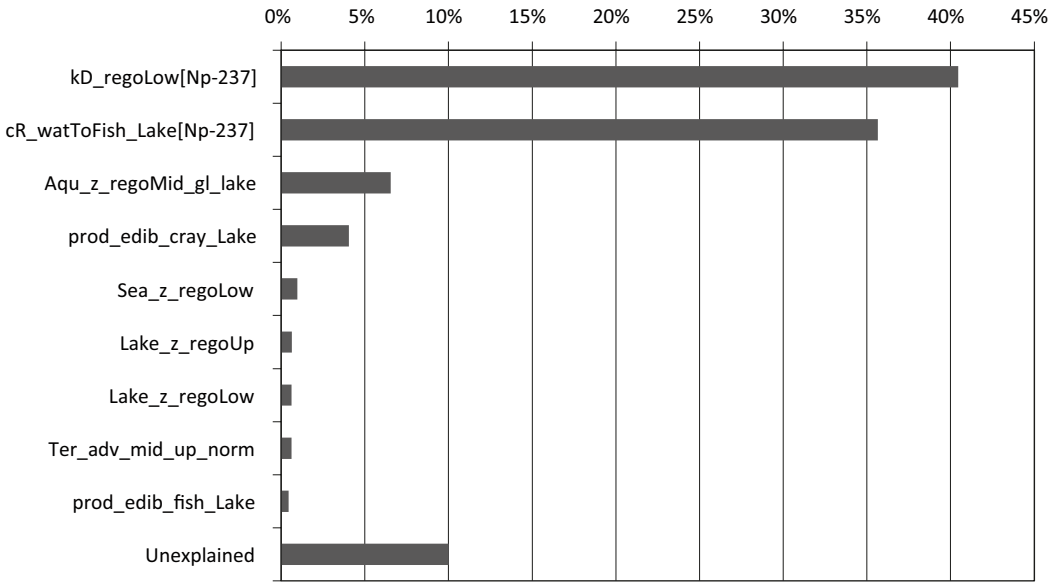


***Figure C-2.*** *First order sensitivity indexes of the maximum LDF for Np-237 obtained from probabilistic simulations.*

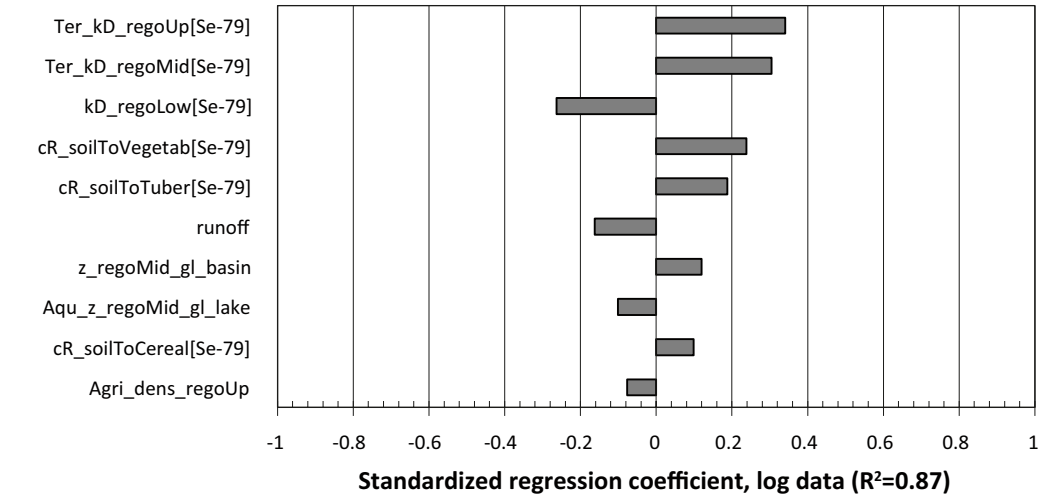


***Figure C-3.*** *Standardized rank regression coefficients of the maximum LDF for Se-79 obtained from probabilistic simulations.*

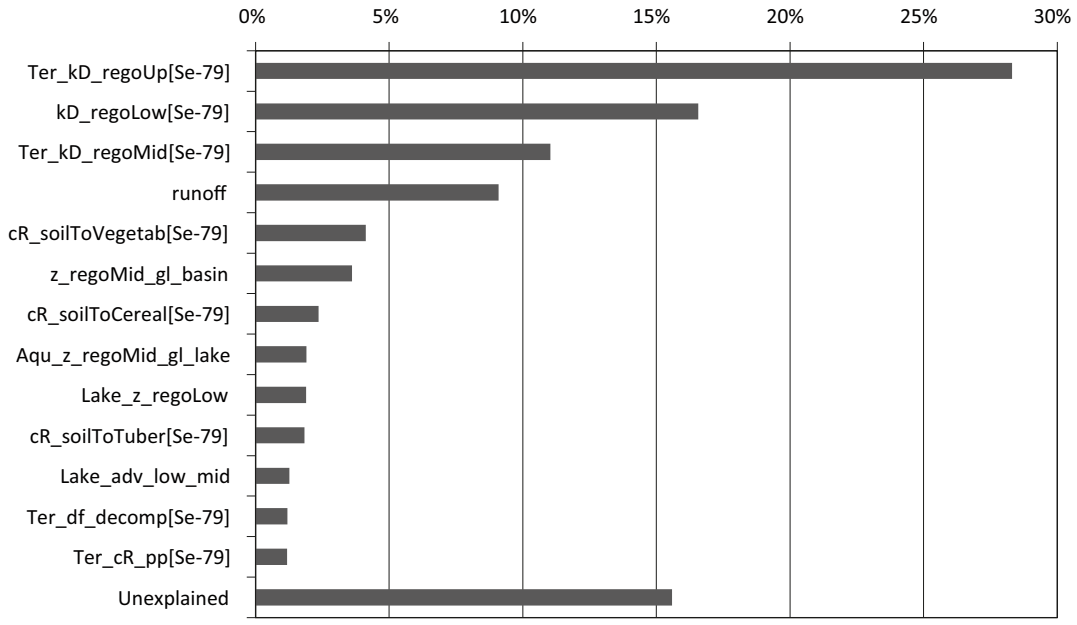


***Figure C-4.*** *First order sensitivity indexes of the maximum LDF for Se-79 obtained from probabilistic simulations.*

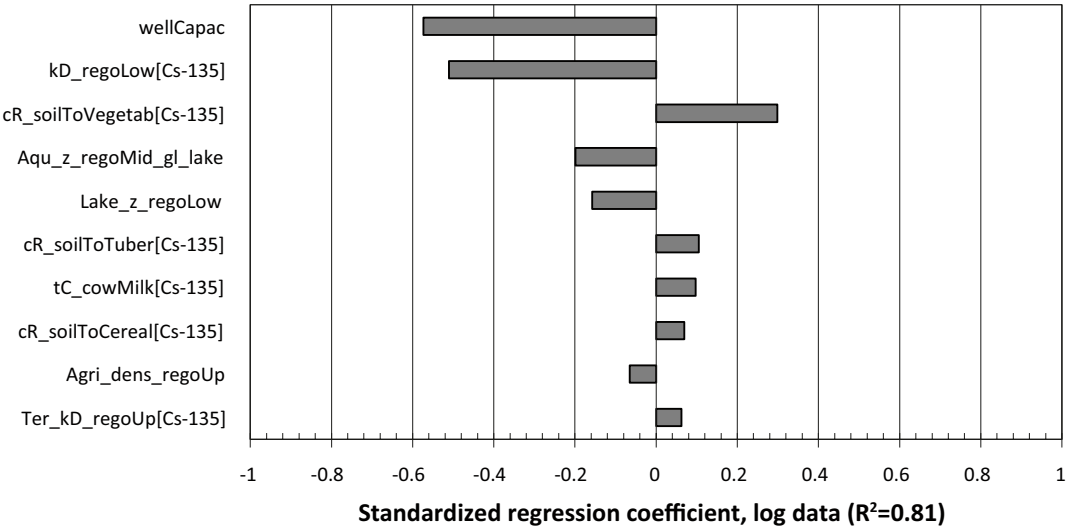


***Figure C-5.*** *Standardized rank regression coefficients of the maximum LDF for Cs-135 obtained from probabilistic simulations.*

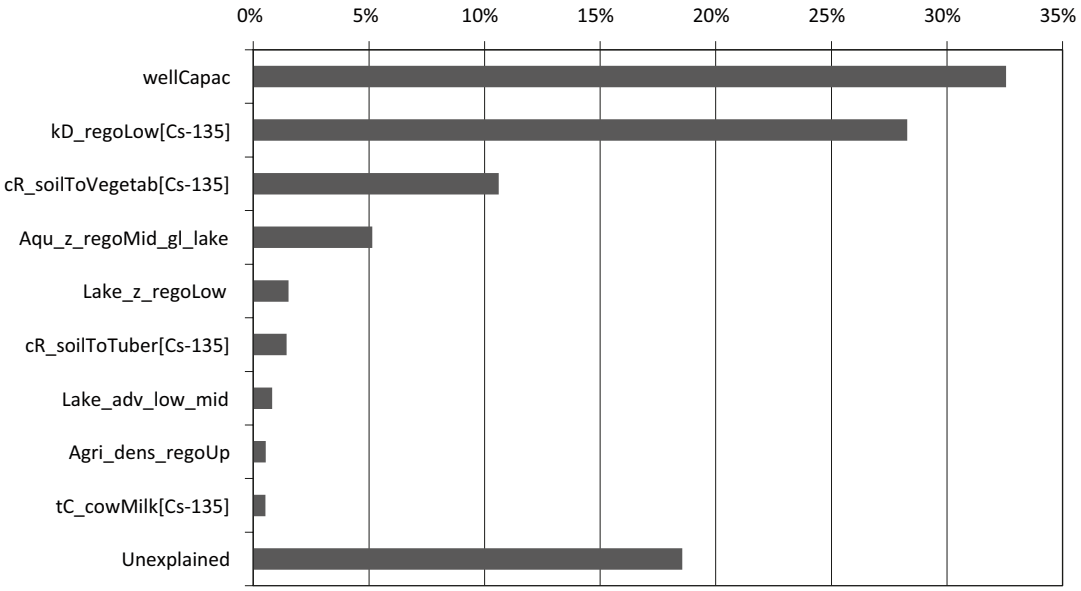


***Figure C-6.*** *First order sensitivity indexes of the maximum LDF for Cs-135 obtained from probabilistic simulations.*

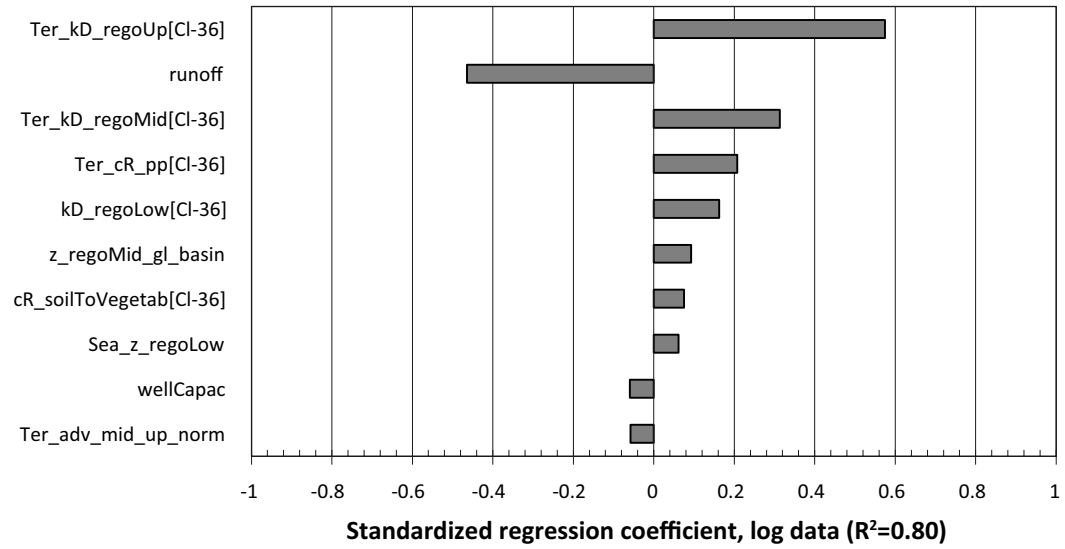


***Figure C-7.*** *Standardized rank regression coefficients of the maximum LDF for Cl-36 obtained from probabilistic simulations.*

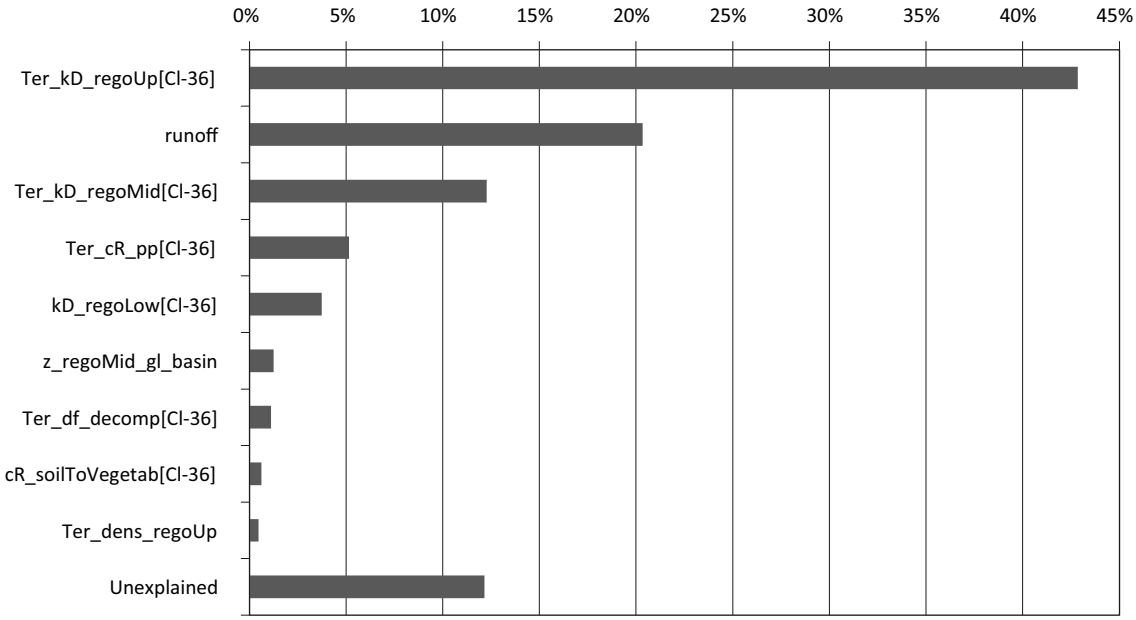


***Figure C-8.*** *First order sensitivity indexes of the maximum LDF for Cl-36 obtained from probabilistic simulations.*